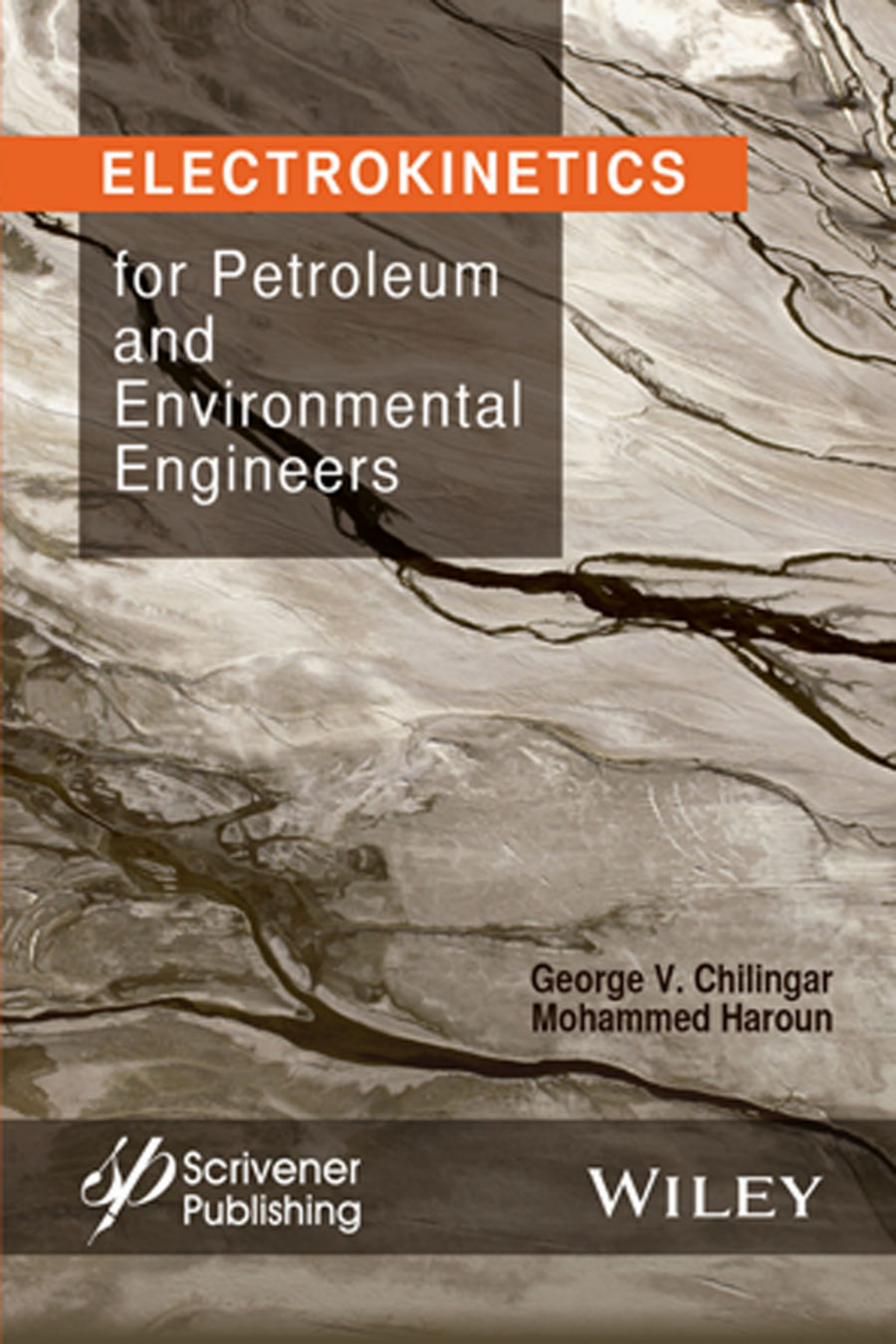
ELECTROKINETICS
for Petroleum and Environmental Engineers
George V. Chilingar
Mohammed Haroun
Scrivener Publishing
WILEY

Electrokinetics for Petroleum and Environmental Engineers

Electrokinetics for Petroleum and Environmental Engineers

George V. Chilingar

Petroleum Engineering, University of Southern California, Los Angeles, USA

Mohammed Haroun

The Petroleum Institute, Abu Dhabi, UAE

WILEY

Co-published by John Wiley & Sons, Inc. Hoboken, New Jersey, and Scrivener Publishing LLC, Salem, Massachusetts.
Published simultaneously in Canada.

Cover design by Kris Hackerott

Library of Congress Cataloging-in-Publication Data:

ISBN 978-1-118-84269-0

Printed in the United States of America

10 9 8 7 6 5 4 3 2 1

Dedication

This book is also dedicated to the memory of the founding father of the U.A.E., H.H. Sheikh Zayed bin Sultan Al Nahyan, whose leadership and vision have been instrumental in driving his ambitious dreams into reality. The authors would also like to dedicate this book to:

H. H. Sheikh Khalifa bin Zayed Al Nahyan, the president of the U.A.E., who has guided this wisdom into all disciplines of our society, making the U.A.E. a world class major educational hub for nurturing our young talent into experts that support the needs of the economy.

H.H. Sheikh Mohamed bin Zayed Al Nahyan, the Crown Prince of Abu Dhabi and Deputy Supreme Commander of the UAE Armed Forces, for his genuine support for the advancement of science and technology, through his endeavors in education and nation building.

Dedication

To Dr. and Mrs. Henry Chuang whose contributions were invaluable in writing this book. Dr. Chuang Yueheng (Henry) is Executive Chairman of the Board of Willie International Holdings Limited. As my former star graduate student and teaching assistant, he was very active in the USC Electrokinetics Laboratory. His contributions for advanced scholarship are helping USC students in Petroleum Engineering. He reflects great honor upon himself and the petroleum industry. We are proud of You!

The principal author dedicates this book to Dr. John Mork, President and Chief Executive of Energy Corporation of America (ECA), who's passion for academic excellence is witnessed by his generous contributions promoting advanced scholarship here at USC in the area of Petroleum Engineering. As one of my former stellar graduate students at USC he shined and now is a recognized pioneer and giant in the petroleum industry. We are proud of You!

The principal author is pleased to dedicate this book to Dr. Erle C. Donaldson with whom he has enjoyed many professional adventures (trips to conferences in foreign lands) and endeavors that have culminated in the birth of the "Journal of Petroleum Science and Engineering" and books on unique topics such as microbial enhanced oil recovery, subsidence, and petrophysics.

Contents

Foreword

I am pleased to write the foreword to the book by Dr. G. V. Chillingar, and Dr. M. Haroun. *Electrokinetics for Petroleum and Environmental Engineers* addresses the advances made in the science of electrokinetics (EK) as it applies to environmental and petroleum engineering. What was once a technology for dewatering clays and soils is now being positioned for use in environmental remediation and enhanced oil recovery. This reference book includes chapters by the foremost researchers in the world conducting research in the area. Top academic researchers from USC, Lehigh University, the University of Vermont and the Petroleum Institute of Abu Dhabi contributed to the book. You will learn about the most recent advances for the use of EK to assist in the cleanup of contamination in soil and ground water. You will also learn about the application of the EK technology for extracting oil as an innovative Enhanced Oil Recovery (EOR) Process.

Electrokinetics was introduced to the US by Leo Casagrande, of Harvard University, in the 1950s. He had used the technology extensively in Europe, for construction site soils stabilization, prior to, and during World War II. In the 1950s, Dr. G. V. Chilingar, and his students at USC conducted a series of laboratory experiments, which suggested that electrokinetics could be utilized to increase flow in permeable formations and for Enhanced Oil Recovery (EOR). About the same time, researchers at a General Electric (GE) facility were conducting field investigation, which indicated that electrokinetics could be an effective and efficient EOR technology. Later, some of these researchers left GE, taking the EK technology with them, founded Electro-Petroleum, Inc. (EPI), and have continued to develop an understanding of EK field implementation.

Electrokinetics is a simple concept to move fluids through rocks and soil under a unidirectional electrical current flow. Current research has extended this technology to move contaminants and oil under the same

stressors. The application of Electrokinetics commercially, to date, has been limited to the soil dewatering and soil stabilization and should be extended by those who read this book. Previous field studies have suffered from a lack of knowledge relating to issues which are being defined and addressed in the chapters in this book. The understanding of the transport of heavy metals having different oxidation states and mobility and organic molecules having different adsorbent coefficients are elucidated in the chapters. The volume of research from laboratory studies is large and the hundreds of research papers published in the scientific literature were reviewed to understand the issues surrounding the complexity of EK technology. This basic understanding of the variables surrounding the technology field can be used to design meaningful field tests.

By reading this book you will learn about the most recent laboratory results for the transport of contaminants in soil and ground water, be exposed to research in the use of EK for oil recovery in the previously unexplored use in carbonate rocks. In Chapter three, Dr. D. G. Hill evaluates the use of the EK process in the oilfield showing the potential of the process for releasing previously unrecoverable oil resources around the world.

Finally great strides are being made in the transferring of the laboratory results into a series of models which can be used to predict the transport phenomena in all types of substrates.

The simple and straight forward style of this book will be of useful to the academic researcher following EK technology development, the environmental remediation engineer looking for a state of the art technology for cleaning up contaminated sites and the petroleum executive looking at the next breakthrough in Enhanced Oil Recovery.

J. Kenneth Wittle, Ph.D.
Electro-Petroleum, Inc.
Williamsburg, VA 23185

List of Contributors

DONALD HILL
Petroleum Engineering, University of Southern California, Los Angeles, CA

EHSAN GHAZANFARI
Environmental Engineering, University of Vermont

SIBEL PAMUKCU
Environmental Engineering, Lehigh University

SANGHEE SHIN
Environmental Engineering, Korea Institute of Construction Technology, Seoul, S. Korea

HASAN SHOJAEI
Petroleum Engineering, University of Southern California, Los Angeles, CA

KENNETH WITTLE
Electro Petroleum Inc., Williamsburg, VA

MENGFEI LIU
Petroleum Engineering, University of Southern California, Los Angeles, CA

1

Introduction to Electrokinetics

By George V. Chilingar, Mohammed Haroun, Hasan Shojaei, and Sanghee Shin

1 Introduction

Electrokinetics is a term applied to a group of physicochemical phenomena involving the transport of charges, action of charged particles, effects of applied electric potential and fluid transport in various porous media to allow for a desired migration or flow to be achieved. These phenomena include electrokinetics, electroosmosis, ion migration, electrophoresis, streaming potential and electroviscosity. These phenomena are closely related and all contribute to the transport and migration of different ionic species and chemicals in porous media. The physicochemical and electrochemical properties of a porous medium and the pore fluid, and the magnitudes of the applied electrical potential all impact the direction and velocity of the fluid flow. Also, an electrical potential is generated upon the forced passage of fluid carrying charged particles through a porous medium.

These electrokinetic effects have been recognized for a considerable period of time, with the effects of electroosmosis and electroviscosity being studied and evaluated by many researchers.

1.1 Factors Influencing Electrokinetic Phenomena

The theoretical development of electrokinetic phenomena and electrochemical transport has been studied historically as far back as 1879 by Helmholtz that led to the introduction of the first analytical equation. Helmholtz described the motion of the charged ionic solution from the anode to the cathode and explained it by the presence of a double layer. This double-layer theory is illustrated in figure 1-1, where the negatively charged surface of the clay attracts the positive ions of aqueous medium, forming the immobile double layer. This immobile double layer is followed by a thick mobile layer with a predominance of positively-charged ions (cations), with a few diffused negatively-charged ions (anions).

Later, the analytical solution was further modified by Smoluchowski in 1921 to arrive at the Helmholtz-Smoluchowski's equation for electrokinetic permeability:

$$k_e = \frac{D\zeta}{4\pi F} \tag{1.1}$$

where D is the dielectric constant; ζ is the zeta potential; and F is the formation factor.

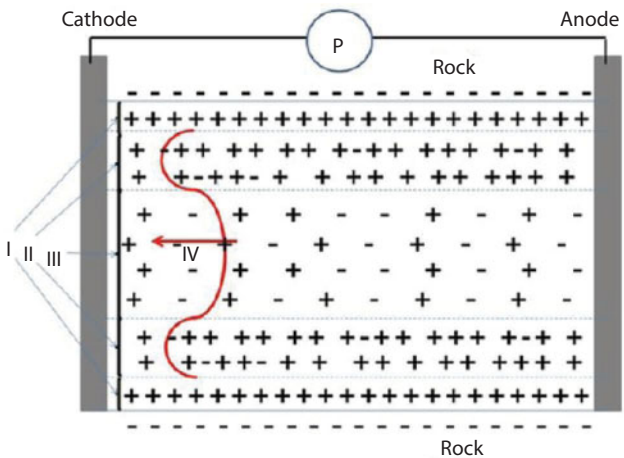

Figure 1.1 Schematic diagram of electrokinetics double layer (I: Immobile Double Layer, II: Mobile Double Layer, III: Free Water, IV: Velocity Profile) as envisioned by Dr. George V. Chilingar. Solid curved line – velocity profile in a capillary. P=DC current power supply. Rock is negatively charged.

The proportionality constant, D, has been verified by several investigators for various types of liquid-solid interfaces. However, extreme sensitivity and complexity of these phenomena have lead to reports of discrepancies in the relative constancy of this term. Probstein and Hicks (1993) have shown the effects of concentration of ionic species within the pore fluid, electric potential, and pH on the zeta potential (ζ). Thus, it doesn't remain constant throughout the electrically-induced transport in soils that are governed by zeta potential, which is defined below.

1.2 Zeta Potential and the Electric Double Layer Interaction

As pointed out by Donaldson and Alam (2008), there is a region at the surface of solids that has a difference in electrical potential across just a few molecular diameters. If a liquid and solid are brought together, an electrical potential develops across a distance of a few molecular diameters at the interface. The changes that are established are characteristic of specific phases and are the underlying cause of many natural phenomena such as electroosmosis, electrophoresis, colloid stability, fluid flow behavior, adsorption, catalysis, corrosion, and crystal growth (Donaldson and Alam, 2008).

The separation of charges is known as the interfacial electrical double layer. It is a complex association of charges illustrated schematically in Fig. 1.2. There is a potential charge (negative or positive) at one or two molecular distances from the surface. This charge may originate from several sources such as: (1) inclusions of extraneous atoms in the lattice structure, (2) dissolution of slightly soluble atoms at the surface of water, (3) chemical reaction (chemisorption) of ions in water with surface atoms forming complex polar molecules on the surface, or (4) exposure of metallic oxides at the surface which react with water to form surface ions. These are some of the major causes of surface charges; others are recognized in suspensions of particles and flocculants in water (Hunter, 1981).

Counterions from the water solution balance the charges at the solid surface and form the immobile Stern layer (Fig. 1.2). The thickness of the Stern layer is only one or two molecular diameters consisting of ions that are adsorbed strongly enough to form an immobile layer. The outer edge of the Stern layer where the ions are mobile is known as the shear plane. There is a linear potential drop across the width of the Stern layer $(\psi_s - \psi_\zeta)$, followed by an exponential potential difference across the diffuse layer between the shear plane and the bulk solution $(\psi_\zeta - \psi_\infty)$. The bulk solution is designated as the reference zero potential. The potential difference between the shear

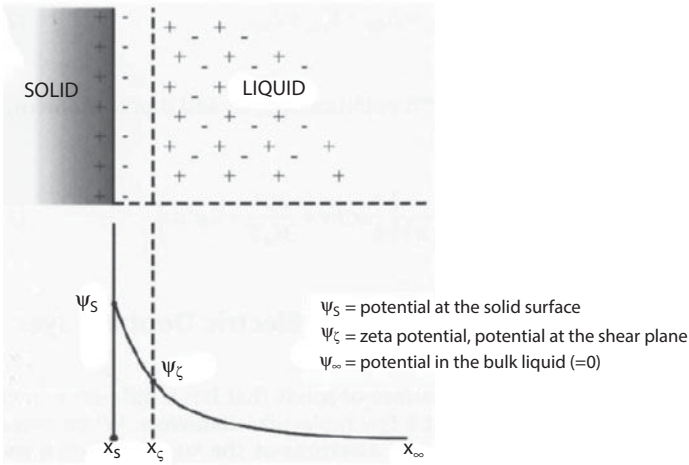

Figure 1.2 Electric double layer at the interface between a solid and liquid: x_s = surface of the solid, x_ζ = shear plane, x_∞ = bulk liquid, $x_\zeta - x_s$ = stern layer, $x_\infty - x_\zeta$ = electrical diffuse (Gouy) layer (Debye length, $1/\kappa$) (after Donaldson and Alam, 2008).

plane and the bulk fluid is known as the zeta potential (Donaldson and Alam, 2008) (see Fig. 1.3).

Cations, anions, and molecules with electrical dipoles can be adsorbed by nonelectrical forces. Grahame (1947) observed that anions are adsorbed by nonelectrical forces with the centers of negative charges lying on an inner plane (within the Stern layer) from the surface known as the inner Helmholtz plane (*IHP* at x_i distance from the solid surface, Fig. 1.4). The *IHP* is followed by the outer Helmholtz plane (*OHP*) drawn through the charges of the hydrated counterions.

The thickness of the Helmholtz layers thus reflects the size of the adsorbed anions and counterions within the Stern layer and is observed by the differences of the measured linear potential differences within the Stern layer. An excellent discussion on the subject was presented by Donaldson and Alam (2008).

The length of the exponential electrical field decay (from the shear plane to the bulk fluid) is known as the Debye length ($1/\kappa$). For example, if the plates of a capacitor have equal charge densities, the zeta potential is the potential difference from the center of the separation to one of the plates (Donaldson and Alam, 2008):

$$\frac{1}{\kappa} = \frac{\varepsilon\varepsilon_o\psi_s}{\sigma_c} = \left(\frac{\varepsilon\varepsilon_o k_B T}{\rho_i z^2 e^2}\right)^{\frac{1}{2}} \quad \left[\frac{C^2}{Jm}\frac{J}{C}\frac{m^2}{C} = m\right] \tag{1.2}$$

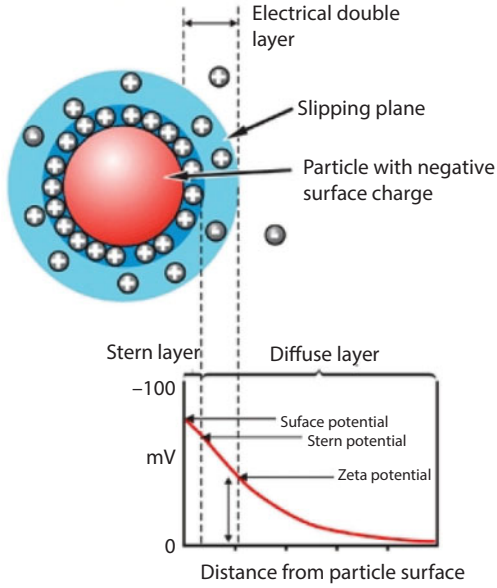

Figure 1.3 Schematic representation of zeta potential (ζ) (after Zetasizer Nano series technical note, Malvern Instruments).

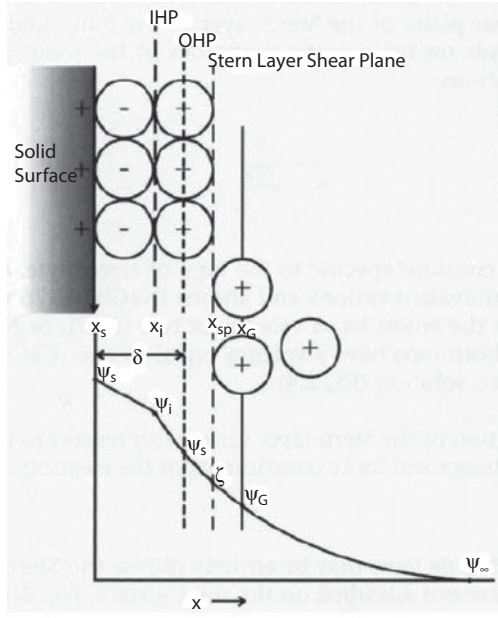

Figure 1.4 Double layer potentials showing the Helmholtz planes and their potentials. *IHP* = inner Helmholtz plane (x_i). *OHP* = outer Helmholtz plane ($x = \sigma$) (after Donaldson and Alam, 2008).

where ε is the dielectric constant (relative permittivity, dimensionless); ε_o is the permittivity of free space [8.854×10^{-12} C^2/J.m=C^2/N.m^2]; k_B is the Boltzmann constant ($1.3806488\times10-^{23}$ J/K); T is the absolute temperature; ρ_i is the number density of ions in the solution; z is the valency; e is the electron charge (1.602×10^{-19} C); $1/\kappa$ is the Debye length; and C is the electrical charge (Coulomb: ampere second). Eq. 1.2 also shows that the charge density of the surface (σ_c) is proportional to the surface potential (ψ_s).

With respect to an ionic solution, the Debye length is the distance from the shear plane of the Stern layer to the bulk fluid. The Debye length depends on the specific properties of the ionic solution. For aqueous solutions (Donaldson and Alam, 2008):

$$\frac{1}{\kappa} = \frac{B}{\sqrt{M}} \tag{1.3}$$

where B is a constant specific to the type of electrolyte. B is equal to 0.304 for monovalent cations and anions (NaCl); 0.176 where either the cation or the anion has a valency of two ($CaCl_2$ or Na_2CO_3); and 0.152 when both ions have a valency equal to two ($CaCO_3$). M is the molarity of the pore solution (see Donaldson and Alam, 2008).

The composition of the Stern layer varies with respect to the nature of the surface charge and ionic constituents of the electrolyte (Castellan, 1971):

1. The double layer may be entirely diffuse (no Stern layer) if ions are not adsorbed on the solid surface (Fig. 1.5). In this case the Stern layer does not exist and the potential difference declines exponentially from the solid surface to the bulk solution.
2. If the concentration of ions in the electrolyte is sufficient to exactly balance the surface charges of the solid, the potential will decrease linearly within the Stern layer to zero at the shear plane. Thus, the zeta potential is zero (equal to the potential of the bulk fluid).
3. If the adsorption of ions does not completely balance the surface charge density, the zeta potential has a finite value with respect to the bulk fluid.
4. If the surface charge is very strong, the Stern layer may contain an excess of ions from the electrolyte. Thus, the zeta potential will have a charge opposite to the surface charge.

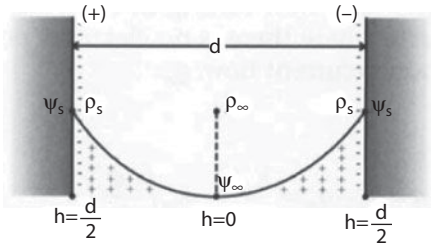

Figure 1.5 Two charged surfaces separated by distance d with a fluid in between. The film thickness on each surface is $h = d/2$. The number density of the counter ions at the surface is ρ_s and the center is designated ρ_∞, which is taken as zero at the reference point in the center. The electric field, which is independent of distance is equal to the electric charge density, D, divided by the electric permittivity, $E_s = D/\varepsilon\varepsilon_o$ (after Donaldson and Alam, 2008).

In aqueous solutions, the zeta potential of mineral surfaces is a function of pH. Usually, acidic solutions promote positive charges at the surface resulting in a positive zeta potential, whereas basic solutions produce an excess of negative charges at the surface because of increase in the hydroxyl ion concentration. The *pH* at which the zeta potential is equal to zero is defined as the zero point charge *(zpc)*. When the negative and positive charges of ions in a solution are equally balanced, the solution is electrically neutral and this condition is defined as the isoelectric point *(iep)* (Donaldson and Alam, 2008). Thomson and Pownall (1989) observed an approximate linear trend of the zeta potential with respect to pH for calcite in dilute solutions of sodium chloride and a mixed solution of sodium chloride and sodium bicarbonate, where $\zeta = -6.67*pH + 40$. The zero point charge occurred at $pH > 6$. Sharma et al. (1987) reported an inverted S-shaped trends where $\zeta = -20*pH + 100$ *(zpc* at $pH \approx 5$*)* for Berea Sandstone cores and dilute sodium chloride solutions (see Donaldson and Alam, 2008).

As the electrolyte passes through a porous material (rock, glass, capillaries, etc.), a potential difference develops which is usually called the streaming potential. The expression for the streaming potential can be written in terms of the zeta potential and the combined resistivities of the electrolyte and solid (Kruyt, 1952):

$$\left(\frac{d\psi}{dx}\right) = \frac{\varepsilon\zeta R_0}{4\pi\mu} \quad \left[\left(\frac{C^2}{Nm^2}\right)(V)\left(\frac{1}{Pa.s}\right)\left(\frac{Vsm}{C}\right) = \frac{V}{Pa}\right] \tag{1.4}$$

where x is the distance; R_0 is the combined resistivities of the electrolyte and solid; and μ is the viscosity.

If the total flow rate of water, q, in a porous medium consists of (1) the flow rate where there is no electrical potential effect, q_n, and (2) an osmotic, countercurrent flow, q_{os}, then:

$$q = q_n - q_{os} = \frac{k_n dp}{\mu dx} - k'_{os}\left(\frac{d\psi}{dx}\right) \tag{1.5}$$

where k_n is the permeability in the absence of electrical phenomena; p is the pressure; k'_{os} is the transport coefficient resulting from the streaming potential, ψ; and μ is the viscosity.

The coefficient, k'_{os} is obtained from the Helmholtz equation for the velocity of electroosmotic flow in a tortuous capillary (Adamson, 1960; Scheidegger, 1974):

$$U_{os} = \frac{e\phi\zeta}{4\pi\mu\tau^2}\frac{d\psi}{dx} \tag{1.6}$$

where ϕ is the porosity and τ is the tortuosity.

Combining Eqs. 1.4 and 1.6 into Eq. 1.5 yields the fluid flow equation that includes the effect of electroosmotic flow (Donaldson and Alam, 2008):

$$q = \left(\frac{k_n}{\mu} - \frac{e^2\phi\zeta^2 R_0}{(4\pi)^2\mu\tau^2}\right)\frac{dP}{dx} = \left(\frac{k_n}{\mu} - \frac{k_{os}}{\mu}\right)\frac{dp}{dx} \tag{1.7}$$

1.3 Coehn's Rule

A general rule for the potential difference of the double layer was given by Coehn in 1909 as follows:

Substances of higher dielectric constants are positively charged in contact with substances of lower dielectric constants. The corresponding potential difference is proportional to the difference of the dielectric constants of the touching substances.

Later, researchers (Smoluchowski, 1921; and Adamson et al., 1963) investigated this qualitative rule.

They found that this rule does not apply to pure organic liquids with low dielectric constants, such as benzene and carbon tetrachloride. However, Coehn's rule is still used to indicate the sign of the zeta potential and, hence, the direction of movement of phases past each other.

The qualitative rule presented by Coehn, seems to represent a very special case where ionic liquid content is very small even when compared to dilute aqueous solutions. The electrochemical behavior of the solid-liquid interface greatly influences these electrokinetic phenomena. In the case of relatively inert surfaces, such as quartz, the electrical charge density depends primarily on the adsorbed electrolytes.

Many researchers, showed a linear logarithmic relationship between zeta potential and concentration (c) (Adamson et al., 1963):

$$\zeta = A - B \log c \tag{1.8}$$

The zeta potential, ξ, goes through a maximum and then approaches zero, which is explained by a combination of two processes: (1) adsorption process of ions on the surface and (2) followed by a neutralization process of the charged surface with opposite sign (Kruyt, 1952).

Rutger et al. (1945) showed the effects of the H^+ and OH^- ions on zeta potential at low concentrations. A small addition of the OH^- increased the negative zeta potential. In the case of larger concentrations, all electrolytes decreased the zeta potential, especially pronounced in the case of polyvalent ions, whereas the addition of H^+ ions decreased the zeta potential.

Although electrolytes can strongly influence the zeta potential, they have no effect on the total potential drop (Adamson et al., 1963.) The addition of multivalent ions may cause the reversal of the zeta potential sign. This can be explained by the adsorbability for these ions in a layer bearing a larger charge than is present on the wall. This will cause a reversal of the charge and potential in the outer part of the double layer (Kruyt, 1952), in order to maintain the electro-neutrality of the system.

The theory of the diffuse double layer leads to the conclusion that the concentration of the electrolyte varies inversely with the effective thickness of the diffuse part of the double layer, (and zeta potential.) The larger the ionic charges, the fewer the ions needed for charge compensation, whereas the larger the ionic charges, the larger the electric forces between the diffuse layer and the inner fixed layer. The fewer ions that are needed for charge compensation, the larger the valences of the adsorbed ions (Adamson et al., 1963).

1.4 Combined Flow Rate Equation

In some of the experiments performed by researchers at USC (Chilingar et al., 1970), an electric potential was applied across a core where oil was already flowing hydrodynamically. When the imposed electrical potential

gradient and pressure drop were in the same direction, the oil flow rate was increased.

If the direction of the hydraulic pressure gradient coincides with the direction of DC electric field current, i.e., Darcy's flow and the electrokinetic transport occur in the same direction, a one-dimensional mathematical model can be used to show the main mechanisms of the species' transport. In this case, redistribution of the species concentration in space can be described as a result of the combined influence of three mechanisms: Darcy flow, electrokinetics and diffusion. The first two relate to the contaminants' solution flow with respect to the solid soil matrix, whereas the last redistributes the species inside the flowing fluids (Chilingar et al., 1997).

For the purpose of simplified analysis, it is reasonable to consider a one-dimensional fluid flow in the direction from anode to cathode. The total fluid flow rate can be obtained by adding the electroosmotic relation to the Darcy equation (Chilingar et al., 1968):

$$q_t = Ak\Delta p / (\mu L) + Ak_e E / (\mu L) \tag{1.9}$$

where A is the cross-sectional area; k is the Darcy permeability; L is the length of the core; k_e is the electrokinetic permeability and E is the imposed electrical potential gradient. This equation can be presented in a dimensionless form by normalizing the flow rates and, thus, eliminating the viscosity, area and length terms:

$$q_t / q_i = 1 + k_e E / k\Delta p \tag{1.10}$$

and

$$(q_t - q_i) / q_i = k_e E / k\Delta p \tag{1.11}$$

where q_i is the initial hydrodynamic stabilized flow rate.

Equation (1.10) shows that an increase in flow rate is dependent upon the zeta potential, dielectric constant, brine concentration, Darcy permeability, and pressure drop. If the dependence of k_e on k is not considered, then Eq. (1.11) would suggest that as the hydrodynamic permeability decreases, the percent increase in flow rate caused by electrical potential would become more significant. This means the electrokinetic technique is especially effective in cases when hydraulic permeability k is very small,

which is valid, for example, for clays or clayey sands. Electrokinetic flow rate increases with increasing clay content in sands. For sands it is possible to raise the hydrodynamic component of the total flow by injection of special purging solutions (Shapiro and Probstein, 1993).

Calculated k_e/k can be used as an index for predicting the probability of success and applicability of Electrically Enhanced Oil Recovery (EEOR). The larger the ratio, the better the chance of success in dewatering sand and increasing the relative permeability to oil. In very tight formations, k_e may exceed k causing an increase in the degree of electric dewatering at the wellbore.

Electrical field application in situ, as a rule, leads to an increase in temperature. In turn, the temperature increase reduces the viscosity of hydrocarbon-containing fluids that, according to Eq. 1.9, would result in an increase of the total flow rate (Chilingar et al., 1968). Analyzing the results of "in situ" trials and verifying corresponding mathematical models, one should keep in mind this additional positive side effect to avoid possible misinterpretations of electrokinetic efficiency. This effect is insignificant for the dissolved gaseous hydrocarbons (like butane and methane). For crude oils (e.g., California crude oils), however, the viscosity can be reduced more than twenty times by heating from 50 to 100 °C (Ungerer et al., 1990). This (at least in theory) would increase the total fluids flow twenty times.

Discussing an electrical field application for the acceleration of fluids transport in situ, one needs to consider also electrical properties of soils (electrical resistivity, for example) and ionization rate of the flowing fluids that can considerably affect the total flow rate. In addition, Chilingar and his associates (Chilingar et al., 1970) discovered that application of DC field to some soils leads to an increase of their hydraulic permeability that, in turn, can considerably accelerate the fluids transport. In addition, some clays are destroyed (become amorphous) upon application of direct electric current, possibly as a result of driving the interlayer water out (do not swell any longer).

1.5 Dewatering of Soils

Electrokinetics has long been applied in soil engineering. Several patents on the removal of water from clayey and silty soils by electrokinetic were issued in Germany before World War II. Later, the method was widely and successfully used in Germany, England, the U.S.S.R., and Canada

in drying waterlogged soils for heavy construction. The development of these practical applications has been largely due to the work of Casagrande (1937-1960) who has carried out continuous research on their feasibility in relation to various soil characteristics.

Literature on civil engineering, soil mechanics, and highway research has reported investigations made by Winterkorn (1947-1958), Casagrande (1937-1960), and others on the nature and scope of the electrical treatment of soils.

Some examples of electrokinetics treatment in civil engineering are described here for the purpose of illustration.

Railway cut, Salzgitter, Germany (Casagrande, 1947): Difficulties that arose during the construction of a double-track railway cutting, in a loose-loam deposit due to the flow of soft soil, were overcome by a large-scale drying operation using electrokinetics. In sections of 100 m, well electrodes 7.5 m deep and 10 m apart were used. Before the application of electrical potential, the average rate of flow of water was 0.4 m^3/day/20 wells. An electrical potential, with an average tension of 180 volts and average current of 19 amps/well, was applied. During an eight-week period, the flow continued at an almost constant rate of 60 m^3/day/20 wells, i.e., at 150 times the flow rate before the application of electrical potential.

U-boat pen, Trondheim, Norway: Several attempts to make an excavation about 14-meters deep in a very thick stratum of clayey silt interspersed by seams of sand in the proximity of the sea were doomed to failure because of the very active uplift phenomenon. The application of electrokinetics to cause water to flow away from the excavation site was tried next. The salt deposits, which increased the electrical conductivity of the soil, required high consumption of current.

Before the application of electrical potential, the flow rate varied from 1 o 50 liters per hour per well. A current of 26 amps at 40 volts tension was used. The application of current increased the flow rate up to 11-479 liters per hour per well. The average power consumption was estimated to be 0.4 KW-hr per cubic meter of soil excavated.

Lime sludge deposits: Some tests were made by Casagrande on dewatering lime-sludge deposits (Wulprath, Germany) having a uniform water content of 120 % of dry weight. The application of electrical potential with 70-volt tension and a current of 50 amps for 14 days obtained a 25 % decrease in moisture content. The reduction lines of water content indicated that the electrokinetics dewatering process took place uniformly along the lines of equal potential strength.

1.6 Use of Electrokinetics for Stabilization of Week Grounds

Casagrande (1930) found that a permanent stabilization of soil could be obtained by using aluminum electrodes. These aluminum electrodes were found to be greatly corroded and aluminum compound deposits were noticed around the electrodes. Encouraged by the model tests, Casagrande (1937) undertook a full scale experiment and came to the conclusion that electrochemical treatment could be used for increasing the bearing capacity of piles.

Casagrande (1960) attributed the increase in the bearing capacity of piles after electrochemical treatment to the following:

1. Water was transported from one electrode to another, causing a change in the water saturation.
2. The loosely attached low valence ions to the clay-plate surface were displaced with higher valence ions by base exchange, such as the replacement of Na ions by Al ions.
3. Metal derivatives were deposited around the anode and $CaCO_3$ around the cathode, acting as cementing agents between soil particles.

Probably, the best example of the use of electrokinetics to increase the bearing capacity of piles was in a bridge foundation over the Big Pic River, near Marathon, Ontario, Canada (Casagrande et al., 1950). The ultimate bearing capacity of piles driven 110 ft into the ground was constant over a one-year period at 30 tons. The piles were about 23 ft apart. A potential of 100-volt tension was used to give an average current of 15 amps per pile. The bearing capacity of the piles increased from 30 to 100 tons after this treatment was maintained for four weeks.

Russian scientists have made significant contributions to the investigation of the electrochemical stabilization of soil and the induration of weak rocks, through the continued addition of different electrolytes at the anodes and by the use of electrodes of various materials. Tolstopiatov (1940), Zhinkin (1952-1959), Rebinder (1957), Titkov et al. (1961) and others seem to agree that upon electrochemical treatment, soil and weak rocks underwent major physicochemical changes. All investigation indicated that these physicochemical changes led to the formation of a new soil structure (coagulation-crystallization structure). Zhinkin (1958) further indicated that these changes were irreversible, and that more strength was obtained progressively by the newly-formed clay structure even after the discontinuation of electrochemical treatment.

Titkov et al. (1961) have introduced the idea of indurating weak rocks in the wall of the borehole by electrochemical treatment. This is carried out by the continued introduction of special electrolytic solution at the anode during the electrical treatment. They have thoroughly investigated the electrochemical treatment of different types of geological formations using various combinations of electrolyte solutions. The investigation was performed on a variety of formation samples in the laboratory, as well as on specially selected field sites. In addition, they tested the use of different electrode material, such as aluminum, iron, and carbon.

Electrochemical induration of weak rocks is dependent on the formation of a new and stronger authigenic cementing material. The formation of new minerals (gibbsite, allophane, aluminite, limonite, hisingerite, calcite and gypsum) were reported (Titkov et al. 1961) to have occurred during electrochemical treatment. Cylindrical movable electrodes with variable diameters were designed by Titkov et al. (1961) in order to test this treatment in the wall of drillholes. With stationary or circulating fluid, it was possible to obtain favorable results in indurating the walls of drillholes for different lengths of time at varying depths from 10 to 116 m. The circulating fluid was varied from pure electrolytic solution to a chemically treated clay-cement mixture. On the basis of tests carried out 13 months later, on the electrochemically indurated drillholes, Titkov et al. (1961) concluded that:

1. The suitability of the electrochemical treatment of weak rocks is quite promising not only at the time of drilling, but also during well exploitation.
2. The walls of a drill-hole may be indurated electrochemically either by the creation of a crust of hardened mixture consisting of clay or loam and binding materials such as cement; or by increasing the stability of clay rocks by transforming them through the electrical action.
3. Reversing the electrodes' polarity during electrochemical treatment will speed up the cementing process.
4. The electrochemical induration of weak rocks is certainly an irreversible process.

1.7 Bioelectroremediation

There is a wide variety of mechanical, physical, chemical, and bioremediation cleaning methods that are applied in contemporary practice for the restoration of contaminated sites. It is even difficult to name all of them

and give their characteristics. A good classification of the bioremediation methods with general recommendations of their applications was presented by Pollard et al. (1994).

For any particular contaminated site, one should select the most appropriate cleanup technology (or the most appropriate combination of different technologies). The choice of a technology (or technologies) depends on many factors, e.g., the site size, type of predominant contamination, the site's future use, and available resources (time and money). Examples of such an approach to the selection of cleanup strategy were presented by Blacker and Goodman (1994) and Fairless (1990). They developed some reasonable selection methodology of cleaning technologies, based on the principles of system analysis from the final goal, through the quantitative characterization of the problem, to the choice of preferable alternatives.

W. Loo and his associates presented many good examples of the successful application of combined technologies. Loo (1994) used a combined system, including primarily passive cometabolic biotreatment and electrokinetic transport of amendments and contaminants in solution for degradation of gasoline and diesel in the soil and groundwater. In one case, spills of gasoline and diesel from an underground storage tank caused soil and groundwater contamination in the clayey Bay Mud, City of Hayward, California. The soil contamination extended to a depth of about 10 ft with a total petroleum hydrocarbons (TPH) concentration of 100 to 3,900 ppm. The gasoline and diesel in the soil were degraded to less than 100 ppm of TPH, and to less than 10 ppm in groundwater. The remediation process was completed in four weeks.

A combination of biodegradation and electrokinetic transport with a hot air venting system and ultraviolet light biocontrol system was used by Loo et al. (1994) for the degradation of gasoline in the clayey soil. The gasoline soil plume covered an area of about 2,400 sq ft, to a depth of about 30 ft. The upper 15 ft. of sediment was composed of highly-conductive marine clay, whereas the lower 15 ft. consisted of well-cemented conglomeratic sandstone. The gasoline concentration ranged from 100 to 2,200 ppm. The process of remediation was completed after about 90 days of treatment. The concentration of gasoline in the soil after treatment was far below the proposed cleanup level of 100 ppm. The cost of treatment was about $50 (US 1997) per ton of soil for this advanced soil treatment process, which provided a cost effective remediation with minimum disruption to business operations at the site (Chilingar et al., 1997).

A closed recovery system for soil and groundwater for a site contaminated with gasoline in Greenville, North Carolina, was developed by Burnett and Loo (1994). The dissolved contaminant plume covered an area

of 18,000 sq. ft. and penetrated to the depth of about 15 ft. The total volume of spill was estimated at 300,000 gallons. The initial concentration of gasoline in the plume averaged about 40 mg/l of total BTEX (Benzene, Toluene, Ethylbenzene, and Xylenes).

A special enhanced bioremediation system was designed to clean this site. The system consisted of two groundwater recovery wells, a treatment unit and an infiltration gallery. The treatment unit consisted of transfer pumps, pressure filters, granulated activated carbon filters, air sprayers, holding tanks, chemical feed system, water heater and monitoring means. The bioenhancement process included heating, addition of nutrient amendments (monoammonium phosphate and trisodium phosphate), and oxygen addition (dilute hydrogen peroxide). In six months of operations, BTEX in the plume had been reduced to a level less than 6.5 mg/l with the passage of 11 pore volumes of displacement.

1.8 Electrical Enhanced Oil Recovery (EEOR)

In 1952, Tchilingarian (Chilingar) suggested the possibility of using direct electric current for the separation of fine sediments into grades on the basis of different cataphoretic velocity exhibited by clay particles of different size. This was achieved on treatment of clays with NaOH, because OH^- ions impart greater negative change to clays and, consequently, greater velocity towards the positive electrode. He started this research because he was questioning the statement in textbooks that "cataphoretic velocity is independent of size and shape of colloids". Also, knowing the success in dewatering of clays by soil engineers, he started research on EEOR together with his students at the Petroleum Engineering Laboratories of the University of Southern California (e.g., Anbah, 1963).

Chilingar and his students (Ace, 1955; Anbah et al., 1964, 1965; Chilingar et al., 1968a,b, 1970,1997) conducted numerous laboratory tests involving electrokinetics since the 1950s, which indicated that this low-power drain mechanism could be used for EOR. Tikhomolova (1993) described similar studies conducted at the University of St. Petersburg, also suggesting electrokinetics as a potential EOR technology. Hill (1997) conducted bench-scale studies, which suggested that hydrocarbons could be transported via electrokinetic mechanisms. Pamukcu et al. (1993) and her students at Lehigh University, demonstrated electrokinetic transport of hydrocarbons (PAH), in clay-rich soils, as a method of remediating manufactured gas plant site contamination.

Upon application of DC current, the mobile Gouy layer migrates toward the (negative) cathode. This motion of the water molecules and cations within the Gouy layer drags the water molecules, cations, and anions, in the free fluid, as well as any non-wetting fluid, along with it (Hill, 1997).

Extensive experimental work, conducted at the University of Southern California (Anbah et al., 1964, 1965; Chilingar et al., 1968a,b, 1970, 1997) showed up to six-fold volumetric fluid flow increases in cores containing clay minerals, compared to only 2-fold increases in pure silica cores (see figure 3-15). Chilingar et al. (1970) speculated that in pure silica core, fluid flow might be, at least partly, due to a thermal effect. Mitchell (1993) maintained that all silicate minerals show this increased flow effect, to some extent. Those with high cation exchange capacity (CEC) exhibit the greatest flow increases.

EEOR is an emerging technology that could significantly improve oil recovery, at costs below other secondary and tertiary oil recovery technologies, in environments where other technologies either do not work or are not attractive. EEOR has a nonexistent water demand, a smaller carbon footprint than traditional EOR technologies, such as steam injection, and does not involve injection of hazardous liquids, as is the case for caustic and/or co-solvent flood. EEOR requires minimal surface facilities. No steam generators, compressors, surface working fluid pumps, and/or hazardous material storage tanks are required.

EEOR involves passing direct current (DC) electricity between cathodes (negative electrodes) in the producing reservoir and anodes (positive electrodes) either at the surface and/or at depth. Anbah et al. (1965) suggested a few electrode arrangements for waterflooding operations (see Chapter 3). Fig. 1.6 shows the originally proposed EEOR field installation (Fig. 1.6).

The use of DC electrical power as an EEOR process was patented by General Electric (GE) (Bell and Titus, 1973, 1974) after it had originally been proposed by Prof. George V. Chilingar in 1950. It is currently being developed by Electro Petroleum, Inc. (EPI) of Wayne, Pennsylvania, USA (Bell et al., 1985; Titus et al., 1985; Wittle and Bell, 2005a, 2005b). These two organizations, collectively, spent several years and millions of US dollars in R&D to overcome encountered field operational difficulties. Their combined efforts resulted in successful EEOR demonstrations in California and Alberta heavy oil fields (Wittle et al., 2008 and 2011). Application of EEOR would return about 25 dollars (2012) per each dollar invested, considering the initial installation cost and that of electricity.

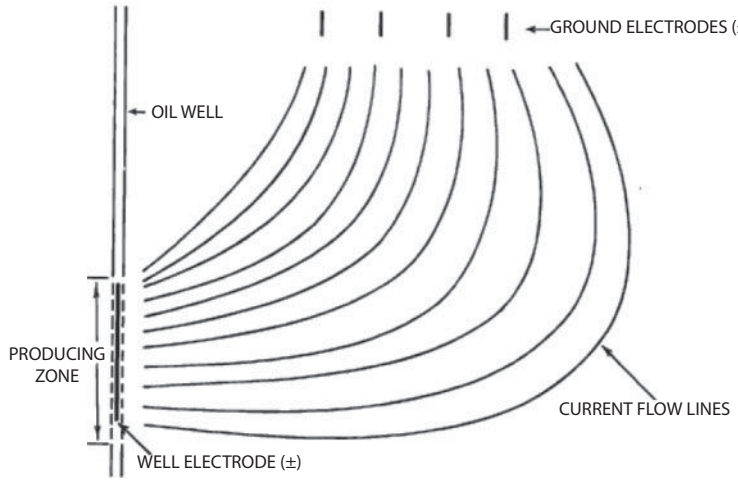

Figure 1.6 Proposed EEOR field installation by Anbah et al. (1965).

1.9 Improving Acidizing of Carbonates

The stimulation of carbonate reservoirs is mainly achieved by acidizing treatments (Hendrickson, 1972; Chilingarian et a1., 1992). Acids may be injected into pores and pre-existing fractures or at hydraulic fracturing rates depending upon the results desired. The acid dissolves the carbonates (limestones/dolomites), enlarging the pores and increasing the width of pre-existing fractures. This gives rise to an increase in permeability. The principal acid commonly used is hydrochloric (HCl), which is pumped through tubing.

In the case of the uniform penetration of acid, the reaction rate declines uniformly with decreasing acid concentration. The weight of carbonate dissolved per increment of distance penetrated declines uniformly until the acid is completely spent. With stronger acid, the spending time decreases.

In the case of matrix acidizing, with enlargement of pores or pre-existing fractures, (1) the specific surface area decreases, (2) the velocity decreases, (3) spending time increases, and (4) the penetration distance increases.

The main problem in acidizing is the fact that the radial distance the acid will penetrate until being spent is short, especially in tight carbonates. When assuming a homogeneous formation and that the volume of acid

injected is equal to the pore volume invaded [$q_i t = \pi\phi h\left(r_a^2 - r_w^2\right)$], the radial distance the acid will penetrate until being spent, r_a (ft), is equal to:

$$r_a = \sqrt{\frac{0.0936 q_i t}{\pi\phi h} + r_w^2} \tag{1.12}$$

where q_i is the acid injection rate (bbl/min); t is the spending time (sec); ϕ is the fractional porosity; h is the formation thickness (ft); and r_w is the wellbore radius (ft).

As shown in Eq. (1.12), in order to increase r_a, either t or q_i should be increased. The injection rate q_i, can be increased considerably by the application of DC current (see Chilingar et al., 1968, 1970, for example). The application of electrokinetics in Abu Dhabi carbonate reservoir rocks has been proven to be very promising by Haroun et al. (2009).

As shown in Fig. 1.7, using electrokinetics, it is necessary to deploy an anode in the well adjacent to the formation being acidized, and a nearby cathode either at the surface or in the adjoining well. The electrokinetic flow will occur from the anode towards the cathode, and thereby acidizing the target formation, enabling the acid to move faster and deeper into the formation in a guided fashion (see Wittle et al., 2008). The two electrodes (anode and cathode) must be connected by cables to the Direct Current

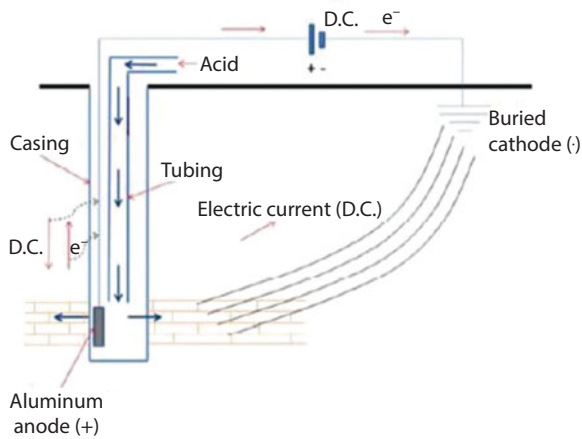

Figure 1-7 Electrodes arrangement for acidizing operation (after Chilingar et al., 2013).

power supply located on the surface. The acid must be injected with corrosion inhibitors into the formation; however, the aluminum anode will also serve as a sacrificial anode.

By applying DC current during acidizing operations, the volumetric rate of flow increases, which, in turn, increases the penetration distance of the acid before it is being spent. Without application of DC current, the penetration distance is usually very short, especially in tight rocks.

1.10 Economic Feasibility

Many assumptions should be made in order to make a rough calculation of economic feasibility of using DC current. The variables which will affect the economic evaluation include: (1) thickness, depth, and resistivity of the pay zone, (2) arrangement of the electrodes, (3) duration of the electrical treatment, (4) labor cost, and (5) price of electricity at the site of application.

In general, the rock resistivity is a function of the amount of interstitial water present, which is determined by the porosity and its type. The flow of electrical current in such a case is not a simple linear flow but follows an irregular path around the individual sand grains. This flow pattern will increase the length of the current flow lines. Inasmuch as the current is mainly transmitted through the rock in the form of electrolytic conduction, the resistivity of the interstitial formation water seems to be the deciding factor in the formation resistivity as a whole. The presence and types of clays, however, greatly affect the electrical resistivity of the formation, especially in the case of fresh formation water (Anbah et al., 1965).

Although the electrokinetics depend mainly on the imposed electrical potential gradient, the associated electrical current is conditioned by the type of formation under consideration and its electrolyte content. There is no simple relation between the amount of liquid transported by electrokinetics and the quantity of electricity consumed. The presence of expandable colloidal matter in the porous media further complicates the picture.

In field application, the energy consumption will depend on the dimensions of the electrodes, the applied electrical potential, and the lithology. If these factors are known, the amount of transmitted electrical current can be estimated. Upon switching the current on, it will drop gradually because the overall resistance will increase.

The total amount of current transmitted (I) for various electrode arrangement can be estimated (Rudenberg, 1945; Casagrande, 1949) by using equations such as those presented below:

a. For two cylindrical electrodes of equal length and cross-sectional area, the required electrical current is equal to:

$$I = \frac{2\pi LE}{\rho \ln \frac{d}{r}} \tag{1.13}$$

where ρ is the formation resistivity in ohm-meters; L and r are the length and radius of the electrode in meters, E is the imposed electrical potential in volts; and d is the distance between the anode and the cathode in meters.

b. For two cylindrical electrodes with different radii:

$$I = \frac{\pi LE}{\rho}\left(\frac{1}{\ln \frac{d}{r_1}} + \frac{1}{\ln \frac{d}{r_2}}\right) \tag{1.14}$$

c. For a row of alternate anodes and cathodes, the amount of electrical current can be given approximately by:

$$I = \frac{N\pi LE}{\rho}\left(\frac{1}{\ln \frac{d}{r_1}} + \frac{1}{\ln \frac{d}{r_2}}\right) \tag{1.15}$$

where N is the number of electrodes in each group.

Before one can proceed with estimating the consumption of power, some assumptions have to be made. The following estimation of the benefit of current application is very difficult because of the decrease in the current flow as a result of increasing overall resistance. On assuming that (1) the electrical current is available at the electrode; (2) the formation resistivity is constant and is equal to 10 ohm-meters; (3) the electrode length and radius are equal to three and 0.1 meters, respectively; (4) the applied potential is equal to 100 volts, and (5) the distance between electrodes is

equal to 40 meters (Anbah et al., 1965) and substituting the above values in Eq. 1.13:

$$I = \frac{2 * 3.14 * 3 * 100}{10 * \ln \frac{40}{0.1}} = 31.4 \text{ amps}$$

Thus, the power consumption is equal to:

$$31.4 * \frac{100}{1000} = 3.14 \text{ KW}$$

The approximate cost of electricity (at \$0.059/KW-h) = 3.14 x 24 x 0.059 = \$ 4.45 per day per well. If the labor cost is assumed to be \$50 per day per well (Gillette, 2006), then the total cost becomes \$54.45 per well per day. It is assumed that the equipment needed (electronic power supply, electrodes, power cables, etc.) will cost approximately \$55,000 per well. If the estimated life of the equipment is five years and its salvage value is 11,000, then by using straight-line depreciation at 6 % average interest, the annual depreciation plus interest is equal to \$10,494 per well (modified after Anbah et al., 1965).

According to laboratory experimental results and the application of electrokinetics in related engineering field, an average increase in the flow rate of oil (corresponding to 3.14 KW-h) can be estimated as 13.9 B/D per well. The annual gross dollar return (at \$70/Bbl) is equal to \$355,145.00, and after CMR tax (at \$6/Bbl) is equal to \$324,704.00. This value minus the annual labor and electricity cost will give a net annual profit of: \$324,704.00 - \$19,874.25 = \$304,829.75. The net profit is approximately equal to 304,829.75/10,494.00 ≈ \$29.05 dollar returned per dollar invested (modified after Anbah et al., 1965).

These rough sample calculations are presented here in order to indicate the possibility of application of electrokinetics in the field (see Chapter 3).

1.11 Releasing Stuck Drillpipe

As pointed out by Helmick and Longley (1957), stuck drillpipe occurs when drillstring embeds itself into a layer of filtercake on the borehole wall (differential sticking). A significant force is required to free the pipe; thus,

various countermeasures are employed to prevent the differential sticking (Brandon et al., 1993).

Khasaev et al. (1983) showed that DC current can reduce the release-torque. Current densities of 0.7-14.4 mA/cm^2 reduced the release torque by 50 % after 0.5-2.5 hours. This was probably due to electrokinetic transport of water to the drillstring-mudcake interface (cathode).

In the laboratory, Bonanos et al. (1993) showed that for polymer-based drilling fluids, the torque required to free the discs decreased by 50-70% on passing 10 mA/cm^2 DC current. Brandon et al. (1993) conducted excellent research on the effect of cathodic currents on friction and stuck pipe release in water-based drilling fluids. They found that the release-torque was reduced by 50 % in polymer-based and 80 % in clay-based drilling fluids.

1.12 Summary

One can summarize the major features and advantages of electrokinetic technology as follows:

- The flow rate of oil and water can be increased by the application of direct current.
- Chemical additives may be used in conjunction with electrical treatment to augment the flow rate of transportable fluids.
- Electrochemical treatment may be used for well stimulation.
- Electrokinetic flow rate increases with increasing potential gradient (or electrical current, *I*), first reaching a maximum, then decreasing with further increase in electrical current.
- It is cost competitive with steam EOR, with no depth constraint.
- Thief zone problems (e.g., in the case of steam injection in EOR) do not exist.
- There is no water or working fluid requirement.
- Reduces water consumption and water cut when compared to steam EOR.
- No hazardous emissions or liquid problems.
- Facility installation can be incremental, allowing the spreading of capital over the lifetime of the desired projects.
- DC current can be effectively applied for releasing the stuck drillpipe in aqueous drilling fluids.

Bibliography

Abramson, H.A., 1934. *Electrokinetic Phenomena and Their Application to* Biology and Medicine. Chemical Catalog Co. New York, N.Y.

Ace, A.G., 1955. *An investigation of the influence of applied electrical potential gradients on flow of fluids in porous media*. M.S. Thesis, Department of Petroleum Engineering, The University of Southern California, Los Angeles, CA.

Adamson, A.W., 1960. *Physical Chemistry of Surfaces*. John Wiley, Interscience, New York.

Adamson, L.G., Anbah, S.A., Chilingar, G.V. and Beeson, C.M. 1963a. Possible use of electric current for increasing volumetric rate of flow of oil and water during primary or secondary recovery. *Chimika Chronika*, 28(1): 1–4.

Adamson, L.G., Chilingar, G.V. and Beeson, C.M., 1963b. Some data on electrokinetic phenomena and their possible application in petroleum production. *Chimika Chronika*, 28(10):121–127.

Adamson, L.G., Chilingar, G.V., Beeson, C.M. and Armstrong, R.A., 1966. Electrokinetic dewatering, consolidation and stabilization of soils. *Engineering Geology*, 1: 291–304.

Al-Sharhan, A.S. and El-Sammak, A.A., 2004. Grain size analysis and characterization of sedimentary environments of the United Arab Emirates coastal area. *J. Coastal Research*, 20 (2): 464–477.

Anbah, A.S., 1963. *Use of direct electrical current for increasing the flow rate of reservoir fluids during petroleum recovery*. Ph.D. Dissertation. The University of Southern California, Los Angeles, CA.

Anbah, S.A., Chilingar, G.V. and Beeson, C.M., 1964. Use of direct electrical current for increasing the flow rate of reservoir fluids during petroleum recovery. *J. Canadian Petroleum Technology*, 3(1):8–14.

Anbah, S.A., Chilingar, G.V. and Beeson, C.M., 1965. Application of electrical current for increasing the flow rate of oil and water in a porous medium. *J. Canadian Petroleum Technology*, 4(2): 81–85.

Anbah. S.A., Chilingar, G.V., and Beeson, C.M., 1965. Application of electrokinetic phenomena in Civil Engineering and Petroleum Engineering. *Annals New York Academy of Science*, 118(14): 585–602.

Atlas, R.M., 1977. Stimulated petroleum biodegradation. *Critical Reviews in Microbiology*, 5: 371–386.

Atlas, R.M., 1981. Microbial degradation of petroleum hydrocarbons. *Microbiological Reviews*, 45: 180–209.

Bear, J., 1973. *Dynamics of Fluids in Porous Media*. Elsevier, Amsterdam.

Bell, C.W. and Titus, C.H., 1973. Electro-Thermal Process for Production of Offshore Oil through Onshore Wells, *US Patent* No. 3,724,543.

Bell, C.W. and Titus, C.H., 1974. Electro-Thermal Process for Promoting Oil Recovery, *US Patent* No, 3,782,465.

Bell, C.W., Titus, C.H., and Wittle, J.K., 1985. In situ Method for Yielding a Gas From a Subsurface Formation of Hydrocarbon Material, *US Patent* No. 4,473,114.

Bell, G.T., 1957. Electrolytically Promoting the Flow of Oil From a Well, *US Patent* No. 2,799,641.

Bhandari, A., Dennis, C.D. and Novak, J., 1994. Soil washing and biotreatment of petroleum-contaminated soils. *J. Environmental Engineering*, 120(5): 1151–1169.

Blacker, S. and Goodman, D., 1994. Risk-based decision making case study: Application at a Superfund cleanup. *Environmental Science and Technology* 28(11): 471–477.

Brandon, N.P., Panesar, S.S., Bonanos, N., Fogarty, P.O., and Mahmood, M.N., 1993. The effect of cathodic currents on friction and stuck drill pipe release in aqueous drilling muds. *J. Pet. Sci. Eng.*, 10: 75–82.

Burnett, W.E. and Loo, W.W., 1994. In-situ bioremediation of gasoline in soil and groundwater: A case history. Paper presented at the *Superfund XV Conference*, Washington, D. C.

Casagrande, I.L., 1937. Full-scale experiment to increase bearing capacity of piles by electrochemical treatment. *Bautechnique,* 15(1): 14–16.

Casagrande, I.L., 1941. The drainage of fine soils. *Strasse,* 8(l9/20): 324.

Casagrande, I.L., 1941. *On the Problem of Drainage of Fine Soils*. Stuttgart 36: 556.

Casagrande, I.L., 1947, The application of electroosmosis to practical problems in foundations and earthworks. *Building Res. Tech. Paper* No. 30. Dept. Sci. Indust. Res. London, England.

Casagrande, I.L., 1948. Electroosmosis. Proc. *Second Int. Conf. Soil Mechanics*, 1: 218–223.

Casagrande, I.L., 1949. Electroosmosis in soils. *Geotechnique,* 1(3): 1–29.

Casagrande, I.L., 1959. *Electroosmosis in Soil*. Harvard Soil Mechanics Series No. 45.

Casagrande, I.L., Soderman, L.G., and Loughney, R.W., 1960. Increase of bearing capacity of friction piles by electroosmosis. Paper presented at *ASCE Convention*. Boston, Mass.

Castellan, G.W., 1971. *Physical Chemistry* (2nd ed.). Addison Wesley Publishing.

Chilingar, G.V., Adamson, L.G., Armstrong, R.A. and Beeson, C.M., 1964. Soils stabilized through electroosmosis. *Southwest Builder and Contractor*, 145(24): 100–102.

Chilingar, G.V., Adamson, L.G. and Rieke, H.H., 1966. Notes on application of electrokinetic phenomena in soil stabilization. In: *Proceedings International Clay Conference*, Jerusalem, Vol. 1, pp. 81 –89.

Chilingar, G.V., Adamson, L.G., Rieke, H.H. and Gray, R.R., 1968. Electrochemical treatment of shrinking soils. *Engineering Geology*, 2(3): 197–203.

Chilingar, G.V., Anbah, S.A. and Beeson, C.M., 1965. Application of electrokinetic phenomena in Civil Engineering and Petroleum Engineering. *Annals New York Academy Science*, 118(14): 585–602.

Chilingar, G.V., Beeson, C.M. and Anbah, S.A., 1968. Uso de corriente electrica directa para aumentar la proportion del fluxo de fluidos en los yacimientos: Effecto del tipo de arcilla sobre la produccion de flujo. *Ingenieria Petrolera*, 5(3): 22–32.

Chilingar, G.V., Buryakovsky, L.A., Eremenko, N.A., and Gorfunkel, M.V., 2005. *Geology and Geochemistry of Oil and Gas*, Elsevier, Amsterdam.

Chilingar, G.V., Chang, K.S., Davis, J.E., Farhanghi, H.J., Adamson, L.G., and Sawabini, S., 1968. Possible use of direct electrical current for augmenting reservoir energy during petroleum production. *Compass of Sigma Gamma Epsilon*, 45(4): 272–285.

Chilingar, G.V., El-Nassir, A., and Stevens, R.G., 1970. Effect of direct electrical current on permeability of sandstone cores. *J. Petrol. Tech.*, 22(7): 830–836.

Chilingar, G.V., Loo, W.W., Khilyuk, L.F., and Katz, S.A., 1997. Electrobioremediation of soils contaminated with hydrocarbons and metals: progress report. *Energy Sources*, 19: 129–146.

Chilingar, G.V., Mannon R.W., and Rieke, H.H., 1972. *Oil and Gas Production from Carbonate Rocks*, Elsevier, New York.

Chilingar, G.V., Shin, S., Haroun, M., Albannay, A., Wittle, K., Meshkati, N., and Pamukcu, S., 2013. Improving acidizing operations. *J. Sustainable Energy Engineering*, 1(1) 1–5.

Chilingarian, G.V., 1991. Comments on: Experimental results on the influence of electric fields on the migration of oil, ionic species and water in porous media, by Lancelot, F., Londiche, H., and de Marsily, G., *J. Pet. Sci. Eng.*, 5: 293–295.

Chilingarian, G.V., Mazzullo, S.V., and Rieke, H.H., 1992 *Carbonate Reservoir Characterization. A Geologic-Engineering Analysis,* Part I, Elsevier, Amsterdam.

Coehn, A., 1909. Über optische Wahrnehmbarkeit und elektrische Wanderung gelöster Moleküle. *Zeitschrift für Elektrochemie und angewandte physikalische Chemie*, 15(17): 652–654.

Cozzarelli, I.M., Herman, J.S. and Baedecker, M. J., 1995. Fate of microbial metabolites of hydrocarbons in a coastal plain aquifer: The role of electron acceptors. *Environmental Science and Technology*, 29: 458–469.

Craft, B.C, Holden, W.R., and Graves Jr., E.E., 1962. *Well Design, Drilling and Production*, Prentice Hall, Englewood Cliffs, N.J.

Donaldson, E. and Alam, W., 2008. *Wettability*. Houston, Texas: Gulf Publishing Company.

Donaldson, E., Chilingarian. G.V., and Yen, T., 1989. *Enhanced Oil Recovery II, Process and Operations. Dev. Pet. Sci.*, 17B, Elsevier, Amsterdam, 604 pp.

El Gawad, E.A., Lotfy, M.M., and Sadooni, F.N., 2008. Sedimentology and hydrocarbon potentiality of arid Sabkha, UAE., *J. Applied Sciences Research*, 4 (9): 1124–1130.

Fairless, B., 1990. Applying total quality principles to Superfund planning, Part II: DQOs in Superfund: A dioxin case study. In: *Proc. Seventeenth Annual National Energy Division Conference, American Society for Quality Control*, Tucson, Arizona.

Gillette, H.P., 2006. *Handbook of Construction Cost*. McGraw-Hill Inc.

Grahame, D.C., 1947. The electrical double layer and the theory of electrocapillarity. *Chemical Reviews*, 41(3): 441–501.

Haroun, M.R., Chilingar, G.V., Pamukcu, S., Wittle, J.K., Belhaj, H.A., and Al Bloushi, M.N., 2009. Optimizing electroosmotic flow potential for electrically enhanced oil recovery (EEOR™) In: Carbonate Rock Formations of Abu Dhabi Based on Rock Properties and Composition. *IPTC*13812, December, 2009.

Haroun, M.H., 2009. *Feasibility of in-situ decontamination of heavy metals by electroremediation of offshore muds*. Doctoral Dissertation in Environmental Engineering, University of Southern California, Los Angeles, CA.

Harton, J.H., Hamid, S., Abi-Chedid, E., and Chilingar, G.V., 1967. Effect of electrochemical treatment on selected physical properties of clayey silt. *Engineering Geology*, 2(3): 191–196.

Helmick, W.E. and Longley, A.J., 1957. Pressure differential sticking of drill pipe and how it can be avoided or relieved. *Drill. Prod. Pract*., 1: 55–61.

Hendrickson, A.R., 1972. Stimulation of carbonate reservoirs. In: *Oil and Gas Production from Carbonate Rocks* (Chilingar, G.V., Mannon, R.W., and Rieke, H.H.), American Elsevier, New York.

Hicks, R.E. and Tondorf, S., 1994. Electrorestoration of metal contaminated soils. *Environmental Science and Technology*, 28(12): 2203–2210.

Hill, D. G., 1997. Enhanced restoration of contaminated aquitards, using electro-osmotic aided remediation, Weiss Associates, Presentation to *California Environmental Protection Agency Department of Toxic Substances Control*, May 7.

Hinchee, R.E., Downey, D.C., Dupont, R.R., Aggarwal, P.K., and Miller, R., 1991. Enhancing biodegradation of petroleum hydrocarbons through soil venting. *J. Hazardous Materials*, 27: 315–325.

Hopper, D.R., 1989. Cleaning up contaminated sites. *Chemical Engineering* (August): 94–110.

Huesemann, M.H., 1994. Guidelines for landtreating petroleum hydrocarbon contaminated soils. *J. Soil Contamination*, 3:299–318.

Huesemann, M.H., 1995. Predictive model for estimation of extent of petroleum hydrocarbon biodegradation in contaminated soils. *Environmental Science and Technology*, 29(1): 7–18.

Hunter, R.J., 1981. *Zeta Potential in Colloid Science: Principles and Applications*, Vol. 125. Academic press, London.

Katz, S.A., Khilyuk, L.F. and Chilingar, G.V., 1996. Sensitivity analysis and multivariant modeling for formation pressure and temperature fields in inhomogeneous media. *J. Petroleum Science and Engineering*, 16: 95–108.

Kendall, C.G., Alsharhan, A.S. and Whittle, G.L., 1995. Holocene carbonates/evaporites of Abu Dhabi, United Arab Emirates-Field trip guidebook, *International Conference on Quaternary Deserts and Climatic Change*, published by the United Arab Emirates University.

Khasaev, R.M., Kuliev., R.B., and Dzhabrailov, G.A., 1983. Freeing stuck drilling tools by the electro-osmotic method under high temperature and pressure conditions. *Neft. Khoz*., 5:22–24 (in Russian).

Kruyt, H.R., 1952. *Colloid Science*, 1: 389. Elsevier Pub. Co., New York, N.Y.

Lageman, R., Pool, W., and Seffings, G., 1989. *Chem. Ind.* 18575.

Lancelot, F., Londiche, H., and De Marsily, G., 1990. Experimental results on the influence of electric fields on the migration of oil, ionic species and water in porous media. *J. Petroleum Science and Engineering*, 4: 67–74.

Langnes, G.I., Robertson, J.O., and Chilingar, G.V., 1972. *Secondary Recovery and Carbonate Reservoirs*, Elsevier.

Leahy, J.G., and Colwell, R.R., 1990. Microbial degradation of hydrocarbons in the environment. *Microbiology Review*, (54): 305–315.

Lee, M.D., Thomas, J.M., Borden, R.S., Bedient, P.B., Ward, C.H. and Wilson, T.J., 1988. Biorestoration of aquifers contaminated with organic compounds. *CRC Critical Reviews in Environmental Control*, 18: 29–89.

Loo, W.W., 1991. Heat enhanced bioremediation of chlorinated solvents and toluene in soil. *Proc. HMCRI R & D Conf.*, Anaheim, Calif., pp. 133–136.

Loo, W.W., 1993. Biotreatment of chlorinated solvents in soil and groundwater utilizing glucose as the co-substrate. Presented at the *Hazmacon Conf.*, San Jose, Calif.

Loo, W.W., 1994. Electrokinetic enhanced passive in situ bioremediation of soil and groundwater containing gasoline, diesel and kerosene. Presented at the *Hazmacon Conf.*, San Jose, Calif.

Loo, W.W., Wang, I.S., and Fan, K.T., 1994. Electrokinetic enhanced bioventing of gasoline in clayey soil: A case history. Presented at the *Superfund XV Conference*, Washington, D. C.

Mahaffey, W.R., Compeau, G., Nelson, M., and Kinsella, J., 1991. Developing strategies for PAH and TCE bioremediation. *Water and Environmental Technology*: 3233–86.

McCarty, P.L., 1991. Engineering concepts for in situ bioremediation. *J. Hazardous Materials*, 28: l–10.

Mitchell, J.K., 1993. *Fundamentals of Soil Behavior*, John Wiley and Sons, Inc., New York.

Morgan, P. and Watkinson, R.J., 1989. Hydrocarbon degradation in soils and methods for biotreatment. *Critical Reviews in Biotechnology*, 8: 305–333.

Nash, J.H. and Traver, R.P., 1988. Field application of pilot soil-washing system. *EPA Document EPA/68-03-3450*. Office of Research and Development, US. Environmental Protection Agency, Cincinnati, Ohio.

Nelson, M.J., Montgomery, S.O., Mahaffey, W.R., and Pritchard, P.H., 1987. Biodegradation of trichloroethylene and involvement of an aromatic biodegradative pathway. *Applied and Environmental Microbiology*, 53(5): 949–954.

Nunno, T.J., Hyman, J. A. and Pheiffer, T. H., 1988. Assessment of international technologies for Superfund applications. *EPA Document EPA/540/2-88/003*, 37 pp. Office of Solid Waste and Emergency Response. U.S. Environmental Protection Agency, Washington, DC

Overbeek, J.T. and Lijiklema, J., 1969. *Electric Potential in Colloidal Systems, Electrophoresis*. M. Bier, Ed., Academic Press, New York, 25–35.

Pamukcu, S. and Wittle, J.K., 1993. Electrokinetic treatment of contaminated soils, sludges and lagoons. *DOE Contract No. 02112406.*

Pamukcu, S. and Wittle, J.K., 1994. Electrokinetic removal of coal tar constituents from contaminated soils. *EPRI TR-103320, Project 2879-21.*

Pamukcu, S., Weeks, A. and Wittle, J.K., 1997. Electrochemical extraction and stabilization of selected inorganic species in porous media. *J. Hazardous Materials*, 55: 305 – 318.

Pamukcu, S., Weeks, A., and Wittle, J.K., 2004. Enhanced reduction of Cr(VI) by direct electrical current in a contaminated clay. *Environmental Science Technology*, 38: 1236 –1241.

Pamukcu, S., Hannum, L., and Wittle, J.K., 2008. Delivery and activation of Nano-iron by DC electric field. *J. Environ. Sci. Health*, Part A, 43(8): 934–944.

Pheiffer, T. H., 1990. EPA's assessment of European contaminated soil treatment techniques. *Environmental Progress 49582–587*.

Pollard, S.J., Hrudey, S.E., and Fedorak, P.M., 1994. Bioremediation of petroleum and creosote-contaminated soils: a review of constraints. *Waste Management & Research*, 12(2): 173–194.

Probstein, R.F., Renaud, P.S., and Shapiro, A.P., 1991. Electroosmosis techniques for removing hazardous materials from soil. *U.S. Patent 5074986*.

Probstein, R.F. and Hicks, R.E., 1993. Removal of contaminants from soils by electric fields. *Science*, 260 (5107), 498–503.

Quincke, G. 1861., Pogg. Ann. Physik. 113: 513; quoted in Smoluchowski: 54.

Raymond, R.L., Hudson, J.O., and Jamison, V.W., 1976. Oil degradation in soil. *Applied Environmental Microbiology*, 31: 522–535.

Rebinder, P.A., 1957. Physiochemical mechanics as a new field of knowledge. *Akademiya Nauk SSSR, Vestnik* 27(10): 32–42.

Renaud, P.S. and Probstein, R.F., 1987. Electroosmotic control of hazardous waste. *PhysicoChemical Hydrodynamics*, 9(1/2): 345.

Rudenberg, P.A., 1945. Grounding principle and practice. *Elect. Engr*., 64 (1): 1–15.

Rutgers, A. and de Smet, M., 1945. *Trans. Faraday Soc*., 41: 758.

Scheidegger, A.E., 1974. *The Physics of Flow Through Porous Media*. University of Toronto Press.

Shapiro, A.P. and Probstein, R.F., 1993. Removal of contaminants from saturated clay by electroosmosis. *Environmental Science Technology*, 27(2): 283–291.

Shapiro, A. P., Renaud, P.S. and Probstein, R.F., 1989. Preliminary studies on the removal of chemical species from saturated porous media by electroosmosis. *PhysicoChemical Hydrodynamics*, 11(5/6): 785.

Sharma, M.M., Kuo, J.F., and Yen, T.F. 1987. Further investigation of the surface charge properties of oxide surfaces in oil-bearing sands and sandstones. *J. Colloid and Interface Science*, 115(1): 9–16.

Shin, S., Haroun, M., Ghosh, B., Pillay, A., Al Badawi,M., Chilingar, G.V., Pamukcu, S., and Wittle, J.K., 2010 Electroremediation of heavy metals from offshore muds upon partial chlorine gas removal. The *9th Symposium on Electrokinetic Remediation (EREM)*, June 27-30, Kaohsiung, Taiwan.

Sims, R.S., 1990. Soil remediation techniques at uncontrolled hazardous waste sites: A critical review. *J. Air Waste Management Association*, 40: 704–732.

Smoluchowski, von M., 1921. Electric endosmosis and streaming current. *Handbuch der Elektrizitat und des Magnetismus*, 2: 366–428. Translated by P.E. Bocque. *Univ. Mich. Engr. Res. Bull.* 33: 47–158.

Stinson, M. K., Skovronek, H. S., and Ellis, W.D., 1992. EPA Site demonstration of the BioTrol soil washing process. *J. Air and Waste Management Association*, 42:96–103.

Street, N., 1961. Electrokinetic effects in laboratory permeability measurement. *Producer* Monthly, 25(1) :12–14.

Tchilingarian, G., I952. Possible utilization of electrophoretic phenomenon for separation of fine sediments into grades. *J. Sed. Petr*., 22: 29–32.

Thompson, D.W. and Pownall, P.G., 1989. Surface electrical properties of calcite. *J. Colloid and Interface Science*, 131(1): 74–82.

Tikhomolova, K.P., 1993. *Electro-osmosis*. Harwood, New York.

Titkov, N.I., Korzhuev, A.S., Smolyaninov, V.G., Nikishin, V.A., and Neretina, A.Y., 1961. *Electrochemical Induration of Weak Rocks*. Translated by Consultants Bureau. New York, N.Y.

Titus, C.H., Wittle, J.K. and Bell, C.W., 1985, Apparatus for passing electrical current through an underground formation, *US Patent No.4,495,990*.

Tolstopiatov, B.V., 1940. The problem of electrochemical treatment of the ground. *Pochvovedenie*, 8: 67–82.

Ungerer, P., Burrus, J., Doligez, B., Chenet, P.Y. and Bessis, F., 1990. Basin evaluation by integrated two-dimensional modeling of heat transfer, fluid flow, hydrocarbon generation, and migration. *Petroleum Geology Bull.*, 74(3): 309–335.

United States Patents. 2,211,696 (8-13-1940); 2,217,857 (10-15-1940); 2,283,206(5-19-1942); 2,625,374 (1-13-1953); 2,799,641 (7-16-1947).

Visscher, K., Brinkman, J., and Soczo, E.R., 1990. Biotechnology in hazardous waste management in the Netherlands. *Biotechnology and Biodegradation: Advances in Applied Biotechnology*, 4: 389–403. Gulf Publ. Co., TX.

von Helmholtz, H.L.F., 1879. Studies of electric boundary layers. *Wied. Ann*, 7: 337–382.

Wilson, J. T., 1985. Biotransformation of TCE in soil. *Applied Environmental Microbiology*, 1: 242–243.

Winterkorn, H.F., 1947. Fundamental similarities between electroosmotic and thermoosmotic phenomena. *Proc. Highway Res. Bd.* 27: 443–455.

Winterkorn, H.F., 1948. Physicochemical properties of soils. *Proc. Second Int. Conf. Soil Mechanics,* 1: 23–29.

Winterkorn, H.F., 1952. Surface-chemical properties of clay minerals and soils from theoretical and experimental developments in electroomosis. *ASTM Symposium on Exchange Phenomena in Soils.* Spec. Tech. Pub. 142: 44–52.

Winterkorn, H.F., 1955. Water movement through porous hydrophilic systems under capillary, electrical, and thermal potential. *ASTM Symp. on Permeability of Soils*. Spec. Tech. Pub. 163: 27–35.

Winterkorn, H.F., 1955. Potentials in moisture migration. *Bldg. Res. Bull.* No. 1: 86–101, Canada.

Winterkorn, H.F., 1958. Mass transport phenomena in moist porous systems as viewed from the thermodynamics of irreversible processes. *Highway Res. Bd. Spec. Report* 40: 324–338.

Wittle, J.K. and Bell, C.W., 2005a. Electrochemical process for effecting redox-enhanced oil recovery, *US Patent No. 6,877,556 Bl.*

Wittle, J.K. and Bell, C.W., 2005b. Method for enhancing oil production using electricity, *US Patent Application No. 2005/0199387 AI.*

Wittle, J.K. and Hill, D.G., 2006a. Use of direct current electrical stimulation for heavy oil production*, Society of Petroleum Engineers Applied Technology Workshop - Technologies for Thermal Heavy Oil and Bitumen Recovery and Production*, Calgary, March 14 – 15.

Wittle, J.K. and Hill, D.G., 2006b. Direct current electrical stimulation - A new approach to enhancing heavy oil production, *First World Heavy Oil Conference*, Beijing, November 12 – 15.

Wittle, J.K., Hill, D.G., and Chilingar, G.V., 2008a. Direct current stimulation for heavy oil production. Paper 2008-374. *Second World Heavy Oil Congress*, Edmonton, March 10–12.

Wittle, J.K., Hill, D.G., and Chilingar, G.V., 2008b. Direct current electrical enhanced oil recovery in heavy-oil reservoirs to improve recovery, reduce water cut, and reduce H_2S production while increasing API gravity, *SPE* 114012.

Wittle, J.K., Hill, D.G., and Chilingar, G.V., 2011. Direct electric current oil recovery (EEOR)—A new approach to enhancing oil production. *Energy Sources, Part A: Recovery, Utilization, and Environmental Effects*, 33(9): 805–822.

Zhinkin, G.N., 1952. Experience in using electrochemical soil reinforcement for stabilizing roadbeds. *Leningr. Inst. Inzhenerov Zheleznodorozhnogo Transporta, Sbornik*, 144: 64–79.

Zhinkin, G.N., 1956. Some results of using electrochemical soil stabilization under operating conditions. *Leningr. Inst. Inzhenerov Zheleznodorozhnogo Transporta, Sbornik*, 150: 72–82.

Zhinkin, G.N., 1958. Strengthening of structural bonds in clayey soils as a result of electrochemical stabilization. *Kolloidn. Zh.*, 22(1): 31–36.

Zhinkin, G.N., 1959. Improving the quality of clayey soils by using electrochemical stabilization methods. *Leningr. Inst. Inzhenerov Zheleznodorozhnogo Transporta, Sbornik*, 157: 164–180.

2

Reduction of Contaminants in Soil and Water By Direct Electric Current

Sibel Pamukcu, Ehsan Ghazanfari, and Kenneth Wittle

2.1 Introduction

Applying a low direct current electrical field across a porous medium, such as wet soil induces migration of ionic and surface charged constituents and flow of the pore water to a directed location within the field. Commonly referred to as "electrokinetics", this process is a proven, sustainable technology that can transport water and substances residing in or near the aqueous phase in clayey soil at a significantly higher rate than hydraulic methods. Harmful heavy metal contaminants and radioactive materials, as well as some immiscible fluids can thus be removed in-situ. The process is especially useful in applications where pump-and-treat methods are impractical due to the low permeability of the medium, or in cases where the contaminants persist owing to their affinity to the solid phases in clay soils. Moreover, the application of direct electric current in soils have been

used successfully to transport reactive agents, such as nano-particle slurries to enhance in-situ reactions that convert contaminants, or chelating or surfactant agents to solubilize the contaminants so they can be transported with water advection. More recently, evidence was provided that shows how direct electric current can contribute to success of the desired transformation reactions by not only providing the "driving force" necessary to deliver active reagents, but also by lowering the energy for the redox reactions to occur. This enhancement of transformation reactions was attributed to the double-layer polarization of the clay surfaces leading to Faradaic processes under the applied electric field.

In most field situations, the contaminants are found adsorbed onto soil surfaces, iron-oxide coatings, soil colloids and natural organic matter. Most contaminants are retained in clay interstices as hydroxycarbonate complexes, or present in the form of immobile precipitates and products in soil pore throats and pore-pockets that "lace" the vadose zone. This exacerbates clean-up efforts as the available technologies, such as in-situ bioremediation, chemical treatment or the traditional pump-and-treat method may not be able to treat the entire site effectively in low permeability soils. Electrokinetics treatment, when designed to properly address the site specific features, can potentially reduce the subsurface pollution by transporting and/or transforming contaminants, and enhance resource recovery by extracting trapped materials (i.e., heavy metals, oils and petroleum) which may not be extractable by other means. This chapter first provides an overview of the use of direct electric current for environmental mitigation in the subsurface, and discusses with examples the application of direct electric current to:

i. transport of environmental contaminants for the purpose of extracting them out of subsurface soil and water;
ii. transfer of environmental contaminants for the purpose of their destruction in-situ or conversion to environmentally less toxic/benign compounds; and
iii. recover resource by extraction and accumulation of usable materials from subsurface soil and water.

2.2 Overview of Direct Electric Current in Subsurface Environmental Mitigation

Electrically induced migration of ions and water is a proven method of externally forced mass transport in clay soils for contaminant remediation

purposes (Pamukcu and Wittle, 1992; Probstein and Hicks, 1993, Lageman, 1993; Acar and Alshawabkeh, 1993, 1996a; Acar et al., 1994; Hicks and Tondorf 1994; Eykholt and Daniel, 1994; Shapiro et al., 1995; Yeung et al., 1996; Alshawabkeh and Acar, 1996b; Electorowicz and Boeva, 1996; Reddy and Parupadi, 1997; Dzenitis, 1997; Chilingar et al., 1997). While electoosmosis is analogous to soil washing, ion-migration is probably the primary mechanism of mass transport when the contaminants are ionic or surface charged. Relative contribution of electroosmosis and ion migration to the total mass transport varies according to soil type, water content, ion species, and their concentration. In silts and low-activity clays, electroosmotic flow reaches maximum in comparison to hydraulic flow. But the mass transported by ionic migration is always much higher than the mass transported by electroosmotic advection (Acar and Alshawabkeh, 1993). The effect of electroosmosis decreases significantly when pH and zeta potential drops in the later stages of a sustained electrokinetic process under a constant electric potential (Hamed et al., 1991 and Pamukcu et al., 1997). When micelles (i.e., charged aggregate of molecules or particles) are formed with other species in the processing fluid, or when slurry masses are treated, electrophoresis may become significant (Pamukcu et al., 1995).

Chilingar and co-workers (1997) reviewed and evaluated the electro-bioremediation technologies for remediation of soils contaminated with hydrocarbons and metals. They found many successful applications of the combined technologies (Loo et al., 1994) including: (i) primarily passive biotreatment for degradation of gasoline and diesel in the soil and groundwater, (ii) combination of biodegradation and electrokinetic transport with a hot air venting system and ultraviolet light bio-control system for degradation of gasoline in the clayey soil, (iii) closed recovery system consisting of special enhanced bioremediation for treatment of soil and ground water for a site contaminated with gasoline.

2.2.1 Theoretical Considerations: Transport of Charged Species - Electromigration

As in many electrochemical systems, flow of electric current through a network of a multi-phase material , such as wet soil occurs in different phases simultaneously: in the bulk liquid (electrolyte in the pores), on the surface of the solid (clay particles), and in the interface layer(s) between the solid and the liquid. Flow of the current can be achieved by ionic conduction through the liquid phase and electronic conduction through the solid phase and the interface layer(s). The electronic conduction orthogonal to and along the interface layer(s) takes place via charge transfer. In

the classical treatise of "electrokinetic phenomenon" in colloidal systems (Hunter, 2001; Lyklema, 1995), it is this interface, known as the *electric double layer* (EDL) or *diffuse double layer* (DDL) which plays a critical role in the coupling between the ion motion and the fluid flow. The double layer intrinsically connects the solid and the liquid phase, and mediates the relative motion between the liquid and solid phase through (i) accumulation of charge density; (ii) transport of charge and ions along surface; and (iii) passage of charge to the surrounding electrolyte (Bard and Faulkner, 1980).

The bulk transport of ions in electrochemical systems without the contribution of advection by water is described by Poisson-Nernst-Planck (PNP) equations (Rubenstein, 1990). The well-known Nernst-Planck equation describes the processes of *diffusion,* the process that drives the ions from regions of higher concentration to regions of lower concentration; and *electromigration* (also referred to as *ion-migration*), the process that launches the ions in the direction of the electric field (Bard and Faulkner, 1980). Since the ions themselves contribute to the local electric potential, Poisson's equation that relates the electrostatic potential to local ion concentrations is solved simultaneously to describe this effect. The electro-neutrality assumption simplifies the mathematical treatise of bulk transport in most electrochemical systems. Nevertheless, this "no charge density accumulation" assumption does not hold true at the inter-phase regions of *electric double layer* between the solid and liquid, hence the cause of most electrokinetic phenomenon in clay-electrolyte systems.

The analysis of mass transport by diffusion under chemical ($\partial C/\partial x$) gradient and by migration under electrical ($\partial \Phi/\partial x$) gradient in dilute solutions – for which the interactions between individual species can be neglected – is described by the Nernst-Planck [Eq. 2.1] and the Poisson's [Eq. 2.2], together referred to as the PNP equations:

$$\frac{\partial C_i}{\partial t} = \nabla\left(D^*_i \nabla C_i + u_i z_i F C_i \nabla \Phi\right) \tag{2.1}$$

$$-\varepsilon_s \nabla^2 \Phi = \rho = \sum_i z_i F C_i \tag{2.2}$$

where, C, D^*, u and z are the concentration, diffusion coefficient, mobility and charge number of a single species i, respectively, and F is the Faraday's constant (i.e., a mole of charge); Φ is the electrostatic potential; ε_s is the permittivity of the solvent, and ρ is the charge density.

For many electrochemical systems the local electroneutrality condition is used, which sets the left-hand side of equation 2.2 to zero for zero

charge density. The mathematical implication is then that the electrical potential satisfies the Laplace equation [$\nabla^2\Phi=0$] hence uniform concentration distribution and uniform conductivity within the electrochemical cell. Yet in real electrochemical systems with concentration gradients, the current density of the system can be affected to cause current flow in the opposite direction of the electric field (Newman, 1991). Using the PNP equations and the electroneutrality condition, it can be shown mathematically that the concentration gradients give rise to a spatial variation of conductivity, where a *diffusion potential* arises to ensure ion movement at the same speed to overcome the charge separation and violation of electrical neutrality (Newman, 1991). The charge density accumulation can't be neglected for inter-phase layers, such as the electrical double layer. Using a non-dimensionalized form of equation 2.2, it was shown that the electroneutrality condition is a direct result of the Debye screening length, where the ratio of the Debye length, λ_D to the field length, L is described as follows [Eq 2.3] (Chu, 2005):

$$-\varepsilon\nabla^2\varphi=\sum_i z_i c_i \tag{2.3}$$

where, $\varepsilon=\dfrac{\lambda_D}{L}, \varphi=\dfrac{\Phi}{RT/F}, c_i=\dfrac{C_i}{C_{eq}}, \lambda_D=\sqrt{\left(\dfrac{\varepsilon_s RT}{F^2 C_{eq}}\right)}$

where, R = universal gas constant, 8.3144 J/K mol ; T = absolute temperature, [K]; F = Faraday constant, 96,485 C/mol electrons; C_{eq} = equilibrium concentration in bulk.

As shown in equation 2.3, unless the Laplace compliance holds true - which is not the case for most electrochemical systems owing to the presence of concentration gradients - the electroneutrality of the system can be satisfied when the Debye length λ_D is so small compared to L (s.t., ε <<) that the left hand side of the equation becomes zero. Asymptotic analysis of PNP equations numerically solved at several values of ε showed that for small values of ε - as would be in macroscopic systems - the charge density ρ is zero for majority of an electrochemical cell of length L, except at the boundaries where Faradaic reactions and Stern-layer capacitance are considered (Chu, 2005). As the Debye length approaches to the width of the electric double layer, non-zero charge density distribution appears in the entire electrochemical cell (Chu, 2005). Hence, the electroneutrality in an electrochemical system will hold when the charge density is small compared to total ion concentration, C_{eq} of the bulk fluid. As the charge density approaches to total concentration within the electrochemical cell

(e.g., electric double layer for which Debye length is the width of the layer), electroneutrality can be achieved considering Nernstian boundaries and Faradaic reactions.

2.2.2 Theoretical Considerations: Transport of Water and Its Constituents - Electroosmosis

In 1809, Reuss observed the electrokinetic phenomena when a DC current was applied to a clay-water mixture. Water moved through the capillary towards the cathode under the electric field. When the electric potential was removed, the flow of water immediately stopped. In 1861, Quincke found the electric potential difference across a membrane resulted from streaming potential. Helmholtz first treated electroosmotic phenomena analytically in 1879, and provided a mathematical basis. Smoluchowski (1921) later modified it to also apply to electrophoretic velocity, also known as the H-S theory. Helmholtz-Smoluchowski (H-S) theory describes the migration velocity of one phase of material dispersed in another phase under an applied electric potential. The electroosmotic velocity of a fluid of certain viscosity and dielectric constant through a surface-charged porous medium of zeta or electrokinetic potential (ζ), under an electric gradient, E is given by the H-S equation as follows:

$$v_{eo} = \frac{\varepsilon_s \zeta}{\eta} \cdot \frac{\partial \Phi}{\partial x} = k_{eo} E \tag{2.4}$$

where, v_{eo} = electroosmotic (electrophoretic) velocity
e_s = permittivity of the solvent or the pore fluid
η = viscosity of the solvent or the pore fluid
k_{eo} = coefficient of electroosmotic conductivity
$\partial\Phi/\partial x = E$ = electric field

The zeta (ζ) potential in equation 2.4 has been shown to vary with pH and ionic concentration of the pore fluid, as well as the electric field, therefore is not constant during electroosmotic transport in clay media (Probstein and Hicks, 1993). This makes it difficult to assess a velocity term for temporal and spatial distribution predictions of the electroosmotic transport. The nonlinearity and nonuniformity associated with the electroosmotic velocity became apparent when experiments showed that v_e/E increased with E, hence rendering the other parameters of equation 2.4 to be functions of the electrical field (Ravian and Zaslavsky, 1967). In a given clay deposit in the field, pore cross-sections, the electrical double

layer properties, the fluid viscosity, the dielectric constant, solute distribution and electrical field can vary significantly from one point to another, both along the flow path and in the orthogonal direction. Hence, averaging microscopic parameters (e.g., zeta potential) to use alongside with macroscopic parameters (e.g., E) in an H-S equation can lead to the nonlinear effects.

The zeta, ζ potential is the electrical potential at the junction between the fixed and mobile parts of the electrical double layer. The ζ potential is influenced by the type and concentration of the electrolytes added to the particle suspension (Kruyt, 1952; Smith and Narimatsu, 1993). For clay soils, ζ potential is usually negative because of the net negative charge on clay particle surfaces. The magnitude and sign of this potential highly depends on pore fluid chemistry. As the hydrogen and hydroxyl ions are the potential determining ions, the lower pH will reduce ζ potential in magnitude for most clay. At low enough pH, ζ potential may become positive. Hunter and James (1992) observed that adsorption of partially hydrolyzed metal cations such as Co^{2+}, Cd^{2+}, and Cu^{2+} cause ζ potential reversals for kaolinite. As the concentration of hydrolyzable metal ions increases, ζ potential becomes more positive at low pH levels due to the accumulation of the cations in a compressed electrical double layer bearing a larger charge than is present on the solid surface (Kruyt, 1952). The effect is largest at an intermediate pH, slightly above the value at which precipitation of the metal hydroxide would be expected in the bulk solution. Due to the sorption of hydrolyzable metal ions, the sign reversal of the ζ potential can make the net electroosmotic flow insignificant in clay soils with high pore fluid electrolyte concentrations. In this case, and also for saline soils, electromigration becomes the dominant mechanism of electrokinetic transport.

Recognizing the inability to uncouple v_{eo} from E in the classical H-S equation for macroscopic systems, Khan (1991) proposed a modified theory of electroosmotic flow in clay soil. In Khan's work, the ionic conductance through the bulk fluid and the electronic conduction through the electric double layer at the solid-liquid interface were lumped in series, representing resistances in parallel or conductance in series. When modeling mass flow in the direction of the electric field, it is intuitive to line up the conducting elements in the direction of the electric field. The electrokinetic transport theory clearly shows that it is the electronic conductance at the electric double layer that induce electroosmotic transport and the ionic conductance in the bulk fluid that result in the ionic transport. Hence, the following relations are expected to hold:

$$i = i_s + i_b \tag{2.5}$$

$$E = \frac{R_s i_s}{L} = \frac{R_b i_b}{L} \tag{2.6}$$

$$v_{eo} = k_{eo} \frac{R_s i_s}{L} = \left[\frac{k_{eo} \tau}{\sigma_s n} \right] . \frac{i_s}{A} \tag{2.7}$$

$$v_{eo} A = Q_{eo} = K i_s \tag{2.8}$$

where, k_{eo} is the H-S coefficient of electroosmotic conductivity; *i,* i_s and i_b are the total, surface and bulk currents (Amps or *C/s*), respectively; R_s and R_b (Ohm) are the surface and the bulk resistances; and σ_s is the surface conductivity (l^{-1} Siemens or l^{-1}Ohm^{-1}; where *l* represents the unit of length); τ is the tortuosity; *n* is the porosity; *A* is the total area ($A_{flow} = nA$). The relation between the resistance and conductivity is given as: $R_s = L'/(\sigma_s A_{flow})$, and the tortuosity term τ is included to augment *L* ($L'=L\tau$) because the electric currents may follow a tortuous path through the length, *L* of the electrochemical cell for which the pore walls are assumed lined up with connected electric double layers. In this model, *K* emerges as a factor that relates volume rate of electroosmotic flow of fluid movement per electrical charge.

Shang et al., (1995) looked at the relation of conductivity and apparent polarization in several wet clay systems, where they found that the surface conductivity and the apparent permittivity decreased significantly when the volume fraction of the particles was increased beyond 0.3. They also found that the conductivity of the bulk fluid was at least an order of magnitude higher than the surface conductivity (=> $R_b/R_s \cong 0.1$), and that the surface conductivity increased when the clay was remolded (=> $R_b/R_{sr} \cong 0.2\text{-}0.5$). These findings support Khan's (1991) "parallel resistances" model when the flow direction is implicitly taken to be the direction of the electric current flow. Because the electroosmotic velocity representation using the surface conductivity, $\sigma_{s,}$ would require fully developed electric double layers with connectivity, increasing the dry clay content would inhibit the connectivity of the electric double layers, and hence cause the reduction in the measurement of the surface conductivity for the overall system. The remolding of wet clay pastes has been shown to reduce the repulsion between particles and cause them align in a face-to-face orientation (Mitchell, 1993; Quigley, 1980), and therefore, possibly increase the connectivity of the electric layers in edge-to-edge correspondence. It follows than the preferential alignment of the particles in the direction of the electrical field help increase the surface conductivity, as was shown by Shang and co-workers (1995).

Through laboratory experiments K has been shown to be a constant, independent of the electric field and soil mineralogy for similar major ion concentrations of the bulk fluid (Pamukcu and Wittle, 1992; Wittle and Pamukcu, 1993). In these studies, the volume of electroosmotic flow (V, cc) per electric charge (either in Coulombs or moles of electrons) referred to as the *electroosmotic efficiency coefficient,* K_{ef} (cc/C) were determined from numerous electroosmotic tests of different clay and solute combinations. The relation between the cumulative electrical charge versus the cumulative volume of electroosmotic flow was found to be linear for a given clay type (e.g., kaolinite, montmorillonite, and sand-clay mixtures), at given initial concentration of different ion species (As, Cd, Co, Cr, Cs, Hg, Ni, Pb, Sr, U and Zn), all applied separately in the pore fluid. In these series of experiments (Wittle and Pamukcu, 1993), the clay matrixes used were pure kaolinite (KS), montmorillonite (MS), kaolinite with simulated groundwater electrolytes (KG), kaolinite with humic substances (KH), and a mixture of fine sand and 10% by weight montmorillonite (SS). In all cases the transport experiments were conducted over 48 hours with a constant electric field of 4 V/cm applied across the electrodes. The clay specimens were sandwiched between two electrode chambers housing a set of graphite electrodes in tap water as shown in Figure 2.1.

The K_{ef} was demonstrated to be a constant factor for the soil type, but changed with the initial concentration of the major ion. Figure 2.2 shows this variation for Cd^{+2} as the major metal ion in clay pores. Also shown on the graph is data from a reference soil matrix (Synthetic Soil Reference Soil Matrix, SSRM), which represented a typical well-graded reference soil matrix (USEPA). The behavior of K_{ef} shown in figure 2.2 is typical of all the other major contributing ions tested in these series of experiments (Pamukcu and Wittle, 1992, 1993).

The constancy of K_{ef} with soil type or clay mineral demonstrates that the assumptions made in developing equation 2.8 are valid. The following

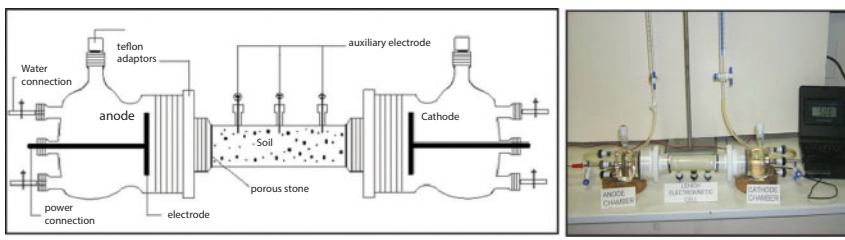

Figure 2.1 Schematic and photo of the Lehigh EK test cell assembly

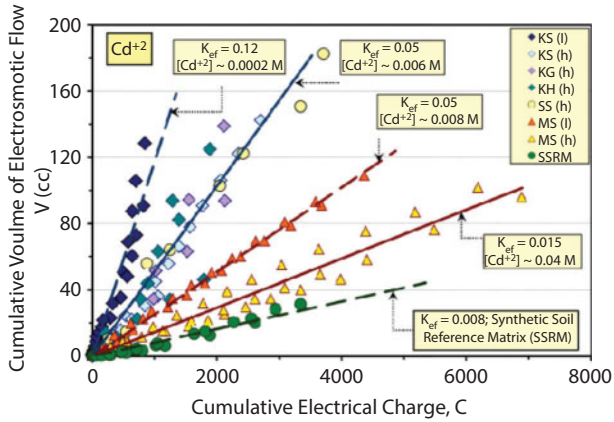

Figure 2.2 Variation of Cumulative Flow with Electric Charge (Pamukcu and Wittle, 1992; Pamukcu, 2009)

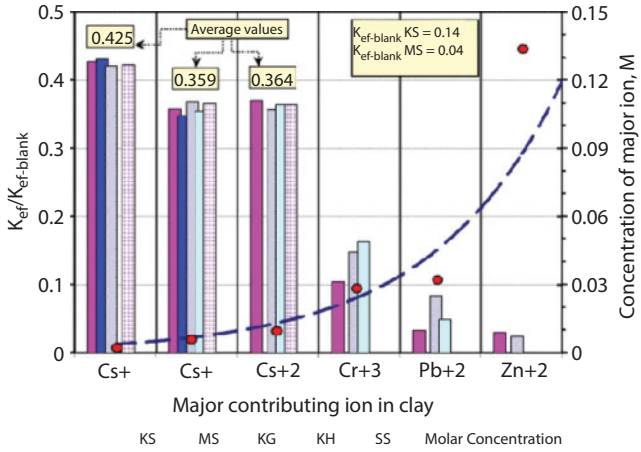

Figure 2.3 Variation of measured K_{ef} factors with ion and soil type at same concentration (Pamukcu and Wittle, 1992; Pamukcu, 2009)

treatise further strengthens the validity of these assumptions. Figure 2.3 presents the variation of the measured K_{ef} for all soils and six selected major contributing ions (Cd, Cs, Cr, Pb, Sr and Zn) in the bulk fluid, all applied separately. There is a clear trend of decreasing K_{ef} factor with increasing ion concentration, where the normalized K_{ef} of different soil types with similar molar concentration cohort of different ions are shown. The values are normalized by the measured K_{ef} values of the respective "blank" clays, those that were mixed and consolidated only with distilled water. At low

concentrations (e.g., Cs, Cd and Sr, all ≤ *0.01 M*), the concentration and the type of the ion appear to control the K_{ef} factor, as all soil types show very close to constant normalized values of K_{ef} for the three ions involved (except MS with Sr). Subsequently, as the concentrations of the major contributing ions increase beyond 0.01 M, fewer soil types comply with the categorization, because the mineralogy of the soil, and its unique chemical interaction with the dominant ion comes into effect. Because of the uniqueness of this interaction the normalized values show greater variation for each ion involved at high concentration (e.g., Cr, Pb, Zn) then the low concentration (e.g., Cs, Cd, Sr) group.

K_{ef} is computed easily by measuring the total volume of flow through the clay matrix and the corresponding total current in the laboratory. In equation 2.5 the total current, i is given as the summation of the bulk current, i_b and the surface current, i_s. Unless the contribution of the surface current is uncoupled, the measured K_{ef} based on total current, i will always display high dependency on soil composition and mineralogy, and the type and concentration of the major contributing ion. During electrokinetic transport, as the bulk fluid chemistry changes so does the electric double layer properties of the clay medium. Equation 2.7 derived earlier, shows a ratio of the H-S coefficient of electroosmotic conductivity k_{eo} and the surface conductivity, σ_s, which should remain constant as they are uniquely related. Only when this constancy (= k_{eo}/σ_s =constant) is true, so is the expression given in equation 2.8. It is important to note here that the use of equation 2.8 necessitates the presence of distributed surface conductivity that enables the surface currents to travel within the electrochemical system for electroosmosis to occur. Yin and co-workers (1995) backed up Khan's theory, which relate electroosmotic mobility and surface conductivity. They found that there is no apparent relationship between electroosmotic mobility and the applied electric field. The term, electroosmotic mobility, defined as the average velocity achieved by the pore water relative to the solid skeleton due to an externally applied electrical field of unit strength (cm^2/s-V), appeared to be directly proportional to the specific conductance (mho/cm) of the specimens at different water saturations in independent tests (Yin et al., 1995).

2.2.3 Theoretical Considerations: Mathematical Modeling of Transport

In the past two decades, many researchers studied and proposed theoretical models of ion transport under electric field as it applied to contaminated clays. In most cases, dilute solutions, rapid dissociation-association

chemical reactions, and small double layer thickness were considered. These models were all based on the Nernst-Planck equation, and each was calibrated to the experimental findings (Shapiro and Probstein (1993); Mitchell and Yeung (1991); Denisov and Probstein (1996); Alshawabkeh and Acar (1996); and Cao (1997)). Cao in 1997 modeled the ion transport considering the effect of changing electrical fields due to the re-distribution of charge concentration. The effect was later shown in a rigorous mathematical analysis by Chu, (2005) where concentration gradients give rise to spatial variation of conductivity to overcome the violation of electroneutrality of the bulk fluid.

In the basic governing equation of advection-diffusion, dispersion refers to the movement of species under the influence of gradient of chemical potential, whereas advection is the stirring or hydro-dynamic transport caused by density gradient or forced convection. A general one-dimensional mass transfer to an electrode is governed by Nernst-Planck equation:

$$J_i(x) = -D_i^* \frac{\partial C_i(x)}{\partial x} - u_i z_i F C_i \frac{\partial \Phi(x)}{\partial x} - C_i v(x) \qquad (2.9)$$

where, J_i = total flux of species *i*, $[Mt^{-1}l]$; $u_i = D^*_i/RT$ = mobility of species *i (Nernst-Einstein relation)* $v(x)$ = advective velocity (= $v_{eo}(x)$, the electro-osmotic velocity)

The mobility of an ion u_i is defined as the limiting velocity of an ion moving in an electric field of unit strength. The minus sign arises because the direction of flux opposes the direction of increasing C_i. Applying Fick's second law, we arrive at another form of Nernst –Planck equation (also given earlier in equation 2.1) with the added advection term:

$$\frac{\partial C_i}{\partial t} = \nabla\left(D^*_i \nabla C_i + u_i z_i F C_i \nabla \Phi\right) + \left(u_i z_i F \nabla \Phi + v\right) \nabla C_i \qquad (2.10)$$

Equation 2.10 is the basic mass transfer equation for an electrochemical system under an electric field. In equation 2.10 the first term is the diffusion; the second term is the migration; and the third term is the advection contribution to the total mass transport of the species *i* in an electrochemical system. In clay soils where the hydraulic advection is negligible compared to electroosmotic advection, the velocity term *v* is simplified as the electro-osmotic velocity (v_{eo}).

The two important system parameters that contribute to the ion flux, and hence the distribution of current density in the system are the

electromigration (v_{em}), and the electroosmotic (v_{eo}) velocities given in summation as the advective velocity (v_{adv}):

$$v_{adv} = v_{em} + v_{eo} \tag{2.11}$$

where, $v_{em} = u_i z_i F \nabla \Phi$
and, from Eqs. 2.4 & 2.7, $v_{eo} = \left[\frac{\varepsilon_s \varsigma \tau}{\eta \sigma_s n}\right] . \frac{i_s}{A}$

The electromigration velocity in equation 2.11 is the speed of ion movement in the pore water caused by an electric field in infinitely dilute solutions. In the pore fluids with finite ion concentrations, which more closely resemble the electrochemical systems of contaminated clays, the influence of the inter-ionic attraction should be considered. Generalized ion mobility that accounts for the possibility of interactions between the ionic species can be used to modify the electrochemical potentials of individual ions in the flux term [Eq. 2.9] when strong chemical reactions between ionic species are considered (Newman, 1991). The resulting relative electric field due to the retardation effects of dissymmetrical ionic atmosphere during ion transport was considered in Cao's model (1997) as described below. The electroosmotic component of the electrokinetic transport is depended on the electroosmotic velocity of the fluid flow. The classical H-S equation expresses this parameter as a function of the field gradient. Due to the tight coupling between the ion concentrations and electric potential – as the ions contribute to the local electric potential themselves – the use of H-S electro-osmotic velocity in transport determination in clay soils can result in nonlinear predictions (Ravian and Zaslavsky, 1967; Chu, 2005). Hence, uncoupling this parameter from the electric potential using the surface conductivity σ_s, and the resulting proportion of the current transferred over the solid-liquid interface i_s, provide an intrinsic electroosmotic velocity dependent on clay surface properties only, as first introduced by Khan (1991) in equation 2.8.

The model predicted distribution and evolution of bulk conductivity, σ_b and field strength, *E,* in kaolinite clay containing $Pb(NO_3)_2$ at the initial concentration of 0.05M in its pore fluid are presented in Figures 2.4 and 2.5, respectively (Cao, 1997). In Figure 2.4, the normalized distribution of the conductivity (normalized by the initial conductivity of *0.28* Siemens/m) shows a consistent decrease in the conductivity at the cathode region, and a steady spread of the lower conductivity towards the anode area over time. Part of this result is attributed to the decrease of dissolved lead concentration, which prevail over the increase of H+ concentration. The change of the conductivity is influenced by combination of three factors: (i) the initial

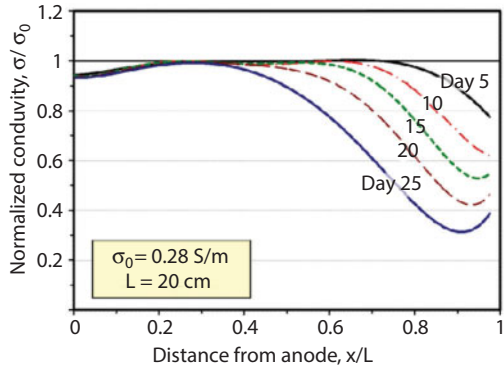

Figure 2.4 Model predicted spatial and temporal variation of conductivity during EK transport of Pb in kaolinite clay (Cao, 1997; Pamukcu, 2009)

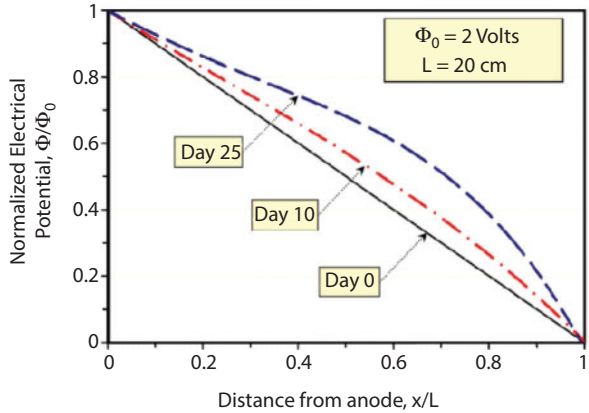

Figure 2.5 Model predicted spatial and temporal variation of electric potential during EK transport of Pb in clay (Cao, 1997; Pamukcu, 2009)

concentrations of the species, (ii) the spatial and temporal distribution of ionic mobility of each species and (iii) the production rate of H+ at anode.

As the conductivity varies, the lower conductive area requires higher potential over it to keep a consistent current with the other parts of the soil column, resulting in a nonlinear electric potential profile across the cell. This tendency is observed in Figure 2.5 where the time evolution of the electric potential distribution is presented. As the electrochemical transport continues, the potential curve becomes less steep over the entire cell except in a narrow region adjacent to the cathode, where the electrical potential is likely to have the largest gradient. This tendency agrees well

with the experimental data reported by Wittle and Pamukcu (1993) and Acar and Alshawabkeh (1996), among many others.

When charged ions transport under the influence of an externally applied electrical field, their concentration distributions change with time which lead to a change in local electrical conductivity, as discussed previously. The change of local electric conductivity directly alters the value of a potential gradient at that specific point. Hence, the changing electric conductivity and electrical field strength describe the transport process of the species implicitly. Furthermore, the mobility of the charged species decreases as they congregate in the direction of their migration. The increasing concentration of the ions leads to a decrease in equivalent conductance in their migration direction (Kortüm and Bockris, 1951). According to Kohlrausch's law of the independent migration of ions, the equivalent conductance of an electrolyte is additively composed of the ionic conductivities of the constituent ions. As ions move under an applied electric field at their terminal ionic velocity (u_i) of infinite dilution, two other phenomena occur, which retard ion velocity and effectively reduce the bulk conductivity. These are called the "retardation" and "electrophoretic" effects. The retardation effect comes about when the ionic atmosphere becomes unsymmetrical about an ion in motion, as the charge density decrease in front of the ion and increase behind it. For a moving positive ion, a net negative charge trail behind it exerting an electrostatic force in the opposite direction. The electrophoretic effect occurs as the negative ions in the ionic atmosphere around the positive ions migrate in the opposite direction taking their solvent sheaths with them. The positive ion therefore travels against a medium moving in the opposite direction, hence a viscous drag. A quantitative formulation of ion mobility, relating the magnitudes of the electrostatic retardation force and the viscous drag force to the radius of the ionic atmosphere directly provides a theoretical basis for the well-known empirical relation known as the "Kohlrausch square root law" (1900), in terms of equivalent conductance, Λ_v [l^2 Ohm^{-1}] (Kortüm and Bockris, 1951). The Λ_v is also the sum of individual ionic conductivities ($F.u_+$ for positive ions; and $F.u_-$ for negative ions), hence the ionic mobility of a given ion, u_i can be expressed in terms of the equivalent conductance (Bard and Faulkner, 1980):

$$u_i = \frac{\Lambda_v t'_i}{F} \tag{2.12}$$

where $t'_i = u_i/(u_+ + u_-)$ is the transference number of the of species *i*.

Equation 2.12 effectively incorporates the retardation effects into the mobility determination for high concentration solutions. As an example,

the variation of the mobility of the positive ion (e.g., H^+, K^+, Na^+) of the 1,1 valence electrolytes HCl, KNO_3 and NaCl in aqueous solutions at room temperature were computed according to Equation 2.12, where Λ_v is described by the "Kohlrausch square root law." These relations are plotted in Figure 2.6. The variation of the transference numbers of the cations with concentration are also plotted to discern its effect on the mobility of each ion. As observed, the reduction of the mobility of each ion with increasing concentration appears to be mostly dependent on Λ_v.

The Cao-model was used to predict the spatial and temporal distributions of four ionic species, Pb^{+2}, NO_3^-, H^+ and OH^- in kaolinite clay. Four one-dimensional advection-dispersion equations were solved simultaneously, one for each ionic species. Changes in electrical potential, conductivity and field strength were considered in the solutions. Figures 2.7 present the spatial distribution of the total lead and the pH for 35 day runs of Cao-model. Superimposed on the numerical solutions are results from the laboratory tests of $Pb(NO_3)$ contaminated kaolinite clay subjected to long-term electrokinetic treatment. The 35-day lead and pH distribution is predicted well by the model, including the accumulation of the metal in a *narrow zone adjacent to the cathode*. The model predictions of the 15-day and the 35-day distribution of lead concentration indicate that migration velocity of the ions become affected by the electrical field distribution over time. The reduction in electrical conductivity at the cathode zone results in higher electrical field in that region. The high electrical gradient hurls the

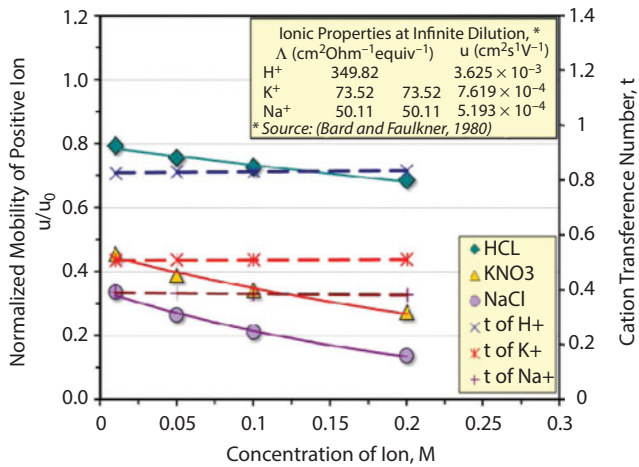

Figure 2.6 Variation of mobility and transference with concentration of selected ions (Pamukcu, 2009)

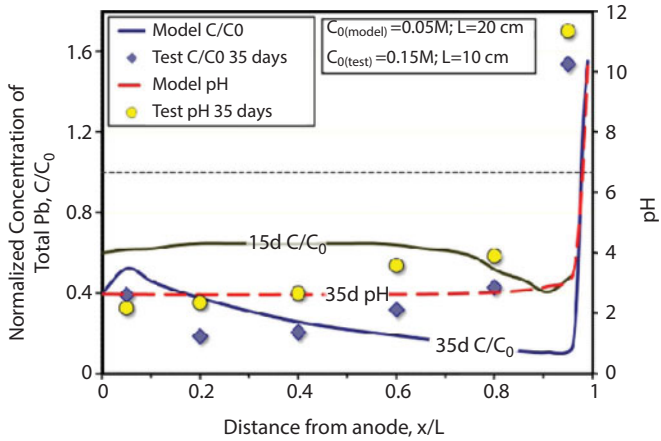

Figure 2.7 Model predicted and measured distribution of pH and total Pb concentration at 35-day EK transport (Pamukcu, 2009)

ions to the narrow high pH zone to be accumulated by precipitation, hence evacuating the region immediately behind it. The progression of this effect is clearly seen by the evolution of lead distribution from 15 to 35 days, as the distribution towards the cathode regions continues to dip behind the high pH zone. The distribution of lead near the anode does not dip at the same rate because the conductivity remains high and the electric potential distribution tends to flatten there. Consequently the ions slow down responding to a lower electric field. Factors such as sorption, retardation and precipitation influence the model predictions, but their relative contributions may be small other than the narrow high pH zone near the cathode.

2.2.4 Theoretical Considerations: Electrochemical Transformations

Transport and extraction of both the inorganic and organic substances from clay pores frequently involve the addition of one or more chemical reagents to the system (Liu and Wang, 2013, Chen et al., 2011, Ryu et al., 2011, Chang et al., 2010, Pazos et al., 2008 and Hansen et al., 2005), introducing with it the possibility of secondary pollution. Recently, "green technology" has been explored for in-situ destruction of contaminants enhancing beneficial electrochemical reactions by electrokinetics. Optimization parameters include changing electric field direction and intensity (Peng et al., 2013), applying a sinusoidal electric field with pulses and a polarity

reversal (Rojo et al, 2012) and the increasing potential gradient (Lei et al. 2012). Diffuse double layer (DDL) processes of clay have been suggested to influence *in situ* conversion of heavy metal soil contaminants to potentially less toxic forms when an external direct current is applied to the clay-electrolyte system (Pamukcu et al, 2004, 2008; Brosky and Pamukcu, 2013). The DDL shrinks, reducing the electrokinetic potential (i.e., zeta potential) of the system in the event of lowered pH and/or increased ionic concentration of the pore fluid due to accumulation of charges in DDL (Israelachvili and Adams, 1978). Therefore when the electrokinetic potential of a clay-electrolyte system changes under varying pH or electrolyte concentration, the system may become prone to spontaneous Faradaic reactions as it tries to restore the equilibrium back. In electrokinetic treatment of clays, the transient acid front movement from anode to cathode, and the regions of low and high pH developing near the electrode sites can set the stage for triggered Faradaic reactions resulting in beneficial transformation of the contaminants.

In soils, all particles with active interfaces (i.e., Inner (IHP) and the Outer Helmholtz Planes (OHP) (Hunter, 1981)), can be regarded to "act" as electrode interfaces when a current is supplied to them, adding up to a significantly large effective electrode surface area. Current flows across these interfaces via two pathways: the Faradiac and non-Faradiac. When an external electric field is applied to water saturated clay of high ionic concentration in the pore fluid, given the incompatibility between the conductivity of two conducting layers in the mixture: 1) the DDL of clay particles with low conductivity (σ_s), and 2) the surrounding electrolyte solution (bulk solution or pore fluid) with high conductivity (σ_b), a large electrical potential is induced across the DDL. This results in compression of the DDL, resulting in higher charge density in this region. This is similar to the effect when salt concentration of the bulk fluid is increased causing the compression or shrinkage of DDL. The electric potential distribution shifts back (i.e., towards the solid) and down, lowering the electrokinetic potential at the shear plane (ς, *zeta potential*) as shown in Figure 2.8a,b,c. The potential distribution shift in this manner increases the intensity of the electric field within the Stern layer (between IHP and OHP), while decreasing the Capacitance, C of the DDL. The reduction in capacitance of the diffuse layer can trigger electron transfer across the diffuse layer towards the solution, giving rise to a Faradaic "cathodic" current (Bard and Faulkner, 1980). The capacitance, C, of the double layer is directly related to the bulk electrolyte concentration and the surface potential of the particle. The capacitance reaches a minimum at the *point of zero charge* (PZC) and sharply increases on either side for the low electrolyte concentrations

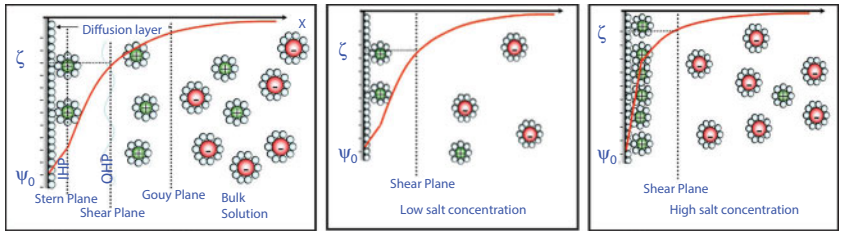

Figure 2.8 **(a)** The distribution of charges against charged clay surface in DDL formation; **(b)** The distribution of charges at low salt concentration; **(c)** The concept of electrolyte ions adsorbing on the surface and reduce the zeta potential without altering the surface potential or charge at high salt concentration. (illustrations courtesy of PERC, *http://perc.ufl.edu/*)

of the bulk solution. The surface charge or electokinetic potential of most clay sharply varies with pH. For example, the PZC for most types of kaolinite clays have been reported to coincide between pH 2.0 and 4.0, depending on the electrolyte concentration of the pore solution (Bard and Faulkner, 1980). Accordingly, as the DDL compresses or expands, Faradaic currents (cathodic or anodic) can generate across Outer Helmholtz Plane (i.e, frequently assumed where the electrokinetic potential and shear surface develops), whereby the concentration gradients are overcome and the electrical equilibrium restored.

Recently Brosky and Pamukcu (2013) proposed that a nonspontaneous change in the oxidation-reduction potential (i.e., E_h) of a clay-electrolyte mixture represents the charge discharge due to the compression of the DDL. They demonstrated a shift in E_h values with increasing clay concentration of an aqueous slurry during electrically enhanced reduction of Cu(II) by Fe(II), as shown in Figure 2.9. The increased clay concentrations promoted electrochemical reduction of Cu^{2+} to more environmentally benign Cu^{+} or Cu^{0} in the system. This is highly relevant to bottom waters and sediments of surface water bodies, where many heavy metal contaminants are found. Electrically treated clay can switch its surface potential sign in time as pH lowers below an 'apparent' PZC. It can be seen from Figure 2.10 that the PZC is achieved for the kaolinite-Cu(II)-Fe(II) test slurries at around pH 2.4. The PZC signifies that the charged layers surrounding the clay particles become saturated with charges from ions in solution as well as electrons from current flow. At this state, the DDL capacitor is storing maximum charge and therefore has reached its minimum capacitance and maximum redox potential. Zeta potential data shows that electrically treated clay can switch in zeta potential sign in time as the pH decreases below the 'apparent PZC' of pH 2.4. Observing Figure 2.9, it appears that the clay systems

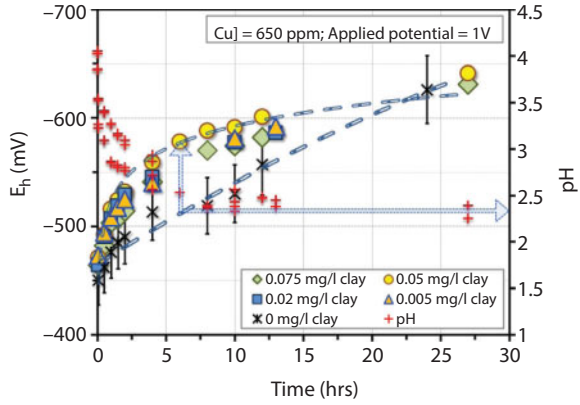

Figure 2.9 Temporal variation and shift of E_h with direct current in Cu(II)-Fe(II) mixtures of clay where maximum E_h shift up is 0.50V (Brosky and Pamukcu, 2013)

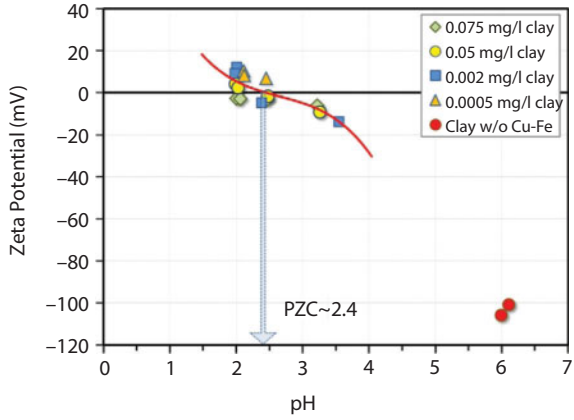

Figure 2.10 Zeta Potential with pH in Cu(II)-Fe(II) mixtures of clay (Brosky and Pamukcu, 2013)

shift from base E_h is maximized (~ between 4-6 hours) when the pH of the system is recorded at around 2.4. This is consistent with the PZC of 2.4 shown in Figure 2.10.

Evidence of DDL-enhanced Cr(VI) reduction to less toxic Cr(III) by direct current application has been reported previously (Banarjee et al., 1987; Pamukcu et al., 2004,2008; Alshawabkeh and Sarahney, 2005; Hannum and Pamukcu, 2007). Electrolytic transformations of selected CHCs and PAHs have also been demonstrated successfully in water and

wastewater (Franz, 2002; Pulgarin et al., 1994). There has also been recent evidence for the double layer-enhanced removal of Pb(II) (Ahn et al., 2010). Previously, controlled laboratory experiments of kaolinite clay (see test set-up in Figure 2.11) injected with Fe(II) showed that an externally applied electric field caused an additional "cathodic current" that drive forth the reduction of Cr(VI) in clay (Pamukcu et al., 2004). These transformations were characterized as to have resulted from the capacitive changes on the clay surfaces. The results in these experiments showed that the system ORP (oxidation-reduction potential) increased by a positive shift from the standard solution ORP in the presence of the clay medium and the induced electrical field. The ORP measurements were plotted against the reaction quotient of the Nernst relation, where the data was categorized by pH, as shown in Figure 2.12. The low pH range (pH range 2=>3) data showed the best agreement with the linear fit, and the relative scatter of data at higher pH values was attributed to poor polarization of the electric layer. At low

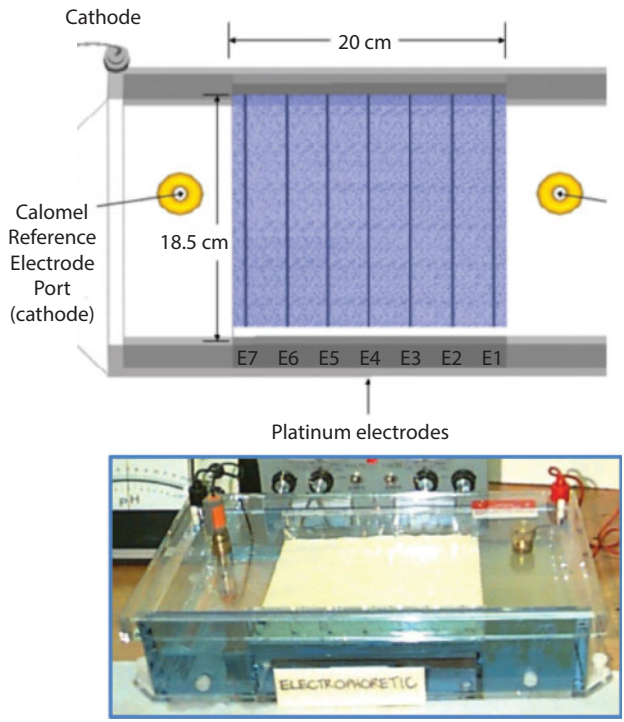

Figure 2.11 The electrophoretic set-up to measure enhanced transformation of Cr(IV) to Cr(III) (Pamukcu et al., 2004, 2008; Hannum and Pamukcu, 2007)

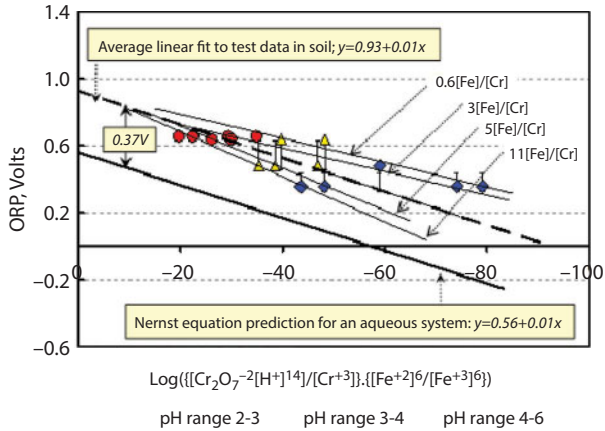

Figure 2.12 Measured and predicted redox potential variation with reaction quotient of species concentration in Nernst relation (average redox potential shift =0.37V) (Pamukcu et al., 2004)

pH, the DDL is compressed with a higher ion concentration, higher electric field (Israelachvili and Adams, 1978), hence higher degree of polarization, and lowered capacitance. At higher pH, the DDL is expanded with reduced degree of polarization, consequently higher capacitance. The ions in an expanded DDL are less restricted to move, therefore discernable fluctuations are likely to occur in the potential development across the diffuse layer.

2.3 Electrokinetically-Aided Environmental Mitigation

The main and best-known advantage of electrokinetically aided environmental mitigation is its ability to move water, dissolved contaminants and, colloidal/micellar particles through low permeability soils and porous formations that are not amenable to hydraulic treatments (Hamed et. al, 1991; Pamukcu and Wittle, 1992; Wittle and Pamukcu, 1993; Acar, et al., 1986, 1989, 1990, 1992; Shapiro and Probstein, 1993, Probstein and Hicks, 1993; Pamukcu et al. 1995, 1997; Pamukcu, 1994, 1998). The electrokinetically aided transport is based on well-known electrokinetic processes (Hunter, 1981; Cassagrande, 1949; Mitchel, 1993), primarily comprised of *electro-osmosis, electrophoresis*, and *ion migration* in wet soil. The electrokinetic treatment involves applying a low direct current (on the order of milliamps per unit cross-sectional area), or a low potential gradient (on the order of few volts per unit distance) between the power electrodes inserted in the

ground. As a result, the contaminants are transported towards the anode or cathode electrode sites by ionic or electrophoretic migration, and electroosmotic advection. The contaminants are then removed at the electrode sites by one of several different methods: electroplating; adsorption; precipitation complexation, or pumping.

The electrokinetic treatment is a powerful soil clean-up technique explored both in the laboratory and the field for the last several decades, particularly for difficult site conditions. The field applications have frequently demonstrated that the success of the treatment is hinged on site specific engineering design of the total system, which includes the enhancement of the transport (Lageman, 1993; Yeung et al., 1996; Acar et al., 1997; Lindgren, 1998). Some of the phenomena experienced with electrokinetic treatment of soils which, interfere with the steady transport of fluid or charged particles to an electrode site are: (i) the spatial and transient variation of soil pH, electric gradient and pore pressures, (ii) surface polarization effects on particles and electrodes, (iii) other electrochemical effects.

The electrolysis reactions that occur at the electrode sites of the applied potential can produce substantial changes in pH of the pore solution. The reactions are oxidation at the anode generating hydrogen (hydronium) ion and oxygen gas, and reduction at the cathode generating hydroxyl ions and hydrogen gas, as follows:

Anode: $H_2O \Leftrightarrow 2H^+ + (1/2)O_2 + 2e^-$ (Standard potential)$E^0 = +1.23$ V
Cathode: $2H_2O + 2e^- \Leftrightarrow 2OH^- + H_2$ (Standard potential)$E^0 = -0.83$ V

The rates at which the hydrogen and hydroxyl ions are produced depend on the current, as such the lower the current density, the lower the rate. The hydrogen and the hydroxide ions are transported into the soil by electromigration. The resulting pH fronts influence the adsorption/desorption and precipitation/dissolution reactions of ionic constituents in the soil pores, as well as the surface chemistry and electrochemistry of the mineral particles. The reduced pH is beneficial in desorption of most metals from soil, as well as dissolution of most metal precipitates. Natural soils with high buffering capacity and carbonate content, or those under the groundwater table tend to neutralize the acid front and maintain a higher pH environment (Pamukcu, 1994). The base front generated at the cathode electrode penetrates the soil a narrow distance creating a zone of high pH, promoting precipitation of the inorganic species into insoluble hydroxide salts in the pore space and also their retention on the clay surfaces. . These side effects may be overcome by continuous adjustment of the pH at the analyte and the catholyte, and/or by adjusting the current density in the soil.

The mitigation outcomes of electrokinetic treatment can be categorized in three general processes, not exclusive of each other: *extraction and separation; immobilization*; and *transformation,* as discussed below:

2.3.1 Electrokinetially-Aided Separation and Extraction

Electrokinetic extraction is analogous to *soil washing* whereby the contaminant is *extracted* from the soil pore space and subsequently collected in aqueous phase in a collection well or deposited at the electrode site. The alkali metals, e.g., Na(I), K(I), and Cs(I), and alkali earth metals, e.g., Sr(II) and Ca(II) tend to remain ionic under a wide range of pH and redox potential values, therefore they are expected to electromigrate and be extracted from soils readily unless they become preferentially sorbed onto solid surfaces and clay interstices in soil. Under ideal conditions, the predominant cation and its accompanying anion may be caused to separate efficiently by electromigration only, for which little or no electroosmotic water advection may be necessary (Weinberger, 1993). The electroneutrality can be maintained by the hydrogen and the hydroxide ions produced by the electrolysis reactions at the electrodes and transported into soil by migration.

Described below are several selected laboratory experiments conducted using the Lehigh Elektrokinetic Test Cell (Wittle and Pamukcu, 1993; Pamukcu, 1994) to exemplify the variety of electrokinetic extraction and separation processes that can be engineered to address site specific situations. The soil samples used in all these experiments were the actual contaminated field soils.

A. NaCl Extraction/Separation: The first example of ionic specie separation and extraction is provided for NaCl removal from drilling mud obtained at an Eastern Pennsylvania site. Figures 2.13 and 2.14 show the separation of sodium (Na) and chloride (Cl) from drilling mud soil samples of different water saturations under constant electric potential. The final pH profiles attained at the end of the tests are superimposed on the graphs. As observed in figure 2.13, close to 100% recovery of the Na is accomplished in the 81% saturated specimen, S1 at the termination of the test, while about 70% of Na is recovered for the 53% saturated specimen, S2. The specimen designated as S1 shows a substantial recovery of Cl (figure 2.14), although not as high a recovery as Na. The inability to account for all the Cl transported

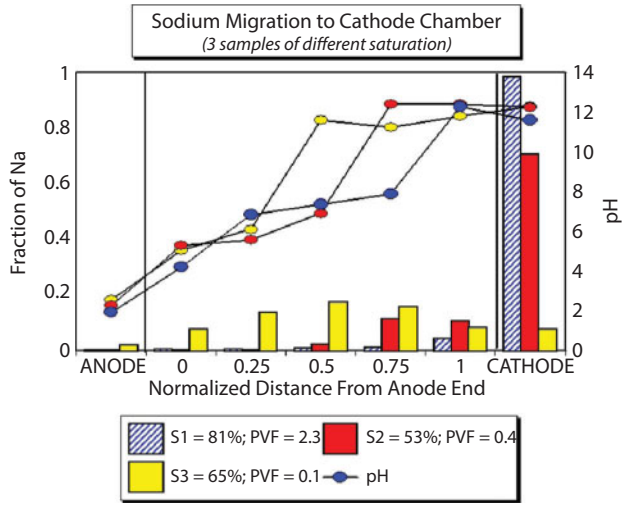

Figure 2.13 Post Electrokinetic distribution of *Na* in drilling mud of various initial water saturation degrees (S1,S2,S3), at various pore volumes of flow (PVF) (Pamukcu and Wittle al.,1993)

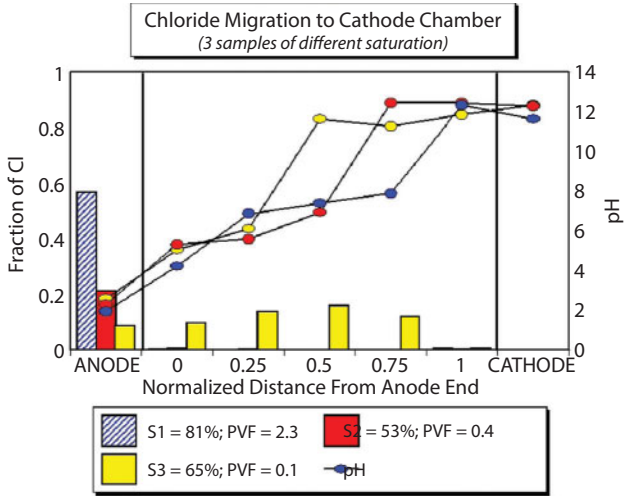

Figure 2.14 Post Electrokinetic distribution of *Cl* in drilling mud of various initial water saturation degrees (S1,S2,S3), at various pore volumes of flow (PVF) (Pamukcu and Wittle., 1993)

to the anode chamber is attributed to formation of gaseous chlorine (at pH below 4) which would have escaped from the anode chamber without accumulation.

B. Perchlorate, ClO4- Extraction: In another example, perchlorate, ClO_4^- contaminated soil samples retrieved from an aviation facility near Rancho Cordova, California were treated to explore the extraction of this species electrokinetically. The soil contained little clay, but mostly fine to medium sand and silt. The packed samples were saturated in the laboratory with the groundwater specimen obtained from the same location that contained high levels of perchlorate. The laboratory test specimens measured 25.7 % water content by dry weight, bulk density of 2.8 g/cm^3, and void ratio of 0.6. Two tests were conducted in parallel one of which served as a control test with no electrical current. In the treatment cell the soil was subjected to constant 30 Volts across the electrodes residing in chambers filled with the local groundwater from site. The results of these tests are presented in figures 2.15 and 2.16.

The current density varied from maximum of 1mA/cm^2 to minimum of 0.006mA/cm^2, as shown in Figure 2.15. The efficiency of extraction (i.e., moles of perchlorate per quantity of electricity) is closely related to the current measured in the soil. The current peaked at 80% removal and diminished thereafter. Although the applied voltage remained at 30V across the electrodes, the voltage potential measured in the soil was transient; decreasing thereafter the maximum removal efficiency was reached. A number of reasons can be offered for this occurrence, some of which are: loss of

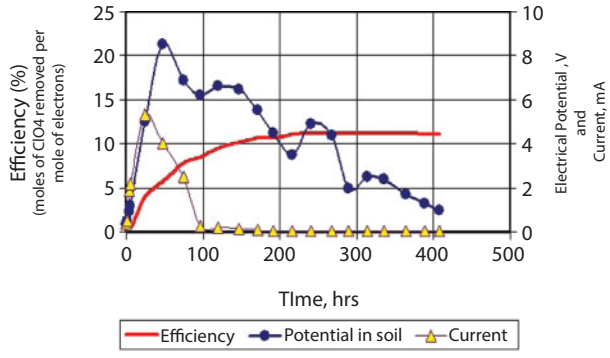

Figure 2.15 Electrokinetic removal of ClO_4^- from soil retrieved from an aviation facility in Rancho Cordova, Ca (Pamukcu and Huang, 2001)

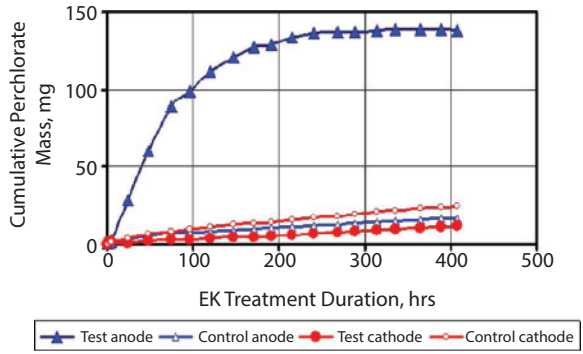

Figure 2.16 Cumulative mass of ClO_4^- removed from soil into the electrode chambers during EK (Pamukcu and Huang, 2001)

electrical energy through the electrolysis of water, changes in soil water chemistry and transient pressure differentials in soil pores (Ray and Ramsey, 1987; Muraoka et al., 2011). This experiment exemplifies one of the typical situations where the majority of the current is carried by the ion flow in pore fluid, and not through the double layers. Therefore, electromigration in pore fluid becomes the dominant mechanism of transport.

As observed in figure 2.16, approximately 99% of the initial mass of the perchlorate (the initial perchlorate concentration was 840 mg/kg) was extracted out of the sample soil by the end of 7 days of electrokinetic treatment. The control specimen showed less than 30% removal by diffusion for the same duration. The rate of electrokinetic removal was significantly faster for the first three days of treatment, by the end of which 80% of the initial mass of perchlorate was removed. Although the soil remained conductive beyond the 3 days, most of the current carriers in the pore fluid were depleted during that time. The electro-osmotic flow of water continued in the positive direction (from anode to cathode) for the first 8 days of treatment, but ceased afterwards. The average equivalent hydraulic conductivity was computed as $1x10^{-5}$ cm/sec, and the electro-osmotic permeability as $1.7x10^{-5}$ $cm^2/sec/V$.

C. Ammonium, NH4+ Extraction: The processed municipal sludge by N-Viro Soil™ technique produces a Ca-rich

material, a potentially inexpensive source of calcium for cement production. The fresh N-viro soil gives out ammonia ($NH_3(g)$) as a by-product of the process, which needs to be mitigated prior to handling the material. Electrokinetic extraction was proposed to reduce the excess ammonia in N-Viro Soil™. The visual and textural observation of the granular material indicated fine sand to silt size mixture with little plasticity. The leachate was a brown colored liquid. Upon arrival, the leachate was acidified to arrest NH_4^+ in the liquid, thereby preserving its original concentration. The test specimens were prepared by mixing the N-Viro soil with the leachate at the reported liquid content of 65%. Two tests were conducted at constant potential of 30 V applied across the electrodes for the 200-hr duration of treatment for each. The voltage gradient measured in the samples remained at approximately 0.3 V/cm. At the termination of each test, the soil was sampled at three points along its length and analyzed for moisture content, pH and NH_4^+ concentration distribution. Figure 2.17 shows the post-electrokinetic distribution of the measured concentration of NH_4^+ and the pH along the soil sample and the anode and cathode liquid chambers. Overall, the concentration of ammonia in the soil samples were reduced from about 150 mg/kg to less than 6 mg/kg in both samples tested.

The mass balance determination showed that for more than 50% of the ammonia was unaccounted. Larger

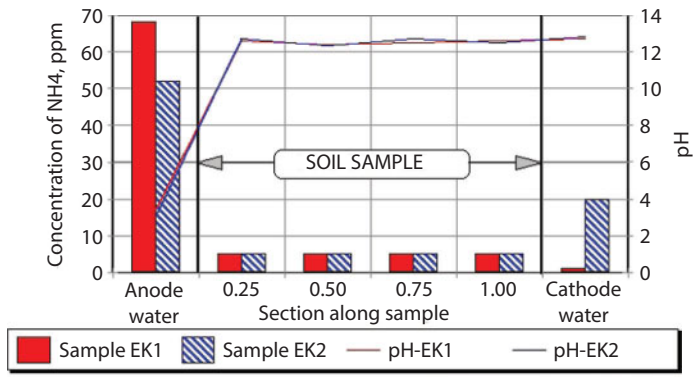

Figure 2.17 Post Electrokinetic Distribution of NH_4 in Processed Municipal Sludge Soil (Pamukcu and Huang, 2001)

concentrations of ammonia were found in the anode chamber in both tests, where pH was at 4. At this pH, the ammonia in the anode chamber would be in the form of ammonium ion. In the cathode chamber where the pH was well above 9.3, the ammonium would readily convert to uncharged ammonia (NH_3). The solubility of ammonia is fairly low in water (Henry's constant, K_H = 57.6 mol/L.atm). Therefore the ammonia removed to the cathode could have converted to vapor phase and escape into the head space of the chamber. Strong ammonia smell was detected when the trapped gasses were released at intervals from the cathode reservoir. The portion of ammonia that was collected in the anode chamber was due to colloidally enhanced transport whereby the positive ion NH_4^+ was expected to collect at the positive electrode by electro-migrating colloids (i.e., bacterial, organic or inorganic). The colloidal transport was observed visually as the anolyte clouded with suspended particles during the treatment. Charged colloids are known to strongly adsorb ions of opposite charge and enhance transport of these substances in porous media (Grolimund et al., 1996).

D. Simultaneous Extraction of Cyanide, CN- and Fluoride F- :

Spent pot-lining sludge from Columbia Falls Aluminum Company was tested to determine the efficacy of electrokinetics in removing cyanide and fluoride metals prior to its disposal. The sludge contained 0.2% cyanide and 9% fluoride by mass, initially. At the end of the 7 days of electrokinetic treatment, about 8% of the cyanide and 2% of the fluoride by mass was removed from 118 g of a sample of the sludge. In these tests 15V of constant potential was applied across the electrodes, and the anolyte and catholyte solutions were replenished with fresh solutions at 29 hrs of this constant potential. As shown in figure 2.18, the electrical potential measured within the sample was small and changed with current when the electrolytes in the electrode chambers were replaced with fresh ones. The current remained high in the range of 15-20 mA in the first stage and dropped to about 7 mA in the second stage. The removal of metals over time, as shown in figure 2.19, demonstrated that preferential removal of CN^- towards anode was prevalent, as the Fl^- transport picked up only after the 4th day against the control value of diffusion to the cathode.

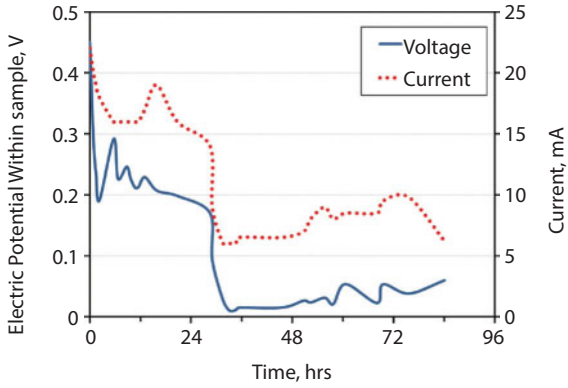

Figure 2.18 Voltage and current evolution in the potlining sludge sample during EK treatment under constant 15V of potential (Pamukcu and Pervizpour, 1998a)

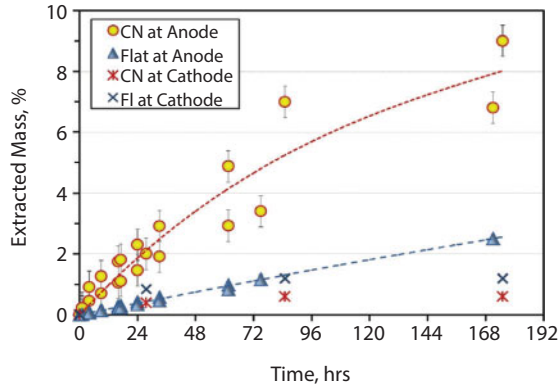

Figure 2.19 Cumulative mass of CN- and Fl-removed from sample into the electrode chambers during EK treatment of sludge (Pamukcu and Pervizpour, 1998a)

E. Hexavalent Chromium, Cr(IV) Extraction:

An example of the influence of diffuse double layer reactions can be observed with hexavalent chromium, in Cr(VI) treatment using electrokinetics. The Cr(VI), which is often found in anionic species of $Cr_2O_4^-$, is readily mobile in soil pore fluid but may not be readily extracted under an electrical gradient. Figure 2.20 shows typical results of electrokinetic extraction of Cr(VI) from a sample of hexavalent chromium contaminated site in Eastern Pennsylvania (Pamukcu and Wittle, 1999 - EPA SITE Demonstration

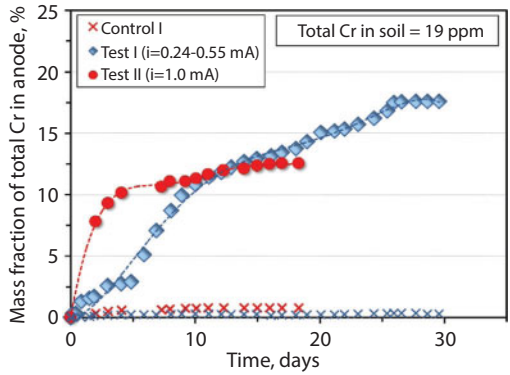

Figure 2.20 Variation of cumulative mass of Cr in anode chamber with EK treatment using constant current (Test I) and (Test II) tests of Aladdin Chrome Plating site soil (Weeks et al., 2001)

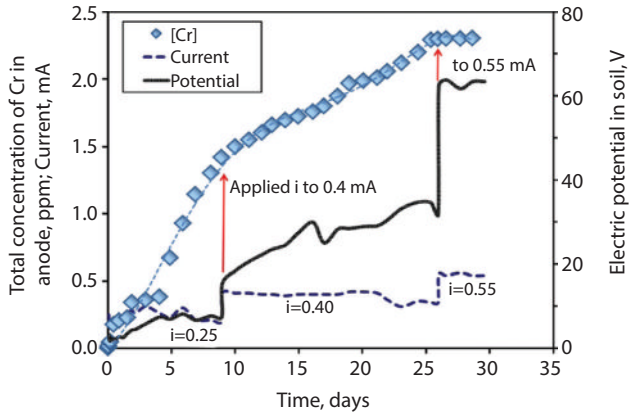

Figure 2.21 Variation of the concentration of Cr, current and potential measured in the test soil in (Weeks et al., 2001)

Program at the Aladdin Plating Site in Chinchilla, Pa). The soil sample was characterized as silty clay. As observed, less than 20 % of the total Cr was removed to the anode chamber, and very little to cathode chamber over 30 days despite the continuing electric field imparted at constant current of up to 1 mA. Figure 2.21 shows that the cumulative concentration increase over the treatment time flattens with each increase in applied current, unlike the previously observed direct correlation between current and removal efficiency.

This result is attributable to tendency of the ensuing electrochemical reactions that reduce Cr(VI) to Cr(III), which subsequently is adsorbed onto the clay surfaces and no longer available for transport.

F. Sulfate, SO4-2, Nitrate, NO3-, and Chloride, Cl- extraction from cationic/anionic soils:

Simultaneous extraction of multiple anionic compounds introduced as lead salts was tested in anionic (positive surface charge) and cationic (negative surface charge) clayey soils. Mixed with medium sand, the clay substrates were predominantly kaolinite (cationic – PZC: 2-4.6) and gibbsite (anionic – PZC:10). The test specimens were prepared by spiking with $Pb(SO_4)$; $Pb(NO_3)_2$, and $PbCl_2$ salt solutions at their respective solubility limits. Electrokinetic tests were conducted over 24 hours, at the end of which the distributions of the anions were measured in the electrode chamber solutions and across the soil specimens at five points. Figure 2.22 shows this distribution for the three anions in two different clay types. As observed, the extraction appears to be influenced both by the anion and the type of substrate. The anions of the soluble salts were extracted into the anode more effectively that the less soluble ones. The cationic soil appeared to release the anions more effectively than the anionic soil, as the anions would have higher affinity to the clay surface in the latter case. Figure 2.23 shows the mass fraction of anions extracted to anode per Coulomb of

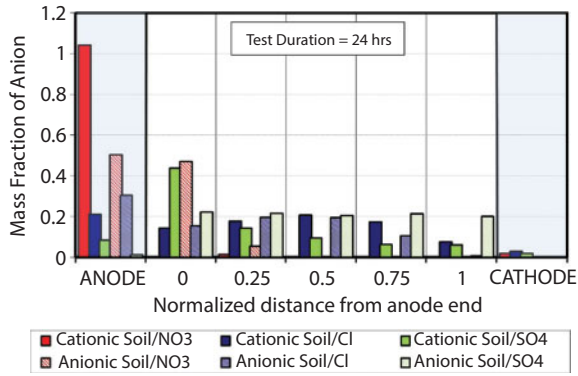

Figure 2.22 Post-EK distribution of mass fraction of anions of lead salts in cationic and anionic clay soils

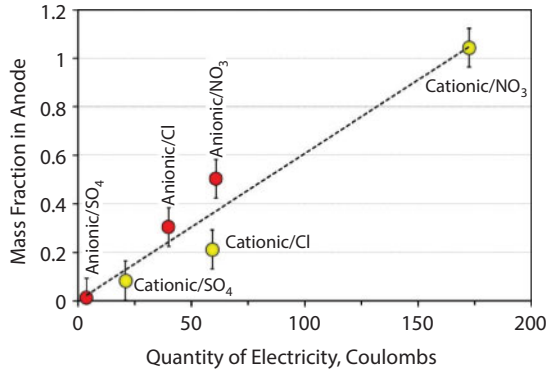

Figure 2.23 Mass fraction of anions extracted into anode per Coulomb of electricity

electricity used. As expected, a linear trend prevails between the extracted mass and the quantity of electricity required. The anionic soil appears to display slightly higher efficiency in energy requirement than the cationic soils for extraction of anions. This is in line with the assumption that the anionic soils will generate electroosmotic flow in the same direction as the anion migration hence will be enhanced for the same quantity of electricity when compared to that of the cationic soil case.

G. Electrokinetic Extraction of Contaminants from Unsaturated Soils:

The application of electrokinetics in the vadose zone has been demonstrated by numerous studies in the past, most notably by Mattson and co-workers (Mattson et al., 2002) and by Banarjee and co-workers (Banerjee et al., 1987). Unsaturated soils pose little difficulty when the electrokinetic transport occurs by ion migration mostly. The mobile ions residing in the liquid phase move to the respective electrodes, provided that there is continuity of the liquid phase over the diffuse layer interfaces. Since in most electrokinetic treatment schemes, clean water is supplied at the anode, the ionic constituents are eventually provided with adequate solution water to migrate in during the course of a treatment. The negative pore pressures that might generate in front or behind the water flux should have little effect on the electromigration of these charged species. This phenomenon is illustrated in the laboratory where kaolinite clay

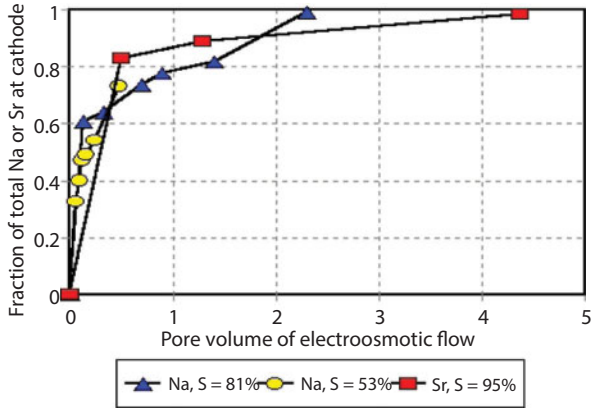

Figure 2.24 Production of Na and Sr at cathode with pore voume of EO flow in **unsaturated** clays (S: degree of saturation) (Pamukcu and Wittle, 1993)

contaminated with strontium and sodium show similar rates of transport per pore volume of liquid despite the different degrees of initial water saturation of the clay, as shown in Figure 2.24 (also see Fig. 2.13 and 2.14). In all three cases, majority of the contaminant is extracted into the cathode before the water advances one full pore distance between the anode and the cathode. However, the same may not hold true for situations where electroosmotic advection is the dominant mechanism of transport, as for non-aqueous phase liquids. In those circumstances, continuous supply of water at the influent electrode (anode-for cationic soils, or soils with pH above PZC point; and cathode for anionic soils, or soils with pH below PZC point) is expected to progressively provide sufficient water concentration in the pores for the NAPLs to partition away from the solid surface.

H. Electrokinetic Extraction of Contaminants from Saturated Soils:

Table 2.1 summarizes average metal concentration reduction (in percentage) in three replicate specimens of fully saturated synthetic soils after 24 to 48 hours of EK treatment of four selected heavy metals (Pamukcu and Wittle, 1993). The measurements provided in the Table were taken at the location of lowest concentration measurement along the specimens, as observed in the spatial distribution of strontium in Figure 2.25. Also shown in Table 1 is the average

Table 2.1 Average Percent Reduction of Metal Concentration and Pore Volume Fraction of Water Transported Toward Cathode Chamber (Pamukcu and Wittle, 1993)

Soil* Type	**KS**		**KH**		**KG**		**MS**		**SS**	
Metal	**% Rem***	**PV***	**% Rem**	**PV**	**% Rem**	**PV**	**% Rem**	**PV**	**% Rem**	**PV**
Cr	93	0.18	97	0.15	95	0.23	95	0.12	97	0.12
Cs	72	0.65	74	0.30	77	0.64	55	0.96	89	0.30
Sr	98	0.41	96	0.88	99	0.44	92	0.53	99	0.63
U	79	0.35	70	0.69	85	0.25	44	0.77	33	0.64

*% **Rem**: percent removal at lowest concentration point

***PV**: Pore volume of water to cathode

***KS**:Kaolinite; **KH**:Kaolinite with humic substances; **KG**: Kaolinite with groundwater salts; **MS**: Montmorillonite; **SS** = Clayey sand with 10% kaolinite

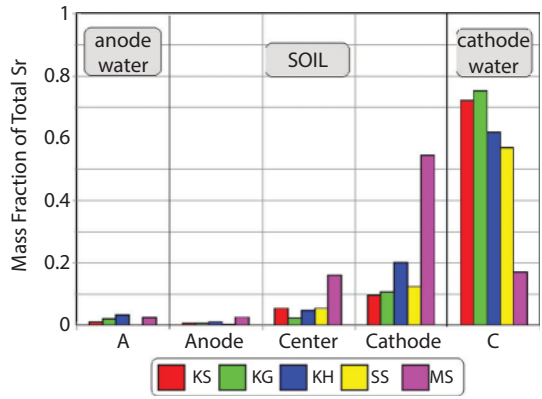

Figure 2.25 Post-EK distribution of mass fraction of Strontioum (Sr) in **saturated** clay soils (Pamukcu et al., 1997)

cumulative fraction of pore volume of water flow toward the cathode electrode compartment during each treatment. The variations in the concentration reduction percentages appear to have little or no correlation with the volume of flow achieved during treatment, but depend on the soil matrix and the metal type mostly. For the cationic species

(Cs, Sr, UO_2) the fraction of pore volume of flow ranged between 0.25 to nearly 1.00. The flow for the anionic form of Cr ($Cr_2O_7^{=}$), was consistently lower than that of the cationic species. This is potentially due to the water dragging action of the hydrated anions as they migrate in the opposite direction of the net flow toward cathode.

Although significant removal of metal into the liquid phase was achieved in most cases, a clear trend of metal accumulation was observed at the discharge locations (cathode end for cations; anode end for anions) in all soil specimens. The accumulation of the metal is due to several conditions. One condition deduced from the experiments is that the time rate of migration of the metal reduces significantly as it approaches to the discharge end. This reduction is triggered by: (i) concentration increase, (ii) precipitation of the metals, and (iii) increased retention capacity of the soil at the discharge ends due to the local pH levels. As the concentration of a particular ion increase near the discharge chamber (anode or cathode), the mobilities of the ions or the micelles decrease (Kohlrausch law). A slight reduction of the contaminant mobility may trigger a progressive concentration build up at that location if the discharge is inhibited by other mechanisms simultaneously. These mechanisms come about by the variation of soil pH from anode to the cathode end.

All the metals, both anionic and cationic, accumulated at their discharge locations creating zones of high concentrations of metal (sometimes over that of the original). These zones are often narrow residing at the interface between the soil and the electrode chamber, which is analogous of deposition of the metal on an electrode as if it was in contact with soil. In the case of cations, the production of hydroxide in the cathode chamber is one of the major causes of the phenomena. As the hydroxide ions (OH^-) migrate into the soil from the catholyte, they create a high pH zone in the soil before they can encounter the oncoming hydronium ions (H^+) and be neutralized. This zone may lessen in thickness as the acid front penetrates deeper toward the cathode side of the soil (Hamed et al., 1991). Subsequently, the high pH generated at the electrode site solution and the lower pH at the soil-water interface can create a large pH gradient across this interface, inhibiting the discharge of the metals. Another effect of high pH is on the adsorption capacity of

the clay soils. Hydroxide ions are potential makers, which subsequently cause the cation adsorption capacity of the soil to increase. Therefore, at high pH the surface potential will increase, leading to thicker diffuse layers and increased surface conductivity. Since, the bulk liquid conductivity would be reduced with precipitation, the combined effect should signal increased electroosmotic water transport and current efficiency. This suggests that with extended duration of treatment, the accumulated metal may eventually be transported into the electrode chamber by the steady but slower action of electroosmotic advection.

Figure 2.26 shows the variation of zeta potential with pH for two clay-electrolyte systems of high ionic concentration. As observed, the PZC of either the Sr or Pb spiked kaolinite clay lie at about 4 pH units. The potential increases in negative values, then reverses at high pH. The changing zeta potential trends can also explain the interfacial accumulation of some compounds in response to reversed EO flow regimes. A typical example of post-EK metal accumulation near the soil-water interface at cathode side is displayed in Figure 2.27 for lead in various clay soils.

I. Extraction of VOCs, PAHs and organic acids:

The application of electrokinetic phenomena to the transport of NAPL pollutants has not been widely investigated. Bruell et al., (1992) showed transport TCE and several gasoline hydrocarbons by electroosmosis, assuming a constant

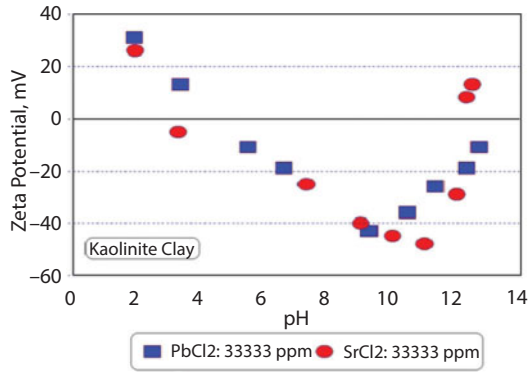

Figure 2.26 Evolution of zeta-potential with pH in kaolinite clay of high salt concentration (Pamukcu et al., 1997)

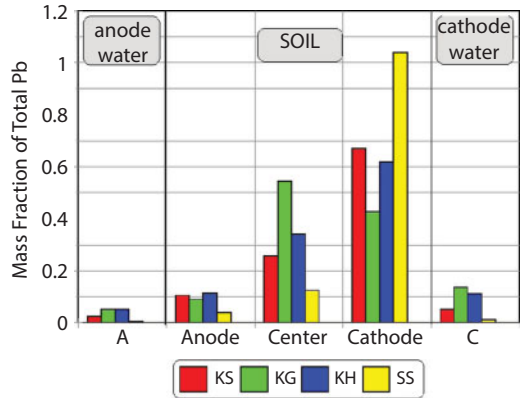

Figure 2.27 Post-EK distribution of mass fraction of Lead (Pb) in **saturated** clay soils (Pamukcu et al., 1997)

rate of electroosmotic flux. Acar et al., (1992) showed that transport of phenol is possible by both electroosmosis and electromigration, owing to the amphoteric nature of the compound. Field experiments by Ho et al., (1995) showed that the dissolved fraction of TCE can be transported by electroosmosis.

Pamukcu (1994) showed that PAH compounds with higher water solubility and lower molecular weight (i.e., naphthalene) in coal tar contaminated soils could be transported by electroosmosis without the aid of surface tension reducing agents. In these tests, extraction of coal tar PAHs, which included : *naphthalene*, *acenaphthylene*, *acenaphthene*, *fluorene*, *phenanthrene*, *anthracene*, *fluoranthene*, *pyrene*, *chrysene*, *benz(a)anthracene*, *benzo(b)fluoranthene*, *benzo(k) fluoranthene*, *benzo(a)pyrene*, *dibenzo(a,h)anthracene*, *benzo(g,h,i)perylene*, and *indeno(1,2,3-c,d)pyrene* were demonstrated using EK process. Figure 2.28 displays the post-process distribution of the normalized mass of total PAHs in the coal tar contaminated soil specimens retrieved from a manufactured gas plant (MGP) site in Champaign-Urbana, Illinois. As observed, the electroosmotic advection transported and accumulated the PAH mass in soil near the cathode interface. Use of an anionic surfactant (sodium dodecyl sulfate (SDS)) with or without a co-surfactant (butanol) appeared to reduce the PAH mass in the soil significantly,

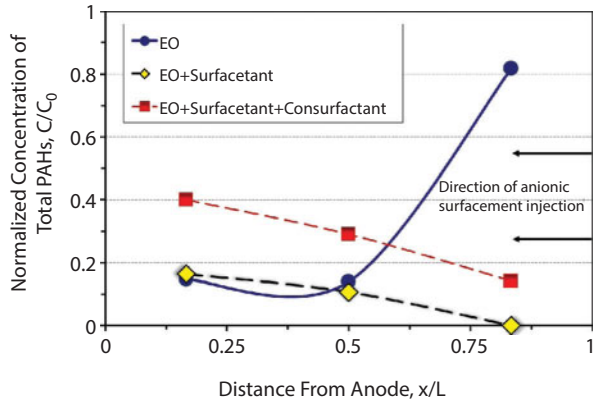

Figure 2.28 Post-EK distribution of the normalized concentration of total PAHs in coal tar contaminated specimens from an MGP site in Illinois (Pamukcu, 1994)

transporting the contaminants into the electrode chambers, mainly to the anode.

Pamukcu and Pervizpour (1998b), through well-controlled experiments, demonstrated the EK aided transport of TCE (trichloroethylene) in contaminated soil samples from Lawrence Livermore DOE Complex site in California. Soil cores were injected with TCE using groundwater collected from the site and spiked with TCE below its solubility limit. The injection of TCE into the soil was accomplished using only electroosmotically aided transport of the solution from the anode (influent) to the cathode (effluent) chamber of the test cell. Figure 2.29 shows the trace and breakthrough of TCE in the cathode, while the concentration of TCE in anode was kept constant under its solubility limit. The breakthrough at the cathode occurred at approximately 1.5 pore volumes of flow. The hydraulic conductivity and the electrosmotic conductivity of the soil specimen were measured as $k_h=10^{-8}$ cm/sec and $k_{eo}= 2x10^{-6}$ cm^2/sec.V, respectively. The equivalent hydraulic conductivity, k_{eh} under EO attained an average value of $5x10^{-6}$ cm/sec, producing steady flux of TCE into the cathode chamber. The tracer curve is indicative of a solute that undergoes partitioning between the solid and the liquid phase, therefore retardation of TCE on the solid phase was expected. Nevertheless, these results

show clearly that the dissolved fraction of a chlorinated hydrocarbon could be transported by EO.

Potassium formate (potassium salt of formic acid), an organic acid used as a drilling fluid additive, was treated using EK. The goal of this treatment was to reduce the potassium content of the mixture by separating the potassium from its anion component (i.e., formic acid) for recycling. Two types of tests, with single and double cell configurations and variable electric potential applications were developed to assess the efficacy of EK. Figure 2.30 shows the conceptual scheme of the proposed separation and the photographs of the test

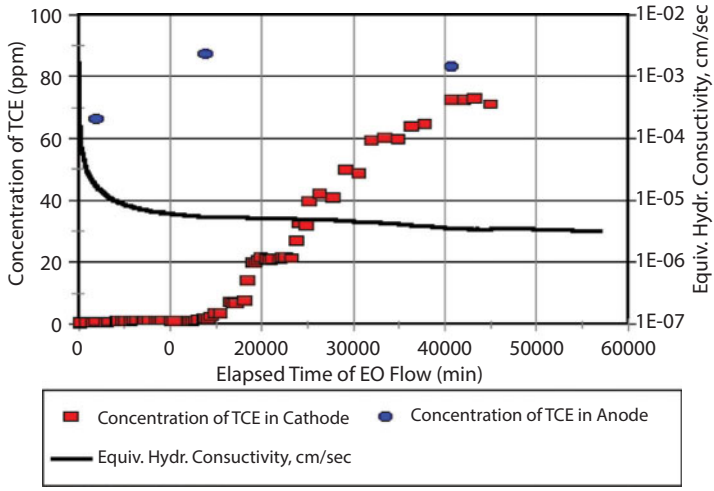

Figure 2.29 The cumulative mass transport of TCE from anode to cathode electrode chamber by EO in soil samples from LLNL DOE Complex site (Pamukcu and Pervizpour, 1998b).

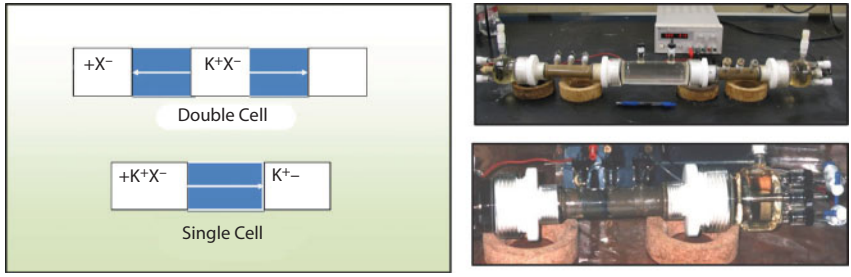

Figure 2.30 Single and double cell EK test configurations and photos of the test cells for extracting K+ from drilling mud

cells. In the double cell configuration, 5% potassium formate solution was placed in the center, anode and cathode liquid chambers whereby the potassium and the formic acid components were expected to filter through the soil into the oppositely charged electrode chambers. In the single cell configuration, 5% potassium formate solution was placed only in the anode electrode chamber and potassium was expected to filter through the soil into the cathode electrode chamber. The results of these tests are presented in figures 2.31 and 2.32. In both tests, the potassium concentration increased at the cathode and decreased in the anode and the

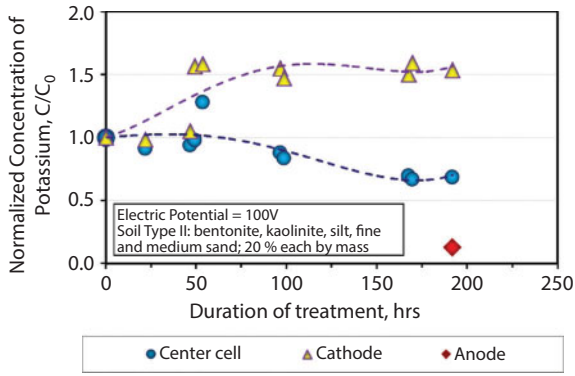

Figure 2.31 Evolution of potassium and concentrations in the electrode sites and center in double cell EK test

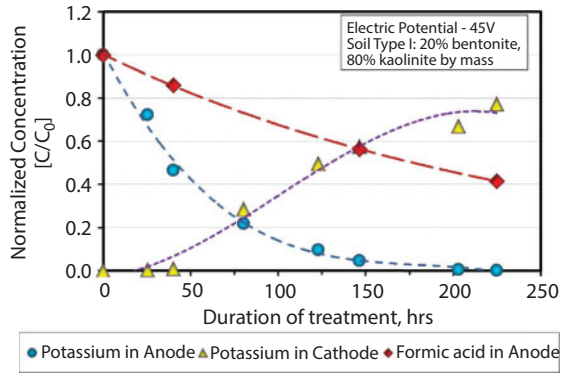

Figure 2.32 Evolution of potassium and formate concentrations in the electrode sites in single cell EK test

center cell compartment. The concentration of the formic acid decreased in the anode chamber pursuant to migration of some of the compound into the soil as well. Lab study confirmed that infield recycling of potassium from drilling fluid is possible by filtering it through soil using EK.

2.3.2 Electrokinetially-Aided Stabilization and Immobilization

In environmental restoration, stabilization is defined as fixing the toxic substance in place thereby rendering it less likely to move elsewhere under the ambient hydrogeological conditions. In the subsurface, stabilization of a toxic substance can be accomplished by delivering an appropriate oxidizing or reducing agent that subsequently will: (i) degrade the contaminant; or (ii) change it to a non-toxic or immobile species; or (iii) enhance stable sorption and incorporation of the contaminant into the clay minerals. Zero-valent iron enhanced degradation of TCE (Ho et al., 1995), and Fe(II) degradation of toxic Cr(VI) to less toxic and less mobile Cr(III) are examples of such processes (Haran et al., 1995; Pamukcu et al., 1997; Pamukcu et al., 2008; Gomes et al., 2012; 2013a; 2013b).

The metals that could be altered in such a manner are those that are least likely to be extracted by electrokinetic treatment. Owing to their complex electrochemistry, metals such as Cr, As, Hg are possible candidates for electrokinetic containment. A good example of electrochemical stabilization may be the relatively well studied reduction of Cr(VI) to Cr(III), by delivering iron (Fe(0), Fe(II), or Fe(III)) with co-reagents in aqueous environments (Powell, et al., 1995; Anderson et al., 1994; Eary and Rai, 1991). Chromium exists in two possible oxidation states in soils: the trivalent Cr(III) and the hexavalent Cr(VI) chromium. At low pH conditions (2 to 6.5) the predominant form of the hexavalent chromium is chromate or dichromate ion. Due to their negative charge they are not readily adsorbed or exchanged at clay surfaces, therefore remain in soil pore water and can be readily transported. At sufficiently low pH, the soil surface may become positively charged and tend to retain and accumulate these anions. Therefore complete removal may not be achieved unless precise control of pH is maintained at the anode during an electrokinetic process. As discussed previously, Figure 2.20 shows a good example where only a small mass of Cr is removed with increasing duration of treatment and applied current.

Hexavalent chromium can be reduced to Cr(III) under normal soil and pH conditions, for which soil organic matter acts as the electron donor (Rai et al., 1987). Bartlett (1991) reported that in natural soils, this reduction

may be extremely slow, requiring years. In subsurface soils where there is less organic matter, the Fe(II) containing minerals reduce Cr(VI) at pH less than 5 (Eary and Rai, 1991). Electrochemically injected Fe(II) into a matrix of soil containing hexavalent chromium should facilitate the reduction of Cr(VI) since electrochemical process produces low pH conditions. The delivery of Fe(II) has also been shown to enhance the formation of a chromium-iron hydroxide solid solution [$(Cr_xFe_{1-x})(OH)_3$(ss)] which has a low equilibrium solution activity then pure solid phases (Powell, et al., 1995). Figure 2.33 shows the formation of chromium-iron oxide hydroxide solutions when Fe(II) was delivered electrokinetically into Cr contaminated soil where the original form of chromium was Cr(IV). As observed, most of the post-EK form of Cr coincided with the solid solution distribution where the Cr is transformed into non-aqueous Cr(III). Figure 2.34 confirms the post EK abundance of Cr(III) per redox-pH measurements shown on Pourbaix diagram. These results confirm that the electrokinetically delivered Fe(II) had successfully transformed and arrested the Cr in soil where it is no longer available for leaching out into the groundwater environment, hence stabilized.

As previously discussed, Faradaic reactions may take place on clay particle surfaces when current pass in the pathways of the diffuse double layers. These reactions can aid in electrically enhanced stabilization and or immobilization of certain contaminants. Hence, external supply of electrical energy can help drive favorable oxidation-reduction reactions on contaminated clay surfaces where most of the contaminants tend to reside because of adsorption or exchange. Controlled laboratory experiments of kaolinite

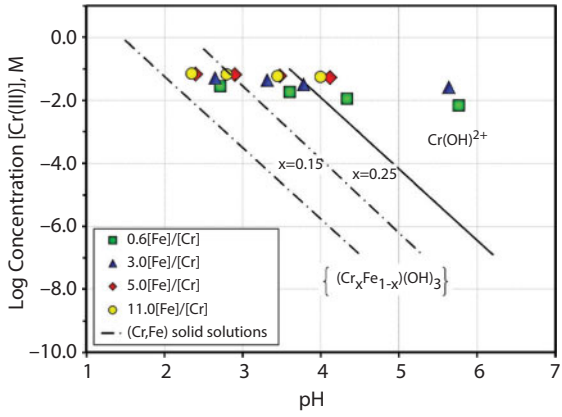

Figure 2.33 Post-EK formation of Cr,Fe solid solutions in soil at various Fe(II) concentration applications (Weeks and Pamukcu, 2001)

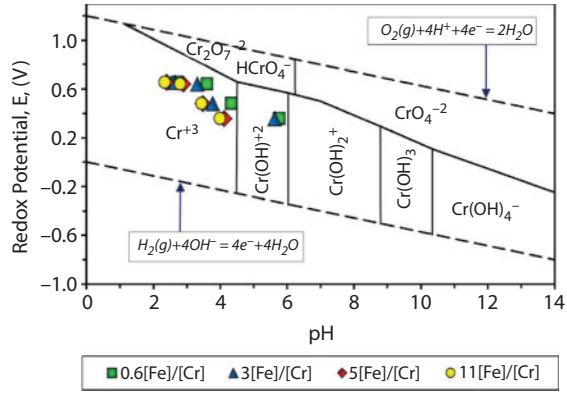

Figure 2.34 Post-EK distribution of Cr species in soil depicted on Pourbaix diagram (Weeks and Pamukcu, 2001)

clay injected with Fe(II) showed that an externally applied electric field caused an additional "cathodic current" that drove forth the reduction of Cr(VI) in clay (Pamukcu et al., 2004). The results in these experiments showed that the system ORP (oxidation-reduction potential) increased by a positive shift from the standard solution ORP in the presence of the clay and the induced electrical field, as was shown earlier in Figure 2.12.

More evidence for electrokinetically assisted surface transformations in kaolinite clay was found when a clean specimen of the clay was permeated with polymer coated dispersed nano-iron particles of positive surface charge (Sun et al., 2006) under an electrical gradient of 0.1 V/cm (Pamukcu et al., 2008). When there is no large concentration of a dominant ion in the clay matrix (i.e. contaminating heavy metals), the primary electron receptors are water and residual dissolved oxygen. Hence, the chemical reactions, which oxidize the nano-iron are:

$$Fe^0(s) + 2H_2O(aq) \rightarrow Fe^{+2}(aq) + H_2(g) + 2OH^-(aq) \qquad (2.13)$$

$$2Fe^0(s) + 4H^+(aq) + O_2(aq) \rightarrow 2Fe^{+2}(aq) + 2H_2O(l) \qquad (2.14)$$

Equation 2.13 is the dominant redox process in presence of overwhelming concentration of water as the solvent. As hydrogen ions are utilized in Equation 2.14, the pH would increase at corrosion locations resulting in simultaneous decline in the solution ORP. The transient ORP measured across a 20cm long, 2 mm thick bed of clay (see Figure 2.11) injected with nanoiron (nZVI) using EK, are presented in Figure 2.35. The ORP

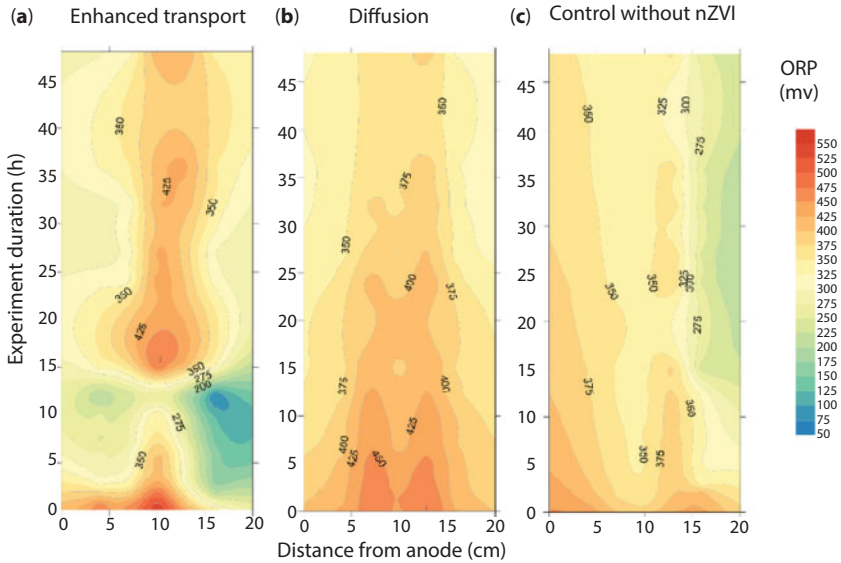

Figure 2.35 Variation of ORP in the kaolin medium in **a)** EK assisted transport of nZVI **b)** diffusion of nZVI and **c)** EK without nZVI; all using 1 mM NaCl as pore fluid electrolyte (Gomes et al., 2013b).

variations for control tests of diffusion and electrokinetics without the nano-iron are also presented. In these tests, the nZVI granules were placed in the clay inside a transverse groove at about 8 cm from the anode end of the clay bed and the tests were run under oxygen poor conditions using 5V across the working electrodes. As observed, the ORP reduced across clay bed for the first 15 hours of transport and increased to above the original values during the rest of the transport period. The ORP for the diffusion only case remained mostly unchanged, and the EK only case showed the typical pH dependent ORP variation expected with EK. Based on the water chemistry of nano-iron (Sun et al., 2006), if the only contributor to the ORP was nano-iron, the change in the ORP of the system would be expected to vary within 50 mV between the pH units of 6.0 to 6.5. The ORP changes for the diffusion tests did remain between *+50 and –50 mV*, over the 48-hour duration without the electric field application. The EK assisted transport of nZVI, on the other hand, displayed larger changes in ORP across the clay bed indicating a synergistic effect of EK and nZVI activation within the first 15 hours of the process. The longer term ORP changes showed the contribution of clay surface interactions with Fe(II) and Fe(III) in presence of electrical potential as the ORP elevated over background values at the average low pH value of 3.

The ORP versus pH obtained from earlier experiments of similar configuration as above (Pamukcu et al., 2008) are plotted in Figure 2.36. The diagram depicts approximate regions of corrosion, passivity and immunity for iron (Davis, 2000). The cluster of data that fell within the *immunity zone* corresponded to the first 6 hours of electrokinetic transport where the ORP at the cathode end was below *–1.0V*. This indicated that the nano-iron particles had already been transported to the cathode side of the clay bed by the end of 6 hours of treatment or earlier. The evidence that corroborated with the visual observations of color change in clay (i.e., indicative of oxidation of iron) was the cluster of data that fell within the *passivity zone.* This data corresponded to measurements made later, from 6 to 46 hours. By the end of 46 hours, the corrosion products with *higher* ORP appeared at the cathode end of the clay bed, as was evidenced by the brown tone color change in that region of the test bed.

The average voltage distributions across the clay bed with and without nZVI are plotted in Figure 2.37 (Pamukcu et al., 2008). As observed, while the EK only test displayed a constant electrical gradient of *0.12 V/cm* (i.e., equation of the linearly fit line) for the 48-hour duration of the test, the electrical gradient fluctuated between adjacent auxiliary electrodes inserted in soil bed for the nZVI case. The magnitude of these oscillations ceased attaining a constant profile in time. Variation of the electric gradient influences the velocity of the migrating particles from one station to the next, causing accumulation in some locations and evacuation in others. Theoretically, the particle velocity is expected to decrease at regions of

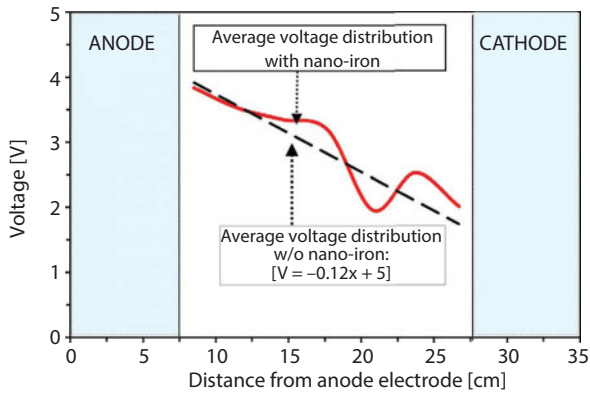

Figure 2.36 Average distribution of voltage in clay with and without nZVI transport over 48 hours of EK (Pamukcu et al., 2008)

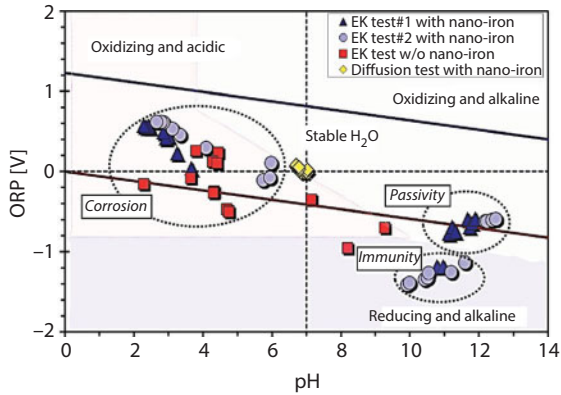

Figure 2.37 pH-ORP (Eh) variation of clay with and w/o nano-iron in electrokinetic transport (Pamukcu et al., 2008)

low electrical fields, causing accumulation and higher charge density; but pick up at regions of higher electric field, hence dilution and low charge density. This process is likely to have a progressive nature that would allow for self-correction by diffusion and Faradic currents to maintain the electrical neutrality. Such a process could also result in the wave shape of the voltage distribution to remain stationary with only the magnitudes of the peaks changing. For example, if initially an accumulation were triggered by a physical obstruction (i.e. agglomeration of the particles in small clay pore-throats), voltage gradient at that locale would increase because of the reduced conduction. The increased charge density would lead to surface capacitance and Faradaic reactions at the location. At the same time, the increased voltage gradient would promote the particles to move and vacate the location, subsequently causing a drop in charge density, and reversal of the surface reactions. It is difficult to capture such potential dynamics through sporadic voltage and ORP measurements in a typical electrokinetic transport testing in clay. Nevertheless, based on the data collected and evaluated, the empirical evidence appears to support that presence of clay and ensuing surface interactions enhance the ORP under direct current electrical field.

The oscillating voltage gradients at high electrolyte concentration environments were observed again in a large-scale test designed to mimic potential application of electrically assisted dewatering of sea-harbor sediments (Muraoka et al., 2011). The model experiment simulated parallel vertical electrodes that can be installed throughout the depth of unconsolidated sediments allowing accelerated drainage laterally. Commercial kaolinite

clay was used to mix a slurry at 35:65 solid:water ratio by mass. The mixing water and the electrode chamber waters were made up of 30,000 ppm electrolyte solution of instant ocean sea salt. Constant voltage, adjusted between 3.5V and 3.0V was applied across the electrodes to maintain a direct electric current of about 100mA. The clay slurry and the electrode chamber waters were filled up to 40 cm from the bottom of the tank. The water levels in the electrolyte chambers were maintained at the mud line to alleviate any change in hydraulic potential. Five water pressure head (piezotubes) and voltage (auxiliary electrodes) measurement probes were placed inside the clay slurry. The electrical gradients and the pore water pressures were measured across the dewatering/settling clay at time intervals.

The long-term experimental results (~ 7 days) showed that the settlement or the dewatering of clay slurry was hindered due to spatially nonlinear and temporally oscillatory voltage gradients, which give way to non-uniform distribution of stagnant pore water pressures within the clay slurry. These results are presented in Figures 2.38 and 2.39 for randomly selected time steps of the voltage gradient and pore-water pressure measurements, respectively. The significance of these observations is that the local voltage gradients appear to have direct influence on the development of local pressure gradients within the electro-osmotic flow region of a high salt content medium. Fluctuating pore water pressures induce competing flow regimes resulting in stagnant pore pressures that can impede electro-osmotic mass transport. In Figure 2.38 the voltage gradient distribution between adjacent probe locations shows clearly zones of high and low gradients, above and below the self-manifesting threshold value of 0.015 V/cm. In final analysis, the nonlinear and oscillatory voltage gradients were

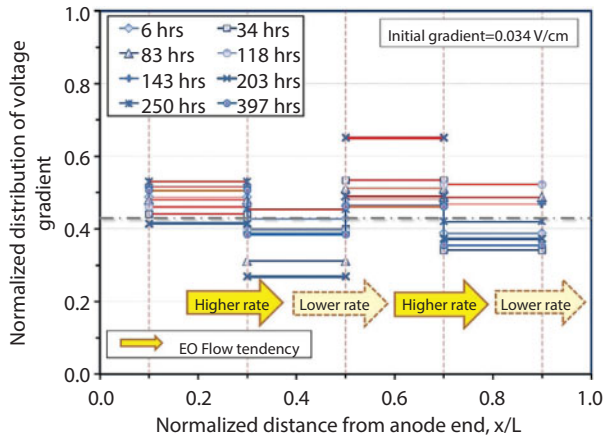

Figure 2.38 Spatial and temporal distribution of voltage gradient across adjacent probes at select times during EK (Muraoka et al., 2011)

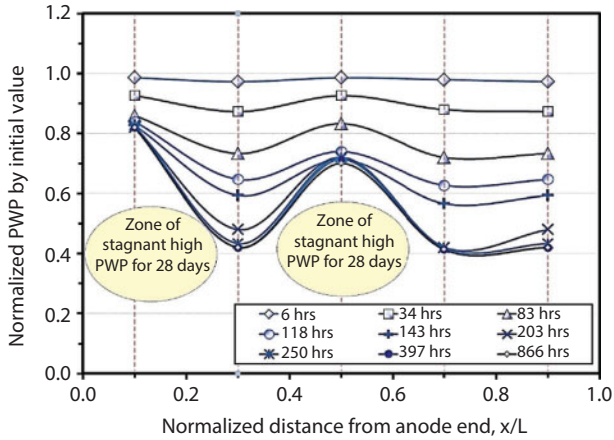

Figure 2.39 Spatial and temporal distribution of normalized pore water pressure (PWP) between adjacent probes at select times during EK (Muraoka et al., 2011)

attributed to streaming potential and migrating fronts of ions in the high salinity environment. The resistance to pore water pressure dissipation was attributed to compression and polarization of particle DDL in the direction of the electric field. The combined consequence of these phenomena is the competing pressure gradients that keep the clay particles from settling and dewatering (Muraoka et al., 2011).

2.3.3 Electrokinetially-Aided Containment

Containment in this publication is defined as causing controlled accumulation of a toxic substance by sorption in a small volume of substrate (i.e., permeable barrier), which can be flushed and regenerated for further use. Electrokinetic containment may be accomplished by causing electromigration or electroosmotic transport of the contaminants to a reactive permeable barrier (Rael et al., 1995; Blowes et al., 1995), strategically situated between the electrodes, where they are attenuated and the filtered water is allowed to pass through (Hansen, 1995; Weeks and Pamukcu, 1996). In actual field applications, such permeable structures could be installed in multiples at various configurations throughout a contaminated site serving as primary and secondary treatment locations.

Pre-contaminated kaolinite samples with lead, Pb(II) (from $Pb(NO_3)_2$ salt) were tested to determine the effectiveness of using permeable reactive caps to contain heavy metals adjacent to the electrode chambers. The reactive permeable caps (GS caps) were comprised of 50% glauconite (green sand), 30% zeolite, and 20 % bentonite clay by mass. The average particle

size of green sand and zeolite was on the order of medium to fine sand. Bentonite was added to enhance the bonding of the matrix. The final water content of the cap mixture was 37.5%, and of the contaminated soil was 60% with initial Pb(II) concentration of 5000 ppm. A constant voltage of 15 volts was applied to all the test samples. The tests were terminated when the current readings diminished to a constant low value.

Figures 2.40 and 2.41 show the average pre- and post-EK mass fraction distributions of Pb(II) in the soil and the electrode chambers with

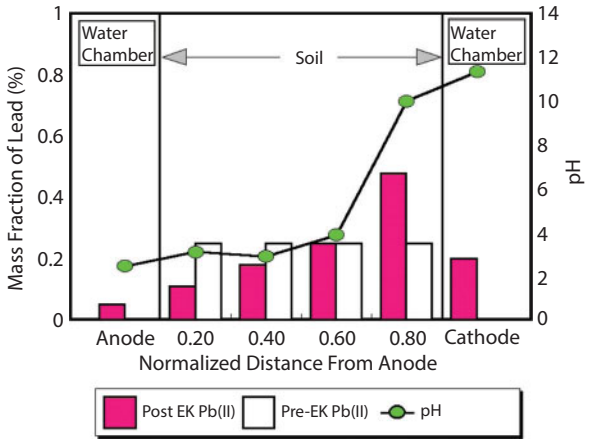

Figure 2.40 Post EK mass fraction (%) of total Pb remaining in soil and liquid tested without the GS Caps; pH superimposed (Pamukcu et al., 1997)

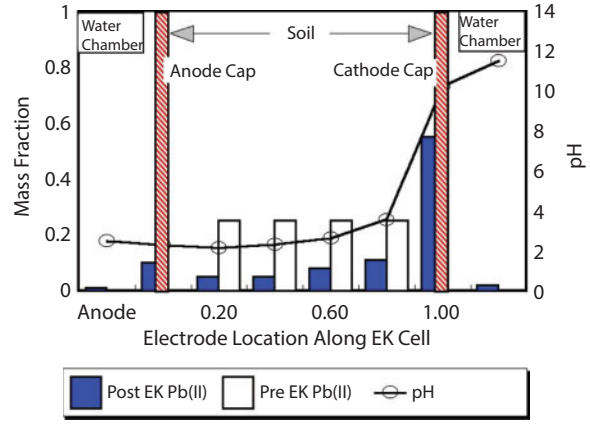

Figure 2.41 Post EK mass fraction (%) of total Pb remaining in soil and liquid tested with the GS Caps; pH superimposed (Pamukcu et al., 1997)

and without the GS caps, respectively. The sample containing the GS caps showed larger concentrations of Pb(II) accumulated in the caps, and very little of the element passed into the electrode chambers. Overall, the results showed that in samples tested without the GS caps more of the Pb(II) remained in the soil; while, the samples containing the caps showed lesser concentrations of Pb(II) in the soil with larger concentrations in the areas of the GS caps for the same duration of electrokinetic treatment. The larger removal of the lead into the GS caps, particularly on the cathode side is attributed to continued flow of higher current and electro-osmotic advection, whereas precipitation of lead at the cathode interface of the soil without the caps inhibited the current and electro-osmotic flow hindering the Pb(II) transport overall. Indeed, the steady low current measured with caps was 3 times larger than the one without the caps. The sorptive capacity of the cathode cap would have kept the Pb(II) and its hydroxide precipitates on the solid surfaces without causing blockage in the porous matrix. These results indicate that application of site and contaminant specific containment packs can work synergistically with EK remediation when the goal is to collect the contaminant in a small volume of substrate from where it can be recovered, while regenerating the substrate for further use.

2.4 Transport and Extraction of Crude Oil

2.4.1 Laboratory Evidence of Oil Extraction

Chilingar and co-workers investigated the use of electrokinetics to augment reservoir energy during petroleum production (Amba et al. 1964,1965; Chilingar et al., 1968a,b). They found that application of direct electric current resulted in several fold increase in the flow rate of oil and water (i.,e., as much as 34 fold) in both synthetic and natural sandstone cores. Synthetic cores were prepared using various percentages of different types of clay admixed with 200 mesh size silica or $CaCO_3$ powder. Also, it was found that the effective permeability to kerosene of core samples containing connate water (i.e., entrapped water in the pores when the rocks were formed) was increased by 50 percent on temporary application of direct potential gradient.

Successful field pilot tests have been reported on the application of EEOR (Electrically Enhanced Oil Recovery) in heavy oil fields in the Santa Maria (California) basin and the Eastern Alberta Plains (Wittle et al., 2007, 2008). In these pilot tests, the EEOR was found to be more efficient than other

conventional heavy oil recovery methods including steam flood or cyclic stream flood. Also, these field pilot studies demonstrated the capability of EEOR in cracking heavy oil in-situ, reducing water cut and increasing oil production rates. The field tests in California demonstrated up to a ten fold increase in the oil production from a field containing 8° API gravity oil.

Haroun and coworkers (Haroun et al., 2009) reported the results of DC electric field application, concurrently with water-flood recovery in mobilizing the connate water and the trapped oil through core-flood studies. In the first set of experiments, DC was applied after ultimate water-flood recovery and in the second set of experiments the DC was applied on oil saturated core plugs concurrently with water flood from the beginning of the test. Comparison of the two processes revealed that application of DC concurrently with water flooding at the beginning of the process recovered approximately 1.5–4% more oil and reduced water requirement by 15–22% in comparison with the water flooding process alone (Alshalabi et al., 2012; Haroun et al., 2009). However, application of DC on a completely water swept core was found to recover 3-9 % additional oil. Also, on repeat application of DC, up to 30% increase in permeability of cores was reported which was attributed to clay dislodgement due to electrophoresis mechanism involved in EEOR. Jihong and coworkers (Jihong et al., 2009) reported that application of DC concurrently with water flooding on core samples containing oil with viscosity of 8 MPa.s, increased the oil recovery rate by more than 5%. Also, the apparent viscosity of the oil was found to decrease as the electric field strength was increased.

The authors (Ghazanfari et al. 2012, 2013b) conducted a series of laboratory experiments on oil-bearing rock core specimens retrieved from a shallow oil formation in Kentucky to investigate the oil extractability and change in the rock-core permeability under applied electric field. The physical properties of the three core specimens (diameter: 36mm; length: 82 mm) are given in Table 2.2. The physical properties of the natural oil in the rock cores and the brine solution used in the experiments as the surrogate formation water are given in Table 2.3. Acurrent density of 1Amp/m^2 was applied to the cores in accordance with the achievable current densities of 1.0-1.5 Amp/m^2 in practical applications in the field.. The total flow generated in each phase (oil and water) was measured periodically for 120 hours. The oil separation and analysis were conducted using standard techniques.

As observed in Table 2.2, most of the oil recovered was produced at the catholyte, while the oil recovered at the anolyte was negligible. The total oil recovered was in the range of 5 to 11% by mass of the initial oil content in

Table 2.2 Physical properties and oil recovery in the natural sand stone cores (Kentucky field)

Core	Porosity (%)	Bulk density (gr/cm^3)	Permeability (mD)	Residual oil (%)	Residual water (%)	Recovered oil at the anolyte (ml)	Recovered oil at catholyte (ml)	Total recovered oil (%)
KY1	10.2	2.48	2.67	12.9	61	0.000	0.021	5.1
KY2	13.6	2.39	11.59	28.1	43.9	0.005	0.104	9.9
KY3	14.7	2.37	41.88	30.2	33.9	0.002	0.157	11.4

Table 2.3 Physical properties of the formation oil and surrogate water (Kentucky field)

Fluid	Properties
Natural formation oil	API 22; Dynamic viscosity = 66.5 cP Specific gravity =0.92 at 20°C
Electrolyte solution (Surrogate formation water)	Salinity= 33,000 ppm; Electrical conductivity = 45,000 μS pH = 7.50; Major elements: Na, Cl, Mg, S, K, Ca, Br

the cores. The oil recovery results suggest a direct relation between the initial oil content of the formation and the measured oil recovery. Modeling studies on two-phase EO flow revealed that the drag force exerted by the mobile water phase on the oil phase increases with water saturation of the pore up to about 50%. The oil production decrease when water saturation is above 50% and oil saturation drops below 50% (Ghazanfari et al. 2013b). The higher recovery of oil with higher initial oil/water ratio is attributed to the availability of more oil.

In a separate set of experiments, sandstone core specimens retrieved from a deep oil formation in Pennsylvania were used in the experiments to assess oil recovery, permeability change, and effect of the magnitude of current density on oil extraction. Unlike the Kentucky cores discussed above, the Pennsylvania cores had very low initial oil content. In order to better control the oil and water saturation, these cores were impregnated with Pennsylvania oil (API 47; Dynamic viscosity = 38.7 cP) and surrogate formation water (i.e., with the same properties as presented in Tables 2.2) prior to testing. First, the cores were dried and vacuumed. Then, oil and water were injected into the cores using a high-pressure injection pump (Quizix Pump) to attain the desired initial oil-water saturations. Once saturated, the cores were tested under a constant current density of 1 Amp/m^2 for 130 hours. The physical properties of the four Pennsylvania cores used in these experiments are given in Table 2.4.

As presented in table 2.4, most of the oil was produced at the catholyte and the oil recovered at the anolyte was negligible. The total oil recovered was in the range of 0.5 to 6% by mass of the initial oil content of the cores. Similar to the Kentucky cores, the highest oil recovery corresponded to core PA3, which had the highest initial oil content and highest hydraulic permeability.

Table 2.4 Physical properties and oil recovery in the oil-impregnated cores (Pennsylvania field)

Core	Porosity (%)	Bulk density (gr/cm^3)	Permeability (mD)	Oil saturation (%)	Water saturation (%)	Recovered oil at the anode side (ml)	Recovered oil at cathode side (ml)	Total recovered oil (%)
PA1	14.5	2.49	3.6	42	58	0.0056	0.0457	1.1
PA2	12.8	2.43	2.3	48	52	0.014	0.23	3.8
PA3	14.4	2.47	8.3	53	47	0.020	0.377	6.3
PA4	11.5	2.45	0.5	40	60	0.0024	0.0198	0.6

2.4.2 Field Evidence of Oil Extraction

A field application case in the Pennsylvania field was monitored over time to investigate the effectiveness of electrically enhanced oil recovery accompanied by water flooding (i.e., water pressure). The cumulative oil and water production was monitored at one of the production wells for 180 days. During this time, some amount of paraffin was observed to produce in the well also. The oil, water, and paraffin production over time are plotted in Figure 2.42. The oil production was about 5% of the water production and the paraffin production was about 4% of oil production by volume.

The oil production decreased with time in general, yet there was no immediate break in oil production when the power was terminated, reversed or re-applied. This is attributed to the build-up of seepage and suction pressures with electro-osmosis, which would require time to dissipate in low permeability formations before the flow regime change or subside (Muraoka et al., 2011). Figure 2.43 shows the oil and paraffin production over time. As observed, the paraffin production increased with power and elevated temperature. When the power was turned off the paraffin production ceased. It is plausible that as pH, ionic concentration and dissolved minerals (e.g., calcite) increase at the production well (cathode), it created the ideal conditions for excess oil to transform to paraffin. A similar phenomenon was observed in lab experiments of core rock samples

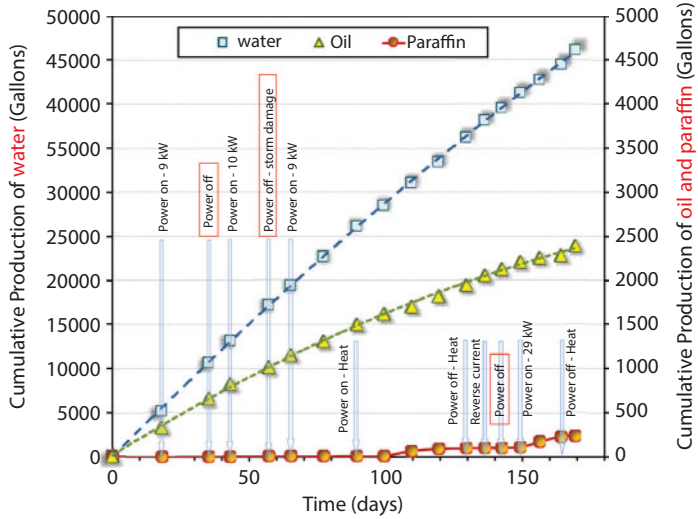

Figure 2.42 Water, oil, and paraffin production (Pennsylvania field) (Ghazanfari, 2013)

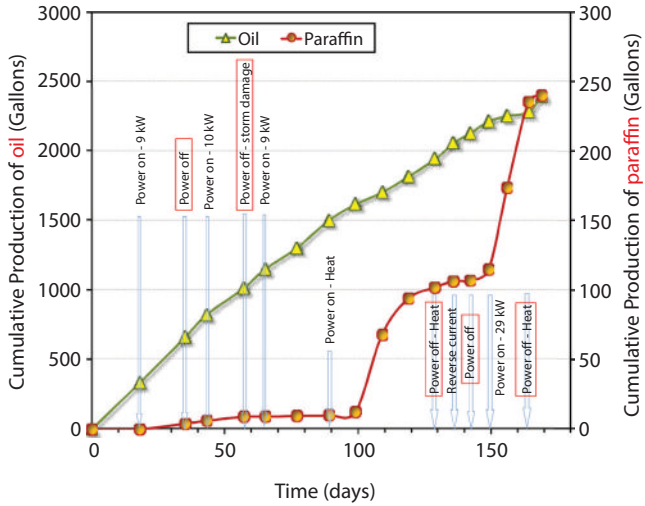

Figure 2.43 Oil and paraffin production (Pennsylvania field)(Ghazanfari, 2013)

with Pennsylvania oil where white -colored *foam* like material was formed in the catholyte, identified as paraffin.

Examining the daily production data, it was determined that when the applied current was reversed, the production of paraffin decreased. This is attributable to the counter current flow resulting in decreased oil production and lowering of the pH at the well. Lower pH and less oil available at the location would potentially reverse the paraffin production. The increase in paraffin production corresponded to the periods of elevated temperature due to sustained power over long term (~ at 100 days), or when the maximum power of 29 kW was applied (~ at 150 days). As observed from Figure 2.43, at times of increased paraffin production, the oil production decreased or completely ceased. Among some of the plausible reasons for this exchange are: the easier transport of existing paraffin in the pore space at elevated temperatures, and the increased availability of oil and mineral components to form paraffin under elevated temperature and power.

2.4.3 Laboratory Evidence of Oil Transformation

The electrochemical reactions result in reduction of the interfacial tension between the formation water and crude oil, as well as reduction in the viscosity of the crude oil. It is postulated that both phenomena eventually lead to increased oil mobility and serve to enhance the oil recovery

under applied DCelectric field. The primary mechanism of interfacial tension reduction under applied electric field is reported as the reaction of electrolysis products of brine/formation water (hydroxyl ions, OH^-) on the acid impurities of oil (carboxylic acids) (Fleureau and Dupeyart, 1988). This results in formation and accumulation of low solubility surface-active carboxylates analogous to that of directly adding a surfactant to reduce the interfacial tension (Sato et al., 1998). The amount of interfacial tension reduction is reported to be proportional to the applied potential (Tao and Xu, 2006).

Interactions between the pore fluids and the solids, which are normally affected by the ambient pH and redox conditions, will be enhanced upon application of DC electric field. These electrochemically enhanced reactions help oil transformation by cracking the heavy molecular structure of crude oil into its lighter components with lower viscosity (Wittle at al., 2007). As a result the functional group fractions of the crude oil, including the Saturates, Aromatics, Resins, and Asphaltenes (SARA) will be affected. As the asphaltene and resin content of the formation oil decrease and the aromatic content increases, it is expected that the viscosity of the oil decrease. The less viscous the crude oil, the higher is its mobility in the formation. Decrease in the oil viscosity under increased electric field intensity has been reported in the literature (Sato et al., 1998; Tao and Xu, 2006; Wittle et al., 2008).

To investigate the oil transformation under applied DC electric field, a series of synthetic cores were prepared and tested. Three of the test cells were run at low current density of $0.1 A/m^2$, three at high current density of $1.0 A/m^2$ and three control cells at no current. The cells were 100 cm in length and 16.2 cm in diameter as shown in Figure 2.44. Titanium

Figure 2.44 Floor scale surrogate core test set-up

electrodes, and ion exchange resin packs were used at the two ends of each cell. The cells were designed in a manner that minimized transport of pH fronts into the cores and they were hydraulically balanced to reduce flow through the cores. Liquid and solid samples were retrieved through the ports placed on the cell walls. Three different crude oils representing a wide range of dynamic viscosity, but the same brine solution was used in preparation of the cores. The physical properties of the fluids used are presented in Table 2.5. The composition of the surrogate formation cores was 52% sand (mean particle size 0.23 mm), 40% silt (mean particle size 0.025 mm), and 8% Georgia Kaolinite clay (mean particle size 0.0011mm). The initial porosity, water, and oil saturation were determined to be 30%, 46%, and 48%, respectively. The representative synthetic core permeability was measured as 510mD.

The viscosity of the oil specimens extracted from 107-day formation samples treated under applied current density of 1 Amp/m^2 showed a significant drop in all regions compared to their control value for the Pennsylvania and Canadian oils, as shown in Figures 2.45 and 2.46. For the Pennsylvania oil sample, the viscosity dropped by 35% in the anode region, 23% in the middle region, and about 13% in the cathode section. For the Canadian oil sample, the viscosity at the anode region dropped by 69% and by 26% in the cathode region.

The post-test SARA analysis (i.e., measures the contents of saturates, asphaltenes, resins and aromatics in oil) of the California and Canadian oil samples are shown in Figures 2.47 and 2.48. In concert with its post-EK

Table 2.5 Physical properties of the formation oils and water

Fluid	Properties
PA field oil	API 47; Dynamic viscosity = 38.7 cP Specific gravity =0.79 at 20°C
CA field oil	API 17.4; Dynamic viscosity = 2782 cP Specific gravity =0.95 at 20°C
Canadian field oil	API 13; Dynamic viscosity = 52000 cP Specific gravity =0.98 at 20°C
Electrolyte solution (Surrogate formation water)	Salinity= 33,000 ppm; Electrical conductivity = 45,000 μS pH = 7.50; Major elements: Na, Cl, Mg, S, K, Ca, Br

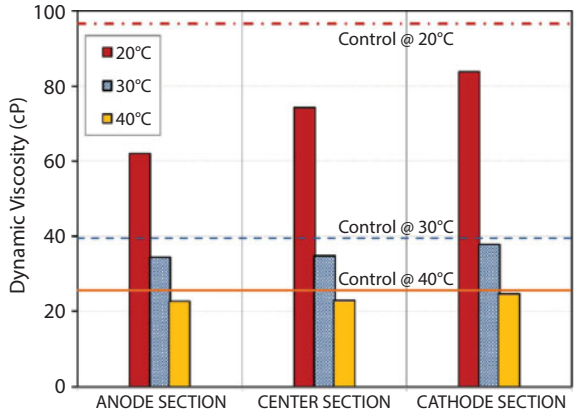

Figure 2.45 The post-test viscosity distribution of **PA** oil cell compared to its control (Ghazanfari, 2013)

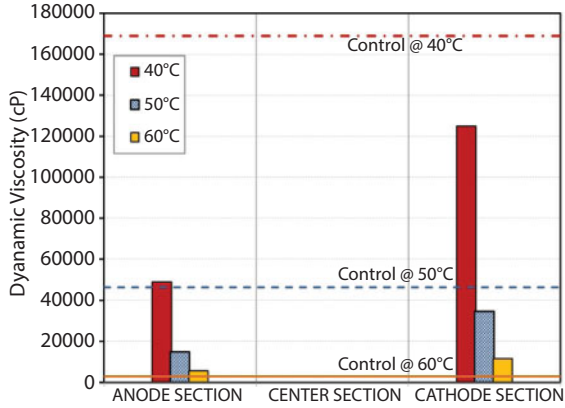

Figure 2.46 The post-test viscosity distribution of **Canadian** oil cell compared to its control (Ghazanfari, 2013)

viscosity which increased, the SARA analysis of the California oil sample showed a decrease in saturates and aromatics while a substantial increase of asphaltenes in the anode region. For the Canadian oil sample, as shown in Figure 2.48, there was a significant increase in the saturate content and a significant decrease in the asphaltene content of the oil both at the anode and cathode regions. The aromatic and the resin contents do not show as large a change from the control.

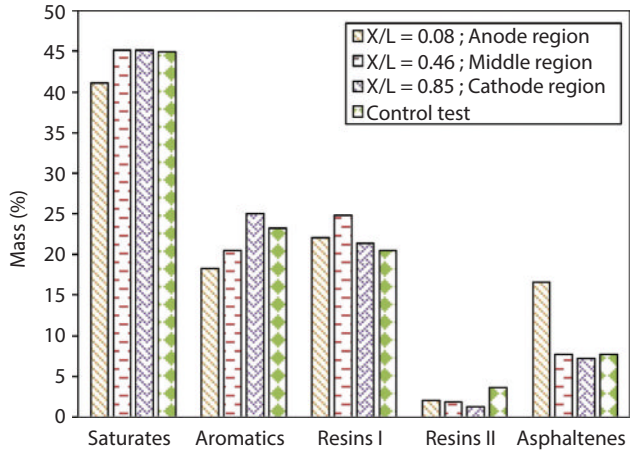

Figure 2.47 The post-test viscosity distribution of **CA** oil cell compared to its control (Ghazanfari, 2013)

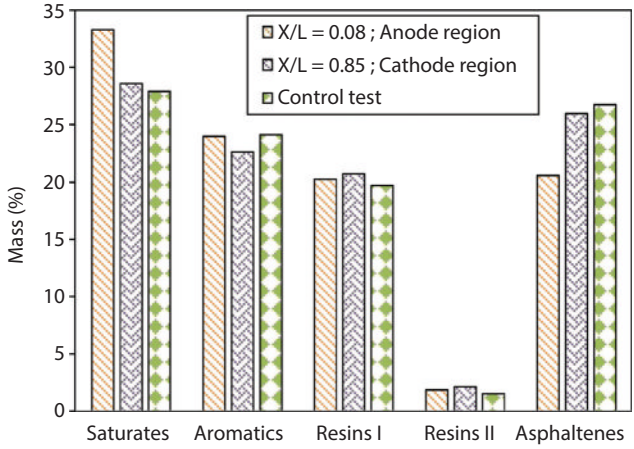

Figure 2.48 T The post-test SARA distribution of **Canadian** core oil compared to its control (Ghazanfari, 2013)

2.5 Summary and Conclusions

The fundamental principles of electrochemical transport and transformations applied to the electrokinetic processing of saturated clays and clayey formations were reviewed, and some findings were presented.

The classical H-S equation expresses the electroosmotic velocity of the fluid as a function of the electric field and the electrokinetic potential of the clay. Both of these parameters vary during electrokinetic transport, and result in a nonlinear process. It was shown analytically and experimentally that the electroosmotic velocity could be uncoupled from the applied electric field when surface conductivity σ_s and the resulting portion of the current transferred over the solid-liquid interface i_s are used as intrinsic properties of the clay to describe the velocity.

The migration of the ions in the bulk fluid were modeled taking into consideration the changing electric field due to migration, and other effects such as retardation and electrophoretic effects that reduce ion mobility. The model appeared to simulate well the long-term ion distribution in the soil as the conductivity and the electric field varied in time and space.

Finally, the experimental results of electrically enhanced extraction, separation, transformation, stabilization and containment in clay and clay rich porous media were presented and discussed in the framework of the theoretical electrochemical and electrokinetic models introduced earlier. The data appeared to support the hypothesis that Faradaic current passage orthogonal to the planes in the electric double layer of clay particles may drive forth redox reactions on clay surfaces.

References

Acar, Y. B., Alashawabkeh, A. N., 1993. "Principles of Electrokinetic Remediation". *Environmental Science and Technology*, 27(13):2638 – 2647.

Acar, Y. B., Hamed, J., Alshawabkeh, A. N., Gale, R., 1994. "Cd(II) Removal from Saturated Kaolinite by Application of Electrical Current," *Geotechnique*, 44(3):239254.

Acar, Y. B., Alshawabkeh, A. N., 1996a. "Electrokinetic remediation I: Pilot scale tests with lead spiked kaolinite," *Geotechnical and Geoenvironmental Engineering*, 122(3):173-185.

Ahn, D.W., Kim, S.S., Han, S.J., Kim B.I., 2010. "Characteristics of electrokinetic remediation of unsaturated soil contaminated by heavy metals-I: Experimental study," *Int. J. Offshore Polar* 20:140-146.

Alshawabkeh, A. N., Acar, Y. B., 1996b. "Electrokinetic remediation II: Theoretical Model," *Geotechnical and Geoenvironmental Engineering*, 122(3); 186-196.

Alshawabkeh, A. N., Sarahney, H., 2005. "Effect of current density on enhanced transformation of naphthalene," *Environmental Science and Technology*, 39:5837-5843.

Al Shalabi, E. W., Haroun, M., Ghosh, B., Pamukcu, S., 2012. "The Application of Direct Current Potential to Enhancing Waterflood Recovery Efficiency," *Petroleum Science and Technology*, Taylor & Francis, 30(20):2160-2168.

Amba, S. A., Chilingar, G. V., Beeson, C. M., 1964. "Use of Direct Electrical Current for Increasing the Flow Rate of Reservoir Fluids during Petroleum Recovery," *Journal of Canadian Petroleum Technology*, 3(1): 8-14.

Amba, S. A., Chilingar, G. V., Beeson, C. M., 1965. "Use of Direct Electrical Current for Increasing the Flow Rate of Oil and Water in a Porous Medium," *Journal of Canadian Petroleum Technology*, 4(1): 81-88.

Anderson, L.D, Kent, D.B, and Davis, J.A., 1994. "Batch Experiments Characterizing the Reduction of Cr(VI) using Suboxic Material From a Mildly Reducing Sand and Gravel Aquifer," *Env. Sci. and Tech.*, 28(1):178-185.

Banerjee, S., Horng, J., Ferguson, J. F., Nelson, P. O., 1987. "Field Scale Feasibility Study of Electrokinetic Remediation", CR811762-01, Risk Reduction Engineering Laboratory, Office of Research and Development, US EPA, Cincinnati, OH, 129 p.

Bard, A. J., Faulkner, L.R., 1980. Electrochemical Methods: Fundamentals and Applications. New York: John Wiley & Sons.

Bartlett, R.J., 1991. "Chromium Recycling in Soils and Water: Links, Gaps, and Methods," *Environmental Health Perspective*, 92:17-24.

Blowes, D.W., Ptacek C.J., Cherry, J.A., R.W. Gillham, and Robertson, W.D., 1995. "Passive Remediation of Groundwater Using In-situ Treatment Curtains," Proc. of the Specialty Conf. GeoEnvironment 2000, ASCE, New Orleans, LA, pp.1588-1607

Brosky, R.T. and Pamukcu, S., 2013. "The Role of DDL Processes During Electrolytic Reduction of Cu(II) in Low Oxygen Environment," *J. of Hazardous Materials*, 262: 878-882.

Bruell, C. J., Segal, B. A., Walsh, M. T., 1992. "Electroosmotic removal of gasoline hydrocarbons and TCE from clay," *J. Environmental Engineering*, ASCE 118(1):68-63

Cao, X., 1997. "Numerical Modeling of Electrokinetically Enhanced Transport Mechanism in Soils". Master of Science Thesis, Department of CEE, Lehigh University, Pennsylvania, USA.

Casagrande, L., 1949. "Electroosmosis in Soils," *Geotechnique*, 1:159-167.

Chang, J.H., Shi, Y.H., Tung, C.H., 2010. "Stepwise addition of chemical reagents for enhancing electrokinetic removal of Cu from real site contaminated soil," *J. Appl. Electrochem*. 40:1153-1160.

Chen, J.L., Yang, S.F, Wu, C.C., Ton, S., 2011. "Effect of ammonia as a complexing agento in electrokinetic remediation of copper-contaminated soil," *Sep. Purif. Technol*., 79: 157-163.

Chu, K. T., 2005. "Asymptotic Analysis of Extreme Electrochemical Transport". PhD Dissertation, Dept. of Mathematics, MIT, Massachusetts, USA.

Chilingar, G. V., El-Nassir, A., Steven, R. G., 1968a. "Effect of Direct Electrical Current on Permeability of Sandstone Core," *Journal of Petroleum Technology*, 22(7): 830-836.

Chilingar, G. V., Sang, C. K., Davis, J. E., Farhangi, H., Adamson, L. G., Sawabini, S., 1968b. "Possible use of direct electric current for augmenting reservoir energy during petroleum production," *Journal of Petroleum Technology*, 4:272-285.

Chilingar, G. V., Loo, W. W., Khilyuk, L. F., Katz, S. A., 1997. "Electrobioremediation of soils contaminated with hydrocarbons and metals: progress report," *Journal of Energy Sources*, 19:129-146

Denisov, G., Hicks, R. E., Probstein, R. F., 1996. "On the kinetics of charged contaminant removal from soils using Electric fields," *Journal of Colloid Interface Science*, 178:309-323.

Davis, J. R., 2000. Corrosion: Understanding the Basics, ASM International, Materials Park, OH, USA.

Dzenitis, J. M., 1997. "Soil Chemistry Effects and Flow Prediction in Electroremediation of Soil". *Environmental Science and Technology*, 31(4):1191-1197.

Eary, L.E. and Rai, D., 1991. "Chromate Reduction by Surface Soils Under Acidic Conditions," *J.American Soil Science Society*, 55:676-683.

Electorowicz, M., Boeva, V., 1996. "Electrokinetic supply of nutrients in soil bioremediation," *Environmental Science and Technology*, 17:1339-1349.

Eykholt, G. R., Daniel. D. E., 1994. "Impact of System Chemistry on Electroosmosis in Contaminated Soil," *Geotechnical and Geoenvironmental Engineering*. 120(5):797-815.

Fleureau, J.M., and Dupeyart, M., 1988. "Influence of an electric field on the interfacial parameters of a water/oil/rock system: application to oil enhanced recovery," *Journal of Colloid and Interface Science*, 123(1).

Franz, A. J., Rucker, J. W., Flora, J. V., 2002. "Electrolytic oxygen generation for subsurface delivery: effects of precipitation at the cathode and an assessment of side reactions," *Journal of Water Resources*, 36:2243-2254

Ghazanfari, E., Shrestha, R., Miroshnik, A., Pamukcu, S., 2012. "Electrically assisted liquid hydrocarbon transport in porous media," *Journal of Electrochimica Acta*, 86:185–191.

Ghazanfari, E., 2013. "Development of a mathematical model for electrically assisted oil transport in porous media". *PhD dissertation*, Dept. of CEE, Lehigh University, Bethlehem, PA.

Ghazanfari, E., Pamukcu, S., Pervizpour, M., Karpyn, Z., 2013b. "Investigation of generalized relative permeability coefficients for electrically assisted oil recovery in oil formations," *Journal of Transport in Porous Media*, Springer, 2012 (in press)

Gomes, I.H., Ferreira, C.D., Ribeiro, A.B., Pamukcu, S., 2012. "Electrokinetic enhanced transport of zero-valent iron nanoparticles for chromium (VI) reduction in soils," *Chemical Engineering Transactions*, 28:139-144.

Gomes H.I., Dias-Ferreira, C., Ribeiro, A.B., Pamukcu, S., 2013. "Direct current assisted transport and transformation of zero-valent nanoiron in porous media," *J. Water, Air and Soil Pollution*, Springer, 224:1710. .

Gomes, H.I., Dias-Ferreira, C., Ribeiro, A.B., Pamukcu, S., 2014. "Influence of electrolyte and voltage on the direct current enhanced transport of iron nanoparticles in low permeability media," *J. of Chemosphere,* 99: 171–179.

Hamed, J., Acar, Y. B., Gale, R. J., 1991. "Pb(II) Removal From Kaolinite by Electrokinetics". *Journal of Geotechnical Engineering*, 117(2):241-271.

Hansen, H.K., 1995. "Practical and Theoretical Aspects Concerning the Use of Ion Exchange Membranes and Resins in Electrokinetic Soil Remediation", Ph.D. Dissertation, Dept. of Physical Chemistry, The Technical University of Denmark.

Hansen, H. K., Rojo, A., Ottosen, L.M., 2005. Electrodialytic remediation of copper mine tailings," *J. Hazard Mater*., 117:179-183.

Hannum, L. and Pamukcu, S., 2007. "Aided Transport of Nano-Iron in Clay Soils Using Direct Electric Field," NSTI-Nanotech2007, V2, pp. 635-38.

Haran, B.S., Zheng, G., Popov, B.N., and White, R.E., 1995. "Electrochemical Decontamination of Soils: Development of New Electrochemical Method for Decontamination of Hexavalent Chromium From Sand," Electrochemical Society Proc., V95-12, pp. 227-251.

Haroun, M. R., Chilingar, G. V., Pamukcu, S., Wittle, J. K., Belhaj, H. A., Al Bloushi, M. N., 2009. "Optimizing Electroosmotic Flow Potential for Electrically Enhanced Oil Recovery (EEORTM) in Carbonate Rock Formations of Abu Dhabi Based on Rock Properties and Composition," Proc. Society of Petroleum Engineers, IPTC 13812.

Helmholtz, H. 1879. Studien uber electrische grenzschichten. *Ann. Phys. Chem*. 7(ser.3):337-382.

Hicks, E. E., Tondorf, S. 1994. "Electrorestoration of Metal Contaminated Soils," *Environ. Sci. Technol.* 28(12):2203-2210.

Ho, S.V., Sheridan, P.W., Athmer, C.J., Heitkamp, M.A., Brackin, J.M., Weber, D., and Brodsky, P.H., 1995. "Integrated In-Situ Soil Remediation Technology - The Lasagna Process," *Env. Sci. and Tech*., 29:2528-2534.

Hunter, R. J. 1981. Zeta Potential in Colloidal Science Principles and Applications. New York: Academic Press.

Hunter, R. J., James, M. 1992. "Charge reversal of kaoliniteby hydrolysable metal ions: an electroacoustic study," *Clay Mineralogy*, 40(6):644-649.

Hunter, R. J. 2001. Foundations of Colloid Science. Oxford: Oxford University Press.

Israelachvili, J. N., Adams, G. E. 1978. "Measurements of Forces Between Two Silica Surfaces in Aqeous Electrolyte Solutions in the Range of 0-100 nm," *Chemical Soc.-Faraday Trans*. 74(4):975-1001.

Jihong, Z., Yu, Haiming, Y., Wang, Yanan, W., Zhang, Gang, Z., Li, Xiaobo, L., 2009. "Experimental research on further enhanced oil recovery by using high DC electric field," IEEE proceedings.

Khan, L. I., 1991. "Study of Electroosmosis in Soil: A Modified Theory and its Applications in Soil Decontamination," Ph.D. Dissertation, Lehigh University, Dept of CEE, PA, USA.

Kortum, G., Bockris, J. M. 1951. Textbook of Electrochemistry. Vol 2. Amsterdam: Elsevier.

Kruyt, H. R., editor, 1952. Colloidal Science. Amsterdam: Elsevier.

Lei, H., Chen, K., Li, Y., 2012. "Electrokinetic recovery of copper, nickel and zinc from wastewater sludge : Effects of electrical potentials," *Environ. Eng. Sci.*, 29:472-478.

Mattson, E., Bowman, D., Robert, S., Lindgren E. R., 2002. "Electrokinetic ion transport through unsaturated soil: 1. Theory, model development, and testing," *Journal of Contaminant Hydrology* 54(1-2):99-120.

Lindgren, E.R., 1998. "Electrokinetic demonstration at the unlined chromic acid pit," Sandia National Laboratories, DOE-Office of Scientific and Technical Information, Springfield, VA, 144p.

Liu, S.H. and Wang, H.P., 2013. "Electrochemical remediation of copper-contaminated soils enhanced by ethylenediaminetetraacetic acid: an in-situ x-ray absorption spectroscopic study," *Int. J. Electrochem. Sci.* 8:4807-4817.

Lageman, R., 1993. "Electro-Reclamation: Applications in The Netherlands," *Environ. Sci. Technol.* 27(13):2648-2650.

Lyklema, J., 1995. Fundamentals of Interface and Colloid Science. Volume II: Solid-Liquid Interfaces. San Diego: Academic Press Limited.

Mitchell, J. K., 1993. Fundamentals of Soil Behavior. 2nd edition. New York: John Wiley and Sons Inc.

Mitchell, J. K., Yeung, T. C., 1991. "Electro-kinetic flow barriers in compacted clay," Transport. Res. Rec. 1288:1-9.

Muraoka, T., Ghazanfari, E., Shrestha, R., Pamukcu, S., 2011. "Electrically Induced Pore Pressures in High Salt Content Clay Slurry," *Separation and Purification Technology*, 79:133–138.

Nernst, W., 1888. Zur kintetik der in losung befindlichen korper. *Z. Phys. Chem*, 2:613–637.

Newman, J., 1991. Electrochemical Systems. 2nd edition. Englewood Cliffs, NJ: Prentice-Hall Inc.

Pamukcu, S. and Wittle, J. K., 1992. "Electrokinetic removal of selected heavy metals from soil," *Environ. Prog.*, 11(3):241-250.

Pamukcu, S., Wittle, J. K. 1993. "Electrokinetically Enhanced Insitu Soil Decontamination", Chapter 13. In: Remediation of Hazardous Waste Contaminated Soils. Wise DL, Trantolo DJ, editors, New York: Marcel Dekker Inc. pp. 245-298.

Pamukcu, S., Filipova, I., Wittle, J.K., 1995. "The Role of Electroosmosis in Transporting PAH Compounds in Contaminated Soils," Electrochemical Techn. Applied to Environmental Problems, Electrochemical Society Trans., PV95-12, 252-266.

Pamukcu, S., Weeks, A., Wittle, J.K., 1997. "Electrochemical Separation and Stabilization of Selected Inorganic Species in Porous Media," *Hazard. Mater.* 55:305-318.

Pamukcu, S. and Pervizpour M., 1998a. "Electrochemical Extraction of Cyanide and Fluoride from Conductive Porous Media," Final Report to EPI, Wayne, Pa, March, 1998. (*available from authors*)

Pamukcu, S. and Pervizpour, M., 1998b. "Electroosmotically Aided Restoration of TCE Contaminated Soil," Final Report to Lawrence Livermore National Laboratory, Environmental Restoration Division, Contract No.B3460123, University of California, Livermore, Ca, November, 52p, 1998.

Pamukcu, S., and Huang, C.P., 2001. "In-Situ Remediation of Contaminated Soils by Electrokinetic Processes," *Chapter 3.1* in Hazardous and Radioactive Waste Treatment Technologies Handbook, Oh, editor, CRC Press LLC.

Pamukcu, S., Weeks, A., Wittle, J. K., 2004. "Enhanced reduction of Cr (VI) by direct electric field in a contaminated clay," *Environ. Sci. Technol.* 38(4):1236-1241.

Pamukcu, S., Hannum, L., Wittle, J. K., 2008. "Delivery and activation of nano-iron by DC electric field," *Environ. Sci. Health A*, 43:934–944.

Pamukcu, S., 2009. "Electrochemical Transport and Transformations," Chapter 2 in Electrochemical Remediation Technologies for Polluted Soils, Sediments and Groundwater, eds. Reddy and Camaselle; John Wiley & Sons, pp. 29-65.

Pazos, M., Gouveia, S., Sanroman, M.A., Cameselle, C., "Electromigration of Mn, Fe, Cu and Zn with citric acid in contaminated clay," *J. Environ. Sci. Heal. A*, 43: 823-831.

Peng, C. Almeira, J.O. Gu, Q. 2013. "Effect of electrode configuration on pH distribution and heavy metal ions migration during soil electrokinetic remediation," *Environ. Earth Sci.* 69:257-265.

Planck, M. 1890. "Ueber die erregung von elektricitat und warme in electrolyten". *Ann. Phys. Chem*. 39(ser. 3):161–186.

Powell, R.M., Puls, R.W., Hightower, S.K., and Sabatini D.A., 1995. "Coupled Iron Corrosion and Chromate Reduction: Mechanisms for Subsurface Remediation," *Env. Sci. and Tech.*, 29(8): 1913-1922.

Probstein, R. F., Hicks, R. E. 1993. "Removal of contaminants from soils by electric fields," *Science*, 260:498–503.

Pulgarin, C., Adler, N., Peringer, P., Comninellis, C. 1994. "Electrochemical detoxification of a 1,4-benzoquinone solution in wastewater treatment," *Water Res*. 28:887–893.

Quigley, R. M., 1980. "Geology, mineralogy and geochemistry of Canadian soft soils: A Geotechnical perspective," *Canadian Geotech.* 20(2):288-298.

Quinke G (1861). Ueber die Fortfuhrung materieller Teilchen durch stromende Electrizitat. *Ann. Phy. Chem.* CXIII, 8:33.

Rai, D., Sass, B., and Moore, M., 1987. "Chromium (III) Hydrolysis Constants and Solubility of Chromium (III) Hydroxide," *J. Chem*., 26:345-349.

Rael, J., Shelton, S. and Dayaye, R., 1995. "Permeable barriers to remove benzene: candidate media evaluation," *J.of Environmental Engineering*, 121(5):411-415.

Ravina, I., Zaslavsky, D., 1967. "Non-linear Electrokinetic Phenomena I: Review of Literature," *Soil Sci.* 106(1):60-66.

Ray, C. and Ramsey, R. H., 1987. "Removal of Heavy Metals in Wastewater in a Clay Soil Matrix Using Electro-Osmosis," *Environ. Progr*., 6(3):145-149

Reddy, K. R., Parupudi, U., 1997. "Removal of Chromium, Nickel, and Cadmium from Clays by In-Situ Electrokinetic Remediation," *Soil Contam*. 6(4):391-407.

Reuss, F. F., 1809. Memories de la Societe Imperial des Naturalistes de Moscow 2:327.

Rojo, A. Hansen, H.K. Cubillos, M., 2012. "Electrokinetic remediation using pulsed sinusoidal electrical field," *Electrochim. Acta*, 86:124-129.

Rubinstein, I., 1990. Electro-Diffusion of Ions. SIAM Studies in Applied Mathematics, SIAM, Philadelphia, PA.

Ryu, B.G., Park, G.Y., Yang, J.W., Baek, K., 2011. "Electrolyte conditioning for electrokinetic remediation of As, Cu and Pb-contaminated soil," *Sep. Purif. Technol*., 79(2):170-176.

Sato, M., Kudo, N., Saito, M., 1998. "Surface tension reduction of liquid by applied electric field using vibrating jet method". IEEE Transactions on Industry Applications, 34(2).

Shang, J. Q., Lo., K. Y., Inculet, I., 1995. "Polarization and Conduction of Clay-Water-Electrolyte Systems". *Geotech. Eng*. 121(3):243-248.

Shapiro, A. P., Probstein, R. F., 1993. "Removal of Contaminants From Saturated Clay by Electroosmosis," *Env. Sci. Tech*., 27:283-291.

Shapiro, A. P., Probstein, R. F., Hicks, R .E., 1995. "Removal of Cadmium (II) From Saturated Kaolinite by Application of Electric Current," *Geotechnique*, 45:355-359.

Smith, R. W., Narimatsu, Y., 1993. "Electrokinetic Behavior of Kaolinite in Surfactant Solutions as Measured by Both the Microelectrophoresis and Streaming Potential Methods," *Miner. Eng*. 6(7):753-763.

Smoluchowski, M., 1914. Handbuch der Electrizitat und des Magnetismus, II. Edit. Graetz, S., 2: 366, Leipzig.

Sun, Y. P., Li, X. Q., Cao, J., Zhang, W. X., Wang, H .P., 2006. "Characterization of zero-valent iron nanoparticles," *Adv. Colloid Interfac. Sci.,* 120:47-56.

Tao, R., and Xu, X., 2006. "Reducing the Viscosity of Crude Oil by Pulsed Electric or Magnetic Field," Energy & Fuels 2006, 20:2046-2051

Weeks, A., Pamukcu S., 1995. "Utilization of Solubilizing and Stabilizing Agents in Electrokinetic Processing of Soils," Proc. 27th Mid-Atlantic Industrial Waste Conference, Technomic Publ. Co., Lancaster, PA, 824-834.

Weeks, Antoinette, 2002. "Electrokinetically Enhanced Reduction of Cr(VI) by Aqueous Fe(II) in Contaminated Clays," *PhD dissertation*, Lehigh University, Bethlehem, PA.

Weeks, A. and Pamukcu, S., 2001. "Electrokinetically Enhanced Reduction of Cr (VI) in Contaminated Soils," Proc. of the XVth Inter. Conf. on Soil Mechanics and Geotechnical Engineering, Balkema Publishers, 3:1935-1938.

Weinberger, R., 1993. Practical Capillary Electrophoresis. Academic Press, San Diego.

Wittle, J. K., Pamukcu, S., 1993. "Electrokinetic Treatment of Contaminated Soils, Sludges and Lagoons," DOE/CH-9206, No. 02112406, Argonne National Laboratories, IL, 65 p.

Wittle, J. K., Hill, D.C., Chilingar, G. V., 2007. "Electro-enhanced oil recovery (EEOR) using direct current," Oil sands heavy oil technologies conference, Calgary, Canada.

Wittle, J. K., Hill, D.C., Chilingar, G.V., 2008. "Direct Current Electrical Enhanced Oil Recovery in Heavy-Oil Reservoirs to Improve Recovery, Reduce Water Cut, and Reduce H2S Production while Increasing API Gravity," Society of Petroleum Engineers, SPE 114012.

Yeung, A. T., Hsu, C. N., Menon, R., 1996. "EDTA-Enhanced Electrokinetic Extraction of Lead," *Geotech. Eng*., 122(8):666-673.

Yin, J., Finno, R. J., Feldkamp, J.R., 1995. "Electroosmotic mobility measurement for kaolinite clay," Proceedings of the Specialty Conference on Geotechnical Practice in Waste Disposal. ASCE, Part 2 (of 2), New Orleans, LA, USA.

3

Application of Electrokinetics for Enhanced Oil Recovery

By Donald Hill

3.1 Introduction

Considerable hydrocarbon resources, of all grades, remain residual oil in many older "depleted" fields, which are being abandoned. Depending upon the reservoir type, light oil (i.e., greater than 20° API gravity) primary and secondary recoveries range from 25% to 75%. This means that at abandonment, as much as 75% of the *Stock Tank Original Oil In Place* (STOOIP) is left behind.

Heavy oil (i.e., less than 20° API gravity) crude recovery is severely limited because of the difficulty in extracting these high viscosity liquids from oil reservoirs. Primary recoveries as low as 10% of the STOOIP reserves are common. Enormous heavy oil resources exist throughout the world (Attanasi and Meyer, 2010; and Meyer, et al., 2007).

Both of these types (i.e., light and heavy) of residual oil resources are known, but are lacking a viable technology for their efficient and economic recovery. Table 3.1 shows a 2007 compilation of world heavy oil and

Table 3.1 World distribution of heavy oil and bitumen resources (after: Meyer et al., 2007)

Region	Heavy Oil		Bitumen	
	Estimated Total Original Oil In-Place (BBO)	Discovered Original Oil In-Place (BBO)	Estimated Total Original Oil In-Place (BBO)	Discovered Original Oil In-Place (BBO)
Eastern Hemisphere	1,617.4	1,617.4	854.96	771.46
Western Hemisphere	1,781.0	1,750.0	4,650.0	3,740.0
World	3,398.4	3,367.4	5,504.96	4,511.46
Africa	83.1	83.1	46.0	13.5
East Asia	168.0	168.0	10.5	10.5
Europe	75.3	75.3	17.0	17.0
Middle East	971	971	0.0015	0.0015
North America	651.0	650.0	2,390.0	1,670.0
Russia	182.0	182.0	347.0	296.0
South & Central America	1,130.0	1,100.0	2,600.0	2,070.0
South Asia	17.6	17.6	0.0	0.0
Southeast Asia & Oceania	68.0	68.0	4.46	4.46
Transcaucasia	52.4	52.4	340.0	340.4

bitumen resources. Whereas the numbers outside of North America are quite speculative, they do give an idea of the potential resource waiting for the right technology to recover it.

The shallowest unrecoverable oil reservoirs, such as the Shallow Athabasca Tar Sands, of Alberta, and McKittrick Field, of California, may be mined, if surface hydrocarbon extraction from the mined rock is economic. Various forms of steam-assisted recovery may work well for deeper

heavy oil reservoirs. Steam assisted recovery has also been utilized as a finishing technique for lighter oil reservoirs (Blevins et al., 1984).

Steam assisted oil recovery, however, may not always be an option. The maximum depth for steam extraction has been increasing but the practical limit still appears to be between 2,000 and 2,500 ft. Deeper unrecovered oil resources require alternative technologies. Many reservoirs also contain reactive matrix minerals, which can cause irreversible reservoir damage from steam recovery technologies.

Steam assisted oil recovery may also not be appropriate for very shallow resources (e.g., less than 500 ft.), because of the potential danger of steam breakthrough to the surface (Staff, 2011). Finally, steam assisted oil recovery may face environmental hurdles, in areas where water is in short supply, waste water disposal is a problem, and/or steam generators, compressors, and pumps require air permits.

Direct Current (DC) Electrokinetically Enhanced Oil Recovery (DCEOR) may be a viable alternative to steam assisted oil recovery because:

- It is operational outside of the above steam assisted oil recovery depth windows
- It has a negligible water demand
- It generates no waste-water streams, beyond that of normal water cut
- It appears to actually reduce water cut, below primary recovery levels
- It has a negligible to positive impact on reactive minerals
- It may actually clear pore throats of colloidal and fine grained particles
- It has negligible air quality impacts
- It may also reduce the production of noxious and toxic gases, such as H_2S

3.2 Petroleum Reservoirs, Properties, Reserves, and Recoveries

Before discussing Electrokinetically Enhanced Oil Recovery, we need to briefly review petroleum reservoirs, reserves, and multi-phase saturation, as well as primary, secondary, and enhanced recovery. This background is needed to better understand the impact of direct electrical current on oil production.

3.2.1 Petroleum Reservoirs

Unfortunately, some jurisdictions refer to petroleum reservoirs as *pools*, which conjures up images of vast underground lakes of petroleum. In reality, most petroleum reservoirs consist of porous rocks, which more closely resemble fine-grained sponges, rather than caverns filled with gas or lakes of liquid petroleum.

3.2.2 Porosity

Reservoir rocks may be though of as being made up of solids (matrix) and voids (pores). The percentage of rock volume occupied by pores is called porosity, Ø.

3.2.3 Reservoir Saturations

The pore spaces in reservoir rocks are usually filled with water, as well as oil and/or gas. Economic gases are light (C_1 – C_3) hydrocarbons. Common non-economic gases are air, N_2, and CO_2. Toxic gases include H_2S. Liquid petroleum is made up of the heavier (i.e., C_4 and above) hydrocarbon chain and ring molecules. Liquid contaminants are sulfur and heavy metal hydrocarbon compounds

Oil and water are immiscible, fluids, with neither particularly soluble in the other. Gas is soluble, to a point, in oil. Beyond that point, however, it becomes a separate phase. The same is true for gas and water.

Oil is (usually) less dense than water and gases are less dense than either oil or water. Because of these density differences, if all three are present in a given reservoir, they will segregate on the basis of density, with gas at the top and water at the base (i.e., much like Jell-O 1-2-3®). Pore throat surface effects at the contact between the fluids and rock matrix, however, will insure that these contacts are not always very sharp.

The types and amounts of fluids, which will co-exist at any given depth, will depend upon reservoir temperature and pressure, as well as pore space capillarity, surface tension between the immiscible fluids, wettability between the rock matrix and fluids, and the contact angle between the different immiscible fluids and the matrix. Clastic (sand and shale) reservoir rocks tend to be preferentially *water wet*, because of the polar nature of water and the net negative charges on the pore throat surfaces, due to cation substitution in silicate minerals. This results in some water, coating the pore throats, throughout the reservoir, making it preferentially water wet. Carbonate reservoirs tend to be preferentially non-water wet. If, however,

the carbonate reservoirs are lined with clay minerals they will also become partially to preferentially water wet.

The percentages of the pore space filled with water, oil, and/or gas, at any depth, is called water, S_w, oil, S_o, and/ or gas, S_g, saturation, respectively.

3.2.4 Initial Reserves

Initial reserves are the amounts of oil and/or free gas in the reservoir, before any production has taken place. For oil the definition is:

$$STOOIP = \frac{7758Ah\phi(1-S_w)}{B_{oi}}, \tag{3.1}$$

where: *STOOIP* is stock tank original oil in place, in bbls.
A is the reservoir closure area, in acres.
h is the average reservoir (net) thickness, in feet.
φ is the average reservoir decimal porosity.
S_W is the average reservoir decimal water saturation.
B_{oi} is the initial oil formation volume factor.
7758 is the acre-ft to bbls conversion factor (*different conversion constants will be required, for other unit systems*).

A similar relationship also exists for gas reserves.

3.2.5 Primary Oil Production and Water Cut

Wells are drilled into petroleum reservoirs to recover the oil and/or gas. Reservoir energy determines whether an oil well will flow (*without assistance*) or must be pumped. The reservoir energy is provided by dissolved gas, mechanical compaction, and/or hydraulic pressure within the reservoir. As a reservoir is depleted, more than one fluid type will be produced. For oil reservoirs, not only will oil be produced, but also associated gas (*gas cut*) and/or water (*water cut*).

3.3 Relative Permeability and Residual Saturation

Figure 3.1 is a generic representation of an oil/water (two phase) relative permeability determination, for a preferentially water-wet reservoir rock. For multi-phase systems, the relative permeability is a measure of the amount of each fluid, which can be produced from a reservoir and under

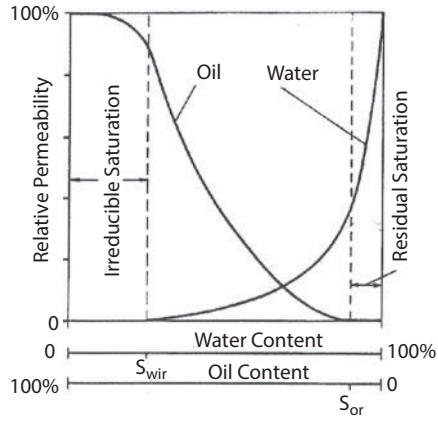

Figure 3.1 Generic relative permeability curves, for preferentially water wet reservoirs (after Cohen and Mercer, 1992)

what conditions. Laboratory relative permeability measurements are utilized by reservoir engineers to aid in depletion planning.

The oil/water ($k_{o/w}$) relative permeability curves are complex functions of:

- The pressure gradient within the reservoir
- The relative viscosities of the oil and water phases
- The interfacial tension, between the two immiscible phases
- The matrix wettability
- The capillary forces at the pore throat restrictions, within the matrix
- The amounts of oil and water (S_o and S_w) in the reservoir rock

At irreducible water saturation (S_{wir}), only oil will be produced. At residual oil saturation (S_{or}), only water can be produced. Comparing the relative permeability values at intermediate S_w and S_o values provides estimates of the oil production and water cut.

For depletion management, the goal is to keep as high on the oil saturation (S_o) curve as (economically) possible, by managing what can be managed (usually field balanced production rates) for primary recovery. In this fashion, oil production is maximized and the water cut is minimized, increasing income and reducing disposal costs.

During primary production, the reservoir drive declines and secondary measures, such as gas lift, gas flood, miscible gas injection, and water flood

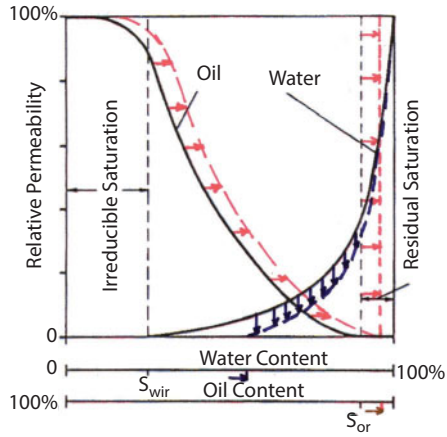

Figure 3.2 Enhanced oil recovery modification of oil/water (ko/w) and water/oil (kw/o) relative permeability, as well as residual oil (Sor) and irreducible water (Swir) saturations (after Hill, et. al., 2010)

are utilized to maintain production rates. However, even these measures will still leave considerable residual oil behind.

3.4 Enhanced Oil Recovery

The goal of *Enhanced Oil Recovery* (*EOR*) technologies is to reduce S_{or} and shift the $k_{o/w}$ curve to the right, as illustrated in figure 3.2, by changing the physical conditions of the reservoir, resulting in increased oil recovery, reduced water cut and lower S_{or}. This is accomplished by modifying one, or more, of the following reservoir matrix and/or fluid properties:

- The viscosities of the oil and water phases
- The interfacial tension, between the two immiscible phases
- The matrix wettability
- The capillary forces at the pore throat restrictions within the matrix

Different EOR technologies modify different combinations of the above reservoir matrix/fluid properties.

3.5 Electrokinetically Enhanced Oil Recovery

Electrokinetic electrical enhanced oil recovery involves inducing electrical current, from antennas, or passing electrical current, between electrodes, in the producing reservoir and either at the surface and/or at depth. These applications have seen several different incarnations. When electrical current is introduced into the ground, several electro-chemical processes can, and usually do occur. Optimum application of electrical current for maximum effectiveness resides in the art of application.

3.5.1 Historical Background

Several groups and individuals have considered using electrical current for enhanced oil recovery (EOR). One of the earliest proposed electrical EOR technologies was by Workman (1930). His patent (which does not appear to have progressed beyond hypothesis) proposed conducting electrolysis in the water legs of oilfields to release gases (presumably hydrogen and oxygen):

> *". . . which permeate, or are absorbed by the oil to render the same lighter and more mobile which facilitates its release from the sand and causes it to rise to the top of the water in the well".*

There is no documentation that this inventor ever attempted to evaluate or implement his ideas. The reference is included only as a benchmark that someone had considered using electricity for EOR as early as 1930.

Sarapuu (1957) proposed using high-density electrical currents to *"carbonize"* hydrocarbons to enhance extraction via well bores. Bell (1957) proposed using high density DC current to drive oil from reservoirs into wells. Again, there is no evidence that either of these technologies progressed beyond the patent stage.

Gill (1970, 1972) and Crowson and Gill (1971) proposed using alternating current (AC) electricity to heat oil reservoirs, which would decrease the oil viscosity and enhance its recovery. Low frequency alternating current (AC) heating was evaluated in Canadian heavy oil fields (McGee, 2008; McGee et al., 1999). Electro-magnetic (EM) heating was evaluated by Cute et al. (1987), Chute and Vermeulen (1988), and Sahni et al. (2000). Radio frequency (RF) induction EOR was evaluated by Kasevich et al. (1994). All of these authors have advocated EM for near wellbore heating to reduce oil viscosity. AC current, however, poses problems such as corrosion of all electrodes, inductive energy loss, and shallow penetration away from the

electrodes or antennas. By contrast DCEOR does not experience any of these problems

Downhole resistive heaters have also been proposed for heating the near wellbore (Sandberg et al., 2013; Vinegar and Bass, 2007; and Vinegar et al., 2006a, 2006b, & 2007).

Several major oil company research and development (R&D) subsidiaries and national laboratories have investigated various AC, Electromagnetic, Radio Frequency, Microwave, and downhole heaters for EOR (e.g., Sahni et al., 2000).

3.5.2 Geotechnical and Environmental Electrokinetic Applications

Electrokinetics have been applied for geotechnical and environmental restoration problems, as well as EOR. Knowledge gained in any of these applications can, and should be, applied to understanding the others.

Leo Casagrande pioneered the use of electroosmosis for construction soil dewatering and stabilization (Anon, 1966; Casagrande, 1952, & 1959; Casagrande et al., 1961). Farris (1968) described the use of anodes and cathodes in a formation as a mechanism for dewatering it. Mitchell (1970) also described using electroosmosis to dewater soil, and was actually retained as a consultant for stabilization attempts at the Campanile at the Cathedral of Pisa, Italy. Gray and Mitchell (1967) provided the current electrochemical basis of electroosmosis: i.e., that the electroosmotic membrane is not a physical membrane but a cation-selective membrane due to the Helmholtz double layer filling pore-throat constrictions. Mitchell (1993) also has an extensive discussion of the electrochemical basis for electro-osmosis. Gray and Schlocker (1969) described electrokinetic alteration of clay minerals. Tchillingarian (1972) described the use of electrophoresis to move fine-grained clays through porous rocks.

Acar and Alashawabkeh (1993) and Acar and Gale (1992) discussed using electrokinetics to decontaminate heavy metal contaminated soils. Bruell et al. (1992), Hill (1994, 1997, 1998), and Hill et al. (1997) utilized electroosmosis to remove gasoline hydrocarbon and TCE contamination of soils. Chilingar et al. (1997) utilized electrokinetic remediation of hydrocarbon and metallic soil contamination. Döring (1993, 1996), Döring et al. (2000, 2001, & 2008), Iovenitti et al. (2003), and Lageman et al. (1989) also applied electrokinetics for the remediation of both organic and inorganic soil contamination, with some rather dramatic case histories. Döring (1993 1996) and Döring et al. (2000, 2001) demonstrated the destruction of organic contamination by breaking down complex organic molecules

into simpler daughter products. Wittle and Pamukcu (1993) and Pamukcu (1994) utilized electrokinetics for treatment of soils and sludges contaminated with hydrocarbon and metals.

3.5.3 Direct Current Electrokinetically Enhanced Oil Recovery

Direct Current Electrokinetically Enhanced Oil Recovery (DCEOR) was originally conceived of at a unit of General Electric (Bell and Titus, 1973 & 1974). The DCEOR technology is currently being evaluated and commercial applications developed by start-up organizations in the U.S., Canada, and Argentina (Bell et al., 1985; Hill et al., 2010; Stainoh, 2011; Titus et al., 1985; Wittle and Bell, 2005 & 2008; Wittle and Hill, 2006a & 2006b; and Wittle et al., 2006a, 2006b, & 2011). These private organizations, collectively, have spent several years and millions of U.S. dollars in R&D to evaluate and overcome field operational difficulties encountered during development. Their combined efforts resulted in successful DCEOR demonstrations at California, Alberta, and in Argentina's heavy oil fields.

During the 1950s and 1960s, George V. Chilingar and his students, at the University of Southern California (USC), conducted numerous laboratory tests involving electrokinetics. These tests suggested that this low power drain DC electrical mechanism could be used for EOR (Ace, 1975; Amba et al., 1964, 1965; Chilingar et al., 1968, 1970, 1997). Tikhomolova (1993) described similar studies conducted at the University of St. Petersburg also suggesting electro-osmosis as a potential EOR technology. Sibel Pamukcu and her students at Lehigh University have conducted numerous laboratory tests investigating potential DCEOR mechanisms and effects (Al Shalabi et al., 2012; Ghazanfari et al., 2012 & 2013).

3.6 DCEOR and Energy Storage

Several authors (Chelidze, 1969; Hill, 1972; Howell and Licastro, 1961; Katsube, 1975; Keller and Licastro, 1975; Rokityansky, 1959; Scott et al., 1967; and Ward and Fraser, 1967) have used Lossy dielectrics as analogues for the electrical behavior of rocks. Rocks and soil can store electrical energy, much like a battery or supercapicator (Conway, 1999; Mayper, 1959a & 1959b; and Wait, 1959). If a step potential is introduced between two electrodes in the ground, the current passing between them will not follow a step function, but will rather spike and then decay exponentially with time to some steady state value. If the step potential is removed, the

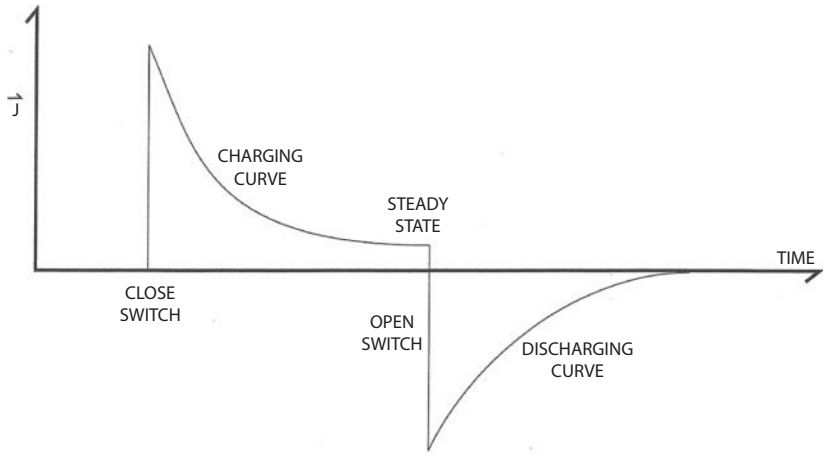

Figure 3.3 Generalized rock/soil charging and discharging current (after Hill, 1999)

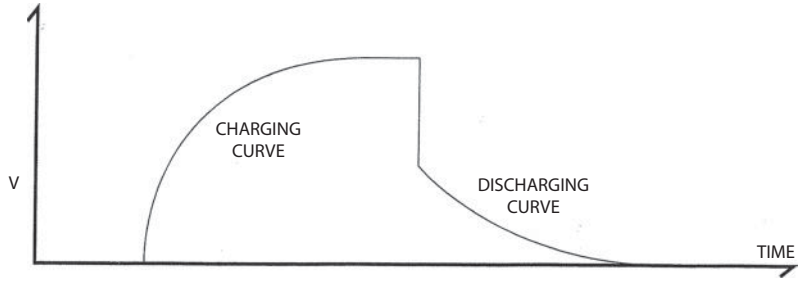

Figure 3.4 Generalized rock/soil charging/discharging potentials (after Hill, 1999)

current will change polarity, spike, and then decay to zero. This is shown schematically in figure 3.3.

The potential difference between two potential electrodes (i.e., NOT the two current electrodes) will rise asymptotically to some limiting value. If the current is then cut off, the potential will drop sharply, to some intermediate value and then decay exponentially to zero, as shown in figure 3.4. The earth responses, shown in figures 3.3 and 3.4, are similar to that of a capacitor in an electrical circuit and are indicative of (electrical) energy storage (Hill, 1999).

Conrad Schlumberger first observed the phenomena shown in figures 3.3 and 3.4 and disclosed his observations in a 1912 German Patent (Sumner, 1976). Schlumberger named the phenomenon *polarisation provoquée* (*PP*), which has the excepted translation of "Induced Polarization" (IP) in the geophysical community (Schlumberger, 1920; Sumner, 1976). Schlumberger

attributed the phenomenon to the presence of metallic mineralization, but claimed that background effects often masked metallic mineral PP (IP) anomalies, to the extent that they were difficult to identify. Later studies identified the source of these anomalies as due to *Membrane Polarization* in clay mineral sand mixtures (Hill, 1999; Komarov and Shmarova, 1961; Mayper, 1959a & 1959b; and Sumner, 1976). Faced with the *polarization provoquee* signal/noise problem, Conrad Schlumberger concentrated on using surface equal potential and resistivity mapping to locate ore bodies and later gravitated to making wireline measurements in oil wells, co-founding the oilfield services firm, Schlumberger, which bears the family name.

3.6.1 Mesoscopic Polarization Model

If one imagines that the subsurface rocks can be thought to host a mesoscopic (i.e., pore scale and larger) distribution of polarization sites, then in the absence of an electrical field, these polarization sites remain unpolarized (see figure 3.5). In the presence of an electric field, however, these sites become polarized over time, as shown in figure 3.6, resulting in a volume polarization field, in opposition to the electrical field. If the electrical field is removed, the polarization sites gradually decay, resulting in a current in opposition to the charging current. This discussion, as well as figures 3.5 and 3.6, provide a qualitative explanation of the observations, shown schematically, in figures 3.3 and 3.4.

Note: The current discussion and the schematic models of figures 3.5 and 3.6 are mechanism independent.

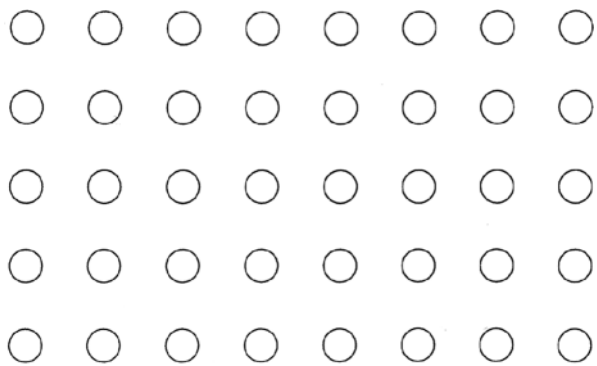

Figure 3.5 Schematic representation of polarizable rock/soil as a mesoscopic distribution of unpolarized polarization sites (after Hill, 1999)

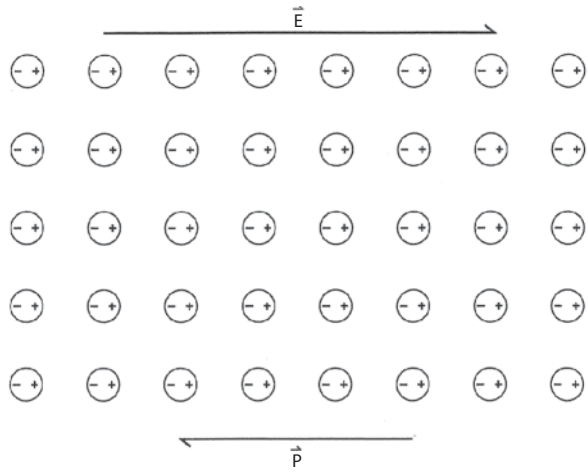

Figure 3.6 Schematic representation of figure 3.5. Rock/soil polarized by an electric field, E (after Hill, 1999).

3.7 Electro-chemical Basis for DCEOR

When electrical current is passed between electrodes embedded in the earth, several phenomena can, and usually do, occur. The best way to treat this situation is via the concept of coupled flows, introduced by Lars Onsager (1931a, 1931b), for which he received the 1968 Nobel Prize in chemistry (Onsager, 1969).

3.7.1 Coupled Flows and Onsager's Principle

Five mechanisms appear to be operative, in DCEOR, based on available field and laboratory data:

- Joule heating
- Electromigration
- Electrophoresis
- Electroosmosis
- Electrochemically enhanced reactions

These mechanisms are often collectively called *electrokinetics*. Figure 3.7 is a qualitative representation of the relative energy requirements for these mechanisms (with the middle three merged as "electrokinetic mass transport"), as well as that required for electrically fusing (melting) the rock.

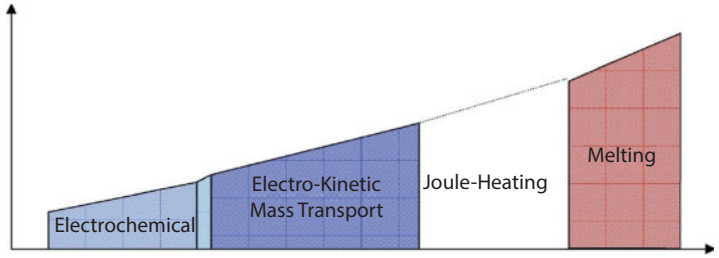

Figure 3.7 Schematic representation of the energy requirements of various electrokinetic mechanisms and electrical melting (after Wittle et al., 2008c)

All of the above five mechanisms are coupled reactions. Nourbehecht and Madden (1963), as well as Mitchell (1993) provide simple linear algebra and tensor representations.

In matrix notation, Onsager's relationships can be represented as:

$$\begin{bmatrix} \mathbf{J}_1 \\ \mathbf{J}_2 \\ \mathbf{J}_3 \\ \mathbf{J}_4 \\ \mathbf{J}_5 \\ \mathbf{J}_6 \end{bmatrix} = \begin{bmatrix} \mathbf{L}_{11} & \mathbf{L}_{12} & \mathbf{L}_{13} & \mathbf{L}_{14} & \mathbf{L}_{15} & \mathbf{L}_{16} \\ \mathbf{L}_{21} & \mathbf{L}_{22} & \mathbf{L}_{23} & \mathbf{L}_{24} & \mathbf{L}_{25} & \mathbf{L}_{26} \\ \mathbf{L}_{31} & \mathbf{L}_{32} & \mathbf{L}_{33} & \mathbf{L}_{34} & \mathbf{L}_{35} & \mathbf{L}_{36} \\ \mathbf{L}_{41} & \mathbf{L}_{42} & \mathbf{L}_{43} & \mathbf{L}_{44} & \mathbf{L}_{45} & \mathbf{L}_{46} \\ \mathbf{L}_{51} & \mathbf{L}_{52} & \mathbf{L}_{53} & \mathbf{L}_{54} & \mathbf{L}_{55} & \mathbf{L}_{56} \\ \mathbf{L}_{61} & \mathbf{L}_{62} & \mathbf{L}_{63} & \mathbf{L}_{64} & \mathbf{L}_{65} & \mathbf{L}_{66} \end{bmatrix} \begin{bmatrix} \nabla\phi_1 \\ \nabla\phi_2 \\ \nabla\phi_3 \\ \nabla\phi_4 \\ \nabla\phi_5 \\ \nabla\phi_6 \end{bmatrix}. \tag{3.2a}$$

or, using the simpler tensor notation, they are:

$$\mathbf{J}_i = \sum_{j=1}^{6} \mathbf{L}_{ij} \nabla\phi_j \,. \tag{3.2b}$$

where: J_i are generalized flow, or flux vectors.
$\nabla\emptyset_j$ are generalized potential gradient, or force, vectors.
L_{ij} are generalized conductivity, or coupling coefficient (second rank) tensors.

The direct flow, or main diagonal terms, L_{ii}, of Equation 2a relate non-coupled fluxes to their potential gradients, whereas the off diagonal terms, L_{ij}, relate coupled fluxes.

Reviewing Equations 3.2a and 3.b2b, one can observe that:

- If J_1 is electrical current density and $\emptyset_1$ is electrical potential, then L_{11} is the electrical conductivity tensor, σ, whereas

the coupled flow coefficient, $L_{1,3}$, includes junction potential and the coupled flow coefficient, $L_{1.5}$, includes Streaming Potential and Membrane Potential.

- If J_2 is heat flow and $\emptyset_2$ is temperature, then L_{22} is thermal conductivity tensor, K, while the coupled flow coefficient, $L_{2,1,}$ includes Joule Heating.
- If J_3 is ionic flux and $\emptyset_3$ is ionic concentration, $L_{3,3}$ is (ionic) diffusion coefficient, $D_{i,}$ then the coupled flow coefficient, $L_{3,1}$, includes electro-migration.
- If J_4 is charged particle flux and $\emptyset_4$ is charged-particle suspension density, $L_{4,4}$ is the (charged particle) diffusion coefficient, D_p, and the coupled flow coefficient, $L_{4,1}$, includes electro-phoresis.
- If J_5 is fluid flux and $\emptyset_5$ is pressure, then $L_{5,5}$ is k/μ, k is the absolute permeability tensor, μ is the fluid viscosity, and the coupled flow coefficient, L_{51}, includes electro-osmosis.
- If J_6 is chemical reaction product flux and $\emptyset_6$ is the chemical reactant concentration, then $L_{6,6}$ is the chemical reaction rate constant, and the coupled flow coefficient, $L_{6,1}$, includes electro-chemically enhanced reactions.

If the units of the left hand side (LHS) fluxes J_i and the right hand side gradients, $\nabla\emptyset_j$, of equations 3.2a & 3.2b are such that their products, $J_i \bullet \nabla\emptyset_j$, represent free energy dissipation, then, by *Onsager's Principle*:

$$\mathbf{L}_{ij} = \mathbf{L}_{ji}\,. \tag{3.3}$$

Onsager's Principle (equation 3) is extremely useful because it is often easier to measure one of the pair of coupled coefficients than the other.

The five DCEOR (electrokinetic) mechanisms listed above, as well as Streaming and Membrane Potentials, are all (equations 3.2a & 3.2b) off diagonal and, as such, are coupled mechanisms. Lorenz (1952) discusses the relationship between two coupled flows: Electro-Osmosis and Streaming Potential. The Primary DCEOR mechanisms are described below.

3.7.2 Joule Heating

The formation is heated by the passage of the electrical current through conducting fluids and solids within the reservoir. Electrical heating elements, such as stovetop burners and space heaters, are based on Joule heating. Joule heating of the reservoir matrix and fluids raises the reservoir

temperature and lowers the viscosity of the crude, making it easier to produce. As shown in figure 3.7, Joule Heating requires the largest energy dissipations and consequently the greatest potential (voltage) gradients of the 5 DCEOR mechanisms.

3.7.3 Electromigration

Movement of dissolved ionic components, such as (positively charged) cations and (negatively charged) anions under the influence of an applied electric field. Electromigration forms the basis of electro-refining and electro-plating metallurgical processes, where metallic cations migrate from anode to cathode. Asphaltenes, which are negatively charged, will migrate toward the anode.

3.7.4 Electrophoresis

Charged colloidal particles, suspended in solution, will also migrate under the influence of an electrical field, similar to electromigration. In as much as clays are generally negatively charged, they will move away from the cathode and toward the anode. This process may clear blocked pore-throats and improve permeability, resulting in increased oil production (Tchillingarian, 1952) or be used to transport organisms and nutrients (Chilingar et al., 1997).

3.7.5 Electroosmosis

Helmholtz double layers formed in the connate waters adjacent to clay minerals form cation selective membranes in narrow pore throats, allowing hydrated cations and water molecules to pass through the pore throats, but blocking hydrated anions. The membrane, in this case, is not a physical membrane as it is in membrane filters, but an electrochemical one. This mechanism has been utilized to dewater expansive clays, and increase apparent reservoir permeability, resulting in increased oil production. This is essentially the definition of electroosmosis used by Leo Casagrande (1952, 1959), as well as that used by Gray and Mitchell (1967), Mitchell (1993), and Tikhomolova (1993).

3.7.6 Electrochemically Enhanced Reactions

Reactions between the pore fluids and matrix materials enhanced by Eh/pH changes brought about by the passage of electrical current. Electrochemically enhanced reactions appear to enhance the breakdown

of complex hydrocarbons, resulting in simpler (hydrocarbon) daughter products, which have lower viscosities than the original components, and increase reservoir energy. Both of these conditions will enhance oil production. As shown in figure 3.7, electrochemically enhanced reactions, field experience has demonstrated that this mechanism only occurs in very low potential (voltage) gradient situations (Döring 1993 and 1997; Döring et al., 2000, 2001, and 2003).

Of the five electrokinetic mechanisms, Joule heating requires the largest amount of energy and, consequently, the highest potential (voltage) gradient, while the electrochemically enhanced reactions require the lowest. The other three mechanisms: electromigration, electrophoresis, and electroosmosis, all have intermediate energy and voltage gradient requirements.

3.8 Role of the Helmholtz Double Layer

3.8.1 Dissociation of Ionic Salts

Water is a very unique fluid. The covalent hydrogen - oxygen bonds result in an H-O-H angle of 105°. Because both hydrogen ions are on the same side of the oxygen ion, the water molecule is strongly polar (dielectric constant of 78.54 at STP). It quickly dissociates electrolyte salts (e.g., NaCl) into positive ions, or cations (such as Na^+) and negative ions, or anions (such as Cl^-). The Na^+ ion is one electron short of electrical neutrality, whereas the Cl^- ion has one excess electron. The net result is the Cl^- ion is about twice the size of the Na^+ ion and one-half the size of water molecules. Each of the dissociated (positively charged) cations and (negatively charged) anions, in aqueous solutions, are hydrated, surrounded by envelopes of water molecules with poles of opposite charge (from that of the ion) facing the ions, attempting to neutralize the ionic charges (as shown, schematically in figure 3.8).

In free solutions, the hydrolyzed (in water molecule clouds) ions are free to move and their relative numbers are comparable to what they were in the solid (i.e., crystalline) state. However, this all changes near the matrix of clastic rocks.

3.8.2 Silicates

The most common minerals in clastic rocks are silicates, cations surrounded by silicate radicals. The basic silicate building block is a tetrahedron, with a silicon ion at the center and oxygen ions on the four corners.

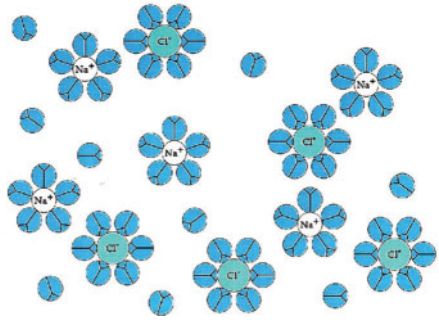

Figure 3.8 Schematic representation of NaCl dissolved in water (after Hill et al, 1997). Water molecules (in blue), with positive poles adjacent to Cl- anions and negative Poles adjacent to Na+ cations.

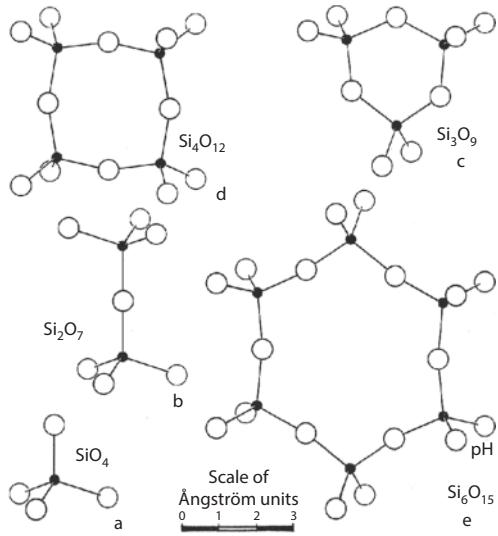

Figure 3.9 Silicate tetrahedra linkage (after Berry and Mason, 1959). a) Independent tetrahedra; b) Double tetrahedra; c – e) Ring structures.

These silica tetrahedra are the building blocks of silicate minerals, much like methane tetrahedra are building blocks of organic molecules (see figure 3.9). Unlike hydrocarbons, most of which are either gases or liquids, at room temperature, however, silicates are all solid crystals.

In addition to the simple silicate tetrahedra, silicates also form single and double chains, as well as sheet structures and three-dimensional networks (see figure 3.9). The common feature, of silicate crystal lattices is that they all consist of cations surrounded by anions and/or silicate radicals.

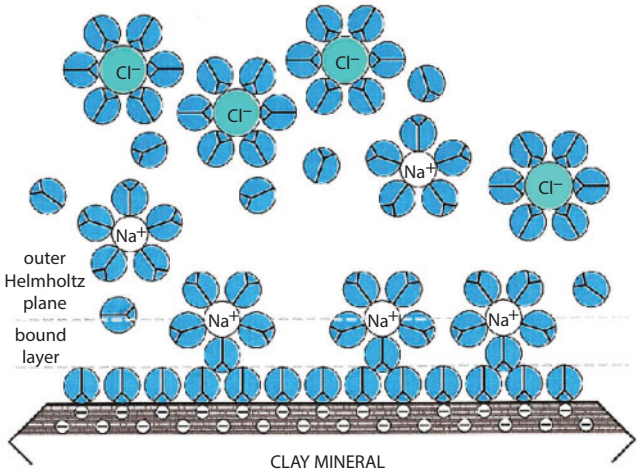

Figure 3.10 Schematic representation of the formation of the Helmholtz Double Layer adjacent to a clay mineral surface (after Hill et al, 1997)

This means that the negative portions of the (neutral) crystals are on their external surfaces.

Many rock-forming minerals do not have fixed chemical formulas, but allow substitutions of cations, within their crystal lattices. In many silicate minerals, this cation substitution involves the substitution of divalent (e.g., Fe^{+2}) for trivalent (e.g., Al^{+3}) cations, or tri-valent (e.g., Al^{+3}) for quadra-valent (e.g., Si^{+4}) cations, in the crystal lattice, resulting in a net negative surface charge on the crystal surface. This net negative charge density on the mineral crystal surfaces attracts the positive poles of water molecules and dissociated cations, while repelling the negative poles of water molecules and dissociated anions in solution (as shown in figure 3.10).

3.8.3 Phillosilicates and Clay Minerals

Reservoir rocks often contain significant amounts of clays (clay-sized particles, and/or clay minerals) within their matrixes. Clay particle size grains are usually phillosilicates or sheet-silicates, such as micas and clay minerals, which have net negative surface charges.

Phillosilicate and clay mineral crystals are composed of composite sheets of AlO_6 octahedra and SiO_4 tetrahedra layers. The substitution of divalent for trivalent cations, in the octahedra layers or trivalent for quadra-valent cations, in the tetrahedra layers leaves strong net negative charge densities on the flat mineral phillosilicate crystal surfaces. Different clay minerals

have differing amounts of excess negative surface charge. This variation in net negative surface charge affects the number of dissociated cations, which will attach themselves to the clay minerals.

This discussion covers silicate minerals and clastic (sand/shale) reservoirs, which tend to be preferentially water wet. This condition results in the continuous electrolytically conductive current pathways along the walls of the reservoir pore throats.

Some of the world's most significant hydrocarbon reservoirs are carbonates, however, which tend to be preferentially *non*-water wet. Except for very high S_w, these reservoirs would not expect to have continuous electrolytic current pathways, because of the hydrocarbons covering the pore-throat walls. If, however, there are significant clay minerals coating the pore throats of the carbonate reservoirs, they should begin to behave much like the clastic reservoirs.

3.8.4 Cation Exchange Capacity

In addition to the net surface charge, phillosilicates and clay mineral crystal structures are composites of layered silicates. The space between the composite layers can be filled with water and/or hydrated cations, as shown in figure 3.11. A measure of the interlayer cation attraction is called cation exchange capacity (CEC) and is measured by determining the number of cations, which can be exchanged on the clay minerals (Mitchell, 1993). CEC is commonly measured in meq/gm. A more useful measure of CEC, for determining the electrochemical and flow behavior of shaly-sands silts, and, perhaps, even shaly carbonates is the CEC/unit pore volume, Q_v, of Waxman and Smitts (1968):

$$Q_v = \frac{CEC}{V_p}, \tag{3.4}$$

where: Q_v is CEC per unit Pore volume, in meq/ml.
CEC is cation exchange capacity, in meq/gm.
V_p is the pore volume, in ml/gm.

The Q_v measure of CEC converts it from a mass measure to a specific volume measure. It also provides a direct link between CEC and:

- The membrane spontaneous potential
- Resistivity behavior of shaly-sands
- Streaming potential

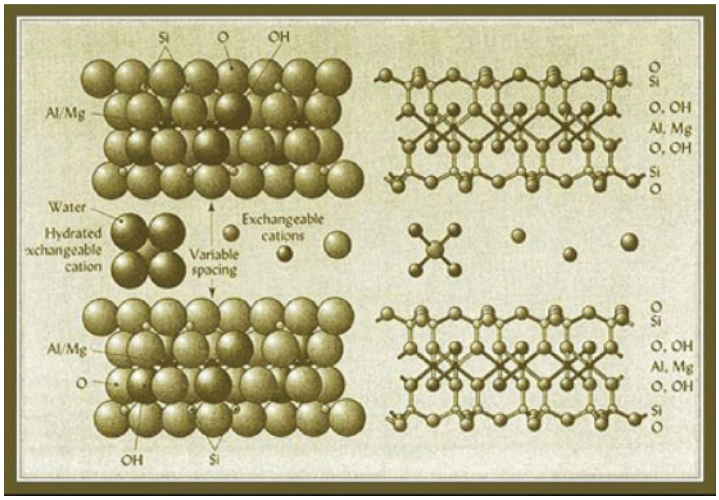

Figure 3.11 Montmorillonite Crystal structure Showing Interlayer Water and Exchangeable Cations (after UBC Website)

- Electro-osmosis
- Induced polarization *Normal Effect* in shaly-sands

Shaly sands with high Q_v, tend to have lower permeability than those with low Q_v.

3.8.5 Electrochemistry of the Double Layer

Water is such a strong polar molecule that it preferentially (over non-polar and weakly polar petroleum molecules) wets the clay mineral surfaces, making them hydrophilic, or preferentially water-wet. The bound layer of water molecules is held tightly enough by the electrostatic attraction from the excess negative charges in the clay mineral surfaces that these water molecules do not move under normal sub-surface forces.

When water comes in contact with clay, or another phillosilicate, the water molecules closest to the surface align themselves with their positive (hydrogen ion) pole opposite the negative charges on the surface of the silicate minerals (figures 3.10 and 3.12). This region of water molecules (which may be from a single-molecule to several-molecules thick) is tightly bound to the surface of the clay minerals, and is variously called the "bound layer", "Stern layer", or "inner Helmholtz layer". The inner layer may or may not contain cations from ionic salts in solution but ***will not contain any anions***.

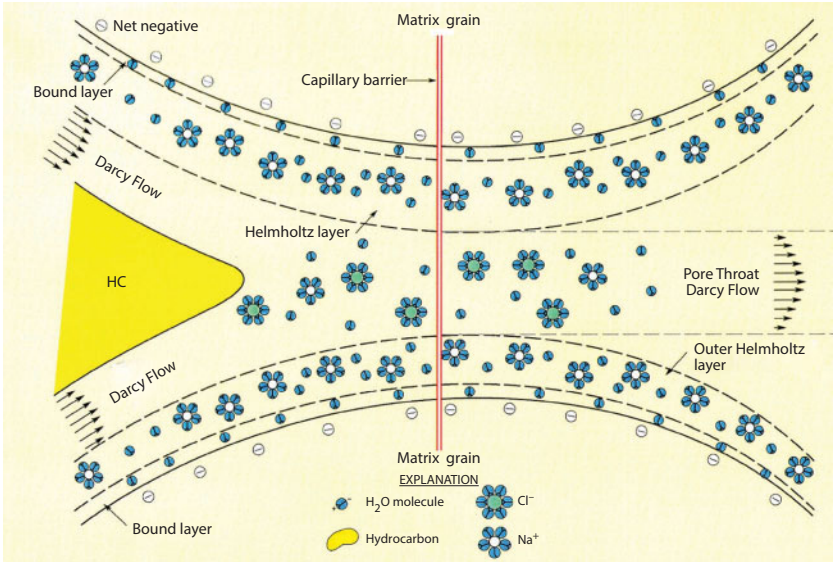

Figure 3.12 Pore throat schematic showing double layers forming adjacent to clay mineral surfaces and restricting darcy flow through the center of the pore throat (after Hill et al., 1999)

Figure 3.12 is a schematic diagram of a pore throat, illustrating the Helmholtz double layer lining. It is formed, in preferentially water-saturated rocks, by the attractive forces between the electrically negative surfaces of minerals and the positive poles of water molecules and positive (cat) ions, in aqueous solution (connate waters). There are no negative anions within the Helmholtz double layer.

This electrical double layer is divided into two electrochemical regions:

- A region of fixed water molecules and cations (Bound, Stern, or Inner Helmholtz layer), held by strong electrostatic forces to negatively charged mineral surfaces.
- A more mobile region of loosely bound cations and water molecules (Outer Helmholtz, or Gouy layer), which are partially shielded from the negatively charged mineral surfaces by the water molecules and cations of the Stern layer. These loosely bound cations and water molecules can move in the presence of an electrical external field.

If the pore throats are large enough, a third electrochemical region (free fluid) exists, containing water molecules, as well as both anions and cations.

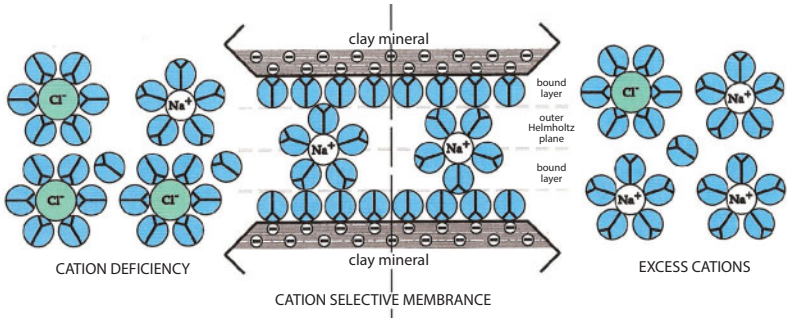

Figure 3.13 Schematic representation of the formation of a cation-selective membrane in a constricted pore throat (after Hill et al., 1997)

In preferentially water wet rocks, this is the portion of he pore throats, where hydrocarbons will reside. If the pore throats are small enough, however:

- The Helmholtz double layers completely fill the pore throat
- The pore throat becomes an electrical cation selective membrane (see figure 3.13)

Even if the Helmholtz double layers do not completely fill the pore throats, capillary forces will restrict the non-wetting fluid from entering the pore throats.

There is a shear, or slipping plane surface between the Stern and Gouy layers, which allows movement of the Gouy layer cations without disturbing the Stern layer. The potential difference between this plane and the free fluid is the Zeta Potential (Chilingar et al., 1970).

Upon application of DC current, the mobile Gouy layer migrates, in the direction of the electrical field, toward the negative (cathode) electrode. This motion of the water molecules and cations within the Gouy layer, results in the following:

- The motion of the water molecules and cations within the Gouy layer effectively opens the diameter of the pore throat to the bound, Stern layer, as shown in figure 3.14.
- Cations, anions, and other fluids in the free fluid will be dragged through the (now enlarged) pore throat.
- Both the wetting and non-wetting fluids will be produced.

Extensive experimental work, conducted at The University of Southern California (Ace, 1955; Amba et al., 1964, 1965; Chilingar et al., 1968,1970,

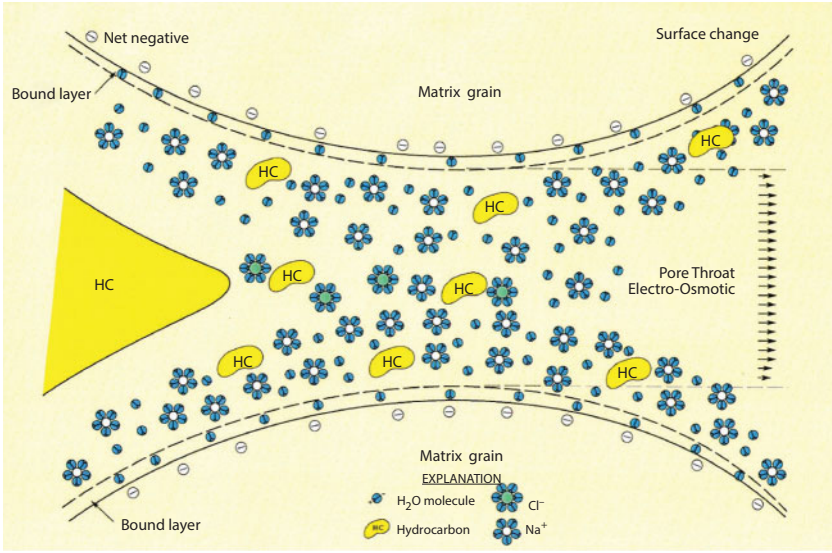

Figure 3.14 Pore throat schematic showing electrokinetic transport of the outer Helmholtz layer, modifying the effective pore throat size for fluid flow (after Hill, 1999)

1997,1997, Tchillingarian, 1952) showed up to forty-fold volumetric fluid flow increases in cores containing clays, compared to only 2 – 3 fold increases in pure silica cores, as shown in figure 3.15. Chilingar, et. al. (1970) speculated that this latter (silica core) fluid flow might be due to a thermal effect. Mitchell (1993) maintained that all silica minerals show increased flow, under DC fields, but that those with high cation exchange capacity (CEC) exhibit the greatest flow increases. The results in figure 3.15 agree with Mitchell's (1993) argument.

For those pore throats completely filled with the Helmholtz double layer, the application of current will develop salinity gradients across the cation selective membranes, which will store energy. Any fluctuation in the local electric fields will result in discharge of this stored energy, similar to discharging a super capacitor (Conway, 1999), potentially inducing a breakdown of complex hydrocarbon molecules, resulting in simpler daughter product molecules.

3.9 DCEOR Field Operations

Figure 3.16 illustrates one possible DCEOR field implementation, where anode(s) are placed near the ground surface and cathode(s) are placed in, or near, producing well(s). An alternative configuration utilizes both

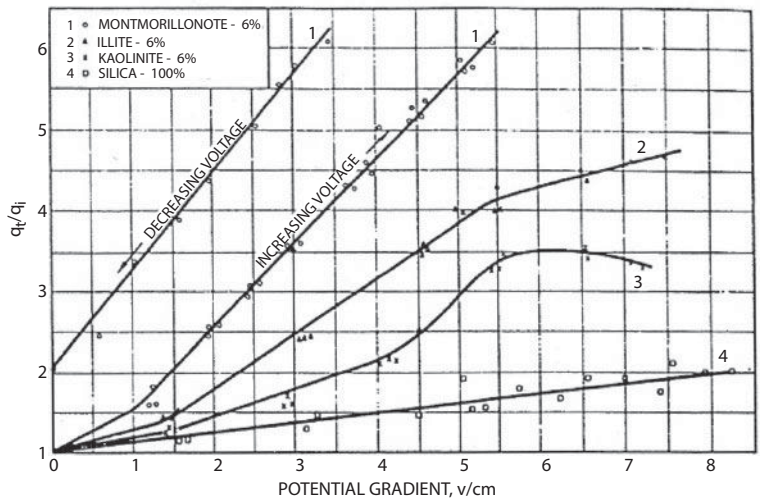

Figure 3.15 Relationship between potential gradient and normalized electrokinetically induced fluid flow, for different silica-clay mineral mixtures. Core No. 1: 94 % silica sand & 6% montmorillonite clay. Core No. 2: 94% silica sand & 6% illite clay. Core No. 3: 94% silica sand and 6% kaolinite clay. Core No. 4: 100% 200-mesh silica sand (after Chilingar, et al., 1970).

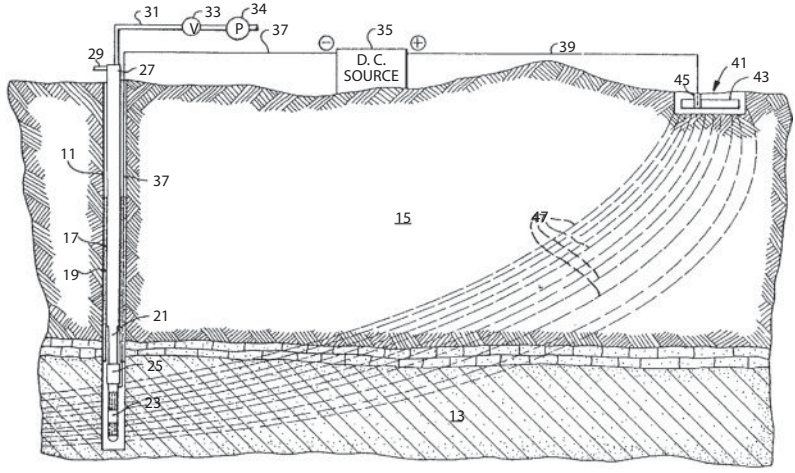

Figure 3.16 DCEOR Field Operation Schematic Rendering (after: Amba et al., 1965; Titus et. al., 1985)

anode(s) and cathode(s) in the subsurface. Successful field pilots have utilized anode-cathode separations of as much as 400 m, or 0.25 mi (Wittle and Hill, 2006a, 2006b; Wittle et al, 2008a, 2008b, and 2008c; Wittle et al, 1011).

3.9.1 Three-Dimensional Current Flow Ramifications

A common misconception is that three-dimensional electrical current flow in the subsurface can be represented by one-dimensional linear (Kirchhoff) circuit theory. For *one-dimensional linear circuit theory*, Ohm's law is:

$$I = \frac{\Delta V}{R} \tag{3.5}$$

or:

$$\Delta V = IR \tag{3.6}$$

Joule heat loss *across a given circuit element*, of resistance R, is given by:

$$P = I\Delta V = I^2 R, \tag{3.7}$$

where: P is the power loss, over the *individual* circuit element, of resistance, R.
ΔV is the voltage drop across the *individual* circuit element.
R is the *individual* circuit element resistance.
I is the current through the *entire* circuit, controlled by the ***total voltage drop across the entire circuit and the sum of all of the resistances*** in the circuit.

In three-dimensions, however, Ohm's law (Equation 3.5) becomes:

$$\mathbf{J} = \sigma\mathbf{E} = \sigma\nabla\phi = \rho^{-1}\nabla\phi, \tag{3.8}$$

or:

$$\nabla\phi = \rho\mathbf{J}. \tag{3.9}$$

*In three-dimensions, the **local** Joule heating power loss* is given by:

$$p_{x,y,z} = \mathbf{J} \bullet \mathbf{E} = \mathbf{J} \bullet \nabla\phi = |\mathbf{J}|^2 \rho \tag{3.10}$$

where: p_{xyz} is the *local* power loss, at the point of interest.
E is the *local* electric field vector, at the point of interest.
$\nabla\emptyset$ is the *local* electrical potential field gradient, at the point of interest.
$\boldsymbol{\sigma}$ is the *local* electrical conductivity tensor, at the point of interest.
$\boldsymbol{\rho}$ is the *local* electrical resistivity tensor (inverse of σ), at the point of interest.
J is the local current density vector, at the point of interest.

I is a constant, in Equations 3.5 to 3.7, dependent only on the total voltage drop across the entire circuit and the sum of the circuit element resistances in the circuit. For a heterogeneous Earth model, however, all of the parameters in Equations 3.8 to 3.10 are functions of position, with the vector and second rank tensor properties, directional, in nature.

Electrical current densities follow paths of least resistance, such that the total Joule power loss;

$$P_T = \iiint p_{xyz}\, dxdydz, \tag{3.11}$$

for the *entire (earth) system*, is minimized. This means that in regions of high resistivity, $|\mathbf{J}|$ is much lower than in regions of low resistivity. Since p_{xyz} depends upon the local $|\mathbf{J}|^2$, Joule power loss is much less in regions of high resistivity than in regions of low resistivity. The exceptions to this rule-of-thumb are in the vicinity of the power electrodes, where the current density is controlled by the geometry of the power electrodes. Even in these situations, however, DCEOR electrode arrays are designed to maximize Joule heating where it is desired and minimize Joule energy loss, where this result is the desired outcome.

3.9.2 Electric Field Mapping

The primary objective of DCEOR is to pass electrical current through the oil reservoirs in an optimum manner to achieve the above mechanisms. This is achieved by electrode array design. Figure 3.17 shows a simple three-layer earth model, used to design electrode arrays. Figures 3.18 and 3.19 illustrate in cross section and plan view, respectively, the equipotential surfaces about parallel sets of three anodes and cathodes, in the model of figure 3.17.

3.9.3 Joule Heating and Energy Loss

Electrode arrays are specifically designed, in DCEOR systems, to produce high current densities, where *high* Joule heating is desired, and low current

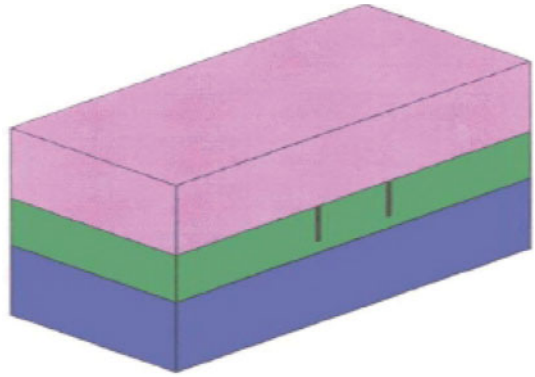

Figure 3.17 Three-layer earth DCEOR field mapping model (after Wittle and Hill, 2006b; and Wittle et al., 2008a, & 2008c)

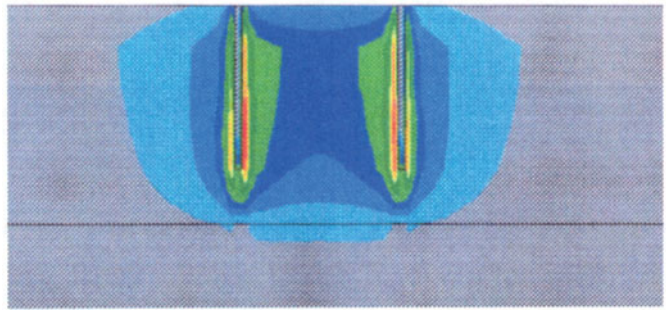

Figure 3.18 DCEOR figure 3.18 model simulation equipotential field cross-section (after Wittle and Hill, 2006a; and Wittle et al., 2008a, 2008b, & 2008c)

densities, where *low* Joule *only* power losses are desired (i.e., high Joule power losses are to be avoided). Figure 3.20 illustrates Joule heating (***no conductive or convective heat transfer***) simulation results in the vicinity of a down-hole electrode within a heavy oil reservoir. Even after 7.5 months of DCEOR, the temperature beyond 14 ft. of the electrode surface is essentially unchanged. Convective and radiative heat transfer, however, would increase the effective heating radius.

3.9.4 Comparison of DC vs. AC Electrical Transmission Power Loss

The power losses, as discussed above, depend only upon resistances (Equation 3.7) or resistivities (Equations 3.10 and 3.11), ***for DC electrical current***.

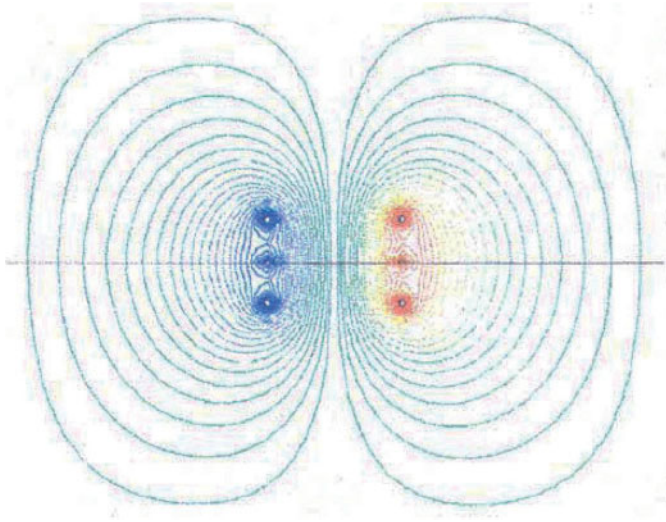

Figure 3.19 DCEOR figure 3.17 model simulation equipotential field plan view (after Wittle and Hill, 2006; Wittle et al., 2008a, 2008b, 2008c

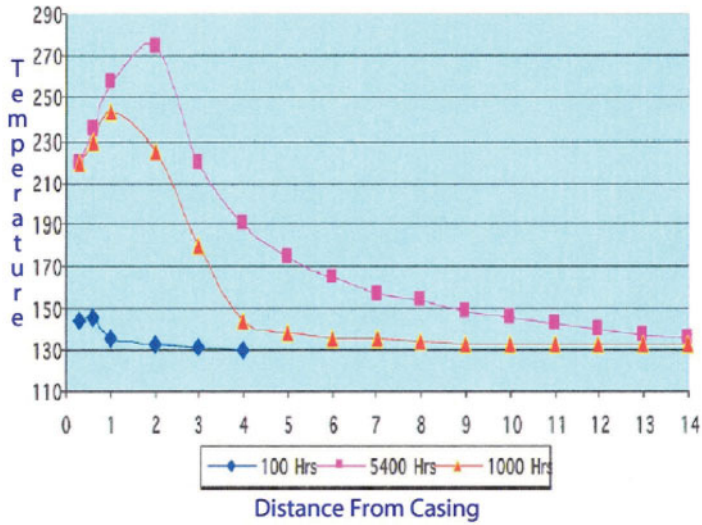

Figure 3.20 DCEOR simulation results: Reservoir temperatures after 100, 1,000, and 5,400 hours of stimulation. temperatures (vertical axis) are in °F and distances (horizontal axis) are in radial feet, from the Casing (after Wittle and Hill, 2006; Wittle et al., 2008a, 2008b, 2008c)

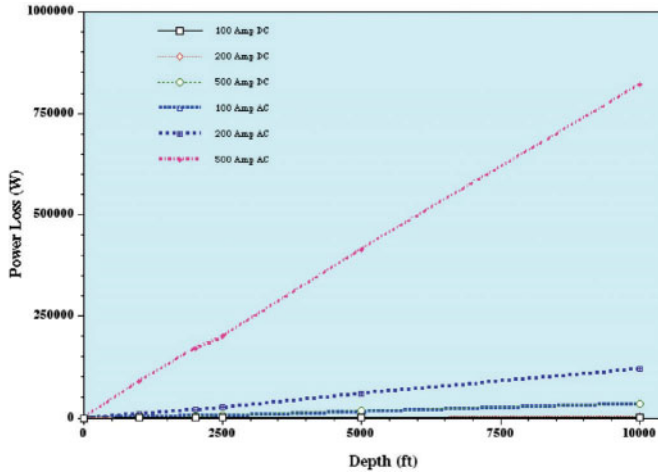

Figure 3.21 DCEOR simulation results: Comparison of AC and DC electrical power loss for various casing depths (after Wittle and Hill, 2006; Wittle et al., 2008a, 2008b, 2008c)

For ***AC electrical current***, however, they ***also depend upon capacitive and inductive losses***. Capacitive loss, in DCEOR, usually involves current leakage to the formation and is generally not a significant concern. Inductive losses for AC signals, however, can become considerable, because of inductive coupling to the earth, from the long cables and/or casing between the generators, at the surface, and the downhole and/or surface electrodes.

Figure 3.21 compares DC and 60 Hz AC power losses for different transmission line current strengths and well depths, using a common vertical (power loss) scale. All of the DC currents (up to 500 A) fall along the horizontal axis of figure 3.21, with insignificant power loss, even to depths of 10,000 ft. By contrast, for a 10,000 ft. well, the 60 Hz 500 A system power loss is over 850 kW. Higher frequencies would fare even worse. This is the reason why AC heating has not been very successful, except for very shallow reservoirs, and extremely short electrode spacings.

3.10 DCEOR Field Demonstrations

Multiple DCEOR field demonstrations have been conducted at heavy oil fields in the Santa Maria Basin of California (USA), Lloydminster Heavy Oil Belt of Alberta and Saskatchewan (Canada), and Golfo San Jorge Basin of Santa Cruz (Argentina).

3.10.1 Santa Maria Basin (California, USA) DCEOR Field Demonstration

The Santa Maria Basin, California (USA) field DCEOR demonstrations, including breaks for data analyses and laboratory testing, lasted over 6 years. Figure 3.22 shows a typical short-term field production test. Within five days of initiating DCEOR, the daily production rate improved approximately tenfold.

The Santa Maria Basin demonstration reservoir was a 100-ft thick unconsolidated sand at a depth of approximately 2,800 ft below ground surface (BGS). Prior *unsuccessful EOR technologies* had included steamflood and cyclic (Huff and Puff) steam injection.

Table 3.2 summarizes the Santa Maria Basin field DCEOR performance, compared to the baseline production. DCEOR increased the oil production by an order of magnitude (10-fold). At the same time:

- The water cut dropped to about 25% of the baseline performance
- API Gravity increased from 8.1° to 10.7°
- Oil viscosity decreased significantly, with the DCEOR produced crude viscosity only about 41% of the baseline value
- Gas production essentially doubled from the baseline value, with DCEOR

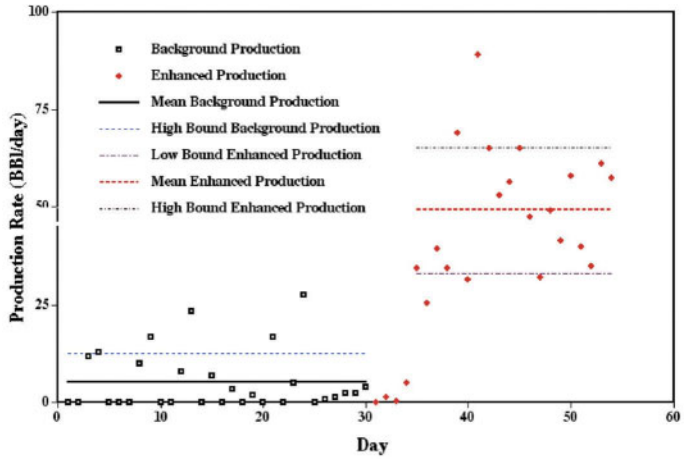

Figure 3.22 Santa Maria Basin (California, USA) short-term DCEOR demonstration, (after Wittle and Hill, 2006a & 2006b; Wittle et al., 2008a, 2008b, 2008c, 2011)

Table 3.2 Santa Maria Basin (California, USA) comparison of DCEOR field demonstration to baseline field performance (after Wittle and Hill, 2006a, 2006b; Wittle et al., 2008a, 2008b, 2011)

Item	Baseline Production	DCEOR Production
Production Rate (BOPD)	5	50
Water Cut (%)	45	12
Oil API Gravity	8.1°	10.7°
Gas Production (SCFPD)	1,750 -2,000	3,800
Produced Gas Energy Content (BTU/SCF)	1.197	1.730
H2S Content (ppm)	2,290	2-40
Viscosity (cps@ 100°C)	51,747	21,275

- The produced gas energy content (PGEC) increased by a factor of 1.5
- The H_2S production dropped from 2,290 ppm to 2 – 40 ppm

The viscosity, API Gravity and PGEC changes are consistent with in-situ *Cold Cracking,* with DCEOR breaking down complex hydrocarbon molecules into simpler liquid hydrocarbons and gases. The near complete destruction of H_2S suggests that the DCEOR is electrochemical, rather than temperature related. These results and conclusions are consistent with those of Döring et al. (2000, 2001, 2003) for DC electrokinetic soil remediation projects.

Table 3.3 summarizes the DCEOR light (C_1–C_9) hydrocarbon and hydrogen (H_2) production, in comparison to the baseline production. With the exception of methane (C_1), these results are consistent with some type of in-situ *Cold Cracking*. The decrease in methane content may be due either to difficulties in capturing this light hydrocarbon, during the baseline production and/or the destruction of methane to hydrogen gas (H_2), which went from non-detect to 1.9%.

Table 3.4 compares the oil production efficiency for DCEOR, cyclic (huff and puff) steam injection, and steamflood, for the Santa Maria Basin field demonstration reservoir. DCEOR was approximately 185 times as efficient as "huff and puff" and 613 – 1,083 times more effective than steam flood.

Table 3.3 Santa Maria Basin (California, USA), DCEOR field demonstration changes in produced gas composition (after Wittle and Hill, 2006b; Wittle et al., 2008a, 2008b, 2011)

Hydrocarbon Species	Baseline (%)	DCEOR (%)
C_1	85.4	45.89
C_2	2.06	4.22
C_3	2.60	10.02
Iso C_4	0.53	2.65
N-C_4	1.35	6.93
Iso C_5	0.69	3.76
HC_5	0.63	3.42
C_6	0.79	3.99
C_7	0.57	2.57
C_8	0.29	0.56
C_9	0.46	0.19
H_2	-	12.90

Table 3.4 Santa Maria Basin (California, USA), Comparison of DCEOR, cyclic steam injection, and steam flood oil production efficiencies (after Wittle and Hill, 2006a & 2006b; and Wittle et al., 2008a, 2008b, 2008c, & 2011)

Recovery Method	BTU/Incremental Bbl Produced
DCEOR	7,014
Cyclic (Huff & Puff) Seam Injection	1,300.000
Steam Flood	4,300,000 – 7,600,000

This reservoir is at a depth of approximately 2,800 ft, significantly deeper than the 2,000 – 2,500 ft practical limit for steam injection. The production efficiencies of Table 3.4 reflect that.

The Santa Maria Basin DCEOR field demonstrations ended when operator was unable to control fines production cost-effectively with the available technology.

3.10.2 Lloydminster Heavy Oil Belt (Alberta, Canada) DCEOR Field Demonstration

The Lloydminster Heavy Oil Belt DCEOR Field demonstrations, including breaks for data analyses and laboratory testing, lasted over 2 years. As with the Santa Maria Basin Field Trial, the Lloydminster Field operator had difficulty with fines production.

The Lloydminster Heavy Oil Belt demonstration reservoir was an 11m (36.3 ft) thick unconsolidated, braided stream sand at a depth of approximately 517 m (1,706 ft) BGS, with a 1.5m (4.95 ft) shale break 3m (9.9 ft) below the top. The well used for this DCEOR demonstration appeared to have missed the main channel sands of the field and, if possible, was an even worse performer than the well used for the Santa Maria Basin demonstration. Baseline production was approximately 2.32 bbl/day (heavy) oil with a 73% BS&W cut, on pump.

The Lloydminster Heavy Oil Belt demonstration evaluated cyclic DCEOR, as shown in figure 3.23. Production rates rose with each power cycle.

Table 3.5 summarizes the Lloydminster Heavy Oil Belt field demonstration. Average DCEOR production was 5.78 Bbl/day with a 2.8 % water

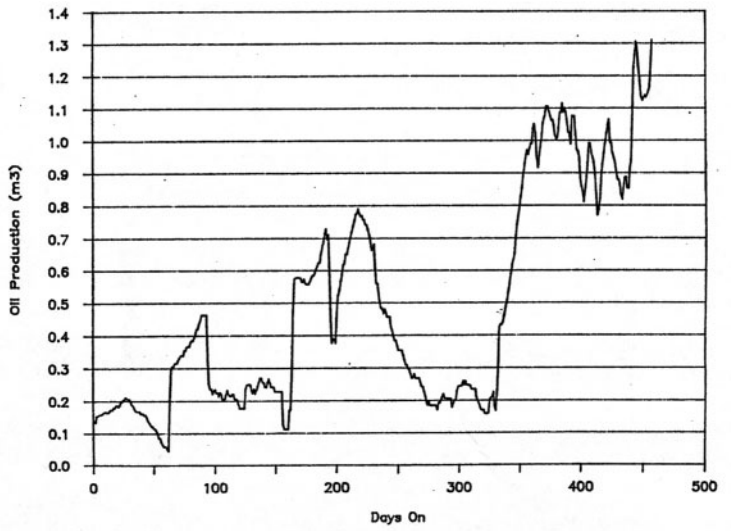

Figure 3.23 Lloydminster Heavy Oil Belt (Alberta, Canada) DCEOR field demonstration, showing the effects of cyclic power application (after Wittle et al., 2008c). Production declines indicate "power off" periods.

Table 3.5 Lloydminster Heavy Oil Belt (Alberta, Canada) comparison of DCEOR Field demonstration to baseline field performance (after Wittle et al., 2008c)

Item	Baseline Production	DCEOR Production
Production Rate (BOPD)	1.32	5.78
Water Cut (%)	31	2.8
Oil API Gravity	NA	N/A
Gas Production (SCFPD)	Nil	Minimal
Produced Gas Energy Content (BTU/SCF)	-	-
H2S Content (ppm)	None	None
Viscosity (cps@ 100°C)	10,275	6,230

cut, compared with baseline values of 1.32 bbl/day and 31 % water cut. This was a 4.38 fold production increase with a 91 % water cut reduction. The fluid level in a nearby observation well also rose approximately 60m, when the DCEOR system was activated. The oil production efficiency was approximately 23.7 BTU/Incremental bbl produced. This DCEOR production efficiency value was comparable to steam flood for this shallow, heavy oil field.

3.10.3 Golfo San Jorge Basin (Santa Cruz, Argentina) DCEOR Field Demonstration

The Golfo San Jorge Basin DCEOR Field demonstration was conducted over a period of 51 days (Stainoh, 2011). Golfo San Jorge Basin reservoirs are interbeded fluvial Cenozoic tuffaceous sandstones (Sylwan, 2001).

The Golfo San Jorge Basin field demonstration reservoir was a 20m (66 ft) thick consolidated, braided stream sand at a depth of approximately 820m (2,706 ft) BGS. The well used for this DCEOR demonstration was a former field production well converted without any modifications to be the DCEOR cathode and production well. Baseline production was approximately 11.46 bbl/day, 15.17° API gravity (heavy) oil with a 96% BS&W cut, on pump.

Table 3.6 summarizes the Golfo San Jorge Basin DCEOR field demonstration. Average DCEOR production was 69.79 bbl /day with a 61 %

Table 3.6 Golfo San Jorge Basin (Santa Cruz, Argentina) DCEOR Field demonstration to baseline field Performance (after Stainoh, 2011)

Item	Baseline Production	DCEOR Production
Production Rate (BOPD)	11.46	69.79
Water Cut (%)	96	61
Oil API Gravity	15.17°	18.42°
Gas Production (SCFPD)	N/A	N/A
Produced Gas Energy Content (BTU/SCF)	-	-
H2S Content (ppm)	N/A	N/A
Viscosity (cps@ 50°C)	2,854	640

BS&W cut, compared to baseline values of 11.46 bbl/day, with a 96 % water cut. This represents a 5.09 fold production increase, with a 34% decrease in water cut.

3.11 Produced Fluid Changes

The DCEOR demonstrations at oilfields in the Santa Maria Basin, Lloydminster Heavy Oil Belt and Golfo San Jorge Basin all suggest that DCEOR may change the chemistry of the produced fluids. These results were not expected, at the time, and have been the subject of considerable discussion, since. Increased oil production and reduced water cut were expected, but not the other results. The higher API gravity, increased gas production and increased BTU content of the produced gasses, were initially attributed to in-situ thermal cracking, due to joule heating of the formation. Joule heating, however, could not explain the dramatic reduction in produced H_2S. The DCEOR field demonstration production wells were also cathodes for the DCEOR system. Because of this, the production of OH^- ions by electrolysis at the cathode was considered a potential explanation for chemical changes in the produced fluids.

A recently developed low current density electrical soil remediation technology (Döring, 1993 & 1996) called Electro-Chemical Geo-Oxidation

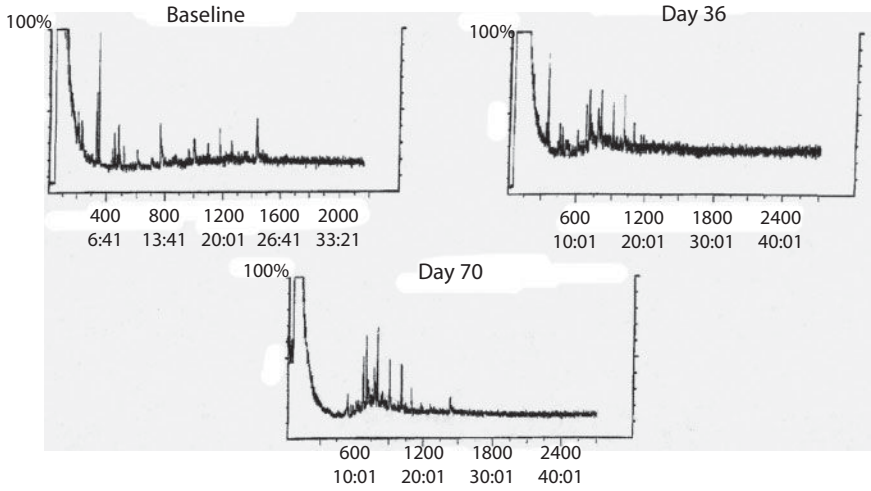

Figure 3.24 EC PAH destruction documented by GCMS changes, with time, During Treatment (after, Döring et al, 2000). Vertical axes are abundance in ppm; horizontal axes time, in minutes.

(ECGO) provides insight for yet another potential explanation of the Santa Maria Basin DCEOR results.

Figure 3.24 shows a series of Gas Chromatography Mass Spectrograph (GCMS) spectras taken at various times during in-situ ECGO remediation a large-scale poly-aromatic hydrocarbon (PAH) contaminated soil site. The GCMS spectra vertical axes are relative to hydrocarbon (HC) species concentration. The horizontal axes are residence times, which are related to the HC species complexity.

The simpler PAH species are vaporized with shorter residence times (left end of the axis), while the more complex species require longer residence times (right end of the axis). Over the course of the site remediation, the GCMS spectra peaks shift from complex to simpler hydrocarbons (i.e., to the left, on the GCMS spectra), suggesting a possible in-situ breakdown of the complex PAH molecules to simpler hydrocarbon daughter products. The measurement samples were ***not*** collected near the electrodes, but from the body of the contaminated soil site. As a result, the chemical changes in the PAH were ***not*** just occurring at the cathodes, or as a result of electrode reactions.

3.12 Laboratory Measurements

The DCEOR demonstrations at oilfields in the Santa Maria Basin, Lloydminster Heavy Oil Belt and Golfo San Jorge Basin all exhibited:

- Increased oil production
- Reduced water cut
- Increases in API gravity of the produced crude

Controlled laboratory tests were developed to further evaluate these field results. Standard petroleum Special Core Analysis Laboratory (SCAL) electrical and flow measurements involve small (1in diameter by 1 – 2 in long) samples housed in Hasler Load Cells, for short term (hours to days) tests. Using these types of tests for investigating the mechanisms involved with DCEOR present the following problems:

- The weeks to months involved in the DCEOR field demonstrations create considerable electrode reaction products at the anodes and cathodes, which could overwhelm any reactions occurring with in the standard petroleum SCAL test sample.
- The very low (μV/m – mV/m) potential gradients involved in the DCEOR field demonstrations are extremely difficult to maintain in a laboratory environment.
- Synthetic surrogate reservoir formation, crude, and brine samples often used for laboratory measurements may not be representative of the actual reservoir material.

To overcome these test design problems, Electro-Petroleum, Inc. (EPI: Wittle and Hill, 2006a and 2006b; Wittle 2008a, 2008b, 2008c, and 2011) and P + P Geotechnik GmbH (P + P: Döring, 1993, 1996) used large (0.5 – 1.0 m^2) samples for laboratory testing.

Figure 3.25 and Table 3.7 describe the progress of a large-scale (~1 m^3 volume sample) laboratory test conducted on a California heavy oil field reservoir rock, via Gas Chromatograph-Mass Spectroscopy analyses of samples collected from the test sample at the start of the DCEOR test (red curve of figure 3.25) and after 74 days (black curve of figure 3.25).

The more complex hydrocarbon molecule abundances (right end of the figure 3.25 spectras) have been reduced, while the simpler molecule abundances (left end of spectras) have increased, as a result of this 74-day

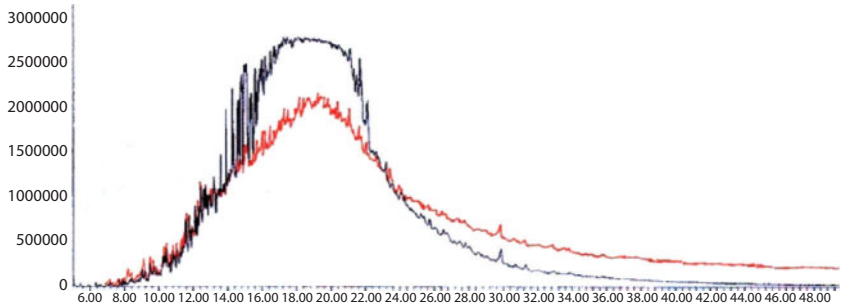

Figure 3.25 Laboratory San Joaquin Valley (California, USA) heavy oil field reservoir rock laboratory DCEOR test (after Wittle and Hill, 2006a & 2006b; Wittle, et al., 2008a, 2008b, 2008c, & 2011). GCMS Spectra: Vertical axis is abundance, while horizontal axis is retention time (corresponding to HC complexity) in minutes. Red curve - start of test. Black curve - after 74 days of DCEOR.

Table 3.7 California heavy oil field reservoir (rock and crude) laboratory test GCMS results

GCMS Spectra Property	Base Line Sample	74 Day Sample
Spectra Peak abundance	2,100,000	2,750,000
Spectra Peak Location (min)	19.05	18.40
Spectra Peak Half-Width Abundance	1,050,000	1,375,000
Spectra Peak Half Width (min)	13.2 – 24.5	14.45 – 22.9
Spectra Tail	Extensive to 49 min	Insignificant after 30 min

DCEOR treatment. As with the case, for the ECGO PAH remediation, the samples for the spectras in figure 3.25 ***were not*** collected at the cathode, but from the ~ 1 m^3 sample.

Figure 3.26 shows viscosity changes during similar large volume DCEOR laboratory tests, involving crudes from two California heavy oil fields. There are significant declines in viscosity (at constant temperature) for both of these crudes, during the course of the tests.

The results shown in figures 3.25 and 3.26 are consistent with the Santa Maria Basin Lloydminster, and Golfo San Jorge Basin field DCEOR results as well as the ECGO GCMS spectra of figure 3.24.

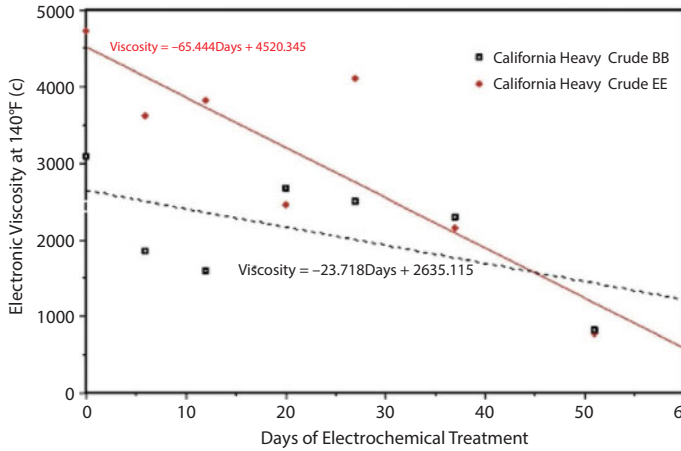

Figure 3.26 California, USA, Heavy Crude viscosity changes during DCEOR laboratory tests (after Wittle et al., 2008a, 2008b, 2008c, & 2011)

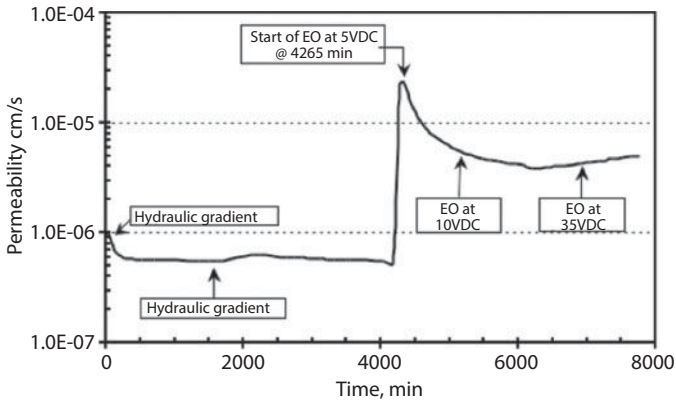

Figure 3.27 Changes in effective permeability, due to the passage of DC current (after, Pamukcu, and Pervizpour, 1997)

3.12.1 Electrokinetics and Effective Permeability

Figure 3.27 illustrates the effect of DC current application on fluid flow in a micro-darcy fine grained silty-clay. The effective permeability, in this laboratory test, increases 1 to 1.5 orders of magnitude, when electrical current is applied. This is consistent with the approximately 60m rise in the fluid level of a monitoring well, during the Lloydminster Heavy Oil Belt, DCEOR field demonstration, and the USC electro-osmosis results described earlier and with the results of Chilingar et al. (1970).

Several successful laboratory and field tests, using DC electrical currents to introduce bacteria and nutrients into fine-grained sediments were conducted at the University of Southern California (Chilingar et al., 1997). The process, termed "Electro-Bio-Remediation", utilized DC electrical currents to force bacteria and nutrients into these very low permeability soils and rocks to remediate light hydrocarbon (gasoline and diesel) contamination from spills.

3.12.2 Sulfur Sequestration

The dramatic Santa Maria Basin H_2S reduction, during DCEOR, raised questions as to whether these results were due to preferential production, or actual sulfur sequestration. Table 3.8 summarizes some preliminary laboratory results, which suggest that DCEOR moves sulfur from the hydrocarbons to the brines, *in-situ*.

3.12.3 Carbonate Reservoir Laboratory Tests

An earlier discussion (above) indicated that carbonate reservoirs, because they tend to be preferentially non-water wet, might behave differently than

Table 3.8 Laboratory evaluation of DCEOR sulfur sequestration studies (after Wittle, 2007)

Oil System Sample	Initial % Sulfur in Oil	Initial % Sulfur in Electrolyte	Final % Sulfur in Oil	Final % Sulfur in Electrolyte
Thriophene in Mineral Oil	1.24	0.00	0.20	2.96
Thriophene in Mineral Oil	1.33	0.01	0.15	1.31
Thriophene in Mineral Oil	2.71	0.00	0.30	1.50
Thrianapthalene in Mineral Oil	3.77	0.00	5.23	0.80
Thrianapthalene in Mineral Oil	6.17	0.07	4.90	0.64
Crude Oil	6.13	0.00	4.57	0.80
Crude Oil	6.13	0.00	4.57	0.80

clastic reservoirs, unless the carbonate reservoir throats were lined with clay minerals. Muhammad Haroun, and his students at the Petroleum Institute Abu Dhabi, have conducted a series of small scale (1 in diameter by 1.5 in long core plug) laboratory carbonate DCEOR assisted water flood experiments Ansari, et al, 2012; Haroun et al, 2009, 2013).

The small sample size is subject to the electrode reaction product risks, cited above, in spite of the authors' best attempts, including flushing the sample holder electrode chambers during the tests. The potential gradients of 2 V/cm are much higher than possible for field operations and may skew the results. Finally, the aggressive core cleaning and restoration utilized by the authors risks irreversibly altering the electrochemical properties of the cores. Timur (1992) attributed the following quote from M. R. J. Wyllie:

> *"The only thing we can say, for certain, about core measurements is that they come from rocks which are no longer part of the reservoir"*

With the above disclaimers:

- Haroun, et al. (2009) reported increased waterflood and surfactant injection rates with DCEK aided flow.
- Ansari et al. (2012) and Haroun et al. (2012) reported increased oil recovery with DCEK assisted waterflood.

3.13 Technology Comparisons

Any emerging technology needs to be compared to both existing and other emerging technologies.

3.13.1 Comparison of DCEOR and Steam Flood Efficiency

Table 3.4 compares DCEOR oil recovery efficiency (energy expended/incremental oil produced) during the Santa Maria Basin, California field demonstration to steam flood and cyclic (Huff and Puff) steam injection, in the same field. For this particular field, with the reservoir at a depth of about 2800 ft BGS, DCEOR was considerably more efficient than either steam flood or cyclic steam injection.

The Lloydminster Heavy Oil Belt well pay zone was much shallower (517 m or about 1,700 ft BGS). No details on these tests are available, but the DCEOR and steam injection efficiencies for this well were considered to be comparable.

The Santa Maria Basin vs. Lloydminster efficiency comparisons reflect the practical depth range of steam injection EOR.

3.13.2 Comparison of DCEOR and Steam Flood Costs

Table 3.9 compares the costs of a potential 20 acre DCEOR operation to that of a comparable 20 acre San Joaquin Valley, California (USA), steam flood operation. This comparison was developed jointly with a representative of a major San Joaquin Valley heavy oil producer, with extensive steam flood experience. The dollar cost figures are in 1998 U$S, not adjusted for inflation.

While the capital, design and installation cost estimates, for the two EOR technologies are close, steam flood installation costs are front-loaded, while the DCEOR system can be added incrementally, spreading its costs over the life of the project. Current approaches, involving intermittent energizing of individual subsurface cathodes, would reduce the number of surface power converters and anode arrays needed. This new approach could significantly reduce DCEOR capital costs. Annual energy costs are

Table 3.9 Comparison of DCEOR and Steam-Flood cost estimates (Wittle and Hill, 2006a, 2006b). All costs are in terms of 1998 U$S, uncorrected for inflation.

Item	Steam-Flood[1]	DCEOR[2]
Capital, Design, & Installation Costs (U$S)[3]	$3,400,000	$3,125,300
Annual Energy Costs (U$S)[4]	$ 620,800	$ 86,200
Non-Energy O&M Costs (U$S/Bbl)[5]	$2.23	$0.45
Equipment Life Expectancy (yr.)	7	10

[1]Steam-Flood figures from San Joaquin Valley, California, for 8 x 2.5 A 5-spots (20 A total), with 8 steam injectors and 15 1,500 ft. production wells with associated generation, compression, and transmission equipment.

[2]DCEOR figures extrapolated from Santa Maria Basin and Lloydminster Heavy Oil Belt Field Demonstrations, for 6 power converters, and surface anode arrays with 23 subsurface cathodes located in production wells covering a 20 A footprint.

[3]Exclusive of normal production well costs. Steam-Flood costs are front loaded, whereas DCEOR costs can be incremental, over the project life cycle.

[4]Steam-Flood: 155,200,000 cu ft/yr Natural gas at U$S 0.40/Therm

DCEOR: 862,000KW-hr/yr at U$S 0.10/kW-hr.

[5]Exclusive of Lifting Costs.

much lower for DCEOR, than for steam flood. Non-energy O&M costs for DCEOR are also much lower than those for steam flood. DCEOR equipment is virtually maintenance free, and can be monitored remotely. This also translates into longer equipment life expectancy and lower operating costs than that needed for steam injection technologies.

3.13.3 Comparison of DCEOR to Other EOR Technologies

Table 3.10 compares DCEOR to other emerging, as well as commercial EOR technologies. DCEOR appears to have the following advantages:

- Heat is generated in-situ, via joule heating
- It does not use a working fluid
- It does not need a significant water supply
- It reduces water cut
- It is independent of permeability
- There are no Thief Zone concerns
- There is no apparent depth limit
- There are no emissions concerns
- There are no hazardous chemical concerns
- It increases apparent permeability
- Electro-kinetics positively influence produced fluids and flow

The biggest DCEOR limitation, to date, appears to be its limited field application portfolio. This will change with additional field experience.

3.14 Summary

The following conclusions can be drawn, about DCEOR:

- There have been three encouraging field demonstrations, to date
- It appears to facilitate beneficial chemical changes in the produced fluids
- It appears to be cost competitive, to steam flood, for shallow reservoirs, and less expensive for deeper reservoirs
- There are no Tight Zone or Thief Zone problems
- There is no water or other working fluid requirement
- It reduces water cut

Table 3.10 Heavy Oil EOR technology maturity, asset, and limitation comparison (after, Wittle and Hill, 2006a, & 2996b; Wittle et al., 2008a, 2008b, 2008c, & 2011) .

Process Limitation	DCEOR	Steam Flood	CO2¬ Flood	Fire Flood	Surfactant Flood	Co-Solvent Flood
Front End Costs	Power Supply Cables Electrodes	Steam Generator				
Compressor Transmission Lines	C2 Supply Compressor Transmission Lines	Compressor Transmission Lines	Mixing Tanks Pumps Transmission Lines	Mixing Tanks Pumps Transmission Lines		
Uniform Sweep	Yes	No – Thief Zones	No – Thief Zones	No – Thief Zones	No – Thief Zones	No – Thief Zones
Depth Limitations	No	≤ 2,500 ft	No	No	No	No
Water Demand	Nil	Very High	None	None	High	Variable
Operational Limitations	None	Emission & water Supply Limits	None	None	Hazardous Chemicals	Hazardous Chemicals
Reservoir & Crude Type	High & Low Permeability	High Permeability Non-Reactive Matrix	High Permeability	High Permeability	High Permeability	High Permeability
Maturity	Field Demonstrated	Commercial	Commercial	Commercial	Pilot Tested	Pilot Tested

- There are no greenhouse gas emission or hazardous liquid problems
- Facility installation is incremental, so that capital costs can be spread over the life of the field
- There appear to be no depth limits to the DCEOR technology

Nomenclature

AC = Alternating Current
Bbl = Barrels
BGS = Below ground surface
BOPD = Barrels oil per day
BTU = British thermal unit
BTU/SCF = British thermal unit/standard cubic foot
COF = Cost of finding
COL = Cost of Lifting
D_i = Ionic diffusion coefficient tensor
D_p = Particle diffusion coefficient tensor
DC = Direct Current
E = Local Electric Field Vector
ECGO = Electro-Chemical Geo-Oxidation
DCEK = Direct Current Electrokinetics
DCEOR = Electro-Enhanced Oil Recovery
Eh = Electron activity
EM = Electro-Magnetic
EOR = Enhanced Oil Recovery
EPI = Electro-Petroleum, Inc.
GCMS = Gas chromatograph mass spectrograph
GE = General Electric
I = Electrical current
J = Electrical current density vector
$\mathbf{J}_i$ = Generalized flux (vector)
K = Thermal conductivity tensor
k = Absolute Permeability tensor
L_{ij} = Generalized coupling coefficient (tensor)
O&M = Operations and maintenance
P = Circuit element power loss
P_T = Total power loss
p_{xyz} = Local power loss
PAH = Poly-Aromatic Hydrocarbon

PGEC = Produced gas energy content
pH = Hydrogen ion activity
R = Resistance
RF = Radio Frequency
SCFGPD = Standard cubic feet gas per day
SAGD = Steam Assisted Gravity Drainage
USC = University of Southern California
US$ = Dollars, U.S.
ΔV = Circuit element voltage drop
∇ = Vector gradient operator
$\oplus$ = Dot (inner) vector product
$\iiint$ = Volume integral with no limits
$| |$ = Magnitude
μ = Fluid viscosity
σ = Local electrical conductivity tensor
ρ = Local electrical resistivity tensor
$\emptyset$ = Electrical potential field
$\emptyset_j$ = Generalized potential field

References

Anon., 1966, Electro-Osmosis Stabilizes Earth Dam's Tricky Foundation, *Engineering News-Record*, 176 (25): 36–37, 40, 45.

Acar, Y. B., and Alashawabkeh, A. N., 1993, Principles of Electrokinetic Remediation, *Environ. Sci., Technol.,* 27 (13): 2638–2647.

Acar, Y. B., and Gale, R. J., 1992, Electrochemical Decontamination of Soils or Slurries, *United States Patent No. 5,137,608.*

Ace, A. G., 1955, *An Investigation of the influence of Applied Electrical Potential Gradients on Flow of Fluids in Porous Media,* M. S. Thesis, Department of Petroleum Engineering, The University of Southern California.

Al Shalabi, E. W., Haroun, M., Ghosh, B., and Pamukcu, S, 2012, The Stimulation of Sandstone Reservoirs, Using DC Potential**,** *Petroleum Science and Technology*, 30 (20): 2137–2147.

Amba, S. A., Chilingar, G. V., and Beeson, C. M., 1964a, Use of Direct Electrical Current for Increasing the Flow Rate of Reservoir Fluids During Petroleum Recovery**,** *J. Canadian Petrol. Technol.*, 3 (1): 8 – 14.

Amba, S. A., Chilingar, G. V., and Beeson, C. M., 1964b, Application of Electrokinetic Phenomena in Civil and Petroleum Engineering, *Annals of the New York Academy of Sciences*, 3 (1): 8 – 14.

Amba, S. A., Chilingar, G. V., and Beeson, C. M., 1965, Use of Direct Electrical Current for Increasing the Flow Rate of Oil and Water in a Porous Medium: *J. Canadian Petrol. Technol.*, 4 (1): 8 1–88.

Ansari, A., Haroun, M., Sayed, N. A., Al Kindy, N., Ali, B., Shrestha, R. A., and Sarma, H., 2012, A New Approach Optimizing Mature Waterfloods with Electrokinetics-Assisted Surfactant Flooding in Abu Dhabi Carbonate Reservoirs, *Soc of Pet. Engr.,* SPE-163379.

Attanasi, E. D., and Meyer, R. F., 2010, Natural Bitumen and Extra-Heavy Oil, in: *2010 Survey of Energy Resources,* Trinnaman, J., and Clarke, A., ed. World Energy Council, pp. 123 – 150.

Bell, C. W., and Titus, C. H., 1973, Electro-Thermal Process for Production of Offshore Oil through Onshore Wells, *US Patent No. 3,724,543.*

Berry, L. G., and Mason, B., 1959, *Mineralogy – Concepts, Descriptions, and Determinations,* W. H. Freeman and Company, San Francisco.

Bell, C. W., and Titus, C. H., 1974, Electro-Thermal Process for Promoting Oil Recovery, *US Patent No. 3,782,465.*

Bell, C. W., Titus, C. H., and Wittle, J. K., 1985, In Situ Method for Yielding a Gas from a Subsurface Formation of Hydrocarbon Material, *US Patent No. 4,473,114.*

Bell, G. T., 1957, Electrolytically Promoting the Flow of Oil from a Well, *US Patent No. 2,799,641.*

Blevins, T. R., Duerksen, J. H, and Ault, J. W., 1984, Light-Oil Steamflooding An Emerging Technology, *J. Petrol. Technol.,* (36) 7: 1115–1122.

Bruell, C. J., Segall, B. A., and Walsh, M. T., 1992, Electroosmotic Removal of Gasoline Hydrocarbons and TCE from Clay, *J. Environmental Engineering, ASCE,* 118 (1): 68 – 83.

Casagrande, L., 1952. Electro-Osmotic Stabilization of Soils, *J. Boston Society of Civil Engineering,* 39 (1): 285–317.

Casagrande, L., 1959. A Review of Past and Current Work on Electro-Osmotic Stabilization of soils, *Harvard Soil Mechanics Series*, No. 45 Harvard College, Cambridge.

Casagrande, L., Loughney, R. W., and Matich, M. A. J., 1961, Electro-Osmotic Stabilization of a High Slope in Loose Saturated Silt, *Proc., 5th. ICSMFE,* v. 2, pp. 555–461.

Chelidze, T. L., 1969, The Effect of Surface Polarization on the Electrical Properties of Rocks in Variable Fields, *Izv., Earth Physics,* 10: 80–87.

Chilingar, G. V., Chang, K. S., Davis, J. E., Farhangi, H. J., Adamson, L. G., and Sawabini, S., 1968, Possible Use of Direct Electrical Current for Augmenting Reservoir Energy During Petroleum Production, *The Compass,* 45 (4): 272–285.

Chilingar, G. V., El-Nassir, A., and Stevens, R. G., 1970, Effect of Electrical Current on Permeability of Sandstone Cores, *J. Petrol. Technol.,* 22 (7): 830–836.

Chilingar, G. V., Loo, W. W., Khilyuk, L. F., and Katz, S. A., 1997, Electrobioremediation of Soils contaminated with Hydrocarbons and Metals, *Energy Sources,* 19: 129–146.

Chute, F. S., and Vrmeulen, F. E., 1988, Present and Potential Applications of Electromagnetic Heating in the In-Situ Recovery of Oil, *OSTRA J. Research,* 4: 19–33.

Chute, F. S., Vrmeulen, F. E., and Stevens, L. G., 1987, Study of the Technical and Economic Feasibility of an Electric Preheat Process for In-Situ Recovery from Athabasca Oil Sands, *OSTRA J. Research*, 3: 139–154.

Cohen, R. M., and Mercer, J. W., 1992, *DNAPL Site Evaluation*, C. K. Smoley/CRC Press, Boca Raton.

Conway, B. E., 1999, *Electrochemical Supercapacitors – Scientific Fundamentals and Technological Applications,* Kluwer Academic/Plenum Publishers, New York.

Crowson, F.I., and Gill, W.G., 1971, Method and Apparatus for Secondary Recovery of Oil, *US Patent No. 3,605,888.*

Döring, F, 1993, Verfahren und Einrichtung zur Beseitigung von Schadstoffen, insbesondere im Erdbodenbereich, *European Union Patent No. 0 578 925 A1.*

Döring, F, 1996, Verfahren zur Abtoetung von Mikrooganismen und/order Mineralisierung von Organischen Substanzen im Boden Und im Grundwasser mittens elektrischen Stromes, *European Union Patent No. 0 792 796 A1.*

Döring, F., Iovenitti, J. L., Döring , N., Satre, R.. I., McIlvride, W. A., and Hill, D. G., 2000, ElectroChemical Remediation Technologies for Soil and Ground Water, *Proc. EREM 2000 International Conference on Nuclear and Hazardous Waste Management,* Chattanooga, September 24–28.

Döring, F., Iovenitti, J. L., Döring , N., Satre, R.. I., McIlvride, W. A., and Hill, D. G., 2001, ElectroChemical Remediation Technologies for Soil and Ground Water Remediation, *EREM 2001, 3rd Symposium on Electrokinetic Remediation,* Karlsruhe, April 18–20.

Döring, R., Pamucku, S., Wittle, K., and Zanko, L., 2003, The Electrochemical Remediation of Petroleum Hydrocarbons: Theory and Results, from a Soil Recycling Plant, *Electro-Petroleum, Inc.,* Wayne, PA.

Feris, S. R., 1968, Well Treating Process Using Electro Osmosis, *US Patent No. 3417823.*

Ghazanfari, E., Miroshnik, A., Shrestha, R. Pamukcu, S. and Wittle, K., 2013 , Investigation of Underlying electrochemical Processes in Electrically Enhanced Oil Recovery, *SPE Journal,* in review.

Ghazanfari, E., Shrestha, A. R., Miroshnik, A., and Pamukcu, S., 2012, Electrically Assisted Liquid Hydrocarbon Transport in Porous Media, *Electrochemica Acta,* 86: 185–191.

Gill, W. G., 1970, Method and Apparatus for Secondary Recovery of Oil, *US Patent No. 3,507,330*.

Gill, W. G., 1972, Electrical Method and Apparatus for the Recovery of Oil, *US Patent No. 3,542,066*.

Gray. D. H., and Mitchell, J. K., 1967, Fundamental Aspects of Electro-Osmosis in Soils, *J. Soil Mechanics and Foundations Division, ASCE,* 93 (SM6): 209–236.

Gray, D. H., and Schlocker, J., 1969, Electrochemical Alteration of Clay Soils, *Clays and Clay Minerals,* 17: 309–322.

Haroun, M., Ansari, A. A., Wittle, J. K., Shrestha, R. A., and Chilingar, 2013, Electrokinetic Assisted Waterflooding in Abu Dhabi Carbonate Reservoirs, *EREM2013*, Boston, June 23–26

Haroun, M., Chilingar, G. V., Pamukcu, S., Wittle, J. K., Belhaj, H. A., and Al Bloushi, M. N., 2009, Optimizing Electroosmotic Flow Potential for Electrically Enhanced Oil Recovery (EEOR®) in Carbonate Rock Formations of Abu Dhabi Based on Rock Properties and Composition, *International Petroleum Technology Conference*, IPTC 13812.

Hill, D. G., 1972, A Laboratory Investigation of Electrical Anisotropy in Precambrian Rocks, *Geophysics*, 37 (6): 1022–1038.

Hill, D. G., 1994, Electro-Osmotic Aided Remediation for Non-Aqueous Liquid Contamination of Fine-Grained Aquitards, *Weiss Associates*, Emeryville, CA, August.

Hill, D. G., 1997, Enhanced Restoration of Contaminated Aquitards, Using Electro-Osmotic Aided Remediation, *Weiss Associates*, Presentation to California Environmental Protection Agency Department of Toxic Substances Control, May 7.

Hill, D. G., 1998, Enhanced Restoration of Contaminated Aquitards, Using Electro-Osmotic Aided Remediation, *Environmental Management and Technology Expo*, Long Beach. CA, November 17–19.

Hill, D. G., 1999, Geophysical Basis for Electro-Chemical Geo-Oxidation Mechanisms, *Weiss Associates*, Emeryville. CA.

Hill, D. G., Iovenitti, J. L., and Cooke, M. A., 1997, Enhanced Restoration of Contaminated Aquitards Using Electro-Osmotic Aided Remediation, *HazWaste World SuperFund XVIII*, Washington, DC, December 2–4.

Hill, D. G., Wittle J. K., Fricker, D. J., and Chilingar, G. V., 2010, Moving Goo: Direct Electric Current Oil Recovery (EEOR)—A New Approach to Enhancing Oil Production, *Sacramento Petroleum Association*, November 17.

Howell, B. F., and Licastro, P. H., 1961, Dielectric Behavior of Rocks and Minerals, American Mineralogist, 46: 269–288.

Iovenitti, J. L., McIlvride, W. A., Döring, F., Hill, D. G., and Döring, 2003, Electrochemical Remediation Technologies for Organic and Metal Contaminants in Soil, Sediment, and Ground Water; Presentation of Case Histories, *Air and Waste Management Association Annual Conference and Exhibition*, San Diego.

Kasevich, R.S., Price, S.L., Faust, D.L., and Fontaine, M.F., 1994, Pilot Testing of a Radio Frequency Heating System for Enhanced Oil Recovery From Diatomaceous Earth, *SPE Annual Technical Conference and Exhibition*, New Orleans.

Katsube, T. J., 1975, The Electrical Polarization Mechanism Model for Moist Rocks, *Geo. Surv. Canada,* Paper *75-1C*: 353–360

Keller, G. V., and Licastro, P. H., 1959, Dielectric constant and Electrical Resistivity of Natural-State Cores, *USGS Bulletin 1052-H*: 257–285.

Komarov, S. G., and Shmarova, V. P., 1961, Membrane Potential of Clays, *Prikladnaya Geofizika*, (31): 288–293.

Lageman, R., Pool, W., and Seffinga, G., 1989, Electro-Reclamation: Theory and Practice, *J. Chemistry & Industry*, 9: 585–590.

Lorenz, P. B., 1952, Phenomenology of Electro-Osmosis and Streaming Potential, *J. Physical Chemistry*, 56: 775–778.

Marshall, D. J., and Madden, T. R., 1959, Induced Polarization, A Study of its Causes, *Geophysics*, 24 (4): 790–816.

Mayper, V., 1959a, The Normal Effect – Part I, in*: Overvoltage Research and Geophysical Applications*, J. R. Wait, ed., Pergamon Press, New York.

Mayper, V., 1959b, The Normal Effect – Part II, in: *Overvoltage Research and Geophysical Applications*, J. R. Wait, ed., Pergamon Press, New York.

McGee, B. C. W., 2008, Electro-Thermal Pilot in the Athabasca Oil Sands: Theory versus Performance, *World Oil*, (11): 47 – 54.

McGee, B. C. W., Vermeulen, F. E., and Yu, L., 1999, Field Test of Electrical Heating with Horizontal and Vertical Wells, *J. Canadian Petrol, Technolo*, 38 (3): 46–53.

Meyer, R. F., Attanasi, E. D. and Philip A. Freeman, P. A., 2007, Heavy Oil and Natural Bitumen Resources in Geological Basins of the World, *Open File Report 2007-1084,* U.S. Geological Survey.

Mitchell, J. K., 1970, In-Place Treatment of Foundation Soils, *J. Soil Mechanics and Foundations Division, ASCE*, 96 (SM1): 73–110.

Mitchell, J. K., 1993, *Fundamentals of Soil Behaviour*, John Wiley and Sons, Inc., New York.

Nourbehecht, B, and Madden, T. R., 1963, *Irreversible Thermodynamics in Inhomogeneous Media and Geoelectric Applications*, Massachusetts Institute of Technology, Cambridge.

Onsager, L. 1931a, Reciprocal Relations in Irreversible Processes I, *Physical Review*, 37: 405 – 426.

Onsager, L., 1931b, Reciprocal Relations in Irreversible Processes II, *Physical Review*, vol. 38, December, pp. 2265–2279.

Onsager, L., 1969, The Motions of Ions: Principles and Concepts (Nobel Laureate Lecture), *Science*, 166 (3911): 1359–1364.

Pamukcu, S., 1994, Electrokinetic Removal of Coal Tar Constituents from Contaminated Soils, *EPRI TR-103320*, Electric Power Research Institute.

Pamukcu, S., 1997, Electro-Chemical Technologies for In-Situ Restoration of Contaminated Subsurface Soils, *Electronic Journal of Geotechnical Engineering*, http://geotech.okstate.edu/ejge/ppr97031/.

Pamukcu, S, and Pervizpour, M, 1997 *Electroosmotic Aided NAPL Remediation of Contaminated Soil: Stanford Linear Accelerator Site*-Final Report to Weiss Associates, Emeryville, Ca, November.

Rahner, D., and Röhrs, 2002, Electrochemically Induced Reactions in Soils – A New Approach to the in-Situ Remediation of Contamination Soils? Part 1: The Microconductor Principle, *Electrochemical Acta*, 47: 1395–1414.

Röhrs, J., Ludwig, G., and Rahner, D., 2002, Electrochemically Induced Reactions in Soils – A New Approach to the in-Situ Remediation of Contamination Soils? Part 2: Remediation Experiments with a Natural Soil Containing Highly Chlorinated Hydrocarbons, *Electrochemical Acta*, 47: 1405–1403.

Rokityansky, I.I., 1959, The Nature of Induced Polarization of Ion-Conducting Soils, *Izv. Geophysics Series*, 1055–1060.

Sahni, A., Kumar, M., and Knapp, R. B., 2000, Electromagnetic Heating Methods for Heavy Oil Reservoirs, *SPE/AAPG/SEG Western Regional Meeting*, Paper SPE-62550, Long Beach, CA, June 19–23.

Sanberg, C. L., Hale, A., and Kovscek, 2013, History and Application of Resistance Electrical Heaters in Downhole Oil Field Applications, *SPE/AAPG/SEG Western Regional Meeting,* Paper SPE-165323, Monterey, CA, March 19 – 25.

Sarapuu, E., 1957, Method of Underground Electrolinking and Electrocarbonization of Mineral Fuels, *US Patent No. 2,795,279*.

Scott, J. H., Carroll, R. D., and Cunningham, D. R., 1967, Dielectric Constant and Electrical Conductivity Measurements of Moist Rock, *J. Geophys Research*, 72 (20: 5101–5115.

Schlumberger, C., 1920, *Étude sur la Prospection électrique du sous-sol*, Gauthier-Villars, Paris.

Smythe, W. R., 1968, *Static and Dynamic Electricity,* John Wiley & Sons, Inc., New York.

Staff, 2011, Total E&P Canada Ltd., Surface Steam Release of May 18, 2006, *Energy Resources Conservation Board*, Edmonton, Alberta.

Stainoh, M., 2011, *QOR Test Report: Sur Rio Deseado Este Oilfield*, Roach SA, Buenos Aires.

Sylwan, C. A., 2001, Geology of the Golfo San Jorge Basin, Argentina, *J. Iberian Geology*, 27 123–157.

Sumner, J. S., 1976, *Principles of Induced Polarization for Geophysical Exploration*, Elsevier Scientific Publishing Company, New York.

Tchillingarian, G. V., 1952, Possible Utilization of Electrophoretic Phenomenon for Separation of Fine Sediments into Grades, *J. Sedimentary Petrology*, 22: (1): 29-32.

Timur, A. 1992, *personal communication*.

Tikhomolova, K. P., 1993, *Electro-Osmosis*, Ellis Horwood, New York.

Titus, C. H., Wittle, J. K., and Bell, C. W., 1985, Apparatus for Passing Electrical Current Through an Underground Formation, **US Patent No. 4,495,990**.

Vacquier, V., Holmes, C. R., Kintzinger, P. R., and Lavergne, M., 1957, Prospecting for Ground Water by Induced Polarization, *Geophysics*, 22 (3): 660–687.

Vinegar, H. J., and Bass, R. M., 2007, In Situ Recovery from a Hydrocarbon Containing Formation Using Conductor-in-Conductor Heat Sources with an Electrically conductive Material in the Overburden, *US Patent No. 7,165,165*.

Vinegar, H. J., Berchenko, I. E., de Rouffignac, E. P., Fowler, T. D., Ryan, R.C., Wellington, S. L., and Zhang, E., 2006a, In Situ Thermal Processing of an Oil Reservoir, *US Patent No. 7077199*.

Vinegar, H. J., Coles, J. M., de Rouffignac, E. P., Hunsucker, B, G., Menotiti, J. L., Pratt, C. A., and Wellington, S. L., 2007, Installation and Use of Removable Heaters in a Hydrocarbon Containing Formation, *US Patent No. 7,156,176*.

Vinegar, H. J., Veenstra, P., Giles, S. P., Sandburg, C. L., Rambow, F. H. K., Picha, M. G., Zhang, E., Beer, G., Carl, F. G., Bai, T., Kim, D. S., Fairbanks, M. D., and

Sanz, G., P., 2006c, In Situ Thermal Processes for Subsurface Formations, *US Patent No. 7121342*.

Wait, J. R., ed., 1959, *Overvoltage Research and Geophysical Applications*, Pergamon Press, New York.

Ward, S. H., and Fraser, D. C., 1967, Conduction of Electricity in Rocks, in: *Mining Geophysics, Vol. II*, Hansan, D. A., Heinrichs, W. E., Holmer, R. C., MacDougall, R. e., Sumner, J. S., and Ward, S. H., Society of Exploration Geophysicists , pp. 198–223.

Waxman, M. L., and Smitts, L. J. M., 1968, Electrical Conductivities of Oil-Bearing Shaly Sands, *SPE J. AIME Trans.,* 243 (1): 107–122.

Wittle, J. K., and Bell, C. W., 2005, Electrochemical Process for Effecting Redox-Enhanced Oil Recovery, *US Patent No. 6,877,556 B2*.

Wittle, J. K., and Bell, C. W., 2008, Method for Enhancing Oil Production Using Electricity, *US Patent No. 7,325,604 B2*.

Wittle J. K., and Hill, D. G., 2006a, Use of Direct Current Electrical Stimulation for Heavy Oil Production, *Society of Petroleum Engineers Applied Technology Workshop – Technologies for Thermal Heavy Oil and Bitumen Recovery and Production*, Calgary, March 14 – 15.

Wittle J. K., and Hill, D. G., 2006b, Direct Current Electrical Stimulation – A New Approach to Enhancing Heavy Oil Production", *First World Heavy Oil Conference*, Beijing, November 12 – 15.

Wittle, J. K., Hill, D. G., and Chilingar, G. V., 2008a, Direct Current Electrical Enhanced Oil Recovery in Heavy-Oil Reservoirs to Improve Recovery, Reduce Water Cut, and Reduce H_2S Production While Increasing API Gravity, *SPE-114012*, Society of Petroleum Engineers.

Wittle, J. K., Hill, D. G., and Chilingar, G. V., 2008b, Electro-Enhanced Oil Recovery (EEOR) Using Direct Current, *Oil Sands and Heavy Oil Technologies Conference*, Calgary.

Wittle, J. K., Hill, D. G., and Chilingar, G. V., 2008c, Direct Current Stimulation for Heavy Oil Production, *Second World Heavy Oil Conference*, Edmonton, Paper No. 2008-374.

Wittle, J. K., Hill, D. G., and Chilingar, G. V., 2011, Direct Current Oil Recovery (EEOR) – A New Approach to Oil Production, *Energy Sources, Part A: Recovery, Utilization, and Environmental Effects,* 33 (9): 805 – 822.

Wittle, J. K., and Pamukcu, S, 1993, Electrokinetic Treatment of Contaminated Soils, Sludges, and Lagoons, *DOE/CH-9206*, U. S. Department of Energy.

Workman, P. E., 1930, Method of Recovering and Increasing the Production of Oil: *US Patent No. 1,784,214.*

Websites

http://www.landfood.ubc.ca/soil200/components/mineral.htm

4

EEOR in Carbonate Reservoirs

By Mohammed Haroun, George V. Chilingar, Arsalan Ansari* and Nabeela Al Kindy*

4.1 Introduction

This chapter is presented to show that EEOR is not only applicable to sandstone but also to carbonate reservoirs. Numerous experiments were conducted in one of the most active electrokinetics laboratories by the principal author on numerous carbonate reservoir cores from Abu Dhabi producing oilfields. Haroun et al. (2009ab, 2012ab, 2013) published numerous papers on the subject.

Research on EEOR in carbonates is continuing at the University Research Center of the Petroleum Institute in Abu Dhabi. The first onshore pilot test in a carbonate reservoir in Abu Dhabi will also be made in the near future under the supervision of the authors.

* Petroleum engineering graduate students, Petroleum Institute, Abu Dhabi

4.2 Electrically Enhanced Oil Recovery (EEOR) – EK Assisted WF

Many waterflooding operations in carbonates present serious problems because of the plugging of pores by clays, bacteria, etc. Even greater problems occur in tight carbonate rocks, i.e., when water "does not move in". By applying DC current, the water moves in much better (e.g., see figure 4.1 and figure 4.2).

This increase in the oil recovery obtained from application of DC electrokinetics can be explained due to the hydrodynamic flow supported by the electrokinetic flow, which is the motion of liquid induced by an applied potential across a porous material, capillary tube, membrane, micro channel, or any other fluid conduit. This electrokinetic phenomenon is significantly enhanced when the flow takes place across small conduits especially in oil-wet reservoirs where most of the oil is by-passed.

The increment in displacement efficiency of about 10-17% results in an increase in residual water saturation of about 4-17%. This is due to the decrease in oil saturation in the cores as the core plug turns into water-wet from an oil-wet initially.

The average reservoir flow rate of 0.1 ml/min was used corresponding to the average flow rate of 1 ft/Day in carbonate reservoirs. It was shown that a lower flow rate of 0.1ml/min yielded higher oil displacement efficiency

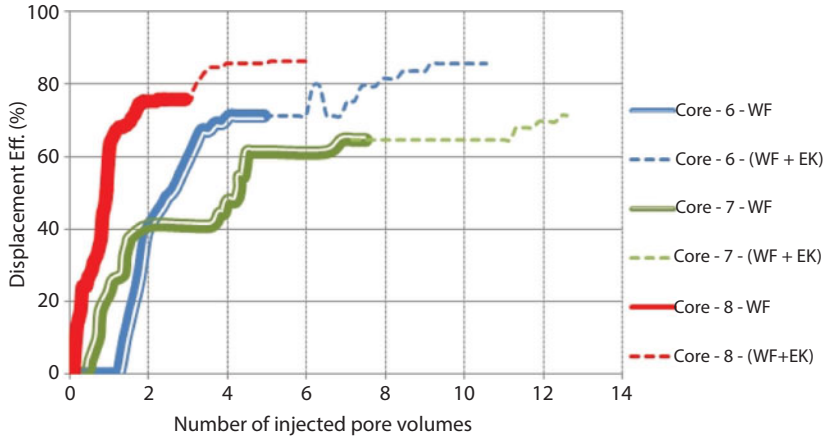

Figure 4.1 Displacement Efficiency (%) versus number of injected pore volumes in experiments conducted on a 1-in core at a flow rate of 0.1 ml/min.

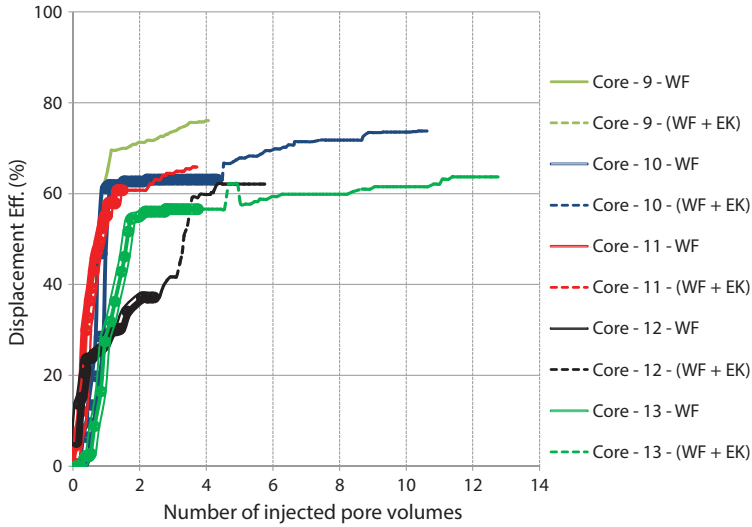

Figure 4.2 Displacement Efficiency (%) versus number of injected pore volumes in experiments conducted on a 1.5 -in core at a flow rate of 0.25 ml/min.

for EK-assisted waterflooding; about 3-4% more when compared to what was achieved during high flow rate experiments. This is due to an extended contact time of brine with the core plug leading to a greater migration of the oil left in the formation pores as mentioned by Amba *et al.* (1965). Furthermore, there is also continuity of a significant oil recovery in the EK assisted waterflooding as a small pore volume is injected for a longer period of time, effectively dragging the oil molecules along the interface of the mobile layers.

It was observed that electrochemically enhanced reactions resulted in an upgrade of the crude oil, while Joule heating also increased the mobility of fluids further.

4.3 SMART (Simultaneous/Sequential Modified Assisted Recovery Techniques)

The main objective of surfactant flooding in carbonates is wettability alteration and the reduction of interfacial tension (IFT). For more details on conventional surfactant-flooding, see Ziegler (1988), Wu et al. (1996), Seethipalli et al. (2004), Manrique et al. (2004,2007), Xie et al. (2005), Alkafeef et al. (2007), and Haiyang et al. (2011).

EK- Surfactant/EK-Nano/EK-Low Acid Concentration:

1. **Conventional flooding**
   Chemical EOR has a number of different advantages of enhancing recovery in carbonates as follows:

   - Reduces interfacial tension
   - Alters wettability
   - Enlarges displacement efficiency particularly in oil-wet reservoirs
   - Increases Recovery Factor

   Conventional acidizing has a number of different advantages of enhancing recovery in carbonates as follows:

   - Enhances permeability
   - Increases connectivity of previously uncommunicating pores through enlarged conduits and, therefore, increases oil recovery

   However, this technology is limited due to:

   - High consumption costs during injection of chemicals due to losses by adsorption/absorption.
   - The depth of penetration of acid, nano or surfactant in the rock formation is very low.
   - It may not be economically feasible.

2. **Sequential/Simultaneous EK-assisted surfactant-flooding/ EK-assisted nanoflooding / EK-assisted low HCl concentration EOR**

   SMART EOR provides an approach for having efficient and precise flooding in carbonates resulting in:

   - Reduced IFT, altering wettability and enlarging displacement efficiency particularly in oil-wet reservoirs
   - Negligible or minimal losses by adsorption/absorption on the rock surfaces
   - Precise targeting of by-passed oil

- Guiding acid/surfactant/nano through the micropore throats by EK
- Increasing Recovery Factor
- Enhancing depth of penetration
- Reducing surfactant and water consumption
- Better economic and environmental feasibility

The tested core plug where conventional acidizing was performed, revealed significant fractures penetrating all the way to the surface, rather than precisely delivering the acid front throughout the core plug. However, in the tested core plug with application of SMART EOR, the acid front exhibited a deeper depth of penetration and in turn, preserved the outer surface of the core plug from reacting with the injected acid.

4.4 (SMART EOR) Electrokinetic-Assisted Nano-Flooding/Surfactant-Flooding

Nanoparticles are used to enhance the recovery (Fletcher and Davis, 2010). Nanoparticles alter the properties of oil in order to assist in releasing the trapped oil. Ayatollahi and Zerafat (2012) showed that injecting particles 1-100 nm in size reduced the viscosity of oil, allowing for greater mobility of fluids. They tested several compounds, including aluminum oxide (Al_2O_3) and iron oxide (Fe_2O_3), with Al_2O_3 giving the best results.

Wettability can be affected by nanoparticles also (Ogolo and Onyekonwu, 2010, 2012). For example, polysilicon nanoparticles (PSNP) change the wettability of a rock surface. Lipophobic and hydrophobic PSNP (LHPN) change wettability from oil-wet to water-wet or water-wet to strongly water-wet (Ogolo and Onyekonwu, 2012). According to them, this would increase the oil mobility. Haroun et al. (2012) tested Fe_2O_3, CuO, and NiO (50 nm) nanoparticles. Some of the results comparing simultaneous vs sequential application of EK assisted nano-flooding are presented in figures 4.3 and 4.4. Comparison between the EK-assisted nanoflooding and EK-assisted surfactant-flooding is presented in figure. 4.5.

Nano EOR application flooding has demonstrated promising potential in carbonate reservoirs by modifying the viscosity of the displacing fluid to yield increased oil recovery. Some nanoparticles have displayed stability at high temperature, high pressure and high salinity, making them compatible with some of challenging carbonate reservoirs in the Middle East.

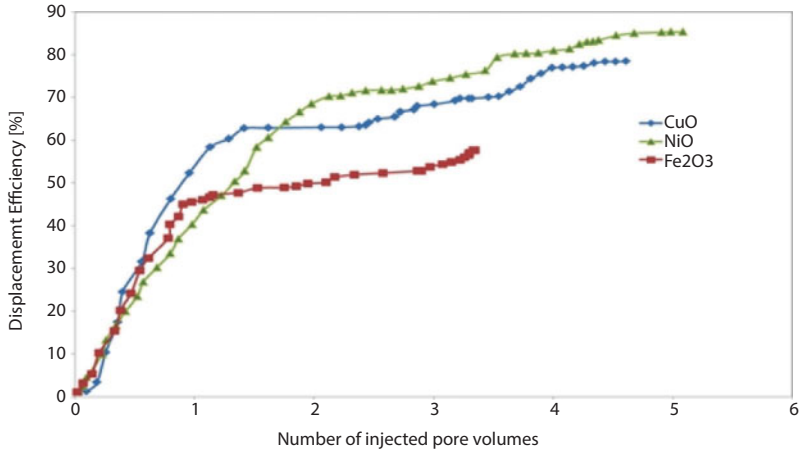

Figure 4.3 Displacement Efficiency using sequential application of EK-assisted nanoparticles (Haroun et al., 2012)

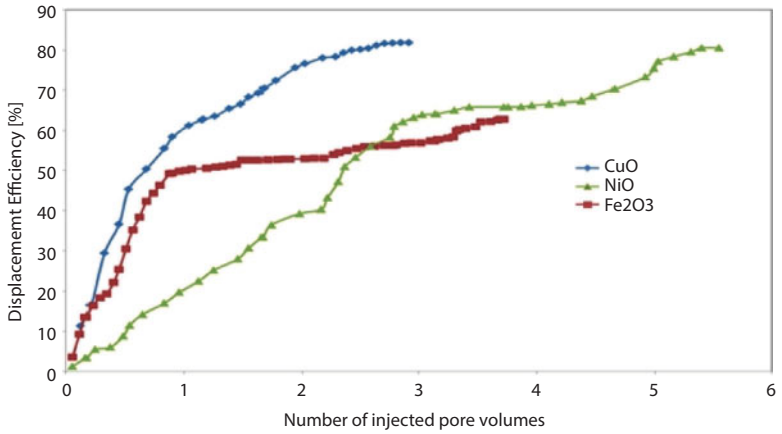

Figure 4.4 Displacement Efficiency using simultaneous application EK-assisted nano-flooding in water-wet carbonate core plugs (Haroun et al., 2012)

It was found that oil-wet core plugs experiments require approximately 10 times the water consumption than that of water-wet core plugs at room temperature (figure 4.6). In addition, there was a higher yield in oil-wet reservoirs as EK-assisted sequential nano-EOR produced 60% of the original displacement efficiency in oil-wet core plugs, while producing 35% of original displacement efficiency factor in water-wet core plugs. However, the

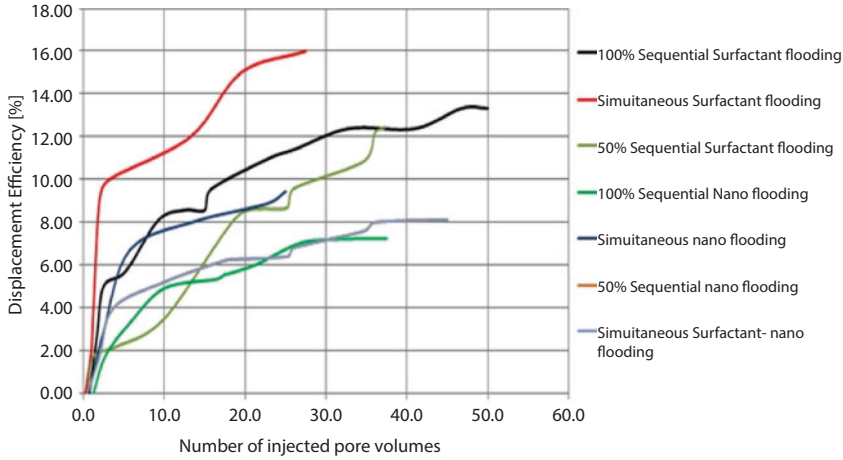

Figure 4.5 Displacement Efficiency using SMART EOR in oil-wet carbonate core plugs. Comparison between EK-assisted nanoflooding and EK-assisted surfactant-flooding (at room temperature).

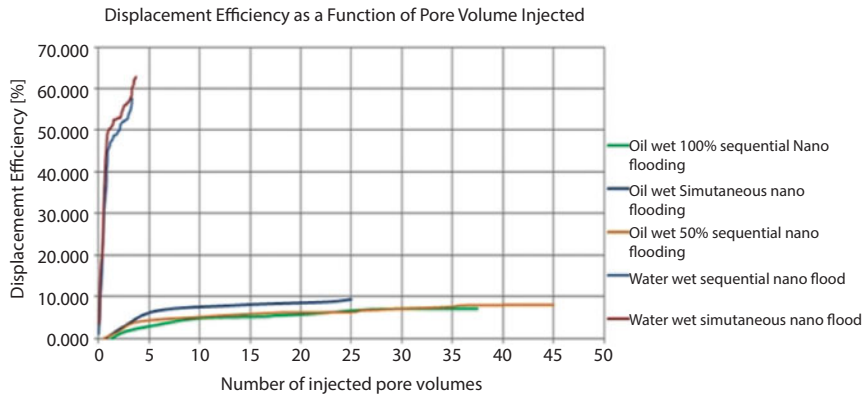

Figure 4.6 Displacement Efficiency in water-wet vs. oil-wet carbonate core plugs using EK-assisted nano-flooding as a function of injected pore volume (at room temperature)

highest displacement efficiency of 41% was observed in oil-wet core plugs at room temperature when SMART EOR was applied using EK-assisted nano-flooding in conjunction with surfactant and low concentration acid.

The simultaneous flooding reduces nanoparticles/surfactant and water consumption by 76% resulting in lower costs of CAPEX and OPEX. Additionally, the small amount of surfactant used reduces adverse environmental impact as it can be easily disposed. However, an increased amount

of power consumption of approximately 18% will be required which can be reduced by optimizing certain parameters when up-scaling future experiments currently being conducted at the PI-EKRC.

Smart EOR utilizes nanotechnology together with EOR. Nanotechnology and surfactant-flooding introduces catalysts into the formation to modify surface properties of the reservoir rock. EK Direct Current activates the catalytic activity. EK Direct Current is used as a driving force to transport oil, water and nanoparticles/surfactant in the formation.
SMART EOR:

- Reduces IFT
- Reduces adsorption capacity of injected fluid on surface of carbonate reservoir rock
- Effectively uses EK driving force to guide low concentration acid nanoparticles, surfactants through the tortuous path with the smaller conduits in carbonate reservoirs.
- Alters wettability
- Increases permeability
- Increase displacement efficiency
- Targets the unswept oil by increasing depth of penetration of acid/nano/surfactant injected solution

Ansari *et al.* (2012) showed that the application of waterflooding on the carbonate cores of Abu Dhabi yields displacement efficiency of 46-60%, with additional 8-14% incremental displacement efficiency upon application of EK. Also, an additional 8-20% displacement efficiency was achieved by the application of EK-assisted surfactant flooding (e.g., see figure 4.7).

SMART EOR using EK simultaneous surfactant flooding generated better results by reaching a maximum displacement efficiency of 87% due to the precise targeted transport of surfactant through the micro-pores towards the cathode (producer) when compared to EK sequential surfactant flooding displacement efficiency of 76%. In addition to this, there was also a 200% reduction in required injected pore volume during application of SMART EOR using EK simultaneous surfactant flooding when compared to EK sequential surfactant flooding.

Therefore, EK-assisted simultaneous surfactant flooding achieved an early displacement efficiency plateau providing potentially increased environmental and economic feasibility. As a result, it can be summarized that EK-assisted simultaneous flooding enhances displacement efficiency by 6%, with an increased power consumption of 18%, and reduced water/surfactant consumption by 76%.

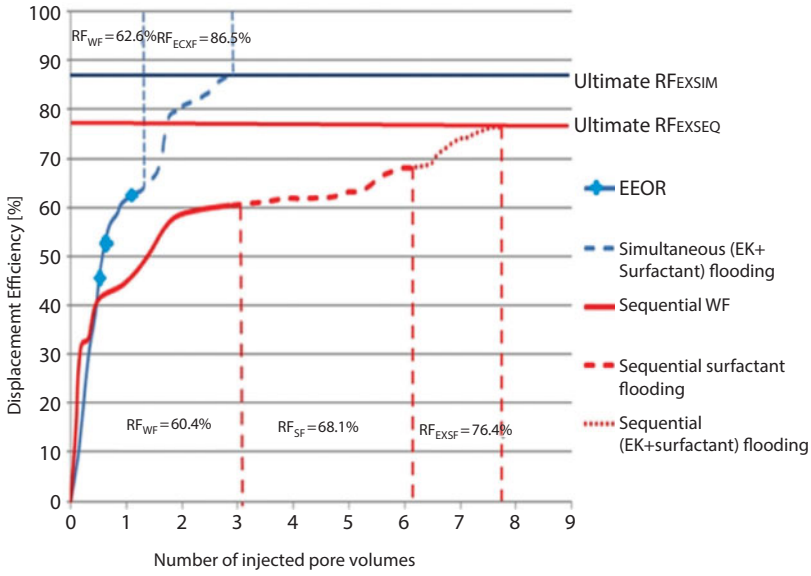

Figure 4.7 An example of different stages in SMART EOR (After Ansari et al., 2012)

4.4.1 Electrokinetic-Assisted Surfactant Flooding (SMART EOR) on Mixed to Oil-Wet Core Plugs

Simultaneous surfactant flooding produced 2.7% higher displacement efficiency or 20% more displacement efficiency related to original recovery when compared to sequential surfactant flooding. This was accomplished while reducing the surfactant/water consumption by 55%. EK sequential surfactant flooding produces almost the same displacement efficiency while providing up to 25% reduced water consumption when EK is initiated after waterflooding at the 50% water cut instead of after waterflooding at the 100% water cut. Therefore, if EK is applied in a mature reservoir early enough, the efficiency of the EK process would be further enhanced due to a significant reduction in water footprint. Furthermore, sequential surfactant flooding requires a lower current density and power consumption when compared to the simultaneous surfactant flooding (figure 4.8).

It was found that oil-wet core plugs require approximately 10 times more water consumption than water-wet core plugs at room temperature. In addition, SMART EOR resulted in a higher yield in mixed to oil-wet reservoirs as EK-assisted sequential surfactant EOR produced 56% of the

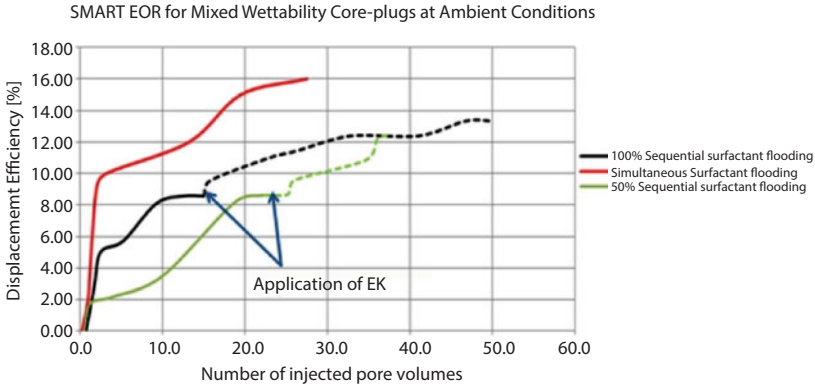

Figure 4.8 Displacement efficiency of mixed to oil-wet core plugs by EK-assisted surfactant flooding (at room temperature)

original displacement efficiency factor in oil-wet core plugs, while producing 28% of original displacement efficiency factor in water-wet core plugs.

4.5 Electrokinetics-Assisted Waterflooding with Low Concentration of HCl

Haroun *et al.* (2013) conducted experiments using a low concentration of hydrochloric acid (up to 1.4% strength) in EK-assisted waterflooding (e.g., see figures 4.9 and 4.10) in carbonates. The results demonstrate an exponential relationship between the acid concentration and permeability enhancement. This indicates that the rate of increment of permeability enhancement is dropping with increased acid concentration as the acid properties change significantly with increasing concentration (Harris *et al.*, 1966). This is due to the significant increase in production of fines and clay colloidal particles that block the pore throats, reducing the permeability. Therefore, there might be an optimum acid concentration at which there is a maximum permeability enhancement (approximately 1.2% HCl), which can be determined if experiments are conducted on a wide range on tight core plugs.

An increase in voltage gradient to 2 V/cm enhances permeability only by 36%. This may be due to the fact that an increase in voltage gradient increases the EK driving force reducing the contact time between the rock and acid. Driving the acid faster lowers the rate at which the electro-chemically enhanced reactions can take place. A voltage gradient of 1 V/cm gives

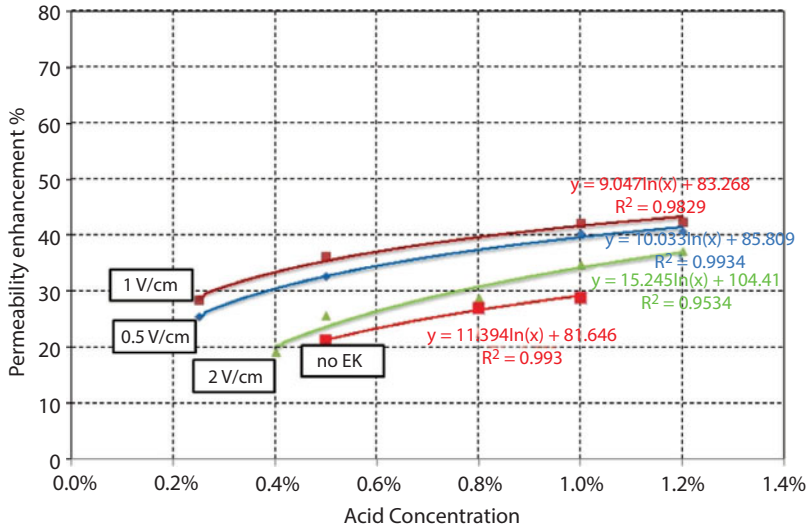

Figure 4.9 Effect of SMART EOR using low concentration acid on permeability enhancement using 0.5, 1, and 2 V/cm.

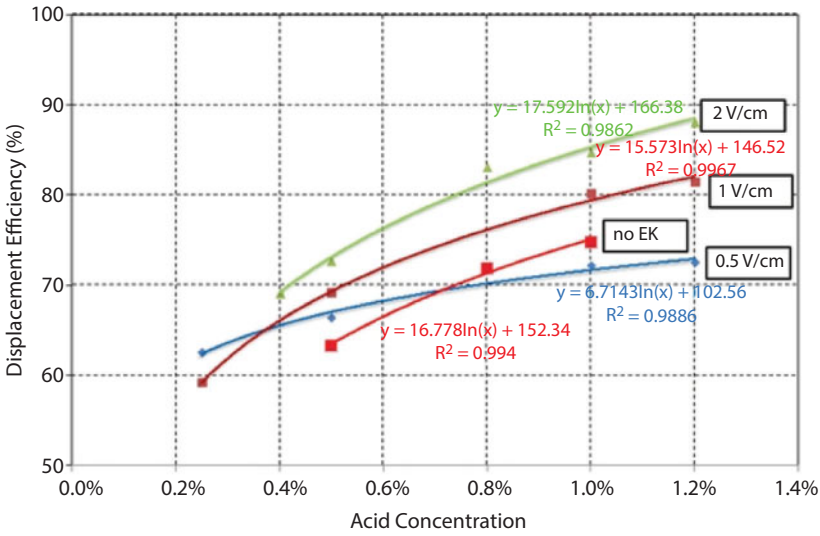

Figure 4.10 Effect of SMART EOR using low concentration acid on oil displacement efficiency using 0.5, 1, and 2 V/cm.

rise to a higher permeability enhancement of 43%, which is 5-9% higher than that with a gradient of 0.5 V/cm (41% enhancement). This is due to the electrophoresis phenomena of EK (Haroun *et al.,* 2009) that results in a rigorous migration of clay colloids and micelles or fines emptying the pore throats and, thus, potentially increasing the permeability. Therefore, there is an optimum voltage gradient of about 1 V/cm which will be verified by further experimental work.

In addition to this, it was also observed that 1-inch core plugs achieve higher values of permeability enhancement by about 20-30% as compared to the 1.5-inch core plugs with a maximum of 70% enhancement in permeability. This may be due to the reduced heterogeneity of 1-inch core plugs.

The displacement efficiency demonstrates an exponential relationship with the acid concentration. The increment in displacement efficiency decreases with increasing acid concentration as the curve approaches an optimum concentration beyond which the displacement efficiency factor starts to drop. The clogging of pore throats beyond the optimum concentration may decrease the oil recovery due to a significant reduction in permeability.

Another significant observation is that the effect of voltage gradient in increasing the displacement efficiency is not very dominant at lower acid concentrations. This indicates that an increase in acid concentration can significantly increase the displacement efficiency factor more than increasing the voltage gradient. This is potentially caused by a reduction in the rate of movement of ions (anions and cations) between the anode and the cathode, reducing the electromigration effect (Wittle *et al.,* 2008 and Pamukcu *et al.,* 2009).

At higher concentrations above 0.5%, the differences in displacement efficiency are observed and the maximum displacement efficiency of 89% was recorded in the case of 2V/cm potential gradient, as it produces the maximum EK driving force. At 1.0% acid concentration, when the voltage gradient increases from 0.5 V/cm to 1.0 V/cm, the displacement efficiency increases by 8%, but when the voltage gradient increases from 1 V/cm to 2 V/cm, the displacement efficiency increases by 5%. Thus, the optimum voltage gradient needs to be determined.

4.6 Effect of EEOR and SMART EOR in Carbonate Reservoirs at Reservoir Conditions

Following are the first laboratory results to date on EEOR and SMART EOR at elevated temperature and pressure. The displacement efficiency was

further enhanced at temperature up to 120 °C and pressures upwards of 3,000 psi, representative of some of the carbonate reservoirs around the world. It was interesting to note that the capillary number increased by up to 200% allowing increased recovery of the previously by-passed crude oil. In order to conduct representative tests of EEOR and SMART EOR, the reservoir temperature, pressure and formation water composition was used in these tests. The formation water contained approximately 270,000 ppm TDS, allowing the required current density to be achieved with lower applied voltage.

A comparison of EEOR and SMART EOR results at elevated temperatures and pressures has been summarized below (see figures 4.11 & 4.12 a and b).

A new index, incremental displacement efficiency to incremental pore volume injected ratio (Incremental D.E.:PVi index), has been proposed to track the efficiency of the EEOR and SMART EOR process vs conventional chemical EOR. It was observed that the Incremental D.E.:PVi index ranged from 2 to 4 for conventional EOR, while ranging from 6 to 10 for EEOR and 15 to 27 for SMART EOR. This provides an indication of the improved EOR performance as a function of water footprint, providing a clear justification on the environomics of each tested EOR process.

4.7 Economics

The laboratory results of power consumption per incremental barrel of oil produced in reducing OPEX for EEOR on a current density basis are shown

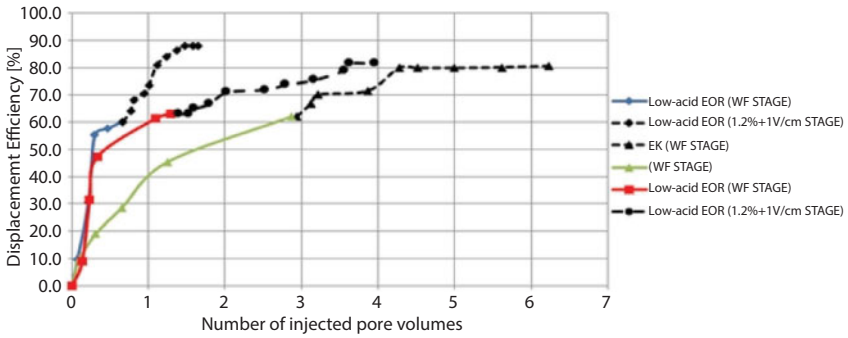

Figure 4.11 SMART EOR at elevated reservoir temperature and pressure (formation water composition 270k ppm TDS) – 30% increased oil displacement and more than 50% reduced water injected

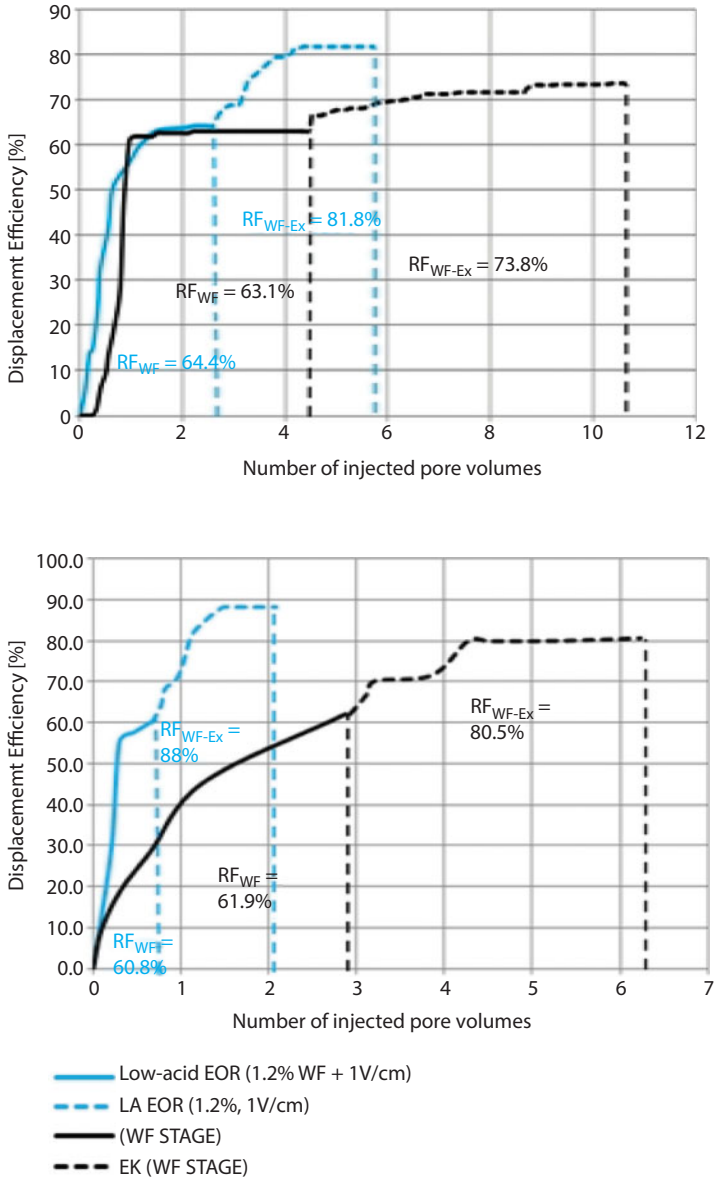

Figure 4.14 a and b EEOR vs SMART EOR at ambient conditions (a) vs. elevated reservoir temperature and pressure (b) in carbonate reservoir core plugs

by Al-Kindy *et al.* (2013). This was be achieved by identifying the desired target current density as a function of lithology, mineralogical content, wettability, oil resistivity and formation water composition. Based on the field retrieved samples from producing Abu Dhabi oil fields, the optimum range of current density can be managed to reduce power consumption per incremental barrel of oil produced according to the desired anode to cathode electrode spatial distance in the field. These results were comparable to those achieved by Wittle et al. (2008), on the EEOR pilot tests in Santa Maria, California, when using a spatial distance of 800 m between anode and production well (cathode).

Conclusions

Based on lab results, keeping in mind the experimental conditions and limitations, the following conclusions have been drawn:

- EK-assisted simultaneous flooding increased the oil displacement efficiency by 6%, with an increased power consumption of 18%, and reduced nano/surfactant consumption by 76%. The following sequential trend was observed for the recovery under the four EOR strategies (WF, N/S, EKSQ and EKSM) studied.
- EK-assisted simultaneous CuO nanoflooding produced superior results compared to EK simultaneous NiO nanoflooding:
  - Displacement efficiency was enhanced by an additional 10.34%
  - Power consumption was reduced by 53%
  - Water consumption was reduced by 57%
- EK-assisted sequential NiO nanoflooding also produced superior results to EK sequential CuO nanoflooding:
  - Displacement efficiency was enhanced by an additional 6.9%
  - Power consumption was reduced by 40%
  - Water consumption was reduced by 21%
- EK-assisted simultaneous surfactant flooding generates 2.7% enhanced displacement efficiency over EK sequential

surfactant flooding, while reducing the surfactant/water consumption by 55%.

- EEOR yield higher displacement potential in oil-wet reservoirs as EK-assisted sequential surfactant EOR produced 56% of the original recovery in oil-wet, while producing 28% of original recovery in water-wet core plugs.
- The maximum enhanced oil displacement efficiency of 41% was observed in oil-wet core plugs at room temperature when smart EOR was complemented by EK assisted low concentration acid (450% increase from original yield) (Ansari *et al*., 2013).
- The incremental displacement efficiency due to EK is higher (30% increase from original yield on average) in oil-wet core plugs when compared to water-wet core plugs.
- SMART EOR produced a maximum of 89% oil displacement efficiency while consuming 1.7 pore volume injected at HTHPHS: elevated temperature of 110°C, pressure of 5000 psi and formation water salinity of 270k ppm TDS.
- Overall SMART EOR produced up to 27% increase in the ratio of incremental oil displacement efficiency to pore volume injected, while conventional chemical (nano/surfactant) produced 2-4% increase in the ratio of incremental oil displacement efficiency to pore volume injected.
- SMART EOR can be customized based on reservoir fluid composition, rock mineralogy, oil specific gravity and resistivity under HTHPHS to significantly improve oil displacement while optimizing both power and water consumption levels.

Nomenclature

ADCO	Abu Dhabi company for onshore oil operations
ADNOC	Abu Dhabi National Oil Company
APG	Alkyl Polyglycoside
CAPEX	Capital Expenses
DC	Direct Current
DE	Displacement Efficiency (Oil recovery in one dimensional flow across core plug)
D.E.:PVi	Incremental displacement efficiency: incremental pore volume injected index

EOR	Enhanced Oil Recovery
EEOR	Electrically Enhanced Oil Recovery
EK	Electrokinetics
EKSM	Simultaneous Electrokinetics-Assisted Flooding
EKSQ	Sequential Electrokinetics-Assisted Flooding
EKLAEOR	Electrokinetics Low Concentration Acid EOR
HTHPHS	High temperature-high pressure-high salinity
LHPN	Lipophobic and Hydrophilic Polysilicon Nanoparticles
OOIP	Original Oil-in-Place
OPEX	Operational Expenses
OW	Oil-wet
PI-EKRC	Petroleum Institute Electrokinetic Research Center
PSNP	Polysilicon Nanoparticles
N/S	Nano/Surfactant
RF	Recovery Factor = DE* Volumetric sweep
Sequential	WF followed by conventional chemical EOR followed by EEOR
Simultaneous	Chemical EOR applied simultaneously with EEOR
SMART	Simultaneous/Sequential Modified Assisted Recovery Techniques
V/cm	Volt per centimeter
WF	Waterflooding
WW	Water-wet

References

Alkafeef, S.F. and Alforgi, M.Z., 2007. Review of and Outlook for Enhanced Oil Recovery Techniques in Kuwait Oil Reservoirs, *IPTC* 11234.

Al Kindy N., Haroun M., Ansari A. and Sarma H., 2013. Application of Electrokinetics to achieve Smart Nano-Surfactant EOR in Abu Dhabi Carbonate Reservoirs. *ADIPEC*.

Amba, S.A., Chilingar, G.V. and Beeson, C.M., 1964. Use of direct electrical current for increasing the flow rate of reservoir fluids during petroleum recovery. *J. Canad. Petrol. Technol.,* 3 (1): 8–14.

Amba, S.A., Chilingar, G.V. and Beeson, C.M., 1965. Application of electrical current for increasing the flow rate of oil and water in a porous medium. *J. Canad. Petrol. Technol.,* 4 (2): 81–85.

Ansari, A., Haroun, M., Abou Sayed N., Al Kindy, N., Ali, B., Shrestha, R., and Sarma, H., 2012. A new approach optimizing mature waterfloods with electrokinetics-assisted surfactant flooding in Abu Dhabi carbonate reservoirs.

SPE 163379 *SPE Kuwait International Petroleum Conference and Exhibition*, Kuwait, 10–12 Dec.

Ayatollahi, S. and Zerafat, M.M., 2012. Nanotechnology-assisted EOR techniques: New solutions to old challenges. *SPE* 157094 *SPE International Oilfield Nanotechnology Conference*, Noordwijk, Netherlands, 12–14 June.

Chilingar, G., El-Nassir, A., and Stevens, R., 1970. Effect of direct electrical current on permeability of sandstone cores. *J. Petrol. Technol.*, *22*(7): 830–836.

Fletcher, A. and Davis, J. 2010. How EOR can be transformed by nanotechnology. *SPE* 129531 *SPE Improved Oil Recovery Symposium*, Tulsa, OK, 24–28 April.

Haiyang, Y., Yefei, W., Yani, Z., Peng, Z. and Wuhual, C., 2011, Effects of displacement efficiency of surfactant flooding in high salinity reservoir: Interfacial tension, emulsification, adsorption. *Advances in Petroleum Exploration and Development,* 1 (1): 4–5.

Haroun, M., Ansari, A. and Al Kindy, N., 2014. Applying EK to achieve SMART (simultaneous assisted recovery techniques) EOR in conventional and tight carbonate reservoirs of Abu Dhabi. *Electrochemistry Gordon Research Conference*, Ventura, CA.

Haroun, M., Chilingar, G.V. and Wittle, J.K.., 2012. Optimizing our mature waterfloods by application of electrokinetics in Abu Dhabi carbonate reservoirs – *Stimulating the Formation with EEOR*. 2012 *Electrochemistry Gordon Research Conference*, Ventura, CA, Jan.

Haroun, M., Alhassan, S., Ansari, A., Al Kindy, N., Abou Sayed, N., Abdul Kareem, B., and Sarma, H., 2012. Smart Nano-EOR process for Abu Dhabi carbonate reservoirs. *SPE* 162386 *SPE Abu Dhabi International Petroleum Conference and Exhibition (*ADIPEC).

Haroun, M., Ansari, A., Al Kindy, N., Abou Sayed, N., Ali, B., Shrestha, R., and Sarma, H., 2013. Application of electrokinetics to achieve smart EOR in Abu Dhabi oil-wet carbonate reservoirs. Presented at the *Electrokinetic Remediation Conference*, June 23–26.

Haroun, M., Chilingar, G.V., Pamukcu, S., Wittle, J., Belhaj, H., and Al Bloushi, M., 2009. Optimizing electroosmotic flow potential for electrically enhanced oil recovery (EEOR™) in carbonate rock formations of Abu Dhabi based on rock properties and composition. *International Petroleum Technology Conference (IPTC)*, Doha, Qatar, 7–9 Dec.

Haroun, M., Chilingar, G.V., Pamukcu, S., Wittle, J., Belhaj, H., and Al Bloushi, M., 2010. The feasibility of using electrokinetics (EEOR) in carbonate rock formations of Abu Dhabi. 2010 *Electrochemistry Gordon Research Conference*, Ventura, CA, Jan.

Haroun, M., Wittle, J.K. and Chilingar, G.V., 2012. Publication No. WO/2012/074510. Title of the invention: "*Method for Enhanced Oil Recovery from Carbonate Reservoirs*." Applicants: ELECTRO-PETROLEUM, INC. (US). Inventors: Mohammed Haroun (AE), J. Kenneth Wittle (US) and George Chilingar (US), June 12.

Haroun, M., Wittle, J.K., Chilingar, G.V. and Ghosh, B., 2012. Publication No. WO/2012/158145 A1. Title of the invention: "*Method for Electrokinetic Prevention of Scale Deposition in Oil Producing Well Bores*." Applicants: ELECTRO-PETROLEUM, INC. (US). Inventors: Mohammed Haroun (AE), J. Kenneth Wittle (US), George Chilingar (US) and Bisweswar Ghosh (AE), Nov. 22.

Haroun, M., 2013. Emerging EOR technologies. *OPEC R&D Forum*, OPEC Secretariat, Vienna, Austria, May 7–8.

Manrique, E., Gurfinkel, M. and Muci, V., 2004. Enhanced oil recovery field experiences in carbonate reservoirs in the United States. 25th *Annual Workshop on Enhanced Oil Recovery International Energy Agency*, Sept.

Ogolo, N. and Onyekonwu, M.O., 2010. Investigating the use of nanoparticles in enhancing oil recovery. *SPE* 140744 *SPE Nigeria Annual International Conference and Exhibition*, Tinapa, Nigeria, 31 July-7 Aug.

Ogolo, N. A., Olafuyi, O.A., and Onyekonwu, M.O., 2012. Enhanced oil recovery using nanoparticles. *SPE* 160847 presented at the *SPE Saudi Arabia Section Technical Symposium and Exhibition*, Al-Khobar, Saudi Arabia, 8–11 April.

Seethepalli, A., Adibhatla, B., and Mohanty, K.K., 2004. Physicochemical Interactions During Surfactant Flooding of Fractured Carbonate Reservoirs. *SPEJ* 9(4): 411–418. *SPE*-89423-PA. *DOI*: 10.2118/89423-PA.

Wu, Z., Reynolds, A.C., and Oliver, D.S., 1999. Conditioning Geostatistical Models to Two-Phase Production Data. *SPEJ* 4(2): 142–155. *SPE*-56855-PA.DOI: 10.2118/56855-PA.

Xie, X., Weiss, W.W., Tong, Z., and Morrow, N.R., 2005. Improved Oil Recovery from Carbonate Reservoirs by Chemical Stimulation. *SPEJ* 10 (3): 276–285. *SPE*-89424-PA. *DOI*: 10.2118/89424-PA.

Ziegler, V.M., 1988. Laboratory investigation of high-temperature surfactant flooding. *SPERE* 3 (2): 586–596. *SPE*-13071-PA. *DOI*: 10.2118/13071-PA.

5

Mathematical Modeling of Electrokinetic Transport and Enhanced Oil Recovery In Porous Geo-Media

Ehsan Ghazanfari and Sibel Pamukcu

5.1 Introduction

EK application for the recovery of reservoir oils has gained a lot of attention over the past decades. It has been reported to have great potential as a viable energy resource recovery application (Amba et al., 1964; Amba et al., 1965; Chilingar et al., 1968, 1970; Killough and Gonzalez, 1986; Wittle et al., 2006 a,b, 2008 a,b,c, 2011; Haroun et al., 2009; Hill et al., 2010; Ghazanfari et al., 2012a, 2012b; Al Shalabi et al., 2012; Ghazanfari, 2013). Upon application of direct current to the reservoir, EK phenomenon is activated near the solid-liquid interfaces inside the pores and a multiphase flow is generated and sustained by the EK assisted transport. Based on the available reports, the process has emerged to have advantage as a

non-drilling operation compared to other conventional methods and oil production is enhanced by simultaneous reduction of oil viscosity (Wittle et al., 2008 a,b; 2011; Haroun et al., 2009; Hill et al., 2010; Al Shalabi et al., 2012; Ghazanfari, 2013).

Mathematical models for petroleum reservoir simulation are valuable tools in predicting the oil production and visualizing reservoir flow patterns. Mathematical modeling of EK enhanced oil recovery (EKEOR) is complex because of the need to integrate multi-phase flow and the EK transport processes. In this chapter, we first review the basics of EK transport modeling and then provide results of initial work on modeling of EKEOR.

5.2 Basics of EK Transport Modeling

Laboratory and field observations on EK remediation of contaminated soils help to better understand the EK transport process. Many features of this transport can be understood from laboratory tests and field observations and employed to describe the physical process in a mathematical model, including the coupled flow and ion migration. A mathematical model of EK transport upgrades our understanding of the EK processes from direct observation to the general principles (Cao, 1997) and helps predict the efficiency of the EK remediation of a specific contamination substance (e.g., heavy metal ion), in a specific soil type. The EK transport models are usually calibrated using controlled laboratory experiments. Ultimately the model should support the field observations adequately so it can be used to predict the success of EK remediation process in the field application, for specific contaminant types.

Mathematical modeling and simulation of the EK transport in porous geo-media (i.e., soil, rock) necessitates mathematical formulation of multiple transport processes, which are controlled by different variables. These variables include the products of the electrolysis reactions at the electrodes, soil pH and soil-surface chemistry, equilibrium chemistry of the aqueous system, electrochemistry of the contaminants, and geotechnical/hydrogeological characteristics of the porous medium (Shapiro and Probstein, 1993; Alshawabkeh, 1996). The EK transport models are based on a generally accepted transient coupled flow equation, which maintains conservation of mass and energy.

The complexity of transport processes necessitates simplifying assumptions that enables us to conduct numerical simulation. These assumptions include: (i) the soil medium is isotropic and saturated, (ii) the porous

medium is a solid framework of cation exchange surfaces with the pore space occupied by chemically reactive species in aqueous solution, (iii) all fluxes are linear homogeneous functions of all driving forces (or potential gradients), (iv) isothermal conditions prevail (coupled heat transfer is neglected), (v) all the applied voltage is effective in fluid and charge transport, (vi) electrophoresis is not present, (vii) soil particles are treated as electrically nonconductive (insulators), (viii) surface conductance and streaming potential are negligible, and (ix) hydraulic conductivity, coefficient of EO permeability, and coefficient of volume compressibility are constant in time and space (Alshawabkeh, 1996).

Several mechanisms contribute to the transport of mass in porous geomedia under applied electric field including hydraulic or fluid flow, ion, compound, and charge transport. In the following section a description of these transport mechanisms under the aforementioned assumptions is provided.

5.3 Fundamental Governing Equations

5.3.1 Fluid Flux

Fluid flux in a porous medium due to applied hydraulic gradient is given by Darcy's law as:

$$J_w^h = k_h \nabla(-h) \tag{5.1}$$

where, k_h is the coefficient of hydraulic conductivity (LT^{-1}), and h is the hydraulic head (L). Microstructure, fabric, porosity, and pore size distribution of the fine grain soils are the main factors that affect k_h and significantly influence fluid transport under applied hydraulic gradient. Fluid flux due to the applied electrical gradient in a porous medium is given by the Helmholtz-Smoluchowski theory as:

$$J_w^e = k_{eo} \nabla(-E) \tag{5.2}$$

where, $k_{eo} = \frac{\varepsilon \xi}{\mu}$ is electroosmosis permeability coefficient ($L^2V^{-1}T^{-1}$), ε is permittivity of the medium ($Farad.L^{-1}$), ξ is zeta potential (V), E is electric potential (V), and μ is dynamic viscosity of pore fluid (FTL^{-2}). Electroosmosis (EO) permeability coefficient depends mainly on porosity and zeta potential of the soil. The total fluid flux due to applied hydraulic and electrical gradients is given by:

$$J_w = k_h \nabla(-h) + k_{eo} \nabla(-E) \tag{5.3}$$

The total one-dimensional fluid flux can therefore be found as:

$$J_w = -k_h \frac{\partial h}{\partial x} - k_{eo} \frac{\partial E}{\partial x} \tag{5.4}$$

Under combination of applied hydraulic and electrical gradients, consolidation of soil is expected to take place and influence the hydraulic conductivity value (k_h) (Acar, et al., 1997). However, in the mathematical formulation of the process, k_h is generally assumed to be constant in time and space because of: (i) the lack of theoretical mechanisms that can describe and capture the effect of pore fluid chemistry on soil fabric and consequently the hydraulic conductivity, and (ii) the uncertainties in evaluating the hydraulic conductivities are more significant than the changes expected in its values. Also, the value of k_{eo} is usually assumed to be constant during the EK process as long as there is no change in the concentration of ions or pH of the pore fluid, which is not always a valid assumption (Gray and Mitchell, 1967; Lorenz, 1969; Hunter, 1981).

The ratio of coefficient of EO permeability (k_{eo}) to hydraulic conductivity (k_h) significantly affects the contribution of each applied gradient to the total flux. Soil type, microstructure, and pore fluid conditions are among the factors that impact this ratio. In coarse-grained soils this ratio is very small due to almost non-existing EO flow and relatively high hydraulic conductivities (>10^{-3} cm/sec), whereas in fine-grained soils the ratio becomes significant as is usually in the order of 10^{-5} (cm^2/V.sec), while is less than 10^{-5} cm/sec (10^{-7} cm/sec for clayey soils) (Acar et al., 1997).

5.3.2 Mass Flux

Different coupled potential gradients cause the mass flux of chemical species relative to pore fluids in porous media. Diffusional mass flux (i.e., mass transport due to chemical concentration gradient) and migrational mass flux (i.e., mass transport of charged species due to an electric potential gradient) are the main components that contribute to the mass flux of chemical species in porous media. Advection (i.e., species transport by the flowing fluid) is another component of mass flux of dissolved species, as well as surface neutral micelles and immiscible fluids.

Fick's first law describes the diffusive mass flux of chemical species in a saturated soil medium under chemical concentration gradients as:

$$J_i^d = D_i^* \nabla(-C_i) \tag{5.5}$$

where, J_i^d is the diffusive mass flux of the ith chemical species per unit cross sectional area of the porous medium ($ML^{-2}T^{-1}$), C_i is the molar concentration of the ith chemical species (ML^{-3}), and D_i^* is the effective diffusion coefficient of the ith chemical species (L^2T^{-1}). The migrational mass flux of the free ionic species in the soil pore fluid due to the applied electrical gradient is given by:

$$J_i^e = u_i^* C_i \nabla(-E) \tag{5.6}$$

where, J_i^e is the migrational mass flux of the ith species ($ML^{-2}T^{-1}$), and u_i^* is the effective ionic mobility of the ith species ($L^2T^{-1}V^{-1}$) defined as:

$$u_i^* = \frac{D_i^* Z_i F}{RT} \tag{5.7}$$

where, Z_i is the charge of the ith species (Coulomb), F is Faraday's constant (96,485 C/mo1 electrons), R is the universal gas constant (8.3144 J/Kmol), and T is the absolute temperature (K). The other contributing mechanism to the flux of species is advection by the soil pore fluid. The advective mass flux of species i relative to the soil particles is:

$$J_i = C_i J_w = C_i \left[k_h \nabla(-h) + k_{eo} \nabla(-E) \right] \tag{5.8}$$

where, C_i is the molar concentration of pore fluid. The total species mass flux (diffusion, migration, and advection) is given as:

$$J_i = D_i^* \nabla(-C_i) + u_i^* C_i \nabla(-E) + C_i \left[k_h \nabla(-h) + K_{eo} \nabla(-E) \right] \tag{5.9}$$

Figure 5.1 shows a schematic of mass transport profile of cationic and anionic species based on the assumption that water advection components (EO and hydraulic) act from anode to cathode. As observed in figure 5.1, the advective EO flow enhances transport of cationic species migrating from anode toward cathode, and retards transport of anionic species migrating from cathode to anode (Shapiro and Probstein, 1993; Acar et al., 1997).

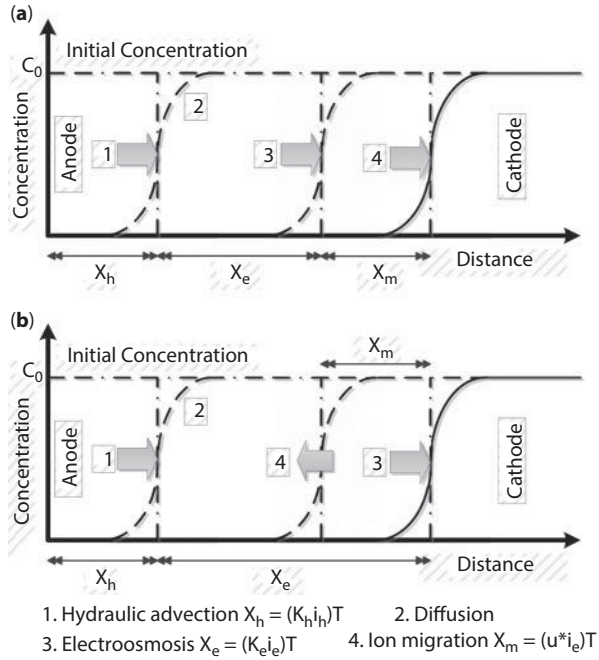

Figure 5.1 Transport mechanisms of (a) cations and (b) anions (After Acar et al., 1997)

Further simplification of equation 5.9 results in:

$$J_i = D_i^* \nabla(-C_i) + C_i\left(D_i^* + k_{eo}\right)\nabla(-E) + C_i k_h \nabla(-h) \qquad (5.10)$$

For one dimensional flow, the total mass flux of species i, is given by:

$$J_i(x) = -D_i^* \frac{\partial c_i(x)}{\partial x} - C_i\left(D_i^* + k_{eo}\right)\frac{\partial E}{\partial x} - C_i k_h \frac{\partial h}{\partial x} \qquad (5.11)$$

As equation 5.10 implies, an applied electrical gradient results in two mass transport mechanisms, ion migration and EO advection. The relative contribution of the two mechanisms to species transport depends on soil and contaminant characteristics (Acar et al., 1997; Cao, 1997). Presence and content of clay minerals, the ionic strength of pore fluid, and pH significantly affects the EO flow. For instance, acidic pore fluid conditions could reverse the charge on the clay mineral surface, and consequently the direction of EO flow (Lorenz 1969; Hunter 1981; Stumm 1992; Eykholt

and Daniel 1994). On the other hand, ionic migration can occur in all soil types, including sand and gravel, and is affected by ionic strength and pH to a lesser extent compared to EO flow.

5.3.3 Charge Flux

Upon application of direct current to a saturated soil medium, the electric field causes charge transport. The main components of charge flux in a saturated soil medium are migration flux, and diffusion flux (due to the diffusion of charged species). There is no contribution of the advective fluid transport to the charge transport.

The current density in the pore fluid due to applied electrical gradient is given by Ohm's law as:

$$I = \sigma^{*}\nabla\left(-E\right) \tag{5.12}$$

where, I is the electric current density ($CL^{-2}T^{-1}$), and σ^{*} is the effective electric conductivity of the porous medium given as:

$$\sigma^{*} = \sum_{j=1}^{N_{species}} Z_j F u_j^{*} C_j \tag{5.13}$$

The migration charge flux can be related to the migration mass flux of species using Faraday's law for equivalence of mass flux and charge flux as:

$$I^{e} = \sum_{j=1}^{N_{species}} Z_j F J_i^{e} = \sum_{j=1}^{N_{species}} Z_j F u_j^{*} C_j \nabla\left(-E\right) \tag{5.14}$$

Similar to the migrational charge flux, the diffusional charge flux due to the diffusional mass flux of charged species is evaluated using Faraday's law of the equivalence of mass flux and charge flux as:

$$I^{d} = \sum_{j=1}^{N_{species}} Z_j F J_i^{d} = \sum_{j=1}^{N_{species}} Z_j F D_j^{*} \nabla\left(-C_j\right) \tag{5.15}$$

The electrical neutrality of free pore fluid is preserved by:

$$\sum_{j=1}^{N_{species}} C_j Z_j = 0 \tag{5.16}$$

The total charge flux (migration and diffusion charge flux) can be found as:

$$I = \mathrm{F}\sum_{\mathrm{j=1}}^{\mathrm{N_{species}}} \mathrm{Z_j} D_j^* \nabla\left(-\mathrm{C_j}\right) + \sigma^* \nabla(-\mathrm{E})] \tag{5.17}$$

For one dimensional applications, the total charge flux will be given by:

$$I = -\mathrm{F}\sum_{\mathrm{j=1}}^{\mathrm{N_{species}}} \mathrm{Z_j D_j} \frac{\partial c_j}{\partial x} - \sigma^* \frac{\partial E}{\partial x} \tag{5.18}$$

5.3.4 Conservation of Mass and Charge

Applying the conservation of fluid, mass and charge equation to fluid flux in saturated soil medium results in the following expression:

$$\frac{\partial \varepsilon_V}{\partial t} = -\nabla J_w = m_V \frac{\partial u}{\partial t} = m_V \gamma_w \frac{\partial h}{\partial t} \tag{5.19}$$

where, ε_V is the volumetric strain of the soil mass, m_V is the coefficient of volume compressibility of the soil, u is the pore water pressure, γ_w is the unit weight of water, h is hydraulic head, and t is time. Equation 5.19 is Terzaghi's classical consolidation equation which describes the change in hydraulic head due to soil volume change. This equation becomes important in cases where hydraulic gradients are also used to enhance transport under applied electrical gradient.

The mass conservation equation describes transient reactive transport of i chemical species under hydraulic, electric, and chemical concentration gradients. Applying the conservation equation to mass transport of species i results in:

$$\frac{\partial n C_i}{\partial t} = -\nabla J_i + n R_i \tag{5.20}$$

where, R_i is the production/consumption rate of the i^{th} aqueous chemical species per unit fluid volume due to geochemical reactions, and n is the porosity of the soil.

Applying conservation of charge to the charge flux equation, results in:

$$\frac{\partial T_e}{\partial t} = -\nabla I = C_p \frac{\partial E}{\partial t} \tag{5.21}$$

where, T_e is the volumetric charge density of the soil medium (CL^{-3}), and C_p is the electrical capacitance per unit volume ($Farad.L^{-3}$). The equation describes the rate of change in the electrical potential required to maintain electrical neutrality of the medium. For zero net change in charge, zero electric capacitance (C_p) is assumed for the soil.

5.3.5 Geochemical Reactions

In equation 5.20, reactive transport of charged species is controlled by rates of geochemical reactions (R). Electrolysis reactions at the electrodes significantly affect the pH and chemistry conditions at the boundaries (Alshawabkeh, 1996; Cao, 1997). The chemistry boundary conditions results in a complex system of geochemical reactions that include sorption, redox, and precipitation/dissolution reactions. The term could be written as:

$$R_i = R_i^s + R_i^{aq} + R_i^p \tag{5.22}$$

where, R_i^s represents the sorption term, R_i^{aq} is aqueous reactions terms, and R_i^p represents precipitation/dissolution reactions. Two approaches have been developed and used to describe chemical reactions in the literature including (i) the instantaneous equilibrium approach, and (ii) the kinetics approach (Kirkner and Reeves, 1988; Davis and Kent, 1990; Alshawabkeh and Acar, 1992, 1996; Stumm and Morgan, 1995; Cao, 1997). In the instantaneous equilibrium reactions species concentrations reach equilibrium instantaneously whereas in kinetic reactions approach concentrations in solution vary with time until they reach equilibrium (Acar et al., 1997). For several species, chemical reactions have been found to vary with time before reaching equilibrium. The kinetics approach is expected to be more realistic for modeling these reactions. However, one could assume chemical reactions reach equilibrium at a very short time (relative to transport time) and can use instantaneous equilibrium. Different geochemical models exist and one could incorporate these models for predicting rates of geochemical reactions during electric field applications. In the following section an overview of these reactions is provided.

5.3.5.1 Sorption reaction

The following general term is considered for sorption evaluation:

$$R_i^s = \frac{\rho}{n}\frac{\partial S_i}{\partial t} = \frac{\rho}{n}\frac{\partial S_i}{\partial t}\frac{\partial C_i}{\partial t} \quad \text{i} = 1,2,\ldots\text{N} \tag{5.23}$$

Where, ρ is the bulk dry density of the soil, S_i is the adsorbed concentration of the component per unit mass of the soil solids. The reversible term ($\frac{\partial S_i}{\partial t}$) is often used to describe the adsorption rate (Kirkner and Reeves, 1988; Davis and Kent, 1990). The equilibrium partitioning between the adsorbed phase and the aqueous phase of the chemical components are commonly measured under controlled temperature and applied pressure, and the resulting correlations of S_i versus C_i are called adsorption isotherms. Different equilibrium models are used to describe sorption of heavy metals in soils. Assuming instantaneous equilibrium in sorption reactions and linear isotherms:

$$\frac{\partial S_i}{\partial C_i} = K_{di} \tag{5.24}$$

Where, K_{di} is the distribution coefficient of species i. Retardation factor (R_{di}) is also introduced and used in modeling species transport to account for linear sorption expressed as:

$$R_{di} = 1 + \rho \frac{K_{di}}{n} \tag{5.25}$$

The retardation factors of species i (R_{di}) define the relative rate of transport of a non-sorped species to that of a sorped species. For a non-sorped species, R_{di} = 1. Simple isotherm sorption models ignore the potential effects of variations in pH, solute composition and ionic strength, redox potential, or processes such as competitive adsorption. Alternatively, more robust and complicated sorption models include ion-or ligand-exchange, mass action models, and surface complexation models are also reported in the literature (Kirkner and Reeves, 1988; Davis and Kent, 1990; Stumm and Morgan, 1995; Bethke, 1996).

5.3.5.2 Aqueous reactions

In aqueous phase reactions, any complex j is the product of i's reactant components expressed as:

$$\sum_{i=1}^{N_c} a_{ij} \overline{C_i} \leftrightarrow \overline{X_j} \quad j = 1,2,\ldots,\mathrm{N_x} \tag{5.26}$$

where, $\overline{C_i}$ is the chemical formula for component i, $\overline{X_j}$ is the chemical formula for the complex *j*, a_{ij} is the stoichiometric coefficient in complex *j* for component *i*. The law of mass action implies that:

$$X_j = K_j^{eq} \prod_{i=1}^{N_c} C_i^{a_{ij}} \quad j=1,2,\ldots,N_x \tag{5.27}$$

where, K_j^{eq} is the equilibrium constant for aqueous reaction *j*. The rate of accumulation of component *i* due to aqueous reaction *j* (R_{ji}^{aq}) is:

$$R_{ji}^{aq} = a_{ji} R_j \tag{5.28}$$

The total rate of accumulation of component *i* due to all aqueous reactions is given as:

$$R_i^{aq} = \sum_{j=1}^{N_X} R_{ji}^{aq} = \sum_{j=1}^{N_X} a_{ji} R_j \tag{5.29}$$

5.3.5.3 Precipitation/dissolution reactions

It is important to incorporate the precipitation/dissolution reactions in the mass transport model. In precipitation reactions, the chemical components are assumed to be composed of products expressed as:

$$\overline{P_j} \rightarrow \sum_{i=1}^{N_c} b_{ij} \overline{C_i} \quad j=1,2,\ldots,N_p \tag{5.30}$$

Where, $\overline{P_j}$ is the chemical formula for precipitate *j*, b_{ij} is the stoichiometric coefficient in precipitate j for component *i*, and N_p is the number of precipitates for component *i*. The production of the precipitate will not occur until the solution is saturated. Therefore, the law of mass action is written as:

$$K_j^{SP} \geq \prod_{i=1}^{N_c} C_i^{b_{ji}} \quad j=1,2,\ldots,N_p \tag{5.31}$$

where, K_j^{SP} is the solubility product equilibrium constant for precipitate *j*. The total rate of production of component *i* due to precipitation/dissolution reactions (R_j^p) is:

$$R_i^p = \sum_{j=1}^{N_p} R_{ij}^p = \sum_{j=1}^{N_p} b_{ji} R_j^p \tag{5.32}$$

where, R_j^p is the rate of production of precipitate *j*.

5.4 Mathematical Model and Solution of Ek Transport

A mathematical model consisting of system of equations describing the transient reactive multi-component species transport under applied hydraulic, electric, and chemical gradients can be developed to model the transport phenomena in EK remediation of contaminated soils. The system consists of partial differential equations (PDEs) for transport and algebraic equations for geochemical reactions. The transport PDEs are divided into three types. The first type consists of one equation that describes transient fluid flow. The second type consists of N number of equations that describe reactive transport of N species. The third type is described by one equation for charge transport. In the following section the transport PDEs are discussed.

Substituting fluid flux into volume change equation results in the EO consolidation equation expressed as:

$$\frac{\partial h}{\partial t} = C_v \nabla^2 h + \frac{K_e}{m_V \gamma_w} \nabla^2 \Phi \tag{5.33}$$

This equation is necessary to describe the changes in the hydraulic head across the soil, which affects the advective component of mass transport (Acar et al., 1997). The transient reactive PDEs for mass transport are derived by substituting mass flux equation into mass conservation equation given as:

$$\frac{\partial nC_i}{\partial t} = D_i^* \nabla^2 C_i + \nabla (C_i \left[\left(u_i^* + k_{eo} \right) \nabla \Phi + k_h \nabla h \right]) + nR_i \; i=1,2,..., \text{N} \tag{5.34}$$

Changes in the electric potential distribution across the soil as a result of changes in the geochemistry can be found by substituting the charge flux equation in the charge conservation equation as:

$$C_p \frac{\partial \Phi}{\partial t} = F \sum\nolimits_{j=1}^{N} Z_j D_j^* \nabla^2 C_j + \nabla \left(\sigma^* \nabla \Phi \right) \tag{5.35}$$

The total number of differential equations described for this system is N+2 including N equations for mass transport, one equation for charge

conservation, and one equation for fluid flow. The unknowns described in this system are N species concentrations (C_i), one electric potential (Φ), one hydraulic potential (h), and N unknowns for the rate of i chemical reactions. Therefore, 2N+2 unknowns are described by N+2 differential equations. The other N numbers of equations required for this system are the mass balance equations for the chemical reactions (Alshawabkeh and Acar, 1996; Cao, 1997).

5.4.1 Initial and Boundary Conditions

The general system describing mass transport needs to be supplied with appropriate initial and boundary conditions. Initial condition and two boundary conditions are necessary for each species present in the system. Initial conditions can be evaluated by the initial concentration distribution, potential distribution and other values so that an equilibrium state can be maintained at the starting point. Boundary conditions can be obtained through employing different equations, which describe different flow statuses at the boundaries. Generally used boundary conditions are the Neumann boundary conditions, Dirichlet boundary conditions, and mixed boundary conditions. When describing flow problems, a Neumann boundary is an insulated boundary (or impermeable boundary) which means there is no flux at the boundary, while a Dirichlet boundary indicates that the value of head (potential, concentration, etc.) is constant at the boundary.

To simplify the solution procedure, constant boundary conditions can be implemented. However, such boundaries are not able to describe the nature of the EK flow realistically. Due to the existence of flux at boundaries caused by the electrode reactions and advection of fluid, flux boundary condition is more capable of describing EO flow status. The mixed boundary condition can also be implemented in the system. The boundary conditions applied at the inlet and outlet of the soil must express the equality between the flux of solute applied at the inside of the soil boundary and the flux of solute at the immediate outside of the porous medium.

Hydraulic head in the EK transport process is controlled either to provide constant head difference or constant flow rate and hydraulic head boundary conditions can be easily described. In most cases, zero head difference is applied between the cathode and the anode. Boundary conditions for charge conservation equations can be developed from the current density value at the boundary and two types of boundary conditions can

be applied. If the voltage difference between the anode and cathode is kept constant, the following boundary conditions can be used:

$$\Phi\big|_{S1} = \Phi_{\max}; \qquad \Phi\big|_{S2} = 0 \tag{5.36}$$

Where, *S*1 is the boundary surface at the anode and *S*2 is the boundary surface at the cathode. However, if the current density is maintained constant the following boundary conditions can be used (Acar, et al., 1997; Cao, 1997):

$$\left[F\sum\nolimits_{j=1}^{N} Z_j D_j^* \nabla C_j + \sigma^* \nabla \Phi\right]\Big|_{S1} = I \;\; \Phi\big|_{S2}=0 \tag{5.37}$$

Boundary conditions for the species transport equations are evaluated based on the electrolysis reactions at the electrodes. As a result of electrolysis reactions, the chemistry at the electrodes will continuously change. These changes either enhance the EK process (e.g., generation of acid at the anode) or retard the process (e.g., generation of the base at the cathode). In some cases, chemical reagents are introduced at the electrodes to enhance the EK process. Upon identification of the electrolysis reactions type, the boundary conditions can be evaluated from mass equilibrium in electrodes compartments. The rate of concentration change of a specific species in the electrode compartment will be equal to the net mass flow rate of the species (Acar et al., 1997; Cao, 1997).

5.4.2 Preservation of Electrical Neutrality

For a unit volume of the soil, the rate of change in the electric charge equals the total rate of change of chemical species concentrations multiplied by their charge and the Faraday's constant expressed as:

$$\text{Rate of change in electrical charge} = C_p \sum\nolimits_{j=1}^{N} Z_j F \frac{\partial n C_j}{\partial t} \tag{5.38}$$

The charge transport equation preserves the electrical neutrality of the porous medium (Acar et al., 1997; Cao, 1997) so that:

$$\sum\nolimits_{j=1}^{N} Z_j F \frac{\partial n C_j}{\partial t} = 0 \tag{5.39}$$

5.4.3 Numerical Solution Approaches

To solve the general system of equations describing the EK transport processes, usually three different approaches are used. These include:

1. Differential and algebraic equations approach that provides a solution to the mixed differential and algebraic equations in which the transport equations and chemical equilibrium reactions are solved simultaneously as a system (Miller and Benson, 1983; Lichtner, 1985).
2. The direct substitution approach, which consists of direct substitution of the algebraic chemical equilibrium equations into the differential transport equations to form a highly nonlinear system of partial differential equations (Jennings et al., 1982; Lewis et al., 1987).
3. The sequential iteration approach, which consists of iterating between the sequentially solved differential and algebraic equations (Kirkner et al., 1985; Yeh and Tripathi, 1991).

5.5 EK Mass Transport Models

Many researchers have attempted to model mass transport under applied electrical gradient (Acar et al., 1989; Shapiro et al., 1989; Acar et al., 1990; Mitchell and Yeung, 1991; Eykholt, 1992; Alshawabkeh and Acar, 1992; Shapiro and Probstein, 1993; Jacobs et al., 1994; Jacobs and Probstein, 1996; Alshawabkeh and Acar, 1996; Haran et al., 1997; Acar, et al., 1997; Cao, 1997; Al-Hamdan and Reddy, 2008, 2011). Shapiro et al., (1989) and Shapiro and Probstein (1993) described a 1-D model accounting for ion diffusion, migration, and EO advection in predicting the species transport rate. The model solves the charge flux equation in order to evaluate the nonlinear electric field distribution. The governing convective-diffusion equation in their model is given as:

$$\frac{\partial C_i}{\partial t} = \frac{D_i}{\tau^2}\frac{\partial^2 C_i}{\partial x^2} - \frac{\partial}{\partial x}\left[C_i\left[u_{ei} + u_c\right]\right] + R_i \tag{5.40}$$

where, τ describes the tortuosity of the porous medium, and u_c is the convection velocity (the bulk EO velocity) given as:

$$u_c = \frac{1}{\tau^2}\frac{\varepsilon\zeta^{\xi}}{\mu}\left(\zeta^{\xi}\frac{\partial \Phi}{\partial x}\right) \tag{5.41}$$

u_{ei} is ionic species migration velocity (e.i., electromigration velocity), given as:

$$u_{ei} = -v_i Z_i F \frac{1}{\tau^2} \frac{\partial \Phi}{\partial x} \frac{1}{\tau^2} \tag{5.42}$$

Comparison of experimental results with model predictions showed good agreement for a case of acetic acid removal from a 40-cm length kaolinite sample (Shapiro and Probstein, 1993).

Acar et al., (1989) presented a one dimensional model to estimate pH distribution during EK driven mass transport in contaminated soil. The model demonstrated the impact of electrolysis reactions on pH distribution during EK process. Alshawabkeh and Acar (1992) described a modified formulation accounting for the chemical reactions of adsorption/desorption, precipitation/dissolution, and acid/base reactions. The governing equation of one dimensional mass transport due to applied electric, hydraulic, and chemical gradient in their model is given as:

$$\begin{aligned} \frac{\partial n C_i}{\partial t} = D_i \frac{\partial^2 C_i}{\partial x^2} + C_i \left[\left(u_i + k_{eo} \right) \frac{\partial^2 \Phi}{\partial x^2} + k_h \frac{\partial^2 h}{\partial x^2} \right] \\ + \frac{\partial c_i}{\partial x} \left[\left(u_i + k_{eo} \right) \frac{\partial \Phi}{\partial x} + k_h \frac{\partial h}{\partial x} \right] + n R_i \end{aligned} \tag{5.43}$$

The left side of the equation, which is the mass conservation, is also described as:

$$\frac{\partial n C_i(x)}{\partial t} = -\nabla \left(J_i \right) + n R_i \tag{5.44}$$

Where, n is the porosity of the media, J_i is the total mass flux of species, and R_i is the production rate of the i^{th} aqueous chemical species per unit fluid volume due to chemical reactions such as sorption, precipitation-dissolution, oxidation/reduction, and aqueous phase reactions. Alshawabkeh and Acar (1996) enhanced their model to predict the reactive transport of hydrogen, lead, hydroxyl, and nitrate ions. The model accounts for lead hydroxide precipitation/dissolution, lead sorption (assuming linear pH dependent isotherm) and water equilibrium reactions. Comparisons of experimental results with model predictions for different species transport indicated that the model is capable of capturing different EK processes successfully (Acar et al., 1997).

Cao (1997) developed a one-dimensional model to investigate multispecies transport under transient electric field as an extension to the Alshawabkeh and Acar model (1996). The governing equation of mass transport in their model is defined as:

$$\frac{\partial nC_i}{\partial t} = D_i^* \frac{\partial^2 C_i}{\partial x^2} - \frac{\partial \Phi}{\partial x}\left[v_m + k_{eo}\right]\frac{\partial C_i}{\partial x} - C_i\left[v_m + k_{eo}\right]\frac{\partial^2 \Phi}{\partial x^2} + nR_i \qquad (5.45)$$

Where, D^* is effective diffusion coefficient, k_{eo} is effective EO mobility, v_m is effective electro-migration mobility, E is electric potential, and R is the term of chemical reaction rate.

Concentration distributions of charged ions change over time while transporting under applied electric field resulting in change to the local electrical conductivity, which in turn alters the value of the electric gradient. Therefore, the changing electric conductivity and electrical field describe the transport process of the species implicitly. One of the important features of the Cao (1997) model is that the model updates the current density due to ionic motion under applied electric field and diffusion motion under concentration gradient as expressed in the following equation:

$$j_b = \left[F\sum\nolimits_i |Z_i| u_i C_i\right]\frac{\partial \Phi}{\partial x} + F\sum\nolimits_i |Z_i| D_i^* \frac{\partial C_i}{\partial x} \qquad (5.46)$$

The model uses the updated concentration [C_i (x,t)], mobility [u_i (x,t)], and current density [j_b (t)] to update the electric field distribution expressed as:

$$E(x,t) = \frac{j_b(t) + F\sum\nolimits_i |Z_i| D_i^* \left(\frac{\partial C_i(x,t)}{\partial x}\right)}{\sigma_b(x,t)} \qquad (5.47)$$

where, σ_b is the bulk conductivity [$\sigma_b = F\sum\nolimits_i |Z_i| u_i C_i$].

Figures 5.2 and 5.3 present the spatial distribution of the total lead and the pH for 1-day and 35-day runs of this model compared with the results from the laboratory tests of $Pb(NO_3)$ contaminated kaolinite clay subjected to long-term EK treatments (Pamukcu, 2009). Although the initial concentrations of the lead used in the numerical simulator and the experiments were different (0.05 M in the numerical and 0.15 M in the experiment), as

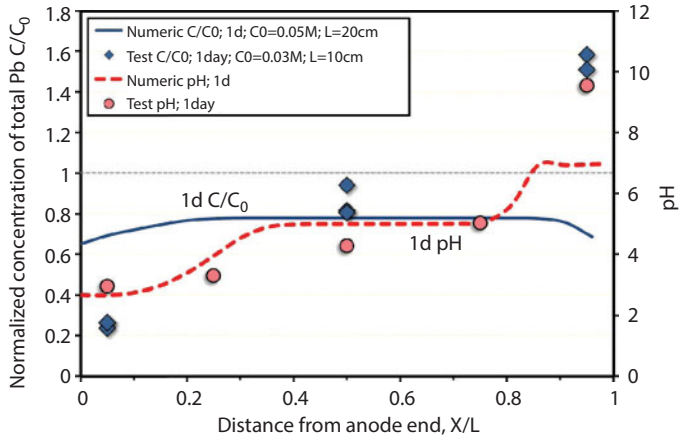

Figure 5.2 Variation of total lead (Pb) concentration and pH distribution as predicted by the Cao (1997) model and measured by experiment for a 1-day duration (After Pamukcu, 2009)

well as the length of the physical and numerical specimens employed, the normalized distributions are comparable.

As shown in figure 5.2, the pH distribution of the model agrees well with the experimental pH after 1 day of treatment, but the distribution of lead does not agree as well for the same duration. The model predicts conservatively a uniform concentration distribution of the metal ion at around 80% of the original, while the available data at three points along the soil column indicate a substantial reduction at the anode and a substantial accumulation at the cathode. It is noted that the model makes a conservative prediction of pH at the cathode end, leading to inadequate capture of the actual lead accumulation by precipitation.

Figure 5.3 shows the long-term model predictions and the matching experimental data from the same series of tests for 35-day treatment. As observed, the model predicts well the long-term behavior of both the lead and the pH distribution, including the accumulation of the metal in a narrow zone adjacent to the cathode.

5.6 Coupling of Electrical and Pressure Gradients

Electrical boundary layers that form a solid-fluid interface in the porous medium create the elektrokinetic potential that result fluid flow under an electric gradient, or charge flow under a hydraulic gradient (Grahame, 1947; Davis et al., 1978). Researchers have investigated the coupling

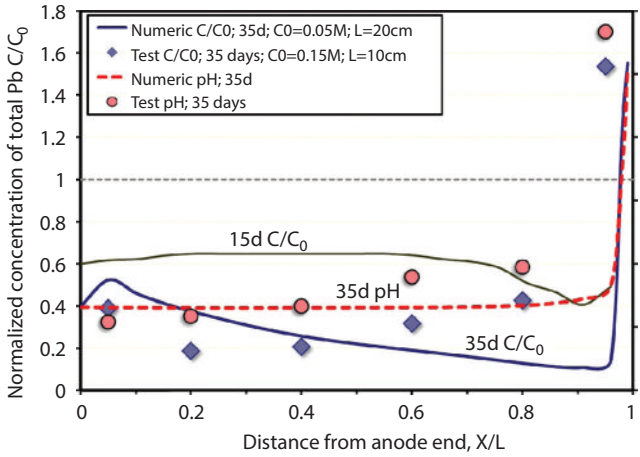

Figure 5.3 Variation of total lead (Pb) concentration and pH distribution as predicted by Cao (1997) model and measured by experiment for a 35.day duration (After Pamukcu, 2009)

between the applied electrical and pressure (hydraulic) gradients (Ishido and Mizutani, 1981, Morgan et al., 1989; Revil and Pezard, 1999; Revil et al., 2007; Saunders et al., 2008; Jackson, 2010). The general relationship between the fluxes of electric current (I) and fluid volume flow (q), and the electric potential gradient (∇E) and fluid pressure gradient (∇P) are given as (Jackson, 2010):

$$\begin{cases} I = -L_{ee}\nabla E - L_{ev}\nabla P \\ q = -L_{ve}\nabla E - L_{vv}\nabla P \end{cases} \tag{5.48}$$

Where, L_{ij} are the phenomenological coefficients. The term $L_{ee}\nabla E$ represents Ohm's law, and the term $L_{vv}\nabla P$ represents Darcy's law. The terms $L_{ev}\nabla P$ and $L_{ve}\nabla E$ and correspond to the coupling effect. In order to give explicit expressions of L_{ij} coefficients for a general porous medium, Ishido and Mizutani (1981) used a capillary tube model with cross-sectional area of A (m^2), overall length L (m) in the direction of general flow, the length of a tortuous pore channel as L_f, and the free cross-sectional area available to flow as A_f. The porosity (n), tortuosity (t), specific internal area S (m^{-1}), and the hydraulic radius h (m) of the model is defined as:

$$n = \frac{A_f L_f}{AL}, \quad t = \frac{L_f}{L}, \quad S = \frac{S_f}{AL}, \quad h = \frac{A_f L_f}{S_f} = nS^{-1} \tag{5.49}$$

Where, S_f is the total internal pore surface area (m^2). The specific conductivity of the sample in this model is given as:

$$L_{ee} = nt^{-2}\sigma_f + t^{-2}S\sigma_s \tag{5.50}$$

where, σ_f and σ_S are the specific conductivity of the fluid in the capillaries ($\Omega^{-1}m^{-1}$) and the specific surface conductivity respectively. The coefficient L_{ev} ($= L_{ev}$) is given as:

$$L_{ev} = L_{ve} = -nt^{-2}\varepsilon\xi/\mu \tag{5.51}$$

where, ε is the dielectric constant of the fluid (Farads per meter), μ is the viscosity of the fluid (Pascal seconds) and ξ is the zeta potential at the slipping plane in DDL (volts). The L_{vv} coefficient is given by Darcy's law as:

$$L_{vv} = \frac{K}{\mu} \tag{5.52}$$

where, K is the intrinsic permeability (m^2). Substituting the coefficients in equation 5.48, Ishido and Mizutani (1981) derived the following equation for the coupled flow:

$$\begin{cases} I = -\left(nt^{-2}\sigma_f + t^{-2}S\sigma_s\right)\nabla E + nt^{-2}\varepsilon\xi/\mu\nabla P \\ q = \left(nt^{-2}\varepsilon\xi/\mu\right)\nabla E - \left(\dfrac{k}{\mu}\right)\nabla P \end{cases} \tag{5.53}$$

Saunders et al., (2006) defined the coupling term as:

$$L_{ev} = L_{ve} = L = \frac{\varepsilon_f \xi}{\mu F} \tag{5.54}$$

where, ε is fluid permittivity, ξ is zeta potential, and $F = \frac{\sigma_f}{\sigma_r}$ is the formation factor, σ_r is the conductivity of the soil/rock fluid system, and σ_f is the conductivity of the pore fluid. For single phase steady state flow, when the electrical current caused by advection is balanced by electrical current caused by conduction, the streaming potential coupling coefficient is defined as (Saunders et al., 2006, 2008):

$$C = \frac{\nabla E}{\nabla P} = \frac{L}{\sigma_r} = \frac{\varepsilon_f \xi}{\mu\sigma_f} \tag{5.55}$$

Measurements of streaming potential have been recently used as a monitoring technique in hydrocarbon reservoirs (Saunders et al., 2006, 2008; Jackson, 2010).

5.7 Mathematical Modeling of EKEOR

EK assisted mass transport of hydrocarbon compounds in natural porous media has gained much attention not only for environmental mitigation of contaminating oils (Pamukcu, 1994; Pamukcu et al., 1995; Pamukcu and Pervizpour, 1998; Kim et al., 2000Yang and Liu, 2001; Reddy and Saicheck, 2004; Reddy et al., 2006; Korolev et al., 2008; Pamukcu, 2009), but also for recovery of reservoir oils over the past decades (Amba et al., 1964; Amba et al., 1965; Chilingar et al., 1968, 1970; Killough and Gonzalez, 1986; Wittle et al., 2006 a,b, 2008 a,b,c, 2011; Haroun et al., 2009; Jihong et al., 2009; Hill et al., 2010; Ghazanfari et al., 2012a,2012b, 2013; Al Shalabi et al., 2012). Some of the contributing factors to the oil production in EKEOR are reported as (i) viscous drag of oil with EO flow of the water phase, primarily controlled by the oil/water ratio and the hydraulic and EO permeability of the formation, (ii) reduction of oil-water interfacial tension due to electrochemical transformation of oil that affect its viscosity, hence increases its mobility, (iii) reduction in the formation oil viscosity due to joule heating, and (iii) increase in the permeability of the formation rock under applied electric field (Chilingar et al., 1968; Wittle et al., 2006 a, 2008 b; Haroun et al., 2009; Hill et al., 2010; Ghazanfari, 2013). Most of the work in this area is experimental work in the laboratory, and the analytical study in this area is limited (Killough and Gonzalez, 1986; Ghazanfari et al., 2013).

In this section, we provide an insight into the mathematical modeling of EK enhanced oil recovery (EKEOR). Although the transient changes in the viscosity of formation oil and the non-isothermal effects contribute to the oil production in EKEOR, viscous drag of oil with EO flow of the water is believed to be the main contributing factor to the oil recovery which is the focus of the model presented here.

5.8 Fundamental Governing Equations for EKEOR Model

Before discussing the governing equations of two-phase flow under applied electrical and pressure gradients, first we review the fundamental governing equations for single and two-phase flow systems under applied pressure gradient in the following section.

5.8.1 Incompressible Single-Phase Flow Under Applied Pressure Gradient

The basic equation describing the flow of a single fluid through a porous medium is the continuity equation which states that mass is conserved and expressed as:

$$q = \frac{\partial}{\partial t}(n\rho) + \nabla[\rho v] \tag{5.56}$$

where, n is the porosity, ρ is fluid density, v is the fluid velocity, and q is the source/sink term (i.e. outflow and inflow per volume). For low-flow velocities, flow through porous media is modeled through the empirical Darcy's law in which the fluid velocity is related to pressure and gravity forces as:

$$v = \frac{-\mathbf{K}}{\mu}(\nabla P - \rho g \nabla z) \tag{5.57}$$

where, K is the intrinsic permeability, μ is the viscosity, g is the gravitational constant, and z is the spatial coordinate in vertical direction. In most real field geological reservoir models, **K** is an anisotropic diagonal tensor (Aziz and Settari, 1979; Allen et al., 1988; Green, 1998; Chen et al., 2006; Aarnes et al., 2007). There are two driving forces in porous media flow including gravity, and the pressure gradient as evident from equation 5.57. Since gravity forces are approximately constant inside a reservoir domain, pressure gradient is considered the main driving force and can be considered as the main unknown parameter for single-phase flow problems. To solve for the pressure, Darcy's equation (eq. 5.57) and the continuity equation (eq. 5.56) are combined. Assuming the constant porosity in time and incompressible fluid, the temporal derivative term in eq. 5.56 vanishes and the following equation for the water (w) pressure is obtained:

$$\nabla . v_w = -\left[\frac{\mathbf{K}}{\mu_w}(\nabla P_w - \rho_w g \nabla z)\right] = \frac{q_w}{\rho_w} \tag{5.58}$$

To complete the single phase flow model, initial and boundary conditions are specified. In reservoir engineering, the common practice is to use no-flow boundary conditions (Aziz and Settari, 1979; Allen et al., 1988, Green, 1998; King, 1992; Chen et al., 2006; Aarnes et al., 2007). For

instance, on the reservoir boundary one can impose the boundary condition as, $v_w.j = 0$, where j is the normal vector pointing out of the boundary. This boundary condition results in an isolated flow system where water cannot enter into or exit from the reservoir.

5.8.2 Two-Phase Immiscible Flow Under Applied Pressure Gradient

To derive the two-phase flow equations for water and oil under applied pressure gradient, several simplifying assumptions are made. These assumptions include (i) the two fluids are immiscible and incompressible and there is no exchange of chemical species among the fluid phases, (ii) the rock matrix is incompressible, (iii) the total flow of oil (as displaced fluid) and water (as displacing fluid) remains constant, (iv) the gradient in phase pressure of the individual phases is the driving force of that specific phase, and (v) the effective permeability for the individual phases is a function of the saturation of each phase.

Assuming Darcy's law holds for flow of both phases (water and oil) and considering the mass conservation in the system, the simplified two-phase flow equations are (Aziz and Settari, 1979; Allen et al., 1985; Ertekin et al., 2001; Chen et al., 2006):

$$\frac{\partial}{\partial t}\left(nS_w\rho_w\right) = -\nabla\left[\rho_w v_w\right] + q_w \tag{5.59}$$

$$v_w = \frac{-k_{rw}\boldsymbol{k}}{\mu_w}\left(\nabla P_w - \rho_w g \nabla z\right) \tag{5.60}$$

$$\frac{\partial}{\partial t}\left[\Phi S_o \rho_o\right] = -\nabla\left[\rho_o v_o\right] + q_o \tag{5.61}$$

$$v_o = \frac{-k_{ro}\boldsymbol{k}}{\mu_o}\left(\nabla P_o - \rho_o g \nabla z\right) \tag{5.62}$$

$$S_w + \mathrm{S_o} = 1 \tag{5.63}$$

$$P_C = P_o - P_w \tag{5.64}$$

Table 5.1 summarizes all the parameters used in the simplified two-phase flow equations. Capillary pressure used in the equations is due to the

Table 5.1 Parameters and descriptions used in simplified two-phase flow equations

Parameter	Description	Unit (metric)
n	Porosity of the media	-
S_w	Water saturation	-
ρ_w	Mass density of water	Kg/m^3
v_w	Velocity of water phase	m/day
q_w	Source/sink term in water phase	m^3/day
$\boldsymbol{k}$	Intrinsic permeability of the medium	m^2
k_{rw}	Relative permeability of water phase	-
μ_w	Dynamic viscosity of the water	Pa.sec
P_w	Hydraulic pressure in water phase	kPa
S_o	Oil saturation	-
ρ_o	Mass density of oil	Kg/m^3
v_o	Velocity of oil phase	m/day
q_o	Source/sink term in oil phase	m^3/day
k_{ro}	Relative permeability of oil phase	-
μ_o	Dynamic viscosity of the oil	Pa.sec
P_o	Hydraulic pressure in oil phase	kPa
g	Gravitational constant	m/sec^2
z	Elevation	m
P_C	Capillary pressure	kPa

curvature and surface tension of the interface between the oil and water phases. This set of equations is supplied with proper initial and boundary conditions and are solved using different solution techniques. One important phenomenon in two-phase flow is the contribution of viscous coupling through momentum transfer between the fluids. The contribution of viscous coupling is ignored in this simple representation of two-phase flow (eq. 5.59 to 5.64). The contribution of viscous coupling in two-phase flow is discussed in the following section.

5.8.3 Contribution of Viscous Coupling

As discussed in section 5.8.2, Darcy's Law for single-phase flow has been directly extended to two-phase flow using effective permeability coefficient (k_α):

$$v_a = \frac{-1}{\mu_a} k_a \left(\nabla P_a - \rho_a g \nabla z\right) \quad \begin{array}{l}[\alpha = w, \text{ for wetting phase;} \\ \quad = n, \text{ for non-wetting phase}]\end{array} \tag{5.65}$$

Where, v_α is the velocity, μ_α is dynamic viscosity, k_α is effective permeability, ∇P_α is pressure gradient, and ρ_α is density of phase α. In reservoir simulation, the relative permeability term ($k_{r\alpha}$) is used widely which is related to absolute and effective permeability through the following expression:

$$k_a = \boldsymbol{K}.k_{ra} \tag{5.66}$$

Where, $\boldsymbol{K}$ is intrinsic permeability, and $k_{r\alpha}$ is relative permeability with respect to phase α. Relative permeability coefficients are typically determined as a function of the wetting phase saturation using standard experimental procedures (Brooks and Corey, 1964; Dake, 1978; Kalaydjian, 1991; Bentsen, 1993; Corey, 1994).

The validity of the key assumption that Darcy's Law holds for two-phase flow equations has been disputed since it implies that the flow of two fluids are essentially uncoupled and each flow has its own channel with own pressure or elevation gradients acting as the driving forces. The generalized immiscible two-phase flow model states that the flow of each fluid phase is a linear function of the gradients of both phases (Kalaydjian, 1991; Liang and Lohrenz, 1994; Avraam and Payatakes, 1995; Bentsen, 1993, 1998; Dullien and Dong 1996; Li et al., 2005). Therefore, fluid flow of each phase depends not only on the gradient of that particular phase but also on the corresponding gradient of the other phase. The generalized two-phase flow models omit the viscous coupling between the two immiscible fluids due to momentum transfer across the fluid-fluid interface. In oil recovery applications, depending on the characteristics of the formation rock, water and the residing oil, viscous drag could have a significant contribution to the quantity of oil produced. Indeed, actual production rates of heavy oil up to 100 times higher than those computed by Darcy approach which omits the viscous coupling has been reported in literature (Yeung, 1996; Tremblay, 1997; Ortiz-Arango and Kantza, 2008).

Four generalized relative permeability coefficients are used in pressure-driven flow. These include two diagonal ($k_{r,ww}$ and $k_{r,nn}$), and the two off-diagonal ($k_{r,wn}$ and $k_{r,nw}$) coefficients. The off-diagonal coefficients capture the contribution of the viscous drag through momentum transfer (Kalaydjian, 1991; Liang and Lohrenz, 1994; Avraam and Payatakes, 1995; Bentsen and Manai, 1993; Bentsen 1998; Dullien and Dong 1996; Li et al., 2005), as given in the following equation:

$$\begin{bmatrix} v_w \\ v_n \end{bmatrix} = -\boldsymbol{K} \begin{bmatrix} \dfrac{k_{r,ww}}{\mu_w} & \dfrac{k_{r,wn}}{\mu_n} \\ \dfrac{k_{r,nw}}{\mu_w} & \dfrac{k_{r,nn}}{\mu_n} \end{bmatrix} \begin{bmatrix} \nabla P_w \\ \nabla P_n \end{bmatrix} \tag{5.67}$$

Where, $\boldsymbol{K}$ is the intrinsic permeability of the porous medium; v_w and v_n are the flow velocities; μ_{w} and μ_{n} are the dynamic viscosities; and ∇P_w and ∇P_n are the pressure gradients in the wetting and non-wetting phases, respectively. In this particular case, the non-wetting phase is oil therefore the subscript identifier "n" is changed to "o", representing oil in the following presentation.

The two diagonal coefficients can be determined as a function of the wetting phase saturation using standard test methods of steady state or un-steady state flow in rock cores. This requires the injection of water and oil simultaneously at constant rates into the core. Once steady state flow is reached, the volumetric flow rate is measured. Given that the intrinsic permeability of the porous medium, pressure gradients, and dynamic viscosity of the fluids are known, the diagonal relative permeability coefficients can be determined at specific saturation levels of the wetting phase. Figure 5.4 shows the experimentally evaluated two diagonal coefficients for a sandstone rock sample (Core C in table 5.2) under applied pressure gradient.

The experimental evaluation of the off-diagonal coefficients ($k_{r,wn}$ and $k_{r,nw}$) is more challenging and only a few studies have reported these coefficients from steady state experiments (Kalaydjian, 1991; Bentsen and Manai, 1993; Liang and Lohrenz, 1994; Bentsen, 1998; Dullien and Dong, 1996). These tests require that upon achieving steady state, the gradient in one phase is set to zero (i.e., the injection of that phase is cut off) while the gradient in the other phase is maintained. Then the volumetric flow rate of the cut-off phase is measured to compute the corresponding off-diagonal coefficient. These coefficients are reported to range between 0 to 24% of the diagonal coefficients depending on the fluids and porous medium

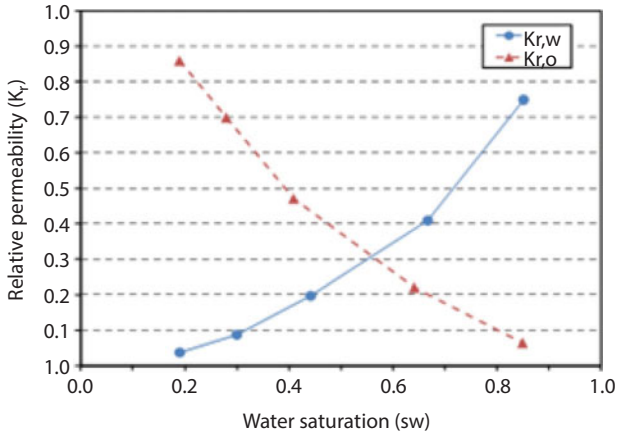

Figure 5.4 Experimentally evaluated diagonal relative permeability coefficients (After Ghazanfari, 2013)

condition. Because of the difficulties associated with the experimental process, various numerical methods, including the Lattice Boltzman Method (LBM) have been employed to evaluate the off-diagonal coefficients (Martys and Hagedorn, 2002; Ramstad et al., 2010).

In the case of applied electric field to the formation in EKEOR application, the contribution of applied electrical gradient in generating flow in both phases should be considered. The EO velocity of a fluid in surface charged porous medium is defined by the Helmholtz-Smoluchowski equation (eq. 5.2) and the EO permeability of the medium is defined as:

$$\boldsymbol{k}_e = \frac{-\varepsilon\xi}{\mu} \tag{5.68}$$

It should be noted that the EO permeability coefficient, $\boldsymbol{k}_e$, in equation 5.68, is the *absolute* EO permeability when only a single fluid (i.e., water) is present in the pores. In here, we consider as the absolute EO permeability coefficient for *water* only.

The coupled flow under applied electrical gradient can be represented through use of four relative permeability coefficients similar to the coupled flow under the pressure gradient (eq. 5.67):

$$\begin{bmatrix} v_w \\ v_o \end{bmatrix} = -\boldsymbol{k}_e \begin{bmatrix} (k_{er,ww}) & (k_{er,wo}) \\ (k_{er,ow}) & (k_{er,oo}) \end{bmatrix} \begin{bmatrix} \nabla E_w \\ \nabla E_o \end{bmatrix} \tag{5.69}$$

Where, the viscous coupling is considered through the off-diagonal coefficients for the water and the oil phases ($k_{er,wo}$ and $k_{er,ow}$) respectively. Equation 5.69 is analogous to the basic equation used in pressure driven two-phase flow (eq. 5.67), where $\boldsymbol{k}_e$ replaces K, and the electrical gradient is the driving force. Analogous to the pressure driven two-phase flow, the generalized off-diagonal relative EO permeability coefficients are used to capture the contribution of the viscous coupling.

5.8.4 Evaluation of EO Transport Coefficients

Reliable prediction of the flow patterns necessitates accurate representation and determination of the relative permeability coefficients under the applied electrical gradient. In this section, relative EO permeability coefficients are evaluated for a specific case of two-phase fluid flow in water-wet porous media, where the second fluid phase is oil. It is postulated that the viscous drag on the oil phase, exerted by the electro-osmotic flow of the water phase is responsible for the transport of oil in the absence of a pressure gradient.

The EO transport of non-conductive liquids (e.g., oil) using conductive liquids (e.g., water) in capillaries, known as EO viscous pumps has been investigated for MEMS devices and microfluidic technologies (Santiago, 2001; Brask et al., 2002; Yao and Santiago, 2003; Gao et al., 2005, 2007; Liu et al., 2009). EO pumps are fabricated mostly of porous glass or fused silica with deprotonated silanol groups on the surface and are based on the EO flow of an electrolyte to generate pressure differentials under a DC electric field (Santiago, 2001; Brask et al., 2002). The performance of EO pumps has been reported to depend on the porosity, tortuosity, and pore size of the porous matrix, pH and ionic concentration of the electrolyte (Santiago, 2001; Brask et al., 2002). The basic premise of EO pumps is that the EO flow of the conducting fluid exerts a drag force on the non-conducting fluid to generate two-phase flow. This is analogous to the postulated process in electrically enhanced oil recovery in water wet porous medium. In EKEOR applications, a similar viscous drag phenomenon leads to oil transport under an applied electric field (Amba et al., 1964; Amba et al., 1965; Chilingar et al., 1968, 1970; Wittle et al., 2006a,b, 2008 a,b,c, 2011; Haroun et al., 2009; Hill et al., 2010; Ghazanfari et al., 2012a, 2012b, 2013a; Al Shalabi et al., 2012).

We discuss here the experimental and analytical approaches on evaluation of relative EO permeability coefficients. In order to evaluate the relative permeability coefficients as a function of water saturation, the porous medium is assumed to be water wet. So, we refer to water as the

wetting phase (i.e., formation water) and to oil as the non-wetting phase. Furthermore, when an electric field is applied to the porous medium, because of the random distribution of the fluids within the pores, it is an accepted assumption that the electric field will be identical in the two phases ($\nabla E_w = \nabla E_o$) (Gladkov, 2003). In the following sections, we discuss the contribution of each of the four relative permeability coefficients to the flow and describe the experimental and analytical approaches used to evaluate them.

5.8.4.1 Diagonal relative permeability coefficient for water phase [$\boldsymbol{k}_{er,ww}$]

The first diagonal relative permeability coefficient ($k_{er,ww}$) was evaluated experimentally for four sand stone rock core specimens as a function of their water saturation. Table 5.2 presents the properties of the rock cores and the flooding fluids used in the experiment. The cores were all 36 mm in diameter and 82 mm in length. Initially, each core was dried and air vacuumed. Then, an electrolyte solution (simulating the formation water of similar salinity) and oil were injected simultaneously at constant injection rate using a high pressure injection pump (Quizix Pump). The core saturation was determined once a steady state flow condition was reached.

Table 5.2 Properties of the sandstone cores and fluids used for relative EO permeability coefficients

Material	Properties
Sandstone core A	Porosity:14.5%, permeability: 3.6 mD , bulk wet density: 2.49 g/cm^3
Sandstone core B	Porosity:14.4%, permeability: 8.3 mD, bulk wet density: 2.43 g/cm^3
Sandstone core C	Porosity:12.8% , permeability: 2.3 mD, bulk wet density: 2.47 g/cm^3
Sandstone core D	Porosity:11.5%, permeability: 0.5 mD bulk wet density: 2.45 g/cm^3
Crude Oil	API 25; dynamic viscosity = 0.0387 pas-sec; Specific gravity =0.79 at 20°C
Electrolyte solution	NaCl; Salinity= 30,000 ppm; Electrical conductivity = 45,000 μS

Then, the core was transferred to the EK test cell. In the EK cell the glass frits separated the core compartment from the formation water in the electrode reservoirs, and the electric field was applied using titanium mesh electrodes placed at the two-end caps of the core.

The typical current densities used in field applications of EKEOR have been reported to be in the range of 1.0-1.5 Amp/m^2 (Wittle et al., 2008a and 2008b). A constant voltage gradient of 4V/cm was applied to the cores in order to achieve current density of 1 Amp/m^2 in the laboratory experiments. The volume production of each liquid was monitored at the cathode reservoir over time for 36 hours. Knowing the measured volume of the produced water, the applied electrical gradient, and the absolute EO permeability of the core (k_e), the $\boldsymbol{k}_{er,ww}$ coefficient could be computed at a specific initial water saturation of the core. For each measurement, the core was dried and air vacuumed and the flooding procedure was repeated to establish the next water saturation level for evaluation of the corresponding $\boldsymbol{k}_{er,ww}$ coefficient. Figure 5.5 shows the measured $\boldsymbol{k}_{er,ww}$ coefficient variation at four different water saturations of the four rock cores designated as A, B, C, and D. As observed, the $\boldsymbol{k}_{er,ww}$ coefficients increased with water saturation, owing to higher water production by the EO flow.

5.8.4.2 *Diagonal relative permeability coefficient for oil phase* [$\boldsymbol{k}_{er,oo}$]

Most crude oils are mixtures of non-polar compounds. Hence unlike water, which is polar and may contain dissolved charged particles, direct application of electric field does not create a notable EO body force in crude oil. To better discern the effect of applied electric field on the oil phase compared to the water phase, the EO permeability of the porous medium is computed using water only and the oil only as the pore fluid. Using Helmholtz-Smoluchowski equation, the computed ratio of k_e (cm^2/V.sec) of a given formation with oil to that with water is significantly low, ranging between10^{-7} to 10^{-3}. This stems from the large differences between the dynamic viscosity and the permittivity of the two liquids. The dynamic viscosity of most crude oils is in the range of 0.038-0.339 Pas.sec (for heavy crude oils the range is 1-5 Pas.sec), while for water it is around 0.001Pas.sec. The range of relative permittivity of most oils is 2.5–5, while for water it is 80. In conclusion, the $k_{er,oo}$ was set equal to zero assuming negligible effect of the applied electrical gradient on the oil phase body force (Ghazanfari, 2013a).

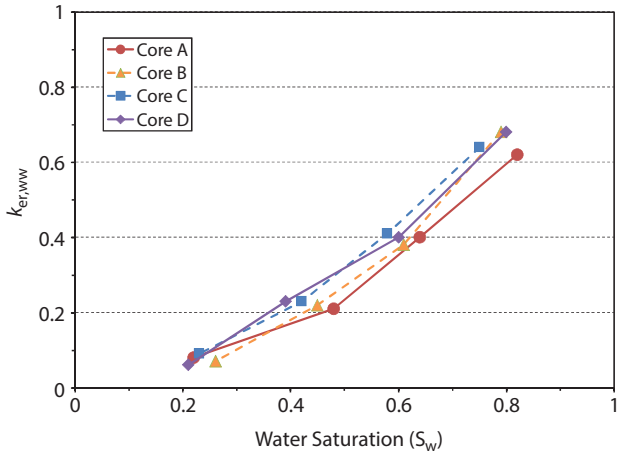

Figure 5.5 Evaluated coefficient for the core samples (After Ghazanfari, 2013a)

5.8.4.3 *Off-diagonal relative permeability coefficients for oil-water coupling* [$\boldsymbol{k}_{er,wo}$ and $\boldsymbol{k}_{er,ow}$]

Evaluation of the off-diagonal relative EO permeability coefficients is one of the major challenges when using two-phase flow principles with coupling between the phases. Experimental procedures similar to those employed in evaluation of the off-diagonal relative permeability coefficients under pressure gradient cannot be used for the electrical gradient application. It is difficult to find experimentally the flow of one phase generated due to the applied electrical gradient in the other phase simply because in practice the electrical gradient cannot be applied solely to one phase in the pore space. To simplify the evaluation, it is assumed that the EO body force occurs in the water phase only since the applied electric field cannot create appreciable EO body force in the oil phase, as discussed above. This implies that even though the electric field is applied to the entire pore fluid simultaneously (both the water and the oil phases), the coupling coefficient, $k_{er,ow}$, can be evaluated experimentally by measuring the quantity of oil phase produced only by assuming that EO body force takes affect in the water phase and not in the oil phase.

The volume of oil production at cathode was monitored for 36 hours during the EK tests of the rock cores designated A, B, C, and D. Once again, knowing the measured volume of the produced oil, the applied electrical gradient and the EO permeability of the core, the $k_{er,ow}$ coefficient could be

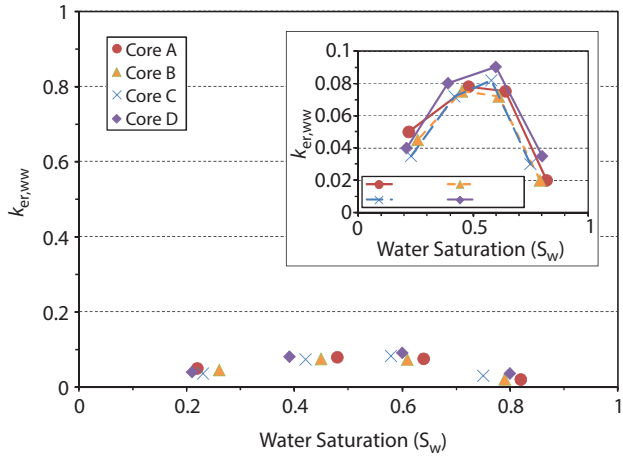

Figure 5.6 Experimentally evaluated $k_{er,ow}$ coefficient for the core samples (After Ghazanfari, 2013a)

computed at a specific water saturation of the core. In these tests a fresh core was used for each measurement to establish the next water saturation level. Figure 5.6 shows the distribution of the evaluated coefficients for the core specimens in two different scales for clarity.

As observed in figure 5.6, the coupling coefficient $k_{er,ow}$ varied from 0.02 to 0.09, on the dimensionless scale of 0 to 1. This coefficient essentially describes the contribution of viscous drag of water on the oil phase, which results in the production of oil by EK. At low water saturations, the dragging capacity of the water is low because there is less water available in the pore space. As the water saturation increases the water mass that creates the momentum to drag oil increases, hence increased oil production. Beyond a critical level of water saturation, the oil production drops despite the increase in the dragging capacity of the water, because there is now less oil available in the pore space.

The $k_{er,ow}$ coefficient, reflecting the contribution of oil to water production, was set to zero since EO body force in the oil phase was assumed to be insignificant, hence no viscous drag by oil exists at the interface to cause water flow.

5.8.4.4 Analytical evaluation of coupling coefficients

It is also possible to evaluate relative EO permeability coefficients analytically, as it may become difficult and tedious to evaluate them experimentally. The analytical representation of coupling coefficients is based on the principles of EO viscous pumps which use conductive liquids (e.g., water)

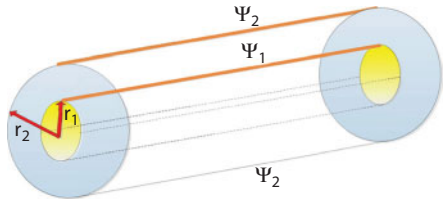

Figure 5.7 Schematic of oil and water filled capillary used in the analysis

to pump non-conductive liquids (e.g., oil) in micro-channels (Santiago, 2001; Brask et al., 2002; Gao et al., 2005, 2007; Wang et al., 2006; Liu et al., 2009). A simple micro-channel (capillary), similar to EO viscous pump, is considered to evaluate the coefficient. Figure 5.7 shows a schematic of the micro-channel filled with the two immiscible fluids. In this depiction, the inner layer is oil (crude oil, assumed to possess no electrical conductivity) and the outer layer, near the channel wall is water (the formation water, with electrical conductivity).

Under an applied electrical gradient, water with EO mobility will be driven by electro-osmosis, and oil with no or negligible EO mobility will be dragged by the interfacial viscous force between the water and oil (Santiago, 2001; Brask et al., 2002; Gao et al., 2005, 2007; Wang et al., 2006; Liu et al., 2009). To evaluate the $k_{er,ow}$ coefficient, the electric field is applied only to the water phase through the two end electrodes. The velocity and volume of flow of each phase can then be calculated and used for evaluation of the $k_{er,ow}$ coefficient as a function of water saturation, or the volume fraction of water in the capillary.

Several simplifying assumptions are needed for this analytical treatise, including i) the two fluids are simple Newtonian fluids, ii) the fluid properties are constant and independent of local electric field, ion concentration, and temperature, and iii) two-phase flow is steady and fully developed with no slip-boundary conditions both at the interface and at the wall. Accordingly, the continuity equations (velocity and momentum) for each phase can be expressed as:

$$\begin{cases} \nabla v_a = 0 \\ \rho_a \left(\dfrac{\partial v_a}{\partial t} + v_a \nabla v_a \right) = -\nabla P_a + \nabla \left(\mu_a \nabla v_a \right) + (\rho_e)_a \nabla E \end{cases} \tag{5.70}$$

where, v_α, ρ_α, and $(\rho_e)_\alpha$ are the velocity, mass density, and the electric charge density of the phase α, respectively. For small Reynolds number

(typical for the range of EO velocities in geological media) the inertial force is zero. Therefore, the continuity equations can be simplified as:

$$\begin{cases} \nabla u v_a = 0 \\ -\nabla P_a + \nabla\left(\mu_a \nabla v_a\right) + \left(\rho_e\right)_a \nabla E = 0 \end{cases} \tag{5.71}$$

The effect of the electrical gradient on the flow can be evaluated by setting to zero the pressure gradients in both phases. Hence, when the electrical gradient is applied to the water phase only, equation 5.71 reduces to:

$$\begin{cases} \mu_w \nabla^2 v_w = -\left(\rho_e\right)_w \nabla E \\ \mu_o \nabla^2 v_o = 0 \end{cases} \tag{5.72}$$

The charge distribution of each phase is required to calculate the phase velocities. The Poisson equation describes the electric potential distribution in cylindrical coordinates (Hunter, 2001):

$$\frac{1}{r}\frac{\partial}{\partial r}\left(r\frac{\partial \psi}{\partial r}\right) + \frac{\partial^2 \psi}{\partial z^2} = \frac{-\rho_e}{\varepsilon} \tag{5.73}$$

Where, ψ is the surface potential and ε is the permittivity of the fluid.

Equation 5.73 can be further simplified based on the assumption of thermodynamic equilibrium and the Debye-Huckel approximation for a low surface potential (Hunter, 2001), as:

$$\frac{1}{r}\frac{d}{dr}\left(r\frac{\partial \psi}{\partial r}\right) = k^2 \psi \tag{5.74}$$

Where, k is the reciprocal of EDL (Electric Double Layer) thickness (Debye length) defined as (Hunter, 2001):

$$k = \left(\frac{2ne^2 {z_0}^2}{\varepsilon K_B T}\right)^{1/2} \tag{5.75}$$

Where, e is the elementary charge; n is the ionic concentration in equilibrium solution, K_B is the Boltzman constant; and T is absolute temperature.

The boundary conditions imposed on the channel wall and at the oil-water interface are (see figure 5.7):

$$\begin{cases} \psi(r_1) = \psi_1 \\ \psi(r_2) = \psi_2 \\ \dfrac{d\psi}{dr} = 0 \quad at\, r = 0 \end{cases} \tag{5.76}$$

Where, ψ_2 is the surface potential on the channel wall, ψ_1 is the potential at the interface between the two fluids, r_1 is the radius of inner layer (oil layer), and r_2 is the radius of the entire channel, as shown in figure 5.7. The electric potential distribution in the channel is found by solving equation 5.74 under boundary conditions specified in equation 5.76 as (Liu et al., 2009):

$$\begin{cases} \psi(r) = \psi_1 \dfrac{I_0(k_1 r)}{I_0(k_1 r_1)} \quad for\ 0 \le r \le r_1 \\ \psi(r) = \psi_2 \dfrac{I_0(k_2 r)}{I_0(k_2 r_2)} + \psi_1 \dfrac{I_0(k_2 (r - 2r_1)}{I_0(k_2 r_1)} \quad for\ r_1 \le r \le r_2 \end{cases} \tag{5.77}$$

Figure 5.8 shows the charge distribution in the capillary for the case when $\psi_1 = \psi_2$ = -25 mV and the water saturation is S_W = 0.8.

The charge density distribution can then be written as:

$$\begin{cases} \rho_e(r) = -\varepsilon_o k^2 \psi_1 \dfrac{I_0(k_1 r)}{I_0(k_1 r_1)} \quad for\ 0 \le r \le r_1 \\ \rho_e(r) = -\varepsilon_w k^2 \psi_2 \dfrac{I_0(k_2 r)}{I_0(k_2 r_2)} + \psi_1 \dfrac{I_0\left(k_2 (r - 2r_1)\right)}{I_0(k_2 r_1)} \quad for\ r_1 \le r \le r_2 \end{cases} \tag{5.78}$$

Where, I_0 is zero order modified Bessel function of the first kind; and k_1 and k_2 are the reciprocal of EDL thickness of the inner and outer layers, respectively; and ε_0 and ε_w are the permittivity of the inner and outer layers, respectively.

Figure 5.9 shows the micro-scale representation of the interfacial forces in the capillary. At the oil-water interface the continuity of velocity and hydrodynamic shear stress can be expressed as (Gao et al., 2007; Liu et al., 2009):

$$\begin{cases} v_w = v_o \\ \tau_o = \tau_w - \rho_e(r_1) \nabla E \end{cases} \tag{5.79}$$

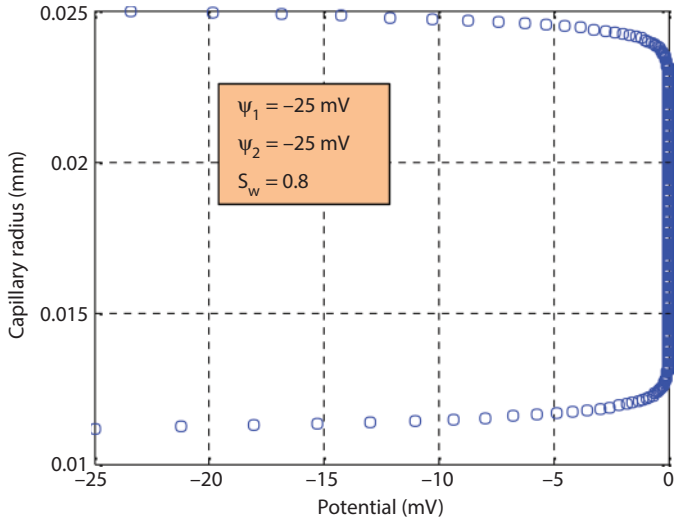

Figure 5.8 Charge distribution in the capillary (After Ghazanfari, 2013)

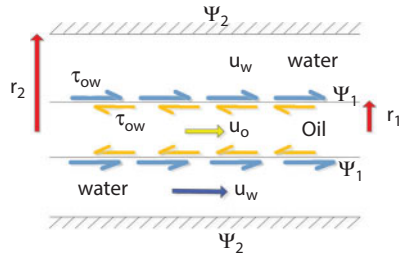

Figure 5.9 Micro-scale representation of the interfacial forces

Where the shear stress at each phase is:

$$\tau_w = \mu_w \frac{\partial v_w}{\partial j} \; and \; \tau_o = \mu_o \frac{\partial v_o}{\partial j} \tag{5.80}$$

Where, j is the normal direction to the interface between the two fluids. The velocity of each phase is found by solving equation 5.72 using the charge density from equation 5.78, and the continuity conditions given in equation 5.79 as:

$$v_o = \frac{\varepsilon_w \psi_2 k^2 \nabla E}{\mu_o}\left[\psi_2 \frac{I_0(kr_1) - I_0(kr_2)}{k^2 I_0(kr_2)} + \frac{\psi_1}{I_0(kr_1)} \int_{r_2}^{r_1} f(r)dr \right. \tag{5.80}$$

$$-[\frac{\psi_1}{I_0(kr_1)}f(r_1)+2\psi_2\frac{r_1I_1(kr_1)}{kI_0(kr_2)}+\psi_1\frac{r_1I_1(kr_1)}{kI_0(kr_1)}\ln\left(\frac{r_1}{r_2}\right)\Bigg]$$

$$v_w=\frac{\varepsilon_w\psi_2k^2\nabla E}{\mu_w}\Bigg[\psi_2\frac{I_0(kr)-I_0(kr_2)}{k^2I_0(kr_2)}+\frac{\psi_1}{I_0(kr_1)}\int_{r_2}^{r}f(r)dr- \tag{5.81}$$
$$\left[\frac{\psi_1}{I_0(kr_1)}f(r_1)+2\psi_2\frac{r_1I_1(kr_1)}{kI_0(kr_2)}+\psi_1\frac{r_1I_1(kr_1)}{kI_0(kr_1)}\ln\left(\frac{r}{r_2}\right)\right]\Bigg]$$

Where, I_1 is first order modified Bessel function of the first kind, and $f(r)$ is defined as (Liu et al., 2009):

$$f(r)=1/2(r-2r_1)^2\,{}_0\bar{F}_1\left[2,\frac{1}{4}k^2(r-2r_1)^2\right]+2r_1(r-2r_1) \tag{5.82}$$
$${}_p\bar{F}_q\left[\frac{1}{2};1,\frac{3}{2};\frac{1}{4}k^2(r-2r_1)^2\right]$$

Where, ${}_0\bar{F}_1$ is the Hypergeometric regularized function, and ${}_p\bar{F}_q$ is the Hypergeometric function (the generalized Hypergeometric function).

Finally, the flow rate of each phase can be found as:

$$\begin{cases} q_o=\int_0^{r_1}2\pi v_o dr \\ q_w=\int_{r_1}^{r_2}2\pi v_w dr \\ q=q_o+q_w \end{cases} \tag{5.83}$$

In order to quantify $k_{er,ow}$ as a function of water saturation, first the oil velocity and oil flow were obtained solving equations 5.80, 5.81, and 5.83 respectively. Then, the expression for $k_{er,ow}$ coefficient was derived for the corresponding $q_0$at a particular water saturation as following:

$$k_{er,ow}=\frac{q_o}{k_e\nabla EA_o} \tag{5.84}$$

Where, A_o is the cross-sectional area of the oil phase. Figure 5.10 shows the velocity profiles at the wall-liquid interface for a capillary with the

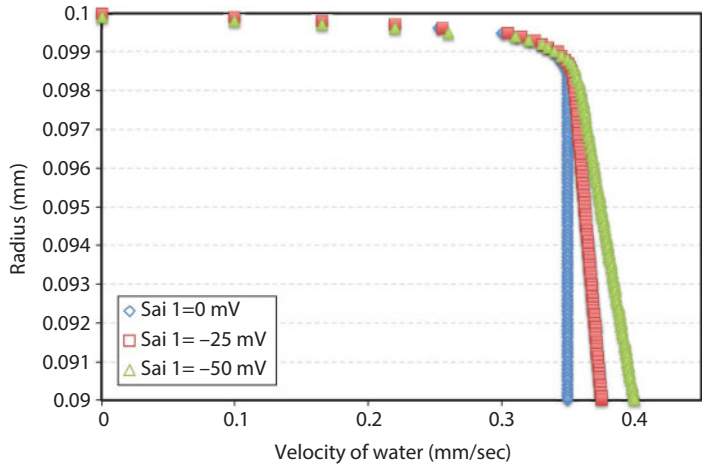

Figure 5.10 Velocity profile across the capillary for variable wall interface potentials

Table 5-3 Properties of the two fluids used in the parametric study

Parameter	unit	value
Oil		
Dynamic viscosity of oil (μ_o)	pas-sec	38.7×10^{-3}
Vacuum permittivity (ε)	Faraday/m	8.854×10^{-12}
Permittivity of oil ($\varepsilon_{o)}$	F/m	~3ε
Formation water		
Element charge (e)	C	1.6×10^{-19}
Boltzman constant (K_B)	J/K°	1.38×10^{-23}
Dynamic viscosity of water (μ_w)	pas-sec	10^{-3}
Permittivity (ε_w)	F/m	~87ε
Working temperature (T)	K°	293
Ionic concentration (n)	M	1×10^{-6}

radius of 0.1mm and $S_w = 0.2$ for three different cases where the wall interface potential varied from zero to -50 mV. As observed in figure 5.10, the velocity of water in the capillary increases with the interfacial potential.

The properties of the two fluids used in the analytical evaluation of $k_{er,ow}$ coefficient are listed in table 5.3. From equations 5.80 and 5.81, it can be

discerned that the parameters affecting the fluid flow are the potential at the interface (ψ_1), potential at the wall surface (ψ_2), reciprocal of EDL thickness for the formation water (k_2), oil/water saturation (determined by the ratio of r_1 and r_2), and the radius of the capillary (r_2). Normally, as the potential at the wall and the interface increases, the EO effect becomes noticeable which results in larger flow rates.

The capillary size, surface potential and water and oil saturation are important input parameters for the analytical solution of the coupling coefficients. The pore throat size of common reservoir rocks varies within the range of 1 to 30μm (Keighin, 1997; Ahr, 2008; Nelson, 2009). For evaluation of $k_{er,ow}$ coefficient, a constant nominal capillary radius of 10μm was adapted to represent the mean diameter of the pore throat size of the cores tested. The zeta potential of common water wet reservoir rock minerals (quartz, kaolinite, and calcite) in contact with connate water varies within the range of -50 to +50 mV (Lichaa et al., 1992; Marinova, 1996; Rodriguez and Araujo, 2006). In this analysis, the representative channel wall surface potential was set to -25 mV. The interface between water and non-polar oil could possess substantial negative charge even in the absence of chemicals that reduce surface tension (Haydon and Taylor, 1960; Rodriguez and Araujo, 2006). Hydroxyl ions, released by the dissociation-association equilibrium of the water molecules are adsorbed at the oil-water interface where they create a negatively charged layer whose charge concentration strongly depend on pH (Haydon and Taylor, 1960; Marinova, 1996). The magnitude of this interface charge depends largely on the ionic composition of the aqueous phase, while the nature of the oil phase is of secondary importance. Typical range of the interface potential is -20± 5 mV (Haydon and Taylor, 1960). In this analysis, the oil-water interfacial potential was set at 0 mV and -15 mV, for two separate solution schemes.

Water and oil saturations were found based on their respective volume fractions in the capillary. The volume fractions of these components were varied by changing the values of r_1 and r_2. Figure 5.11 shows the velocity profile for half of the capillary for the case when the charge density at the oil-water interface is set to zero (ψ_1=0 mV). As observed in figure 5.11, the oil velocity profile is constant, which results in plug flow and the water velocity increases within the EDL and remains constant across the capillary.

The velocity profile for when the interface possess charge (ψ_1= -15 mV) is shown in figure 5.12. In this case, the water velocity increases across the capillary which results in higher water flow. The oil flow remains as plug flow, but at an increased quantity as expected.

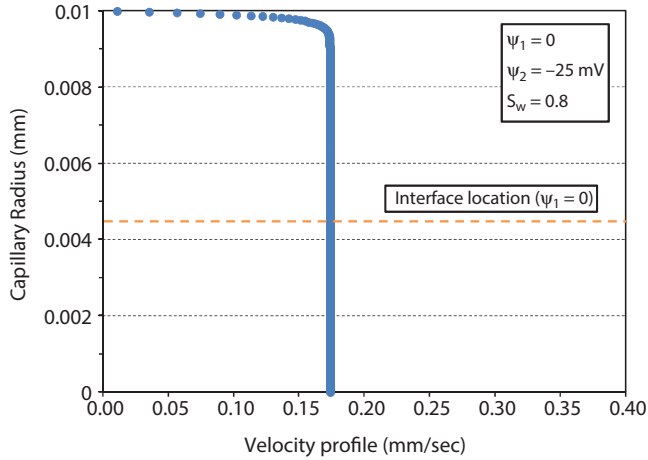

Figure 5.11 Velocity profile across the capillary (zero oil-water interface potential)

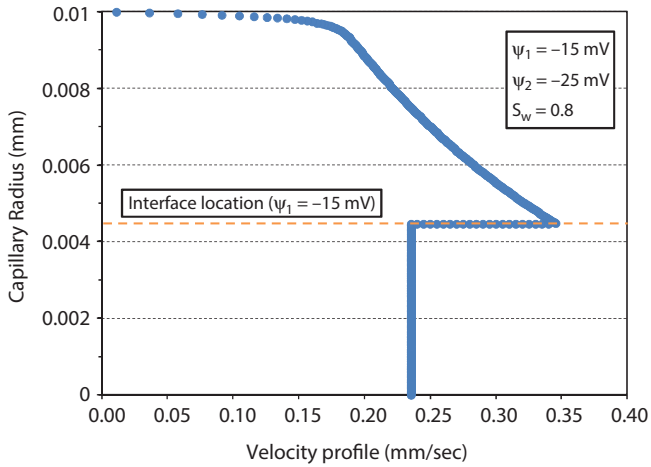

Figure 5.12 Velocity profile across the capillary (with -15 mV oil-water interface potential)

Figure 5.13 shows the analytically evaluated $k_{er,ow}$ coefficient as a function of water saturation. As also observed in the case of experimentally evaluated $k_{er,ow}$ coefficient (see figure 5.6), the coefficient increases with increasing in water saturation initially, to slightly over 0.1 at 50% water saturation. The coefficient decreases beyond the 50% saturation, because of less oil available in the capillary to be produced.

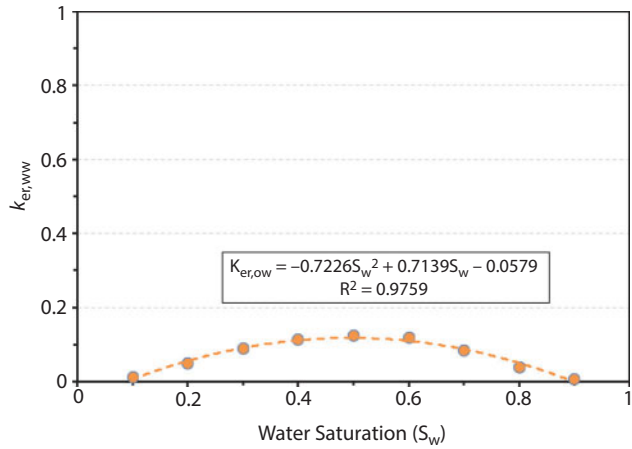

Figure 5.13 Analytically evaluated coefficient as a function of water saturation

5.8.4.5 Scaling issues in evaluation of relative EO transport coefficients for reservoir simulation

The generalized EO permeability coefficients presented above are important pieces of the constitutive relationships in the EKEOR reservoir simulation. It should be noted that reservoir properties are often highly heterogeneous and anisotropic. The up-scaling difficulties and issues in EKEOR reservoir simulation remain the same as other conventional methods. There are several scaling issues between the laboratory experiments and the reservoir scale. Two of the major differences are transient changes in the electric field distribution and non-isothermal effects.

The applied DC current in the laboratory scale over the course of the laboratory experiment is fairly uniform and conveniently manageable. The distribution of electric field strength is uniform and temporal and spatial fluctuations in electric field intensity are not a concern. However, in the reservoir scale, the current density is not uniform in the formation and temporal and spatial fluctuations of the electric field intensity affect the oil production. Also, the temperature in laboratory scale experiment remains fairly constant and thermal effects are negligible. In contrast, the thermal effects could be significant in the reservoir scale, specifically in the regions close to injection and production wells where the electrodes are inserted. This effect is particularly important for extended periods of power application which could generate significant heat due to formation resistivity in the regions close to the injection and production wells.

5.8.5 Two-phase Immiscible Flow Under Applied Pressure and Electrical Gradient

Superimposing electrical gradient to the pressure and elevation gradients, the resulting fluid flow expressions for each phase can be expressed as:

$$\begin{bmatrix} v_w \\ v_o \end{bmatrix} = -\boldsymbol{k}\begin{bmatrix} \frac{k_{r,ww}}{\mu_w} & \frac{k_{r,wo}}{\mu_o} \\ \frac{k_{r,ow}}{\mu_w} & \frac{k_{r,oo}}{\mu_o} \end{bmatrix}\begin{bmatrix} \nabla P_w - \rho_w g \nabla z \\ \nabla P_o - \rho_o g \nabla z \end{bmatrix} - \boldsymbol{k_e}\begin{bmatrix} (k_{er,ww}) & (k_{er,wo}) \\ (k_{er,ow}) & (k_{er,oo}) \end{bmatrix}\begin{bmatrix} \nabla E_w \\ \nabla E_o \end{bmatrix} \tag{5.85}$$

As discussed in section 5.9.4, setting $k_{er,ow}$ and $k_{er,oo}$ coefficients to zero, and $\nabla E_w = \nabla E_o$, Eq. 5.85 reduces to:

$$\begin{bmatrix} v_w \\ v_o \end{bmatrix} = -\boldsymbol{k}\begin{bmatrix} \frac{k_{r,ww}}{\mu_w} & \frac{k_{r,wo}}{\mu_o} \\ \frac{k_{r,ow}}{\mu_w} & \frac{k_{r,oo}}{\mu_o} \end{bmatrix}\begin{bmatrix} \nabla P_w - \rho_w g \nabla z \\ \nabla P_0 - \rho_o g \nabla z \end{bmatrix} - \boldsymbol{k_e}\begin{bmatrix} k_{er,ww} \\ k_{er,ow} \end{bmatrix}\begin{bmatrix} \nabla E_w \\ \nabla E_w \end{bmatrix} \tag{5.86}$$

Having the velocities of each phase under the combined pressure and electrical gradients, the system of equations to be solved is then:

$$\frac{\partial}{\partial t}\left(\Phi S_w \rho_w\right) = -\nabla\left[\rho_w v_w\right] + q_w \tag{5.87}$$

$$v_w = -\boldsymbol{k}\frac{k_{r,ww}}{\mu_w}\left(\nabla P_w - \rho_w g \nabla z\right) - \boldsymbol{k}\frac{k_{r,wo}}{\mu_o}\left(\nabla P_o - \rho_o g \nabla z\right) - \boldsymbol{k_e} k_{er,ww}\left(\nabla E_w\right) \tag{5.88}$$

$$\frac{\partial}{\partial t}\left[\Phi S_o \rho_o\right] = -\nabla.\left[\rho_o v_o\right] + q_o \tag{5.89}$$

$$v_o = -\boldsymbol{k}\frac{k_{r,ow}}{\mu_w}\left(\nabla P_w - \rho_w g \nabla z\right) - \boldsymbol{k}\frac{k_{r,oo}}{\mu_o}\left(\nabla P_o - \rho_o g \nabla z\right) - \boldsymbol{k_e} k_{er,ow}\left(\nabla E_w\right) \tag{5.90}$$

$$S_w + S_0 = 1 \tag{5.91}$$

$$P_C = P_o - P_w \tag{5.92}$$

There are several alternatives in formulation of the partial differential equations in the above system including (i) formulation in phase pressures, (ii) formulation in phase pressure and saturation, and (iii) formulation in global pressure (Crichlow, 1977; Dake, 1978; Aziz and Settari, 1979; King, 1992; Chen et al., 2006; Aarnes et al., 2007). When formulated in phase pressures, simultaneous solution techniques can be used to solve the system of equations. When formulated in phase pressure and saturation, the implicit pressure explicit saturation (IMPES) technique can be used to solve the system of equations. Finally, to reduce the coupling in the system, equations can be formulated in global pressure (Crichlow, 1977; Dake, 1978; Aziz and Settari, 1979; King, 1992; Chen et al., 2006; Aarnes et al., 2007).

5.8.6 Formulation in Phase Pressure (Oil Pressure) and Saturation (Water Saturation)

Capillary pressure is a function of water saturation and the direction of saturation change (drainage or imbibition). Different empirical correlations between saturation and capillary pressure have been developed including the Brooks and Corey (Brooks and Corey, 1964; Corey, 1994) correlation expressed as:

$$P_C = P_d S_w^{(-1/\lambda)} \tag{5.93}$$

Where, P_C is capillary pressure, P_d is entry capillary pressure, and λ is related to the pore size distribution of the porous medium (in the range of 0.2 to 3.0).

Relative permeability coefficients are correlated to wetting phase saturation (usually water saturation). As discussed in section 5.8.3, these coefficients are determined either experimentally for specific porous medium of interest or empirical correlations can be used as an alternative. There are several empirical expressions for relative permeability coefficients as a function of wetting phase saturation including the Brooks and Corey (Brooks and Corey, 1964; Corey, 1994) correlation given as:

$$k_{r,ww} = S_w^{\frac{2+3\lambda}{\lambda}} \tag{5.94}$$

$$k_{r,oo} = S_o^2 \left[1 - \left(1 - S_o\right)^{\frac{2+\lambda}{\lambda}} \right] \tag{5.95}$$

Analytical expressions that correlate EO relative permeability coefficients to the wetting phase saturation for the porous medium of interest can be developed also, as discussed in section 5.8.3.

Assuming that the capillary pressure has a unique inverse function as:

$$S_w = P_C^{-1} \tag{5.96}$$

Equations 5.87 to 5.90 can be combined as follows:

$$\frac{\partial}{\partial t}\left(\Phi S_w \rho_w\right) = \nabla\left[\rho_w\left(\boldsymbol{k}\frac{k_{r,ww}}{\mu_w}\left(\nabla P_o - \frac{dP_c}{dS_w}\nabla S_w\right) + \boldsymbol{k}\frac{k_{r,wo}}{\mu_o}\nabla P_0\right)\right. \tag{5.97}$$
$$\left. + \boldsymbol{k_e} k_{er,ww}\nabla E_w\right] + q_w$$

$$\frac{\partial}{\partial t}\left(\Phi(1-S_w)\rho_O\right) = \nabla\left[\rho_O\left(\boldsymbol{k}\frac{k_{r,ow}}{\mu_w}\left(\nabla P_o\right) + \boldsymbol{k}\frac{k_{r,oo}}{\mu_o}\nabla P_0\right) + \boldsymbol{k_e} k_{er,ow}\nabla E_o\right] + q_o \tag{5.98}$$

To solve the above system of equations, appropriate initial and boundary conditions are needed in the space and time domains. For initial conditions, usually the main unknowns (phase pressures) are specified over the entire space domain at t = 0. For boundary conditions, the possible cases include (i) phase pressure specified as a function of position and time (Dirichlet), (ii) pressure gradient is known (Neumann), (iii) phase pressure and pressure gradient in an impervious boundary are specified (Mixed). In reservoir simulation, usually the no flow boundary condition is used (Aziz and Settari, 1979; King, 1992; Chen et al., 2006). Also, the boundary conditions for applied electric field need to be specified on the reservoir boundaries.

5.9 Solution Strategy

There are multiple solution schemes for the system of equations used in reservoir simulation (Aziz and Settari, 1979; Eymard, 2003; Chen et al., 2006). Among these schemes, IMPES (Implicit pressure, explicit saturation), simultaneous solution, sequential, and adaptive implicit methods are widely used in the petroleum industry. The simultaneous solution method solves the coupled non-linear equations simultaneously and implicitly.

The advantage of this method is its stability and that it can take very large time steps while stability is maintained. The sequential methods solve the set of equations in an implicit fashion without developing a full coupling between the equations (Chen et al., 2006; Aarnes et al., 2007). Compared to IMPES and simultaneous solution schemes, the sequential schemes are less stable but more computationally efficient. The adaptive implicit scheme can be referred to as middle ground between the IMPES and sequential solution schemes as at a given time step, the expensive simultaneous solution scheme is assigned to the blocks that require it, and the IMPES scheme is implemented on the remaining blocks (Chen et al., 2006; Aarnes et al., 2007).

The IMPES technique, developed by Sheldon and coworkers (1959) and Stone and Grader (1970) is widely used in the petroleum industry. The method separates the computation of pressure from saturation. The coupled system is split into a pressure equation and a saturation equation and the pressure and saturation equations are solved using implicit and explicit time approximation approaches. The technique can be implemented for solving the set of equations for two-phase immiscible flow under applied pressure and electrical gradients. In the following section, the pressure and saturation equations for the case of two-phase immiscible flow under applied pressure and electrical gradients are derived to be implemented in IMPES solution technique.

5.9.1 The Saturation Equation for Two-Phase Incompressible Immiscible Flow

The continuity equations for the two phases are expressed as (Aziz and Settari, 1979; Allen et al,, 1988; Ertekin et al., 2001):

$$\frac{\partial}{\partial t}\left(nS_a\rho_a\right)+\nabla.\left[\rho_a v_a\right]=q_a \tag{5.99}$$

The water, oil, and total mobility (functions of water saturation) are defined as (Aziz and Settari, 1979):

$$\lambda_w\left(s_w\right)=\left(\frac{k_{r,w}}{\mu_w}\right) \tag{5.100}$$

$$\lambda_o\left(s_w\right)=\left(\frac{k_{r,o}}{\mu_o}\right) \tag{5.101}$$

$$\lambda = \lambda_w + \lambda_o \tag{5.102}$$

The fractional flow for water and oil phases (function of water saturation) are defined as (Aziz and Settari, 1979; Ertekin et al., 2001):

$$f_w = \frac{\lambda_w}{\lambda}; f_o = \frac{\lambda_o}{\lambda} \tag{5.103}$$

The total velocity and total flow are defined as (Aziz and Settari, 1979):

$$v = v_w + v_o \; q = q_w + q_o \tag{5.104}$$

The saturation equation for the case of two-phase incompressible and immiscible flow under pressure gradient and elevation gradients are extended to the case of two-phase incompressible and immiscible flow under pressure, elevation, and electrical gradients. First, multiplying Darcy's law for each phase with the mobility of the other phase and ignoring the contribution of viscous coupling under pressure and elevation gradients we have the followings:

$$\lambda_o v_w = -\mathbf{K}\lambda_w\lambda_o\left(\nabla P_w - \rho_w g\nabla z\right) \tag{5.105}$$

$$\lambda_w v_o = -\mathbf{K}\lambda_w\lambda_o\left(\nabla P_o - \rho_o g\nabla z\right) \tag{5.106}$$

Subtracting equation 5.105 from equation 5.106 gives:

$$\lambda_w v_o - \lambda_o v_w = -\mathbf{K}\lambda_w\lambda_o\left(\nabla P_c + \left(\rho_o - \rho_w\right)g\nabla z\right) \tag{5.107}$$

To find an expression that only contains the total velocity and the saturation of the wetting phase, we use $v_0 = v - v_w$ (Eq. 5.104) to get:

$$\lambda_w v - \left(\lambda_w + \lambda_o\right)v_w = -\mathbf{K}\lambda_w\lambda_o\left(\nabla P_c + \left(\rho_o - \rho_w\right)g\nabla z\right) \tag{5.108}$$

Considering $s = s_w$ and using the fractional flow of water as $f(s) = \frac{\lambda_w}{\lambda_w + \lambda_O}$ we have:

$$v_w = f(s)v - \mathbf{K}\lambda_o f(s)\left(\nabla P_c + \left(\rho_o - \rho_w\right)g\nabla z\right) \tag{5.109}$$

Inserting this equation into the continuity equation (Eq. 5.96) for the wetting phase we get:

$$\varphi\frac{\partial S}{\partial t}+\nabla.\left[f(s)v-\mathbf{K}\lambda_o f(s)\left(\nabla P_c+(\rho_o-\rho_w)g\nabla z\right)\right]=\frac{q_w}{\rho_w} \quad (5.110)$$

This is the saturation equation. Similarly, the saturation equation for the incompressible and immiscible two-phase flow under pressure and electrical gradients can be derived as (Ghazanfari, 2013):

$$\varphi\frac{\partial S}{\partial t}+\nabla.\left[f(s)v-\mathbf{K}\lambda_o f(s)\left(\nabla P_c+(\rho_o-\rho_w)g\nabla z\right)-\boldsymbol{k_e}\nabla E_w\left(f(s)k_{er,ow}\right.\right.$$
$$\left.\left.+\left(f(s)-1\right)k_{er,ww}\right)\right]=\frac{q_w}{\rho_w} \quad (5.111)$$

5.9.2 Pressure Equation for Two-Phase Incompressible Immiscible Flow

Summing the Darcy's law over the two phases we get the following equation:

$$v=v_w+v_o=-\mathbf{K}\lambda_w\left(\nabla P_w-\rho_w g\nabla z\right)-\mathbf{K}\lambda_o\left(\nabla P_o-\rho_o g\nabla z\right) \quad (5.112)$$

Taking divergence on both sides and considering the fact that $\nabla.[v] = \rho$, we have:

$$\nabla.[v]=-\nabla\left\{\mathbf{K}\lambda_w\left(\nabla P_w-\rho_w g\nabla z\right)+\mathbf{K}\lambda_o\left(\nabla P_o-\rho_o g\nabla z\right)\right\}=q \quad (5.113)$$

This is the pressure equation. Similarly, the pressure equation for the incompressible and immiscible two-phase flow under pressure and electrical gradients can be derived as (Ghazanfari, 2013):

$$\nabla.[v]=-\nabla\left\{\mathbf{K}\lambda_w\left(\nabla P_w-\rho_w g\nabla z\right)+\mathbf{K}\lambda_o\left(\nabla P_o-\rho_o g\nabla z\right)+\right. \quad (5.114)$$
$$\left.\boldsymbol{k_e}\nabla E_w\left(k_{er,ww}+k_{er,ow}\right)\right\}=q$$

The pressure and saturation equations (Eq. 5.111 and 5.114) are nonlinearly coupled primarily through the saturation-dependent mobility (λ_w, and λ_o) in the pressure equation, and through the pressure-dependent velocity (v_w and v_o) in the saturation equation, and also through other terms that depend on pressure or saturation (e.g., viscosity, capillary pressure). To reduce the coupling, a global pressure term (P) can be introduced to replace the phase pressures (P_w, and P_o) (Chen et al., 2006; Aarnes et al., 2007). The global pressure is defined as $P = P_o - P_c$, where the saturation-dependent complementary pressure (P_C) is defined as (Chen et al., 2006; Aarnes et al., 2007):

$$P_c\left(S_w\right)=\int_1^{S_w} f_w\left(\beta\right)\frac{\partial P_{cow}}{\partial S_w}\left(\beta\right)d\beta \tag{5.115}$$

Where, the fractional-flow function $f_w=\frac{\lambda_w}{\lambda}$ measures the water fraction of the total flow. Since $\nabla P_c = f_w \nabla P_{cow}$, then the total velocity can be expressed as a function of the global pressure:

$$\begin{aligned} v = v_w + v_o = -\mathbf{K}\left(\lambda_w+\lambda_o\right)\nabla P+\mathbf{K}\left(\lambda_w\rho_w+\lambda_o\rho_o\right)g\nabla z \\ +\boldsymbol{k_e}\nabla E_w\left(k_{er,ww}+k_{er,ow}\right) \end{aligned} \tag{5.116}$$

Using the total mobility and global pressure, the following pressure equation is obtained:

$$-\nabla.\left\{\mathbf{K}\lambda\nabla P-\mathbf{K}\left(\lambda_w\rho_w+\lambda_o\rho_o\right)g\nabla z+\boldsymbol{k_e}\nabla E_w\left(k_{er,ww}+k_{er,ow}\right)\right\}=q \tag{5.117}$$

The pressure equation is complete for the problem at hand when no-flow boundary conditions are imposed.

5.10 Numerical Implementation

Commonly used numerical methods for solving two-phase flow problems include (i) finite difference method, in which functions are represented by their values at certain grid points and derivatives are approximated through differences in these values, (ii) method of lines, where all but one variable is discretized and the result is a system of ordinary differential equations (ODEs) in the remaining continuous variable, (iii) finite element method, where functions are represented in terms of basic functions and the PDE is solved in its integral form, and (iv) finite volume method, which divides space into regions or volumes and computes the change within each volume by considering the flux (flow rate) across the surfaces of the volume (Aziz and Settari, 1979; Allen et al., 1988; King, 1992; Chen et al., 2006).

When applied to reservoir simulation, finite difference method (FDM) can be very easy to implement and in its basic form is restricted to handle only rectangular shapes. The method introduces considerable geometrical error and grid orientation effects. Finite element method (FEM), on the other hand can handle complicated geometries, and reduces the grid orientation effects. The quality of a FEM approximation is often higher than

in the corresponding FDM approach. However, it is not easy to implement and is slower than FDM (King, 1992; Chen et al., 2006).

In finite volume method (FVM), physical quantities are calculated at control volumes and the method is conservative (i.e., the flux entering a given volume is identical to that leaving the adjacent volume). In a FVM the unknown functions are represented in terms of average values over a set of finite-volumes, over which the integrated PDE model is required to hold. FVM can be viewed as a conservative finite-difference scheme that treats the grid cells as control volumes. FVM is widely used in the petroleum industry and can be formulated to allow for unstructured meshes. FVM is in between FDM and FEM, faster and easier to implement than FEM; and more accurate and versatile than FDM (King, 1992; Chen et al., 2006).

One of the simplest schemes of finite volume method is cell-centered finite-volume method, also referred to as the two-point flux-approximation (TPFA) scheme. The scheme uses two points, the cell-averages quantities, to approximate the flux, and it is frequently used in reservoir simulation.

The pressure and saturation equations developed in here for two-phase immiscible flow under pressure and electrical gradients are solved in a sequential approach. In this approach, each equation is solved separately using IMPES method. Different discretization methods were used to discretize the two fundamentally different equations. For the global pressure and total velocity formulation, a sequential splitting method is used in the following steps (Chen et al., 2006; Aarnes et al., 2007). First, the saturation distribution from the previous time step (or initial data) is used to compute the saturation-dependent coefficients in the pressure equation before the equation is solved for global pressure and total velocity. Then, the total velocity (v) is kept constant as a parameter in saturation equation, while the saturation is advanced in time. Next, the new saturation values are used to update the saturation-dependent coefficients in the pressure equation, and the pressure equation is solved again, and the computation is repeated.

To incorporate the flux resulting from the electrical gradient at a specific time step; first the saturation distribution in the reservoir is found using the TPFA scheme under the pressure gradient. Then, using the Archie's law, the electrical conductivity of cells is approximated at that specific time step. Archie's law is an empirical law in petro-physics that relates the in-situ resistivity of a reservoir rock to its porosity, water saturation, and resistivity of water through the following expression (Fleureau and Dupeyart, 1988):

$$S_w = \left(\frac{R_w}{R_t} \right)^{0.5} \Phi \tag{5.118}$$

where, S_w is the water saturation, R_w is the resistivity of water, R_t is the true resistivity of rock, and Φ is the porosity. From equation 5.118, the bulk electrical conductivity of the reservoir rock can be found as:

$$\sigma^*_t = \frac{S_w^2}{R_w} \cdot \frac{1}{\Phi^2} \tag{5.119}$$

Assuming a uniform current density in the reservoir, the radial distribution of potential (voltage) is solved first. Then, the flux resulting from potential (voltage) difference in cells is found using the TPFA scheme. Finally, the total production due to applied electrical gradient at each time step is added to the production due to the applied pressure gradient at that specific time step and the computation is repeated.

Using the IMPES technique and implementing the TPFA scheme, the numerical simulation of two-phase flow under applied pressure and electric gradients was accomplished on MATLAB. One layer of the model reservoir from the SPE 10 model data (Christie and Blunt, 2001) was used for a two-dimensional simulation of the flow under applied pressure and electrical gradients (Ghazanfari, 2013). The model size is 60 x 220 x 1 cells and the size of each scaled cell is 20 ft x 10 ft x 2 ft (figure 5.14). The fluids are assumed to be immiscible and incompressible. The actual porosity and permeability tensors of the selected layer from the SPE 10 model were used for simulation. The tensor of EO permeability was assumed to be constant as $1x10^{-5}$ (cm^2/V.sec) in the reservoir. The EO relative permeability coefficients evaluated experimentally (see figures 5.5 and 5.6) were used as representative functions of water saturation for the reservoir.

Gravity term and capillary effect were ignored in the simulation. The reservoir was assumed to be initially filled with oil with S_{wc} = 0.2 (connate water saturation) and S_{or} = 0.2 (residual oil saturation). The fluid viscosities were assumed as μ_w = 1 cp and μ_0 = 38 cp. Injection well was set at the lower-left corner and production well at the upper-right corner and no-flow conditions were imposed at the boundaries. Electric field (current density:1 Amp/m^2) was assumed to be applied through electrodes inserted inside the injection and production wells as shown in figure 5.14.

The saturation, production, and oil recovery profiles at three different time steps are shown in figures 5.15 (a), (b), and (c) respectively. In these figures, the left hand side graph shows the saturation profile, the middle graph shows the changes in the production profile over time including the fractional flow of water and oil, and the right hand side graph shows the variation of oil recovery (%) with pore volumes of injected water. To investigate the contribution of applied electric field to the oil recovery, two

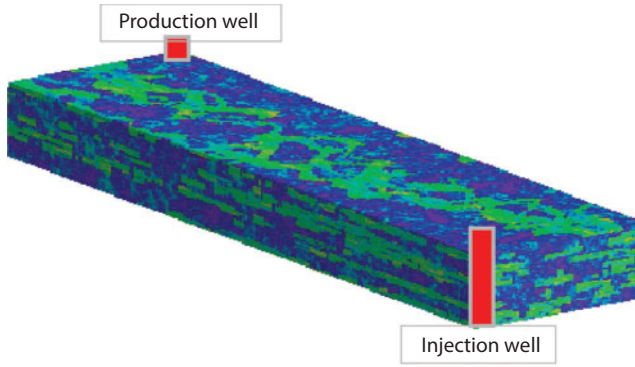

Figure 5.14 Schematic of model reservoir (Christie and Blunt, 2001) and well locations

different cases were considered and developed in the oil recovery graph: (i) only pressure gradient was applied to the reservoir, (ii) electrical gradient was superimposed on top of pressure gradient (i.e. both pressure and electrical gradients were applied to the reservoir).

As observed in figure 5.15 (a), after 100 days, the water has gradually displaced oil toward the production well, but most sections of the reservoir are still filled with oil. The fractional flows of oil and water are 1 and 0 respectively, which means all of the production at this stage is oil and the water has not reached the production well yet. Looking at the oil recovery changes versus water injected pore volumes, only about 5% of the original oil in the reservoir has been extracted. Also, there is no discernible difference in the oil recovery between the two cases of with and without applied electrical gradient after 100 days. This is attributed to the fact that most of the reservoir is still filled with oil and the water saturation has not reached the minimum value to activate the EO flow of water and consequently the contribution of EO generated viscous drag of oil.

After about 650 days, the water has reached the production well and the fractional flow of water drops while that of oil increases at the same time as observed in figure 5.15 (b). At this stage, the water is displacing the oil in most parts of the reservoir and only about 25% of the original oil is recovered. As observed in the oil recovery profile, the contribution of applied electrical gradient is about 4% increase in the oil recovery after 700 days. After 2500 days, the water has filled most parts of the reservoir and the fractional flow of water is about 0.9 and that of oil is about 0.1 as observed in figure 5.15 (c). About 50% of the original oil in the reservoir is recovered with the combined gradient application, to which the contribution of applied electrical gradient is about 7% increase in the oil recovery.

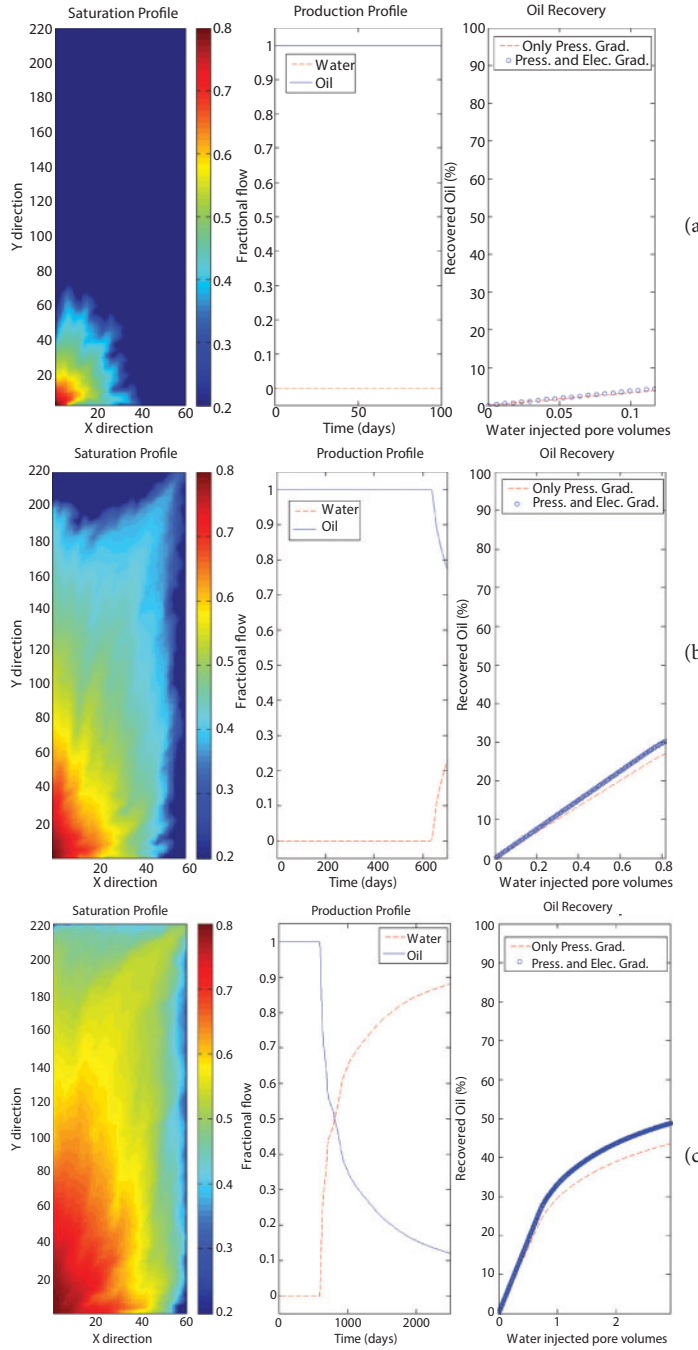

Figure 5-15 Saturation, production, and oil recovery profiles after (a)100, (b)700, and (c)2500 days

5.11 Summary

Mathematical models of EK transport are valuable tools that help predict the efficiency of the EK remediation for a specific contaminated soil. The basic governing equations of EK transport of mass, conservation of mass and charge, and geochemical reactions associated with the EK process were discussed. Existing EK transport models and the coupling between the applied electric and hydraulic gradients were reviewed.

An insight into the mathematical modeling of EKEOR that couples the pressure and electrical gradients applied to the porous medium and incorporates the viscous drag of water on the oil phase under applied electric gradient was provided. EO relative permeability coefficients were evaluated experimentally and analytically as a function of water saturation of the porous medium. A set of governing equations for EKEOR simulation was derived. Implicit Pressure Explicit Saturation (IMPES) solution technique was used to solve the set of governing equations. Numerical solution of the model employed Finite Volume Method (FVM). The predictive capabilities of the model can be enhanced using more realistic parameters about the reservoir, incorporating the transient changes in the viscosity of formation oil, and the non-isothermal effects during extended application of electric field.

References

Acar, Y. B., Gale, R.J., Putnam, G. A., and Hamed, J., 1989. Electrochemical processing of soils: its potential use in environmental geotechnology and significance of pH gradients. *Proc. of 2nd International Symposium on Environmental Geotechnology*, Shanghai, China, Envo Publishing, Bethlehem, PA, Vol. 1: 25.38.

Acar, Y. B., Gale, R. J., Putnam, G. A., Hamed, J., and Wong, R. L., 1990. Electrochemical processing of soils: Theory of pH gradient development by diffusion, migration, and linear convection. *Environmental Science and Health*, A25(6): 687-714.

Acar Y. B., Alshawabkeh, A.N., and Parker R. A., 1997. Theoretical and experimental modeling of multi-species transport in soils under electric fields. Technical report, EPA/600/R-97/054.

Al-Hamdan, A. Z., and Reddy, K. R., 2008. Electrokinetic remediation modeling incorporating geochemical effects. *Geotechnical and Geoenvironmental Engineering*, 134, (1): 91-105

Al-Hamdan, A. Z., and Reddy, K. R., 2008. Modeling of heavy metals transport in high acid buffering soil during electrokinetic remediation. *Proc. of GeoFrontiers 2011*: 836-845,

Al Shalabi, E. W., Haroun, M., Ghosh, B., and Pamukcu, S., 2012. The application of direct current potential to enhancing waterflood recovery efficiency. *Petrol. Sci. and Technol.*, Taylor & Francis, 30 (20): 2160-2168

Allen, M. B., Herrera, I., and Pinder, G. F., 1988. Numerical modeling in science and engineering. *John Wiley & Sons, USA*

Alshawabkeh, A. N., and Acar, Y. B., 1992. Removal of contaminants from soils by electrokinetics: A theoretical treatise. *Environmental Sci. and Health*, A27 (7): 1835.1861.

Alshawabkeh, A. N., and Acar, Y. B., 1996. Electrokinetic remediation: II. Theory. *Geotechnical Engineering, ASCE*, 122(3): 186-196.

Amba, S. A., Chilingar, G. V., Beeson, C. M., 1964. Use of direct electrical current for increasing the flow rate of reservoir fluids during petroleum recovery. *Canad. Petrol. Technol.*, 3 (1): 8 - 14.

Amba, S. A., Chilingar, G. V., Beeson, C. M., 1965. Use of direct electrical current for increasing the flow rate of oil and water in a porous medium. *Canad. Petrol. Technol.*, 4, (1): 81 - 88.

Aarnes, J. E., Gimse, T., Lie, K., 2007. An introduction to the numerics of flow in porous media using geometric modelling. *Numerical Simulation and Optimization, Applied Mathematics at SINTEF*, Springer, 2007: 265.306.

Avraam, D. G., and Payatakes, A. C., 1995. Generalized relative permeability coefficients during steady-state two-phase flow in porous media, and correlation with the flow mechanisms. *Transport in Porous Media*, 20: 135.168

Aziz, K., and Settari, A., 1979. Petroleum reservoir simulation. Applied Science Publishers Ltd., London UK.

Bentsen, R. G., 1998. Effect of momentum transfer between fluid phases on effective mobility. *Petrol. Sci. and Eng.*, 21: 27-42.

Bentsen, R. G., and Manai A. A., 1993. On the use of conventional concurrent and countercurrent effective permeabilities to estimate the four generalized permeability coefficients which arise in coupled two-phase flow. *Transport in Porous Media*, (11): 243-262.

Bethke, C. M., 1996. Geochemical reaction modeling: concepts and applications, Oxford Univ. Press, New York, NY, 1-397

Brask, A., Goranovic, B., and Bruus, H., 2002. Electroosmotically driven two-liquid viscous pump for no conducting liquids. *Micro Total Analysis Systems*, (1):145–147.

Brooks, R., and Corey A., 1964. Hydraulic properties of porous media, *Hydrology Papers*, Volume 3, Colorado State University.

Cao, X., 1997. Numerical modeling of electrokinetically enhanced transport mechanism in soils. *MS Thesis*, Department of Civil and Environmental Engineering, Lehigh University, Bethlehem, PA.

Chen, Z., Huan, G., and Ma, Y., 2006. Computational methods for multiphase flows in porous media. *Soci. for Indust. and Appl. Math.*, Philadelphia, PA

Chilingar, G. V., Sang, C. K., Davis, J. E., Farhangi, H., Adamson, L. G., and Sawabini, S., 1968. Possible use of direct electric current for augmenting

reservoir energy during petroleum production. Compass of Sigma Gamma Epsilon, 45 (4): 272-285.

Chilingar, G. V., El-Nassir, A., and Steven, R.G., 1970. Effect of direct electrical current on permeability of sandstone cores. *Petrol. Technol.*, 22 (7): 830-836

Christie, M. A., and Blunt, M. J., 2001. Tenth SPE comparative solution project: A comparison of upscaling techniques. *SPE Reservoir Evaluation Eng.*, 4(4):308–317, url: www.spe.org/csp.

Corey, A., 1994. Mechanics of immiscible fluids in porous media. 3rd Ed., *Water Resources Publications, LLC*.

Crichlow, H., 1977. Modern reservoir engineering- a simulation approach. *Prentice Hall Inc.*, New Jersey

Dake, L. P. 1978. Fundamentals of reservoir engineering. *Development in Petroleum Science*.

Davis, J. A., James, R. O., and Leckie, J. O., 1978. Surface ionization and complexation at the oxide/water interface: I. Computation of electrical double layer properties in simple electrolytes. *Colloid and Interface Science*, 63 (3): 480–499

Davis, J. A., and Kent, D.B., 1990. Surface complexation modeling in aqueous geochemistry.", *Reviews in Mineralogy*, Vol. 23, pp. 177-260.

Dullien, F. A., and Dong, M., 1996. Experimental determination of the flow transport coefficients in the coupled equations of two-phase flow in porous media. *Transport in porous media*, 25: 97-120

Ertekin, T., Abou-Kassem, J. H., and King, G. R., 2001. Basic applied reservoir simulation. Textbook Series, Society of Petroleum Engineers Publications Department, Dallas, Texas.

Eykholt, G. R., 1992. Driving and complicating features of the electrokinetic treatment of contaminated soils. PhD thesis, Dept. of Civ. Eng., Univ. of Texas at Austin, Tex.

Eykholt, G. R., and Daniel, D. E., 1994. Impact of system chemistry on electroosmosis in contaminated soil. *Geotechnical Eng., ASCE*, 120(5), 797-815.

Eymard, R., Gallou T., and Herbin R., 2003. Finite volume methods. *Handbook of Numerical Analysis*, Vol. 7, pp. 713-1020

Fleureau, J. M., and Dupeyart, M., 1988. Influence of an electric field on the interfacial parameters of a water/oil/rock system: application to oil enhanced recovery. *Colloid and Interface Science*, 123 (1).

Gao, Y., Wong T.N., Yang C., and Ooi K.T., 2005. Two-fluid electroosmotic flow in microchannels. Colloid and Interface Science 284: 306–314

Gao, Y., Wang, C., Wong, T.N., Yang, C., Nguyen, N.T. and Ooi, K.T., 2007. Electroosmotic control of the interface position of two-liquid flow through a microchannel. *Micromechanics and Microengineering*, 17: 358–366

Ghazanfari, E., Shrestha, R., Miroshnik, A., and Pamukcu, S., 2012a. Electrically assisted liquid hydrocarbon transport in porous media. *Electrochimica Acta*, 86: 185–191

Ghazanfari, E., Pamukcu, S., Pervizpour, M., and Karpyn, Z., 2012b. Investigation of generalized relative permeability coefficients for electrically assisted oil recovery in oil formations. *Transport in Porous Media* (In press)

Ghazanfari, E., 2013. Development of a mathematical model for electrically assisted oil transport in porous media. *PhD dissertation*, Lehigh University, Bethlehem, PA

Gladkov S.O., 2003. Dielectric properties of porous media. *Springer*, New York.

Grahame, D. C., 1947. The electrical double layer and the theory of electrocapilarity. *Chemical Review*, 41: 441-501

Gray, D. H., and Mitchell, J. K., 1967. Fundamental aspects of electro-osmosis in soils. Soil Mech. Found. Div., Proc. ASCE, 93(6), 209-236.

Green, D. W., and Willhite, G. P., 1998. Enhanced oil recovery. *SPE textbook series*, Volume 6.

Haran, B. S., Popov, B. N., Zheng, G. and White, R. E., 1997. Mathematical modeling of hexavalent chromium decontamination from low surface charged soil. *Electrochemical Decontamination of Soil and Water, Special Issue of Journal of Hazardous Material*, 55 (1-3): 93-108.

Haroun, M. R., and Chilingar, G. V., Pamukcu, S., Wittle, J. K., Belhaj, H. A., and Al Bloushi, M. N., 2009. Optimizing electroosmotic flow potential for electrically enhanced oil recovery (EEORTM) in carbonate rock formations of Abu Dhabi based on rock properties and composition". *Society of Petroleum Engineers*, IPTC, 13812.

Haydon, D. A., and Taylor, F., H., 1960. On adsorption at the oil/water interface and the calculation of electrical potentials in the aqueous surface phase I. neutral molecules and a simplified treatment for ions. *Phil. Trans. R. Soc. Lond. A*, 253 (1027) 255. 275

Hill, D. G., Wittle J. K., Fricker, D. J., and Chilingar, G. V., 2010. Moving goo: direct electric current oil recovery, a new approach to enhancing oil production. *Sacramento Petroleum Association,* November 17.

Hunter, R. J., 1981. Zeta potential in colloid science. *Academic Press*, New York, N.Y.

Hunter, R. J., 2001. Foundations of Colloid Science. *Oxford University Press*, London.

Jackson, M., 2010. Multiphase electrokinetic coupling: insights into the impact of fluid and charge distribution at the pore scale from a bundle of capillary tubes model. *Geophysical Research*, 15.

Ishido, T., and Mizutani, H., 1981. Experimental and theoretical basis of electrokinetic phenomena in rock-water systems and its applications to geophysics. *Geophysical Research and Solid Earth*, 86, (B3): 1763–1775.

Jacobs, R. A., Sengun M. Z., Hicks, R. E., and Probstein, R. F., 1994. Model and experiments on soil remediation by electric fields. *Environmental Science and Health*, A29(9): 1933-1955.

Jacobs, R. A., and Probstein, R. F., 1996. Two-dimensional modeling of electromigration. *AICHE Journal*, 42(6): 1685.1696.

Jennings, A. A., Kirkner, D. J., and Theis, I. L., 1982. Multicomponent equilibrium chemistry in groundwater quality models. *Water Resources Research*, 18(4): 1089-1096.

Jihong, Z., Yu, Haiming, Y., Wang, Yanan, W., Zhang, Gang, Z., Li, and Xiaobo, L., 2009. Experimental research on further enhanced oil recovery by using high DC electric field", *IEEE proceedings*.

Kalaydjian, F., 1991. Commentary on origin and quantification of coupling between relative permeabilities for two-phase flow in porous media. *Transport in porous media*, 6:469-471.

Keighin, C. W., 1997. Physical properties of clastic reservoir rocks in the Uinta, wind river, and Anadarko basins, as determined by mercury-injection porosimetry. *U.S. geological survey bulletin,* 2146

Killough, L. E., and Gonzalez, J. A., 1986. A fully implicit model for electrically enhanced oil recovery. *Proced. of Soc. of Petrol. Eng.*, New Orleans, LA, DOI: 10.2118/15605.MS

Kim, S. O., Moon, S. H., and Kim, K. W. 2000. Enhanced electrokinetic soil remediation for removal of organic contaminants. *Environmental Technology*, 21(4):417-426.

King, P. R. 1992. The mathematics of oil recovery. Clarendon press, Oxford

Kirkner, D. J., Theis, I. L., and Jennings, A. A., 1985. Multicomponent mass transport with chemical interaction kinetics. *Hydrology*, 76: 107-117.

Kirkner, D. J. and Reeves, M., 1988. Multicomponent mass transport with homogeneous and hetrogeneous chemical reactions: effect of the chemistry on the choice of numerical algorithm. *Water Resources Research*, 24(1): 1719--1729.

Korolev, V. A., Romanyukha, O. V., and Abyzova, A. M. 2008. Electrokinetic remediation of oil-contaminated soils," *Envir. Sci. and Heal.*, *Part A*, 243(8):876-80.

Lewis, F. M., Voss, C. I., and Rubin, J., 1987. Solute transport with equilibrium aqueous complexation and either sorption or ion exchange; simulation methodology and applications. *Hydrology*, 90: 81-115.

Li, H., Pan, C., and Miller, C., 2005. Pore-scale investigation of viscous coupling effects for two-phase flow in porous media. *Physical Review*, E 72, 026705

Liang, L., and Lohrenz, J., 1994. Dynamic method of measuring coupling coefficients of transport equations of two-phase flow in porous media. *Transport in porous media*, 15:71-79

Lichaa P. M., Alpustun H., Abdul J. H., Nofal W. A. and Fuseni A. B. (1992), "Wettability evaluation of a carbonate reservoir rock", reviewed proceedings of the Society of Core Analysis Third European Core Analysis Symposium, P.W. Worthington and C. Chardaire-Riviere (eds.), Paris (1992).

Lichtner, P. C., 1985. Continuum model for simultaneous chemical reactions and mas transport in hydrothermal systems. *Geochem. Cosmochim. Acta*, No. 49: 779-800.

Liu, M., Liu, Y., Guo, Q., Yang, J., 2009. Modeling of electroosmotic pumping of nonconducting liquids and biofluids by a two- phase flow method. *Eelectroanalytical Chemistry*, (636): 86-92

Lorenz, P. B., 1969. Surface conductance and electrokinetic properties of kaolinite beds," *Clays and Clay Minerals*, 17: 223-231.

Marinova, K. G., Alargova, R. G., Denkov, N. D., Velev, O. D., Petsev, D. N., Ivanov, I. B., and Borwankar, R. P. 1996. Charging of oil-water interfaces due to spontaneous adsorption of hydroxyl ions. *Langmuir*, 12, 2045.2051.

Martys, N. S., and Hagedorn, J. G., 2002. Multiscale modeling of fluid transport in heterogeneous materials using discrete Boltzmann methods. *Materials and Structures*, 35: 650-659.

Miller, C. W., and Benson, L. V., 1983. Simulation of solute transport in a chemically reactive heterogeneous system: model development and application. *Water Resources Research*, 19(2): 381-391.

Mitchell, J. K., and Yeung, T. C., 1991. Electrokinetic flow barriers in compacted clay. *Transportation Research Record*, 1288:1-10.

Morgan, F. D., Williams, E. R., Madden, T. R., 1989. Streaming potential properties of westerly granite with applications. *Geophysical Research*, 94 (B9):12449-12461

Nelson, P., 2009. Pore-throat sizes in sandstones, tight sandstones, and shales. *AAPG Bulletin*, 93 (3): 329 - 340

Ortiz-Arango, J. D., and Kantza, A., 2008. Visulaization of viscous coupling effects in heavy oil reservoirs. *SPE/PS/CHOA International Thermal Operations and Heavy Oil Symposium*. Doi: 10.2118/117675.MS

Pamukcu, S., 1994. Electrokinetic removal of coal tar constituents from contaminated soils". *EPRI TR-103320*, 65p.

Pamukcu, S., Filipova, I., and Wittle, J. K., 1995. The role of electroosmosis in transporting PAH compounds in contaminated soils. Electrochemical Technology Applied to Environmental Problems, *The Electrochemical Society*, PV95.12, 252-266.

Pamukcu, S., and Pervizpour, M., 1998. Electroosmotically Aided Restoration of TCE Contaminated Soil," *Final Report to Lawrence Livermore National Laboratory, Environmental Restoration Division, Contract No.B3460123*, University of California, Livermore, CA, November, 52p.

Pamukcu, S., 2009. Electrochemical transport and transformations. Chapter 2: Electrochemical remediation technologies for polluted soils, sediments and groundwater, eds. Reddy, K. R., and Camaselle, C., John Wiley & Sons, pp. 29-65.

Ramstad, T., Fern, P., and Bakke, S., 2010. Simulation of two-phase flow in Reservoir rocks using a lattice Boltzmann method. *SPE Journal*, 124617

Reddy K. R., and Saicheck, R.E., 2004. Enhanced electrokinetic removal of phenanthrene from clay soil by periodic electric potential application. *Environ. Sci. and Heal., Part A,* 39(5):1189-1212

Reddy, K. R., Ala, P. R., Sharma, S., and Kumar, S. N., 2006. Enhanced electrokinetic remediation of contaminated manufactured gas plant soil. *Engineering geology,* 85 (1-2)132-146

Revil, A., and Pezard, P. A., 1999. Streaming potential in porous media: Theory of the zeta potential. *Geophysical Research*, 104(B9): 20,021-20,031

Revil, A. N., Linde, A., Cerepi, D., Jougnot, S. K., Matthai, S., 2007. Electrokinetic coupling in unsaturated porous media. *Colloids and Interface Science*, 313: 315.327

Rodriguez, K., and Araujo, M., 2006. Temperature and pressure effects on zeta potential values of reservoir minerals. *Colloid and Interface Science,* 300 788–794.

Santiago, J. G., 2001. Electroosmotic flows in microchannels with finite inertial and pressure forces. *Analytical Chemistry*, 73(10): 2353-2365.

Saunders, J. H., Jackson, M. D., and Pain C. C., 2006. A new numerical model of electrokinetic potential response during hydrocarbon recovery. *Geophysical research letters*, 33, L 15316.

Saunders, J. H., Jackson, M. D., and Pain C.C., 2008. Fluid flow monitoring in oil fields using downhole measurements of electrokinetic potential. *Geophysics*, 73 (5)

Shapiro, A. P., Renauld, P., and Probstein, R., 1989. Preliminary studies on the removal of chemical species from saturated porous media by electro-osmosis. *Physicochemical Hydrodynamics*, 11(5):785.802.

Shapiro, A. P., and Probstein, R. F., 1993. Removal of contaminants from saturated clay by electroosmosis. *Environmental Science and Technology*, 27(2): 283-291.

Sheldon, J. W., Zondek, B., and Crdwell, W. T., 1959. One dimensional, incompressible, non-capillary two phase fluid flow in a capillary, Trans., *SPE AIME,* (216): 290-296

Stone, H. L., and Garder, A. O., 1970. Analysis of gas cap or dissolved gas reservoir. *Trans., SPE AIME* 222: 92-104

Stumm, W., 1992. Chemistry of the solid-water interface, processes at the mineral-water and particle-water interface in natural systems. *John Wiley & Sons*, *Inc.,* 428p.

Tremblay, B., Seddgwick, G., and Forshner, K., 1997. Simulation of cold production in heavy oil reservoirs: wormhole dynamics, *paper SPE 35387*, 1997

Wang, P., Chen, Z., Chang, H. C., 2006. A new electro-osmotic pump based on silica monoliths. *Sensors and Actuators B*, 113: 500–509.

Ahr, W. M., 2008. Geology of carbonate reservoirs. *John Wiley & Sons, Inc.*

Wittle, J. K., and Hill, D. G., 2006a. Use of direct current electrical stimulation for heavy oil production. *Soc. of Petrol. Eng. Appl. Technol. Workshop* -Technologies for thermal heavy oil and bitumen recovery and production, Calgary, March 14 – 15.

Wittle, J. K., and Hill, D. G., 2006b. Direct current electrical stimulation – a new approach to enhancing heavy oil production. *First World Heavy Oil Conference*, Beijing, November 12 – 15.

Wittle, J. K., Hill, D. G., and Chilingar, G. V., 2008a. Direct current electrical enhanced oil recovery in heavy-oil reservoirs to improve recovery, reduce water cut, and reduce H2S production while increasing API Gravity. *SPE-114012, Society of Petroleum Engineers*.

Wittle, J. K., Hill, D. G., and Chilingar, G. V., 2008b. Electro-enhanced oil recovery (EEOR) using direct current. *Oil Sands and Heavy Oil Technologies Conference*, Calgary.

Wittle, J. K., Hill, D. G., and Chilingar, G. V., 2008c. Direct current stimulation for heavy oil production. *Second World Heavy Oil Conference*, Edmonton, Paper No. 2008-374.

Wittle, J. K., Hill, D. G., and Chilingar, G. V., 2011. Direct current oil recovery (EEOR) – A new approach to oil production. *Energy Sources, Part A: Recovery, Utilization, and Environmental Effects*, 33 (9): 805 – 822.

Yang, G. C., Liu, C. Y., 2001. Remediation of TCE contaminated soils by in-situ EK –Fenton process. *Hazardous Materials*, 137(2):1218-1225

Yao, S., and Santiago J. G., 2003. Porous glass electroosmotic pumps: theory. *Colloid Interface Science*, 268, 133-142.

Yeung, K. C., 1996. Cold flow production of crude bitumen at the Burnt Lake project, Northeastern, Alberta. *Unitar international conference on heavy crude and tar sands*; 1: 515.528

Yeh, G. T., and Tripathi, V. S., 1991. A model for simulating transport of reactive multispecies component: model development and demonstration. *Water Resources Research*, 27(12) 3075. 3094.

Index

Also of Interest

Check out these other related titles from Scrivener Publishing

From the Same Author:

Fundamentals of the Petrophysics of Oil and Gas Reservoirs, by Buryakovsky, Chilingar, Rieke, and Shin. ISBN 9781118344477. The most comprehensive book ever written on the basics of petrophysics for oil and gas reservoirs. *NOW AVAILABLE!*

Petroleum Accumulation Zones on Continental Margins, by Grigorenko, Chilingar, Sobolev, Andiyeva, and Zhukova. ISBN 9781118385074. Some of the best-known petroleum engineers in the world have come together to produce one of the first comprehensive publications on the detailed (zonal) forecast of offshore petroleum potential, a must-have for any petroleum engineer or engineering student. *NOW AVAILABLE!*

Mechanics of Fluid Flow, by Basniev, Dmitriev, and Chilingar, ISBN 9781118385067. The mechanics of fluid flow is one of the most important fundamental engineering disciplines explaining both natural phenomena and human-induced processes. A group of some of the best-known petroleum engineers in the world give a thorough understanding of this important discipline, central to the operations of the oil and gas industry. *NOW AVAILABLE!*

Other Related Titles available from Scrivener Publishing:

Measurement While Drilling (MWD) Signal Analysis, Optimization, and Design, by Wilson C. ChinYinao Su, Limin Sheng, Lin Li, Hailong Bian and Rong Shi, ISBN9781118831687. The only book explaining modern MWD technology, to include hardware design, signal processing and telemetry, offering unique approaches to high-data-rate well logging. *NOW AVAILABLE!*

Formation *Testing: Pressure Transient and Formation Analysis*, by Wilson C. Chin, Yanmin Zhou, Yongren Feng, Qiang Yu, and Lixin Zhao, ISBN

9781118831137. This is the only book available to the reservoir or petroleum engineer covering formation testing algorithms for wireline and LWD reservoir analysis that are developed for transient pressure, contamination modeling, permeability, and pore pressure prediction. *NOW AVAILABLE!*

Electromagnetic Well Logging, by Wilson C. Chin, ISBN 9781118831038. Mathematically rigorous, computationally fast, and easy to use, this new approach to electromagnetic well logging does not bear the limitations of existing methods and gives the reservoir engineer a new dimension to MWD/LWD interpretation and tool design. *NOW AVAILABLE!*

Oil Spill Risk Management: Modeling Gulf of Mexico Circulation and Oil Dispersal, By David Dietrich, Malcolm J. Bowman, Konstantin Korotenko, and Hamish Bowman, ISBN: 9781118290385. This book describes and applies state-of-the-art software designed to help balance cost and profit estimates against risk in the petrochemical industry using oil extracted from ocean bottom deposits. *SEPTEMBER 2014*

Bioremediation of Petroleum and Petroleum Products, by James Speight and Karuna Arjoon, ISBN 9780470938492. With petroleum-related spills, explosions, and health issues in the headlines almost every day, the issue of remediation of petroleum and petroleum products is taking on increasing importance, for the survival of our environment, our planet, and our future. This book is the first of its kind to explore this difficult issue from an engineering and scientific point of view and offer solutions and reasonable courses of action. *NOW AVAILABLE!*

Sustainable Resource Development, by Gary Zatzman, ISBN 9781118290392. Taking a new, fresh look at how the energy industry and we, as a planet, are developing our energy resources, this book looks at what is right and wrong about energy resource development. *NOW AVAILABLE!*

An Introduction to Petroleum Technology, Economics, and Politics, by James Speight, ISBN 9781118012994. The perfect primer for anyone wishing to learn about the petroleum industry, for the layperson or the engineer. *NOW AVAILABLE!*

Ethics in Engineering, by James Speight and Russell Foote, ISBN 9780470626023. Covers the most thought-provoking ethical questions in engineering. *NOW AVAILABLE!*

Zero-Waste Engineering, by Rafiqul Islam, ISBN 9780470626047. In this controversial new volume, the author explores the question of zero-waste engineering and how it can be done, efficiently and profitably. *NOW AVAILABLE!*

Formulas and Calculations for Drilling Engineers, by Robello Samuel, ISBN 9780470625996. The most comprehensive coverage of solutions for daily drilling problems ever published. *NOW AVAILABLE!*

Emergency Response Management for Offshore Oil Spills, by Nicholas P. Cheremisinoff, PhD, and Anton Davletshin, ISBN 9780470927120. The first book to examine the Deepwater Horizon disaster and offer processes for safety and environmental protection. *NOW AVAILABLE!*

Advanced Petroleum Reservoir Simulation, by M.R. Islam, S.H. Mousavizadegan, Shabbir Mustafiz, and Jamal H. Abou-Kassem, ISBN 9780470625811. The state of the art in petroleum reservoir simulation. *NOW AVAILABLE!*

Energy Storage: A New Approach, by Ralph Zito, ISBN 9780470625910. Exploring the potential of reversible concentrations cells, the author of this groundbreaking volume reveals new technologies to solve the global crisis of energy storage. *NOW AVAILABLE!*

WILEY END USER LICENSE AGREEMENT

Go to www.wiley.com/go/eula to access Wiley’s ebook EULA.